THE ORGANIZATION, STRUCTURE, AND ROLE OF ENDOTHELIAL CELLS

DURING ORGANOGENESIS

APPROVED BY SUPERVISORY COMMITTEE

_____

Ondine Cleaver, Ph.D.

_____

Michael Buszczak, Ph.D.

_____

Thomas Carroll, Ph.D.

_____

Michael Dellinger, Ph.D.

DEDICATION

To my parents **Donald Daniel** and **Khana Daniel**,

my brothers **Sargon Daniel** and **Michael Daniel**,

and my wife **Christina Daniel**

for their constant love and support

THE ORGANIZATION, STRUCTURE, AND ROLE OF ENDOTHELIAL CELLS DURING ORGANOGENESIS

by

EDWARD DANIEL

DISSERTATION

Presented to the Faculty of the Graduate School of Biomedical Sciences

The University of Texas Southwestern Medical Center at Dallas

In Partial Fulfillment of the Requirements

For the Degree of

DOCTOR OF PHILOSOPHY

The University of Texas Southwestern Medical Center at Dallas

Dallas, Texas

August, 2019

ACKNOWLEDGMENTS

As the saying goes, “It takes a village to raise a child,” and I could not have written this thesis without the help from many people. First and foremost, I am deeply grateful for my mentor, Dr. Ondine Cleaver. Her guidance and support have been invaluable throughout my graduate education and have helped shape the way I ask and answer scientific questions. Her enthusiasm is infectious and inspires me to maintain the same positive attitude throughout all of my work. Most importantly, she has taught me what it means to be a true scientific mentor. It truly has been an honor to be a member in her lab.

Thank you to my committee members – Dr. Michael Buszczak, Dr. Thomas Carroll, and Dr. Michael Dellinger – for their advice, help, and mentoring over the years. It was clear to me that they wanted me to be the best that I could be. Their many words of advice, scientifically or otherwise, have helped me grow so much as a scientist. Thank you for always pushing me to reach higher goals and serving as my role models.

I must thank the many members of the Cleaver lab that I have had the privilege of working alongside. The lab environment is second to none thanks to all of you, and I will deeply miss working here with you all as I continue on in my career. I want to especially thank Berfin Azizoglu, Annie Ryan, Gabby Sutton, and Yadanar Htike who have directly helped me with the work done here. To everyone else – Caitlin Braitsch, Xiaowu Gu, Simon Lee, David Barry, Haley Barlow, Leilani Marty-Santos, Matthew Hensley, Mitzy Cowdin, Katy Jones, and Seema Neupane – thank you so much for making these last 4 years unforgettable.

The Cleaver lab is a part of an amazing department and surrounded by so many wonderful people. I want to thank the members of the Carroll and Buszczak labs – Alicia,

Varsha, Courtney, Victor, Arnaldo, Phoebe, and many others – for all of the memories we have created. I also want to thank those in the Molecular Biology, GD&D, and MSTP communities that I have had the pleasure of working with over the years, especially Dr. Denise Marciano for her advice and mentorship.

Lastly, thank you to my whole family, new and old: my wife, my parents, my brothers, my new sisters, and my new parents. There's no way I would have been able to go through grad school without their love and support over the years. I am so lucky to have them all in my life. I love you all dearly.

From the bottom of my heart and with everything I am, thank you everyone.

THE ORGANIZATION, STRUCTURE, AND ROLE OF ENDOTHELIAL CELLS DURING ORGANOGENESIS

Publication No. _____

Edward Daniel, Ph.D.

The University of Texas Southwestern Medical Center at Dallas, Graduation Year

Supervising Professor: Ondine Cleaver, Ph.D.

Cellular crosstalk is essential for proper organogenesis. Although originally assumed to be simple conduits for blood, endothelial cells (ECs) actively coordinate organ development through communicating with nearby cell types to generate properly patterned tissues. Despite extensive studies detailing the signaling pathways important for organ development, little is known about how exactly ECs influence these processes. Furthermore, attempts to study ECs in this context have been hampered, in part, by an incomplete understanding of normal endothelial development in specific organs. Here, I characterized the organization, structure, and function of ECs during organ development in the kidney and lung. I first began with an in

depth anatomical analysis of the kidney vasculature over the course of fetal development. I showed that the vasculature grows coordinately with the developing epithelium and stroma from the onset of kidney development and that it forms highly stereotyped structures around these other populations. I then carried out transcriptomic analysis of renal ECs and identified many novel EC-enriched genes expressed in the fetal kidney. From this analysis, I focused on the retinoic acid (RA)-catabolizing enzyme, Cyp26b1, which is enriched in ECs in both the kidney and the lung throughout development. Surprisingly, deletion of Cyp26b1 abrogated development of the lung, but not the kidney. Cyp26b1-null lungs exhibited defects in differentiation of the distal epithelium, leading to neonatal lethality. Transcriptomic and functional analyses suggested that the phenotype observed is due to RA-dependent and RA-independent mechanisms. On the other hand, the kidney appeared to be protected from loss of Cyp26b1 by upregulation of Dhrs3 to maintain normal RA levels. Bypassing Dhrs3 by exogenously administering RA interrupted kidney epithelial development only in mice lacking at least one allele of Cyp26b1. This body of work highlights the importance of EC-mediated cellular communication during development and identifies organ-specific mechanisms that regulate this crosstalk.

TABLE OF CONTENTS

PRIOR PUBLICATIONS

Nam Y.J, Song K., Luo X., **Daniel E**., Lambeth K., West K., Hill J.A., DiMiao J.M., Baker L.A., Bassel-Duby R., Olson E.N. (2013) Reprogramming of human fibroblasts toward a cardiac fate. *Proc Natl Acad Sci U S A*. 110 (14): 5588-93

PRESENT WORK

Daniel, E., Sutton, G.I., Htike, Y., Cleaver, O. (2019) Organotypic roles of Cyp26b1 during lung and kidney organogenesis. *In preparation*

Daniel, E. and Cleaver, O. (2019) Vascularizing organogenesis: Lessons from developmental biology and implications for regenerative medicine. *Curr Top Dev Biol*. 132: 177-220

Daniel, E., Azizoglu, D.B., Ryan, A.R., Walji, T.A., Chaney, C.P., Sutton, G.I., Carroll, T.J., Marciano, D.K., and Cleaver, O. (2018). Spatiotemporal heterogeneity and patterning of developing renal blood vessels. *Angiogenesis*. 21 (3): 617-634

LIST OF FIGURES

CHAPTER 1

CHAPTER 3

CHAPTER 4

LIST OF TABLES

LIST OF DEFINITIONS

3D – 3-Dimensional

Adam10 – A Disintegrin and Metalloprotease Domain 10

Ager – Advanced Glycosylation End-Product Specific Receptor

Angpt1 – Angiopoietin-1

Aqp5 – Aquaporin 5

AT1 – Alveolar Type 1

AT2 – Alveolar Type 2

atRA – All-trans RA

AV – Arteriovenous

β-Gal – β-Galactosidase

BASC – Bronchioalveolar Stem Cell

Bmp – Bone Morphogenetic Protein

BSA – Bovine Serum Albumin

CCSP – Clara Cell Secretory Protein

CD – Cluster of Differentiation

Cdh2 – Cadherin 2

cDNA – Complimentary DNA

CK – Cytokeratin

CKD – Chronic Kidney Disease

Cre-ERT2 – Cre Recombinase Estrogen Receptor T2

CRISPR/Cas9 – Clustered Regularly Interspaced Short Palindromic Repeats/ CRISPR Associated Protein 9

Cx40 – Connexin40

Cxcl12 – C-X-C Motif Chemokine Ligand 12

Cxcr4 – C-X-C Motif Chemokine Receptor 4

Cyp26a1 – Cytochrome P450 Family 26 Subfamily A Member 1

Cyp26b1 – Cytochrome P450 Family 26 Subfamily B Member 1

Cyp26c1 – Cytochrome P450 Family 26 Subfamily C Member 1

DAPI – 4′,6-Diamidino-2-Phenylindole

Dig – Digoxigenin

DNA – Deoxyribonucleic Acid

E – Embryonic Day

EC – Endothelial Cell

E-Cad – Epithelial Cadherin

ECM – Extracellular Matrix

EDTA – Ethylenediaminetetraacetic Acid

Emcn – Endomucin

eGFP – Enhanced GFP

EpCAM – Epithelial Cell Adhesion Molecule

EphB4 – Ephrin Receptor B4

FACS – Flourescence Activated Cell Sorting

FBS – Fetal Bovine Serum

Fgf – Fibroblast Growth Factor

Fgfr – Fibroblast Growth Factor Receptor

FISH – Fluorescent ISH

Fl – Flox

Flk1 – Fetal Liver Kinase 1

FoxD1 – Forkhead Box D1

GBM – Glomerular Basement Membrane

GFP – Green Fluorescent Protein

Gimap4 – GTPase Immune Associated Protein 4

Gpihbp1 – Glycosylphosphatidylinositol Anchored High Density Lipoprotein Binding Protein 1

H&E – Hematoxylin and Eosin

HOPX – Homeodomain-Only Protein

HUVEC – Human Umbilical Vein Endothelial Cell

Hypo – Hypomorph

Icam – Intercellular Adhesion Molecule

IF – Immunofluorescent

ISH – In Situ Hybridization

Lamp3 – Lysosomal Associated Membrane Protein 3

LTL – Lotus tetragonolobus lectin

Meis – Myeloid Ecotropic Viral Integration Site

MET – Mesenchymal to Epithelial

Mfsd2a – Major Facilitator Superfamily Domain Containing 2A

Mmp14 – Matrix Metalloproteinase 14

mRNA – Messenger RNA

N-Cam – Neural Cell Adhesion Molecule

NCC – Sodium Chloride Cotransporter

Nfatc1 – Nuclear Factor Of Activated T Cells 1

NPC – Nephron Progenitor Cell

Nrp – Neuropilin

O.C.T – Optimal Cutting Temperature

PBS – Phosphate Buffered Saline

Pbx1 – Pre-B-Cell Leukemia Homeobox 1

PCA – Principle Component Analysis

PCR – Polymerase Chain Reaction

PDGF-B – Platelet Derived Growth Factor B

Pdgfr – Platelet Derived Growth Factor Receptor

Pdpn – Podoplanin

Pdx1 – Pancreatic and Duodenal Homeobox 1

PECAM – Platelet Endothelial Cell Adhesion Molecule

PFA – Paraformaldehyde

Plvap – Plasmalemma Vessicle Associated Protein

Podxl1 – Podocalyxin

proSP-C – proSurfactant Protein-C

PTA – Pretubular Aggregate

Ptf1a – Pancreas Associated Transcription Factor 1a

qRT-PCR – Quantitative Real Time PCR

RA – Retinoic Acid

Raldh – Retinaldehyde dehydrogenase

RAR – Retinoic Acid Receptor

RARE – Retinoic Acid Response Element

RNA – Ribonucleic Acid

Rsad2 – Radical S-Adenosyl Methionine Domain Containing 2

RV – Renal Vesicle

RXR – Retinoic X Receptor

S1P – Sphingosine-1-phosphate

$S1P_1$ – Sphingosine-1-phosphate Receptor

Sca1 – Stem Cell Antigen 1

Sema3a – Semaphorin 3A

Six2 – Sine Oculus Homeobox Homolog 2

Sftpc – Surfactant Protein C

sgRNA – Single Guide RNA

Slfn5 – Schlafen Family Member 5

Sm22a – Smooth Muscle Protein 22 Alpha

SMA – Smooth Muscle Actin

Sox9 – Sex Determining Region Box 1

Tie1 – Tyrosine Kinase with Immunoglobulin Like And EGF Like Domains 1

Tie2 – TEK Receptor Tyrosine Kinase

Tm4sf1 – Transmembrane 4 L Six Family Member 1

UB – Ureteric Bud

VE-Cad – Vascular Endothelial Cadherin

VEGF – Vascular Endothelial Growth Factor

Vegfr – VEGF Receptor

vWF – Von Willebrand Factor

WGCNA – Weighted Gene Correlation Network Analysis

Wnt – Wingless-Type MMTV Integration Site Family

Wt1 – Wilms Tumor 1

CHAPTER ONE

Introduction – Vascularizing Organogenesis

Blood vessels are the conduits for life. Through them, organ systems across the body communicate to one another through the exchange of nutrients, gas, and signaling factors. Over the last several years, there has been a growing appreciation of the role blood vessels play in paracrine signaling within developing organs. The endothelial cells (ECs) lining blood vessels actively communicate with surrounding stromal (or mesenchymal) and epithelial tissue to ensure proper patterning of both the endothelium and other tissues. In fact, endothelial-derived signals are required for proper development and patterning in organogenesis. One of the main challenges facing vascular biologists today is understanding both what these signals are and how they regulate organ development.

Where do vascular progenitors come from? How do they become patterned to accommodate growing organs? Do they all have the same potential and plasticity? These are all questions that the field of vascular developmental biology is eager to answer. Some general principles have emerged. Amongst them, the concept that angiogenic factors are expressed by non-vascular cells to recruit and maintain blood vessels. In addition, it is now well accepted that blood vessels are not equivalent in all tissues, but rather they adapt to local needs and conform to distinct environments. What is less clear is how ECs in turn influence the tissues they perfuse. Are there identifiable non-nutritional signals? Most cells within tissues are understood to communicate with each other, but what the language of that conversation says remains a significant mystery to decode. Experimental data, often contradictory and spatiotemporally dependent, remains a challenge to interpret.

Many recent efforts have been aimed at generating tissues or organs *in vitro* to replace those that are diseased or defective. Successful clinical application has been of limited success as only rudimental vascularization has been achieved. Whereas these efforts have focused extensively on improving epithelial development in these *ex vivo* organs, there has been limited success to promote proper vascularization. This is, in part, due to the lack in understanding how organs are normally vascularized during development. A better understanding of the coordinated growth of tissues during embryonic development, the interface of blood vessels with different cells within these tissues, and the patterning, remodeling, and heterogeneity of ECs that form these vessels will therefore be critical to develop fully vascularized therapeutically viable tissues for transplant.

In this chapter, I will focus on three important aspects of blood vessel formation in organs: 1) how the vasculature remodels and organizes within developing tissues; 2) establishment of vascular heterogeneity, as vessels display organ specificity and regionalization within tissues; and 3) ways in which the vasculature and surrounding tissues communicate to one another to direct development. I will examine these themes of vascular biology in the context of three vital organs, the pancreas, lung, and kidney with a special focus on the kidney as greater relevant literature is available (**Fig. 1.1**). Lastly, I will highlight the current efforts to apply the principles guiding development towards generating functional kidney tissue *ex vivo* and discuss challenges related to vascularization of these *ex vivo* tissues.

EC DEVELOPMENT, HETEROGENEITY, AND THE CHALLENGES WE FACE

Blood vessels grow via two main mechanisms: *vasculogenesis* and *angiogenesis*. *Vasculogenesis* is the process by which vessels assemble *de novo* from individual endothelial

precursors termed ‘angioblasts.’ These angioblasts coalesce to form a vascular cord, polarize, and open a lumen, differentiating into mature ECs to form a functional blood vessel (Azizoglu and Cleaver, 2016). Conversely, *angiogenesis* is the process by which new vessels grow from pre-existing vessels. ECs in these vessels respond to local cues to undergo morphologic changes to sprout and generate a new lumenized vessel (Azizoglu and Cleaver, 2016). Whether the vessels in an organ form through a vasculogenic or angiogenic process is entirely organ-specific. For example, the early vessels of the yolk sac and dorsal aortae form through vasculogenesis, while the retinal vasculature forms primarily through an angiogenic process (Garcia and Larina, 2014; Siemerink et al., 2013; Strilic et al., 2009). Some vascular beds, such as those in the lung, form through both angiogenesis and vasculogenesis (Herriges and Morrisey, 2014). Through these processes, vessels extend throughout the growing embryo, coalesce, and remodel until they yield a fully functional and hierarchical vascular network.

A fascinating aspect of blood vessels is how different they are in every tissue: some vessels contain small pores called fenestrae, some vessels form strict continuous barriers, and, some form highly discontinuous junctions or sinusoids. In fact, at times it seems the only unifying characteristic is that they carry blood! The concept of endothelial heterogeneity is underscored by organ-to-organ variations in how blood vessels develop. ECs are highly adapted to their specific local environment. The fact that ECs display stark heterogeneity based on their local environment has been known for some time (Aird, 2003, 2007a, b). On a gross scale, the vascular system can be broken down into 3 main components: high pressure arteries that transport blood away from the heart, low pressure veins that bring blood back to the heart, and capillaries where nutrient and gas exchange occurs. ECs in each of these regions possess unique characteristics that facilitate

their functions. Arteries and veins can be distinguished from each other by histology and by gene expression profiles (Chi et al., 2003; Chong et al., 2011; dela Paz and D'Amore, 2009). In fact, arteriovenous (AV) differentiation, the process by which some early ECs commit towards an arterial or venous fate, is one of the first ways in which ECs begin to demonstrate this heterogeneity. AV differentiation is evident as early as E8.0 when the first major vessels, the dorsal aortae and vitelline veins, show signs of formation and transcriptional differences (Chong et al., 2011).

ECs that compose capillaries also display heterogeneous morphology and gene expression, dependent on their resident tissue. Capillaries can be classified as continuous, fenestrated, or sinusoidal/discontinuous based on morphology and vessel permeability (Augustin and Koh, 2017). The permeability of a capillary bed depends on the needs of the organ. For example, the capillaries supplying the central nervous system (CNS) possess a continuous endothelium that contributes to the maintenance of the Blood-Brain Barrier, a highly restrictive interface that tightly regulates the ions, small solutes, nutrients, drugs, water, and other molecules that can be transferred from the plasma into the CNS in order to protect the brain from potentially harmful substances (Zhao et al., 2015). On the other hand, the sinusoids within the liver allow for the free flow of solutes in the blood into the space of Disse adjacent to hepatocytes (Augustin and Koh, 2017). Recently, transcriptional profiling of perfused adult ECs from several different organs – the kidney, liver, lung, heart, testes, brain, muscle, spleen, and bone marrow – and from human fetal kidney, liver, lung, and heart brought new insights into the degree of EC heterogeneity (Marcu et al., 2018; Nolan et al., 2013). ECs from each organ displayed significantly different transcriptomes and functional capabilities. EC heterogeneity has also been observed not only between different

endothelial beds, but also at the cellular level within the same vessel. For example, the ECs that line the aorta demonstrate a mosaic and dynamic pattern of vWF expression (Yuan et al., 2016). Similar mosaicism has also been observed in the developing pancreatic arteries as well (Azizoglu et al., 2016). Taken together, these data clearly demonstrate that ECs display tissue-specific heterogeneity.

Although ECs are understood to be heterogeneous, there are still several challenges facing the field. First, it is unclear what upstream regulators coordinate the transcriptional programs that define ECs in each region. Are these programs dependent on EC intrinsic cues, extrinsic cues from the surrounding microenvironment, or a mixture of both? Next, when is this heterogeneity established during organogenesis? As will be discussed below, EC differentiation – including morphogenesis, AV specification, and mature capillary formation – is entirely organ-dependent. For example, the first evidence of AV differentiation in the pancreas is a single vessel present at E11.5, when connexin40 (Cx40) expression is seen in vessels undergoing coalescence (Azizoglu et al., 2016). In the kidney, arterial development begins at E13.5, possibly due to differences in when the organs begin to develop, and emerges as a hierarchical tree instead of a single vessel (Munro et al., 2017a; Murakami et al., 2019). These questions must be answered to understand how organs form blood vessels adapted to suit their needs.

Currently, the field lacks some basic tools to study organotypic variations between ECs that can help answer these organ-specific questions about the vasculature. The current genetic tools available to study endothelial development rely on broadly expressed endothelial genes, namely VE-Cad or Tie2. While powerful means to study EC biology, there are important limitations to these systems to answer questions in an organ-specific manner. First, deletion of a gene in all ECs

can cause off-target effects independent of the effect in a specific organ. Any gene that prevents ECs from forming a continuous, lumenized network will lead to vascular anomalies with far reaching effects, and possibly to early embryonic lethality (Ferrara et al., 1996; Xu et al., 2011). Additionally, transcriptional profiling of organ-specific ECs revealed that these genes, and other broadly expressed endothelial markers, vary in expression levels between organs (Nolan et al., 2013). Therefore, even the available pan-endothelial promoters used to make reporters or Cre lines expressed in 'all' ECs may not be well suited to answer questions in all organs.

To overcome this challenge and generate both EC- and organ-specific mouse models, one method utilized two recombinase systems to specifically label coronary or brain ECs (Pu et al., 2018). In this method, a Dre recombinase was expressed in ECs using the Tie2 promoter. A second recombinase, a Cre-ERT2, was placed downstream of the Wt1 or Mfsd2a promoters, which are expressed in coronary or brain ECs, respectively, as well as other tissues. This Cre-ERT2 cassette contained Dre-specific Rox sites around the ERT2 cassette (CrexER). In ECs where Dre is expressed, the ERT2 domain will be eliminated and Cre will be able to translocate to the nucleus to undergo additional recombination events. Therefore, Cre-mediated excision will only occur in cell types that express both the Dre and Cre recombinases, providing a means to achieve both endothelial- and tissue-specific expression pattern. Although potentially useful in certain contexts, this approach would only be useful if lines that overlap in expression exist. In addition, it may also not prove suitable in tissues that lack a single tissue-specific promoter like the kidney. It is also limited by the lack of suitable mouse lines with the CrexER transgene. Thus, the tools needed to answer many of the questions about organ-specific vascular biology need to be further developed.

VASCULAR MORPHOGENESIS IN SPECIFIC ORGAN SYSTEMS

Pancreas

Overview of pancreatic vascular development

The pancreas consists of two organs combined into one: an exocrine compartment that secretes digestive proteins into the duodenum and an endocrine compartment that releases hormones that regulate glucose homeostasis, including insulin and glucagon (Pan and Wright, 2011). Both of these lineages arise from the same progenitor population marked by *Pdx1* (Gu et al., 2003). The first morphologic event of pancreatic development occurs with specification and thickening of $Pdx1^{+}$ pre-pancreatic epithelium on both dorsal and ventral sides of the foregut-midgut junction at E8.5-E9.0 (Villasenor et al., 2010a). The dorsal pancreatic epithelium lies in direct contact with the dorsal aortae, while the ventral epithelium is separated from the nearby vitelline veins by a small layer of mesenchymal cells (**Fig. 1.2A**) (Lammert et al., 2001; Yoshitomi and Zaret, 2004). The surrounding mesenchyme also contains fine capillaries and isolated angioblasts (Azizoglu et al., 2016; Katsumoto and Kume, 2011; Yoshitomi and Zaret, 2004). In a process termed the 'primary transition' (from approximately E9.0 to E12.0), the thickened pancreatic epithelium undergoes additional morphogenesis to form a stratified epithelial bud that will give rise to the exocrine and endocrine pancreas (Villasenor et al., 2010a). At this stage, small capillaries, often in direct contact with the epithelium, can be identified in the surrounding mesenchyme around but not within the bud, forming a mesh-like network or plexus (**Fig. 1.2B-C**) (Azizoglu et al., 2016; Pierreux et al., 2010). The majority of these vessels at this stage are not perfused (Shah et al., 2011).

Signs of AV differentiation can be observed in the pancreatic bud as early as E10.5. As vessels expand and coalesce, they initiate expression of ephrinB2^{+} or EphB4^{+} vessels, marking arteries and veins, respectively. Within one day, a central artery, but no large caliber vein, can be seen, indicating that arterial development precedes venous development in the pancreas. Importantly, these early arteries, veins, and capillaries present around the epithelium arise through remodeling of the plexus cords present in the mesenchyme at E9.5 to eventually form a hierarchical tree (Azizoglu et al., 2016). Angiogenesis does not seem to play as significant a role in early pancreatic endothelial development, as pancreatic branches are largely seen to integrate between existing vessel loops rather than via formation of new sprouts. These studies in early pancreatic morphogenesis underscore how closely associated early vessels are with the growing pancreatic epithelium at early stages of organogenesis.

The next phase of pancreatic development beginning around E12.5 is called the 'secondary transition.' This period marks a dramatic change in epithelial growth and differentiation. During this time frame, the stratified epithelial bud begins to resolve into a single-layered epithelium and the epithelium experiences a burst of proliferation. The result is the emergence of two distinct epithelial regions: the distal tips containing acinar cells that secrete digestive enzymes and the trunk region where bipotential cells differentiate to form ductal and endocrine lineages (Pan and Wright, 2011). At this stage, ECs are more sparse around the distal acinar tips, while being more dense around the trunk region, coincident with increased expression of the powerful endothelial mitogen VEGF-A in the trunk (**Fig. 1.2D**) (Pierreux et al., 2010). This organization is maintained through the rest of development.

Endothelium regulates early pancreatic morphogenesis

During initial stages of pancreatic development, ECs promote formation of the early pancreatic bud. Pre-pancreatic endoderm explants form pancreatic-like structures only when co-cultured with the dorsal aorta or other EC-containing tissues (Lammert et al., 2001). Utilizing *Flk1*$^{-/-}$ mutant mouse embryos which lack all ECs to expand upon this observation, Yoshitomi and Zaret observed that early dorsal pancreatic endoderm still expressed Pdx1; however, the dorsal endoderm failed to expand into the early stratified bud while the ventral pancreatic endoderm remained unaffected (Yoshitomi and Zaret, 2004). These results indicate that ECs are required for pancreatic growth but dispensable for initial pancreatic induction (Yoshitomi and Zaret, 2004). These *Flk1*$^{-/-}$ mice also exhibited a loss of Ptf1a, an important driver of the pancreatic fate in the early endoderm (Kawaguchi et al., 2002), which was rescued when cultured with fragments of the dorsal aorta. Experiments performed in chick embryos suggest a reciprocal relationship between ECs and the early pancreas. Early pre-pancreatic endoderm secretes the chemokine Cxcl12, which binds to its cognate receptor Cxcr4 expressed on nearby angioblasts. These angioblasts, in turn, signal back to the endoderm to promote pancreatic development (Katsumoto and Kume, 2011). Together, these experiments demonstrate the promotion of early pancreatic development by vascular structures.

ECs also communicate to the pancreatic bud indirectly by supporting the surrounding mesenchyme. The mesenchyme is necessary for epithelial development from the onset of pancreatic morphogenesis partly through secreting Fgf10 (Bhushan et al., 2001; Landsman et al., 2011). In *Flk1*$^{-/-}$ embryos, the mesenchyme is nearly absent due to increased apoptosis (Jacquemin et al., 2006). Likewise, dorsal mesenchyme explants can only grow when cultured with the dorsal

aorta suggesting that signals from the ECs themselves support mesenchymal growth. Adding Fgf10 to *Flk1*$^{-/-}$ pancreas explants rescued pancreatic growth (Jacquemin et al., 2006). Thus, ECs are not only important for early pancreatic epithelial development through direct endothelial-epithelial crosstalk, but they also communicate via the surrounding mesenchyme to support mesenchyme-epithelial crosstalk.

Systemic factors have also been shown to be important for early pancreas formation. *Cdh2*$^{-/-}$ mice, which are able to form the dorsal aortae but lack blood flow due to cell adhesion defects in the heart, display initiation of Pdx1 expression but failure of dorsal pancreas expansion. Dorsal pancreatic formation was rescued when Cdh2 activity was restored in the heart alone, suggesting that systemic factors may be regulating this phenotype (Edsbagge et al., 2005). Indeed, addition of Sphingosine-1-phosphate (S1P) to *Cdh2*$^{-/-}$ early pancreatic explants rescued dorsal pancreatic morphogenesis. S1P appears to signal through the endothelium as genetic deletion of the endothelial-specific S1P receptor $S1P_1$ also resulted in a dramatic reduction of both dorsal and ventral pancreas growth by E12.5 (Edsbagge et al., 2005; Sand et al., 2011). These data argue that ECs promote growth and differentiation of the early dorsal pancreas both directly via cell-cell communication between the epithelium and endothelium and indirectly via supplying systemic factors and supporting the mesenchyme after the initial specification.

The evolving role of ECs in pancreatic morphogenesis

By the secondary transition, ECs become more dense around the trunk and more sparse around the acinar tips (**Fig 1.2D**). This vascular organization in the developing pancreas suggests that ECs may differentially regulate pancreatic morphogenesis depending on their location. Specifically, ECs may positively regulate trunk development – and the bipotential progenitors

therein – while inhibiting acinar development. In support of this idea, overexpression of VEGF using the Ptf1a promoter (Pierreux et al., 2010) or a TET off system under the control of the Pdx1 promoter (Magenheim et al., 2011) both lead to hypervascularization of the pancreas including around the distal tips, decreased epithelial branching, and inhibition of acinar differentiation. Conversely, inhibition of VEGFR2 in explants decreases vascularization while increasing epithelial growth specifically at the tips but not at the trunk (Magenheim et al., 2011; Pierreux et al., 2010; Sand et al., 2011). These data strongly support the model in which ECs inhibit acinar differentiation during the secondary transition by keeping adjacent epithelial cells in a more immature or progenitor-like state. Therefore, ECs can be argued to serve two opposite roles in pancreatic development: 1) during initial pancreas formation and primary transition, ECs promote expansion and development of the early dorsal pancreatic bud, and 2) when pancreatic organogenesis shifts to the secondary transition, ECs perform the opposite role and inhibit acinar differentiation.

Based on the localization of ECs around the trunk, one could hypothesize that ECs promote the development of trunk cells into ductal and endocrine cell fates. Indeed, the precise role of ECs in directing endocrine fates appears to be time-dependent, mirroring the change in the role of ECs during epithelial development. ECs appear to promote endocrine differentiation early in pancreas development, but inhibit it at later stages. VEGF-A overexpression in $Pdx1^{+}$ cells from the onset of pancreatic development and into perinatal stages leads to islet hyperplasia and ectopic insulin expression in the stomach, suggesting that ECs promote endocrine differentiation (Lammert et al., 2001). Likewise, *Flk1*$^{-/-}$ embryos fail to develop insulin^{+} or glucagon^{+} cells (Yoshitomi et al., 2004). Conversely, deletion of VEGF-A from $Pdx1^{+}$ cells during this same time frame led to a

reduction in endocrine cell mass (Reinert et al., 2013). These results may be due to changes in oxygen levels. Perfused blood vessels lie in close proximity to glucagon$^+$ cell clusters and pancreas explants grown in hypoxia demonstrate decreased endocrine differentiation suggesting that early endocrine differentiation relies on increased oxygen (Shah et al., 2011). Alternatively, inhibition of VEGFR2 in pancreas explants for a short period of time decreased endocrine differentiation, indicating that ECs themselves also play a role in promoting endocrine differentiation (Pierreux et al., 2010). As seen in early pancreatic epithelial morphogenesis, the endothelium promotes early endocrine development both directly and indirectly.

At later stages of pancreas development, ECs inhibit endocrine differentiation. Overexpression of VEGF exclusively in β-cells, which emerge starting at E11.5, led to disrupted islet morphology and decreased endocrine mass by E16.5 (Cai et al., 2012). In a separate series of experiments, ECs were actually shown to inhibit endocrine differentiation in contrast to the previous work (Magenheim et al., 2011). By overexpressing VEGF in Pdx1$^+$ cells using the Tet system *in vivo* and inhibiting VEGFR2 *in vitro*, this study demonstrated that endocrine differentiation is inversely related to the amount of vascularization. Why these studies see disparate responses to hyper- and hypovascularization remain unclear. Potential reasons include differences in 1) the transgenic system utilized, 2) the explant culturing techniques, and 3) the small molecule VEGFR2 inhibitor. All of these variables could introduce unknown additional effects on the developing pancreatic epithelium and the progenitors there in, which ultimately manifest in the different phenotypes observed. The exact mechanism by which ECs influence endocrine differentiation – and how to reconcile these studies – remains to be elucidated.

Lung

Overview of pulmonary vascular development

The lung facilitates the exchange of O_2, CO_2, and other gases between the air and the blood. As such, endothelial-epithelial interaction is central for proper lung development and function. Lung development begins at E9.0 with specification of the early lung progenitors in the embryonic foregut, formation and splitting of the tracheoesophageal ridge, and initial branching events (Herriges and Morrisey, 2014). This early developmental timeframe is termed the 'pseudoglandular stage' due to its resemblance to glandular organs.

During this early morphogenesis, a delicate vascular plexus surrounds the early lung as it courses throughout the mesenchyme (deMello et al., 1997; Parera et al., 2005; Schachtner et al., 2000). By E12.5, the lung progenitors differentiate into two main progenitor populations: one that will give rise to the distal airway spaces where gas exchange occurs and another that generates the proximal (or conductive) airways responsible for transporting gases between the distal airways and external environment. Likewise, the endothelium associated with either of these epithelial compartments is thought to arise from two separate sources. The endothelium of the large caliber pulmonary arteries and veins that form next to the proximal airways arise from $Wnt2^+$ cardiopulmonary progenitors that also give rise to the associated smooth muscle cells (Peng et al., 2013). On the other hand, ECs surrounding the distal airways are thought to arise from a VE-Cad^+ population of ECs present in the trunk at E8.5 before initial lung development (Herriges and Morrisey, 2014). It is striking that the lung endothelium arises from two separate endothelial populations and that they must coordinate to anastomose and form a fully functional endothelial

network. How these two endothelial populations form a vascular network remains to be determined as the current data support both angiogenic and vasculogenic processes for both populations.

Distinct origins determine the role of the pulmonary vasculature

The distinct origin of the two lung EC populations and their relation with the associated airways raises the possibility that endothelial-epithelial crosstalk is region-specific. Early ECs have been shown to be dispensable for initial specification of lung progenitors and vice versa (Havrilak et al., 2017; Peng et al., 2013). Instead, ECs are necessary for proper maturation and branching of the embryonic lung. Studies that investigated how ECs regulate lung development have utilized an indirect approach of modulating VEGF-A levels in specific regions of the lung – which thereby affects EC patterning and function – and assessing changes in the pulmonary epithelium. Overexpression of VEGF-A in proximal epithelial cells (specifically Clara Cell Secretory Protein ($CCSP^+$) cells) during development or after birth led to disruption of the proximal airway morphology and dilation of the associated arteries with minimal to no involvement of the distal airway spaces (Akeson et al., 2005; Akeson et al., 2003; Le Cras et al., 2004). Likewise, overexpression of VEGF-A in distal epithelial cells (specifically Surfactant protein-C ($Sftpc^+$) cells) during development led to disruption of the normal lung vasculature with dilated distal airway spaces (Akeson et al., 2003; Zeng et al., 1998). Proximal airways appeared unaffected in these models. Interestingly, deletion of VEGF-A in these same distal epithelial cells also led to dilation of the distal airways, although this was due to impaired septal formation (Yamamoto et al., 2007). These data indicate that the role of VEGF-A – and, by extension, the role of ECs – during lung organogenesis is spatially defined.

Ex vivo lung explant models and 3-dimensional analyses of *in vivo* lungs have demonstrated that ECs promote branching morphogenesis. The addition of VEGF-A in lung explant models increases epithelial branching morphogenesis through increased Bmp4 and Sftpc expression (Del Moral et al., 2006). This effect seems to be specifically affecting the distal tips of the lung epithelial tree. Conversely, explants cultured with antisense oligonucleotides against VEGF-A or against VEGFR2 demonstrate decreased epithelial branching (Del Moral et al., 2006; van Tuyl et al., 2005). When VEGF-A was blocked *in vivo* through increased production of soluble VEGFR1, the rate of epithelial branching did not change but, rather, the orientation of the branches was disrupted (Lazarus et al., 2011). All of these data show that ECs influence epithelial maturation by modulating epithelial morphogenesis during development.

ECs are also necessary for postnatal maturation of the lung epithelium, specifically the alveoli where gas exchange occurs. The majority of alveoli form in the immediate postnatal period in a process termed 'alveolarization,' which leads to a massive expansion in the surface area for gas exchange to occur (Warburton et al., 2010). Treatment of neonatal pups with antiangiogenic agents or an inhibitor against VEGFR2 resulted in decreased postnatal lung growth, decreased endothelial arborization, and fewer but dilated alveoli, all indicating disrupted alveolar maturation (Jakkula et al., 2000). Likewise, genetic deletion of PECAM-1, an endothelial-specific gene that is necessary for angiogenesis (Cao et al., 2002; DeLisser et al., 1997; Newman and Newman, 2003), resulted in decreased alveolarization and thickened airway spaces in postnatal mice without affecting EC proliferation or apoptosis.

Recently, lung pericytes have also been implicated in directing alveolar maturation. Deletion of the Hippo pathway proteins Yap1 and Taz in PDGFR-β^+ lung pericytes using the

PDGFR-β-CreERT2 inducible mouse line resulted in impaired alveorization leading to dilated airspaces, decreased capillary formation, and reduced pulmonary vasculature (Kato et al., 2018). These phenotypes were likely caused by a decrease in angiopoietin-1, a ligand of the EC-specific Tie2 gene and important modulator of EC activity (Dumont et al., 1994; Suri et al., 1996). This phenotype was recapitulated when angiopoietin-1 was deleted specifically in pericytes. These studies underscore that EC migration and angiogenesis, mediated by crosstalk between each cell population in the lung, must occur for full maturation of the alveolar sacs during the postnatal period when air exchange is necessary

Lung regeneration – vascular contributions

Unlike the other organs discussed in this chapter, the lung displays an incredible ability to regenerate in response to injury. Unilateral pneumonectomy of the left lung induces compensatory expansion of mass and volume of the right lung (Cowan and Crystal, 1975). Alternatively, chemical injury with bleomycin or naphthalene damages distal AT2 ($Sftpc^{+}$) or proximal non-ciliated bronchiolar cells ($CCSP^{+}$), respectively, and induces a set of resident lung stem cells called 'bronchioalveolar stem cells' (BASCs) (defined by coexpression of Sftpc and CCSP) to repair the damage (Aso et al., 1976; Kim et al., 2005; Plopper et al., 1992). In all of these models, ECs play a critical role in directing lung regeneration via expansion of epithelial stem cells. With bleomycin injury, BASCs secrete Bmp4, which activates NFATc1 signaling in ECs to produce Tsp-1 and promote epithelial repair (Lee et al., 2014). Left lung pneumonectomy leads to an alternate response: synergistic activation of VEGFR2, FGFR1, and Cxcr4-Cxcl12 pathways in pulmonary ECs lead to secretion of MMP14, which promotes the expansion of epithelial progenitors through the release of cryptic Epidermal Growth Factor ligands (Ding et al., 2011; Rafii et al., 2015). The

differences in the signaling pathways induced in these studies may be due to the differences in the models employed: whereas chemical injury induces a regenerative response to replace the damaged tissue, pneumectomy leads to hyperplasia of the remaining lung lobes and thus creates new alveolar spaces. Importantly, these multiple models of lung injury confirm that endothelial-epithelial crosstalk is indispensable for proper lung regeneration. The obvious question emerges as to whether these same pathways are also implicated during lung development or if they are injury-specific responses.

Kidney

Blood vessels mirror nephron development

The kidney is a highly patterned and organized organ that carries out a wide variety of vital functions. The primary role of the kidney is to filter the blood and concentrate the urine, thus eliminating wastes from the body and reclaiming important small molecules and water from the filtrate. As a part of these roles, the kidneys help regulate serum ion levels, osmolarity, and pH, adjusting as necessary to fit the needs of the individual at that moment. The kidneys also secrete hormones that regulate blood pressure (renin) and red blood cell production (erythropoietin). Most of these functions are carried out by structures called ‘nephrons,’ which consist of a glomerulus – the filter apparatus – at the proximal end followed by a single, highly-patterned tubule that eventually drains into the ureter. Each region of the tubule is adapted to perform specific cellular duties. For example, the proximal convoluted tubule is better suited for reclaiming ions and small molecules while the descending loop of Henle can only absorb water to concentrate the urine. Not only is the nephron epithelia patterned along its length, the kidney itself is patterned from the

cortex to the medulla whereby different nephron segments and stromal populations are located exclusively in one region or the other.

To be able to carry out all of the diverse roles of the kidney efficiently, the renal vasculature must be highly adapted and regionalized. The path of blood flow through the kidney is the first level of endothelial organization. Blood flows from the 1) renal artery branching off of the abdominal aorta to the 2) segmental arteries, 3) interlobar arteries, 4) afferent arterioles, 5) glomerular capillaries, 6) efferent arterioles, 7) peritubular capillaries in the cortex and vasa recta in the medulla that surround and perfuse the entire nephron tubule, 8) interlobar veins, and 9) the renal vein that drains into the vena cava (**Fig. 1.3**). One of the most striking features of this organization is that the renal vasculature possesses two capillary beds in series: the glomerulus followed by peritubular capillaries and vasa recta. Additionally, ECs in each of these regions carry out regionalized exchanges and must be adapted to fit their role. For example, glomerular capillaries possess fenestrae to allow for filtration of solutes in the plasma. Although the peritubular capillaries and vasa recta represent a "single" endothelial group, the high degree of nephron epithelial patterning suggests that these capillaries may also be patterned along each region of the nephron. Which cues direct the formation of individual capillaries and vasa recta, and how ECs specialize in these individual niches, are currently unknown.

Kidney epithelium and endothelium grow and expand coordinately

Kidney development begins at E10.5 when the Wolffian duct buds into the adjacent metanephric mesenchyme. This mesenchyme contains both $Six2^+$ nephron progenitor cells (NPCs) and $FoxD1^+$ stromal progenitor cells. At this stage, ECs can be identified surrounding (but not penetrating) the metanephric blastema (**Fig. 1.4A**) (Munro et al., 2017b; Robert et al., 1998). Next,

the Wolffian duct bud, called the 'ureteric bud' (or UB), evaginates into the metanephric mesenchyme in response to inductive signals emanating from the NPCs (O'Brien and McMahon, 2014). At the same time, the vasculature surrounding the early metanephric mesenchyme forms a continuous vascular plexus both around and within the developing kidney (**Fig. 1.4B**). Through reciprocal signaling between the UB and NPCs, the UB undergoes extensive growth and branching while the NPCs cluster at distal UB tips to form 'caps' and proliferate. This process is maintained until NPCs are exhausted at around P3 in mice (O'Brien and McMahon, 2014).

Recently, 3-dimensional (3D) imaging of the distal tips revealed that ECs grow coordinately with the distal UB tips and NPC caps. ECs circumscribe each NPC cap in a predictable manner as each new cap forms (Munro et al., 2017b). Notably, these ECs do not directly contact the NPCs and are most likely predominately surrounded by stromal cells. This organization suggests that the endothelium at distal UB tips is patterned, at least in part, by the stroma. Indeed, ablation of $FoxD1^{+}$ stromal cells leads to hypervascularization of the progenitor region and disruption of endothelial structure (Hum et al., 2014), suggesting the stroma acts to restrain EC proliferation. Interestingly, in both mutant and normal mice, the ECs rarely contact NPCs directly (Hum et al., 2014; Munro et al., 2017b). This cellular organization may suggest that NPCs reside in a state of hypoxia. In agreement with this model, kidney explants cultured under hypoxia show an increase in NPC numbers compared to those cultured under normoxia (Rymer et al., 2014); however, the mechanisms that regulate this are unknown at this time.

Current paradigms of the vasculature in nephrogenesis

Beginning around E12.5, some NPCs in the caps will undergo a mesenchymal to epithelial transition (MET) and begin nephrogenesis, the process by which new nephrons are formed. The

first step of nephrogenesis is formation of a pretubular aggregate followed by the renal vesicle (RV) stage when a lumen forms. The RV undergoes extensive morphogenesis to form first a comma-shaped body, then an S-shaped body, and eventually a full nephron. Nephron patterning also begins becoming evident as early as the renal vesicle stage: cells closest to the UB are fated to become the distal nephron, while those farther from the UB will become the podocytes and proximal tubule (Lindstrom et al., 2018e). At the S-shaped body stage, additional discrete regions can be identified using different markers including separation of the proximal tubular and podocyte fates as well as additional intermediate populations between each segment. As NPCs undergo nephrogenesis and new nephrons form, the vasculature integrates with the expanding nephric tree.

Early studies suggested nephrogenesis occurred without significant vascularization until the S-shaped body stage. At this stage, it was proposed that individual angioblasts migrate into the cleft of the developing S-shaped body where presumptive podocytes reside (Eremina et al., 2003; Saxen and Sariola, 1987). A more recent model states that an angiogenic sprout, and not individual angioblasts, is the source of ECs that invade the cleft where presumptive podocytes reside. This model is supported by recent high-resolution live imaging data of embryonic kidney explant cultures that identified an angiogenic sprout invading the developing S-shaped body (Saarela et al., 2017). However, several questions remain concerning the role of ECs during nephrogenesis. First, are ECs involved with nephrogenesis at stages preceding the S-shaped body stage? Previous analyses have relied on imaging thin sections of the kidney, and, therefore, are not adequate to fully assess the entire 3D organization of the developing nephron and associated cell types. Second, although it is clear that all parts of the mature nephron are highly vascularized, at what points during nephron development do each part become vascularized? Is there crosstalk between

the endothelium and epithelium during nephrogenesis or is EC organization along the nephron entirely cell autonomous? Lastly, the epithelium demonstrates clear signs of patterning on the transcriptional level as early as the RV stage that is maintained as the nephron matures (Lindstrom et al., 2018e). Is this true for the endothelium as well? If so, at what stage is this heterogeneity established? Does EC-epithelial crosstalk play a role in establishing heterogeneity in either compartment? Answering these questions will shed new light on the pathways necessary for full nephron development.

Factors regulating glomerular development

The glomerulus is a highly patterned structure responsible for ultrafiltration of the blood. Each glomerulus consists of fenestrated ECs, highly specialized epithelial cells called 'podocytes,' and stromal cells called 'mesangial cells.' During development, ECs and podocytes both lay down several extracellular matrix (ECM) proteins to generate a fused basement membrane called the 'glomerular basement membrane,' or GBM, which is the filtering apparatus of the glomerulus (**Fig. 1.5A**) (Miner, 2012). Although not directly contributing to the GBM, mesangial cells are thought to support the activity of the other glomerular cell types in maintaining proper glomerular function.

Glomerular development requires coordinated crosstalk between the endothelium and developing podocytes. A key angiogenic factor responsible for establishing and maintaining ECs within the glomerulus is VEGF-A. VEGF-A is secreted by presumptive podocytes in the S-shaped bodies. VEGF-A then binds to its cognate receptor VEGFR2 on ECs in the surrounding plexus to induce the ECs to invade the cleft of the S-shaped body (Eremina et al., 2003). Podocyte-specific deletion of VEGF-A leads to hypovascularization of the glomerulus, loss of GBM fenestrations,

and mesangial cell loss in a dose-dependent manner (Eremina et al., 2006; Eremina et al., 2003) (**Fig. 1.5B**). Similar results were seen when newborn mice were administered a neutralizing antibody against $VEGF_{165}$ (Kitamoto et al., 1997). Perhaps not unexpectedly, over-expression of VEGF-A also led to drastic alterations in glomerular function and morphology, indicating that VEGF-A expression must by tightly regulated to ensure proper glomerular development (Eremina et al., 2003; Sison et al., 2010). The VEGF-VEGFR2 axis between podocytes and glomerular ECs is not only necessary during development, but also for postnatal glomerular function. Whole-body deletion of VEGFR2 beginning 9 days after birth leads to pronounced glomerular damage highlighted by loss of glomerular ECs (Sison et al., 2010).

The ligand receptor pair PDGF and PDGFR also play an integral role in glomerular formation. In general, interaction between PDGFs and PDGFRs are known to be important during angiogenesis and vessel maturation. PDGF-B, expressed by sprouting ECs, binds to PDGFR-β on vascular smooth muscle cells to recruit the smooth muscle cells to the developing vessel (Gerhardt and Betsholtz, 2003). The kidney follows a similar paradigm whereby PDGF-B is expressed by the renal endothelium and PDGFR-β is expressed in mesangial cells, vascular smooth muscle cells around the renal arterial tree, and stromal cells in the renal cortex (Lindahl et al., 1998). Germline deletion of either PDGF-B or PDGFR-β both result in aneurysms within glomeruli and a nearly complete absence of mesangial cells (Leveen et al., 1994; Soriano, 1994) (**Fig. 1.5C**). When PDGF-B is specifically deleted from the EC compartment, these results can be recapitulated although the phenotype is more variable and mild compared to the germline knockout, possibly due to incomplete deletion with available Cre lines used for conditional deletion (Bjarnegard et al., 2004). These results suggest that EC-derived PDGF-B is the predominant factor directing

PDGF signaling and mesangial recruitment during glomerulogenesis. Notably, the GBM appeared normal in all mutants, indicating that the PDGF-PDGFR axis mediates the interaction between ECs and mesangial cells but not between ECs and podocytes.

Based on these data, one can build a model of the cell-cell signaling pathways that direct glomerular development and maturation. Initially, VEGF-VEGFR2 is necessary to induce the initial angiogenic sprout to invade the S-shaped body (**Fig. 1.6A**). Soon after this step, PDGF-B secreted by these ECs binds to PDGFR-β on presumptive mesangial cells to recruit them into the glomerulus (**Fig. 1.6B**). This interaction continues during glomerulogenesis to generate multiple capillary loops. Meanwhile, ECs and podocytes communicate to lay down the ECM proteins necessary to form the GBM. Once the glomerulus has fully matured, ECs and podocytes require persistent communication through VEGF signaling in order to properly maintain the GBM and full glomerular function.

Several other signaling pathways have been implicated in directing glomerular formation through communication between ECs, podocytes, and mesangial cells (Mohamed and Sequeira-Lopez, 2018). These pathways include Notch (Alabi et al., 2016; Farber et al., 2018; Lin et al., 2014; McCright et al., 2001), Bmps (Dunn et al., 1997; Ueda et al., 2008) Semaphorins (Bartlett et al., 2017; Reidy et al., 2009), and Angiopoietins and Tie (Jeansson et al., 2011) although direct functional analyses by specifically ablating these genes in the endothelium or mesangium have been relatively sparse (**Table 1.1**). This is due to, in part, the lack of useful genetic tools to answer these questions. Although several podocyte-specific Cre lines exist (Podocin-Cre, Nephrin-Cre) (Belteki et al., 2005; Eremina et al., 2003), such tools do not exist for either glomerular ECs or mesangial cells. Because several of the pathways implicated regulate many non-renal processes,

whole-body or even vascular-specific deletion of these genes can cause several off-target effects, limiting the analyses that can be performed on the kidney. Full understanding of molecular machinery necessary for glomerular formation and function will require development of these tools.

Renal arterial specification and development

The onset of AV specification marks an important initial step in EC differentiation throughout the embryo and each of its tissues. The first evidence of arterial specification in the kidney is relatively late, at E13.5, when vessels expressing the arterial markers Cx40 or Nrp1 can first be identified (Munro et al., 2017a; Murakami et al., 2019). In the adult, the arteries form a highly branched, hierarchical network within the kidney (Nordsletten et al., 2006). Although the onset of arterial development has been established, how these vessels form remains controversial. Some have proposed a model in which arterial ECs form through angiogenic sprouts from the aorta (Stolz and Sims-Lucas, 2015), while others suggest arteries form through vasculogenic remodeling of the existing renal vasculature prior to E13.5 (Sequeira Lopez and Gomez, 2011). Similar coordination of angiogenic and vasculogenic mechanisms have been proposed in other organs, including the lung (Parera et al., 2005; Schachtner et al., 2000). In support of the second model, one group generated EC-deficient kidney organoids that lacked $Flk1^+/CD31^+/Tie2^+$ ECs but contained $Pdgfr\alpha^+$ stromal cells, NPCs, and UB cells from Tie2Cre; tdTomato E11.5 kidneys (Murakami et al., 2019). Upon transplantation under the kidney capsule, these EC-deficient organoids were able to generate $Tomato^+/Cx40^+$ vessels, arguing that a non-$Flk1^+/CD31^+/Tie2^+$ population present in the E11.5 metanephros gave rise to ECs that were able to remodel into arterial-like vessels. It is unclear if a similar process happens during normal development.

Additional careful *in vivo* lineage-tracing experiments will need to be performed to fully determine how the renal arterial tree forms.

The known cues that regulate renal arterial development arise primarily from the stromal and perivascular cells supporting the arterial ECs. Stromal, perivascular, and mesangial cells in the kidney derive from a $FoxD1^{+}$ stromal progenitor population present at the onset of metanephric development (Guillaume et al., 2009; Hatini et al., 1996; Humphreys et al., 2010). Genetic deletion of *FoxD1* or mosaic ablation of $FoxD1^{+}$ cells both lead to drastically altered renal artery formation with arterial vessels perfusing from the outer cortex to the glomeruli instead of from the hilum (Sequeira-Lopez et al., 2015). Whereas all perivascular cells derive from $FoxD1^{+}$ cells in the controls, kidneys with mosaic ablation of $FoxD1^{+}$ cells demonstrated recruitment of perivascular cells that came from a non $FoxD1^{+}$ source indicating that there may be compensatory mechanisms to direct arterial development. The downstream mechanism of how FoxD1 regulates arterial development remains unknown, although it could be attributed at least in part to PDGF signaling. Indeed, deletion of Pbx1, a TALE transcription factor expressed in the mural cells lining the renal arterial ECs, in $FoxD1^{+}$ cells alters normal arterial branching morphogenesis through dysregulation of PDGFR-β (Hurtado et al., 2015). Additionally, the Notch pathway, known to regulate arterial development in other contexts (Deng et al., 2013; Duarte et al., 2004), has also been implicated as a potential mechanism by which the stroma regulates arteriogenesis (Lin et al., 2014). Deletion of RBP-J, a common downstream transcription factor of the Notch pathway, in $FoxD1^{+}$ stromal cells results in kidneys with fewer arterioles that possess a thinner layer of surrounding smooth muscle cells (Lin et al., 2014). Whether other molecular pathways known to regulate arterial development in other contexts, including VEGF (Lanahan et al., 2013; Lanahan

et al., 2010; Simons and Eichmann, 2015), also facilitate stromal-endothelial crosstalk during renal arterial formation remains to be elucidated.

There are several other mechanisms that can affect arterial specification and development that have yet to be explored in the kidney. In the skin, sensory nerves determine where arteries, but not veins, form through VEGF-mediated signaling pathways (Mukouyama et al., 2002). Although where and how nerves form remain to be determined in the kidney, these data suggest that neuronal and arterial development may be co-regulated in the kidney. Additionally, the number of studies identifying EC-intrinsic mechanisms that regulate renal arterial development are limited. One study identified $S1P_1$ as an intrinsic factor regulating renal arterial development. Deletion of $S1P_1$ from the vascular and hemogenic compartments using Scl-Cre resulted in disorganized and dilated renal arterials (Hu et al., 2016). Mechanical factors, namely blood flow, may also be important in kidney arterial development. Blood flow plays a critical role in EC maturation in multiple contexts including arterial-specification in the aorta (Chong et al., 2011; le Noble et al., 2004; Simons and Eichmann, 2015). Although data examining the effects of flow in organoids suggest that flow promotes arterial formation (Homan et al., 2019; Murakami et al., 2019), it is currently unclear if blood flow is an important part of normal renal arterial development *in vivo* as more direct methods to test the effect of blood flow on renal artery development need to be performed.

Patterning of the peritubular capillaries and vasa recta

For the remaining vascular compartments in the kidney - the peritubular capillaries and vasa recta - most work has examined the role of general vascular signaling pathways in regulating their formation. VEGFR2, which is expressed throughout all ECs during kidney development, is

only expressed in glomerular ECs and peritubular capillaries, but not in the vasa recta or arteries in the adult kidney (Dimke et al., 2015). Deletion of its ligand VEGF-A from tubular epithelial cells specifically abrogates peritubular capillary formation without appreciably affecting the vasa recta. On the other hand, angiopoietins and Tie signaling pathways regulate vasa recta formation. Deletion of Tie2 or both Angiopoietin-1 and Angiopoietin-2 in late gestation lead to a decrease in vascular density in the renal medulla (Kenig-Kozlovsky et al., 2018). The decrease in vascular density is due to a loss of ascending vasa recta, while the descending vasa recta appeared normal. These results point to distinct molecular pathways that regulate EC formation and maintenance in region-dependent manners. Outside of the studies described above, surprisingly little has been done to understand the molecular pathways that regulate peritubular capillary and vasa recta formation.

"THERAPEUTIC" DEVELOPMENT – USING DEVELOPMENT TO GUIDE REGENERATION

Chronic kidney disease (CKD) affects approximately 10% of the American adult population and is characterized by a decrease in glomerular filtration as a result of a loss of functional nephrons (Oxburgh et al., 2017; Stevens et al., 2013). Because adult kidneys cannot generate new nephrons, nephron replacement strategies to treat CKD must rely on non-endogenous sources. Allogeneic kidney transplantation is an effective means to treat patients with CKD; however, the demand for kidney transplants far exceeds the supply of transplantable kidney with over 100,000 Americans remaining on kidney transplant waiting lists (Tullius and Rabb, 2018). Thus, an alternative source for functional nephrons is necessary to meet this demand. Regenerative

medicine has the promise to address the gap by directly generating new kidney tissue *ex vivo*. Importantly, the replacement tissue must 1) be able to perform all normal renal functions, 2) be fully vascularized, and 3) be able to integrate with the host vasculature. This section will focus on the current status of regenerative therapies for transplantation and the challenges in developing a fully functional and vascularized *ex vivo* organ.

Using organoid to generate de novo replacement kidney tissue

Current efforts to create organs *ex vivo* have revolved around the use of organoids. Organoids are clusters of cells organized in 3-dimensional culture that contain multiple organ-specific cell types and resemble the intended tissue by morphology, gene expression, or function (Lancaster and Knoblich, 2014). Organoids demonstrate a greater potential for regenerative therapies than directed differentiation of pluripotent stem cells into a single cell type because they more closely mimic normal developmental programs as they generate multiple organ cell types in parallel. To date, organoids have been generated for several different organs, including the kidney (Bantounas et al., 2018; Freedman et al., 2015; Morizane et al., 2015; Takasato et al., 2015), intestines (Spence et al., 2011; Workman et al., 2017), lung (Chen et al., 2017; Dye et al., 2015; Lee et al., 2014), cerebrum (Eiraku et al., 2008; Jo et al., 2016; Lancaster et al., 2017; Lancaster et al., 2013), retina (Eiraku et al., 2011; Nakano et al., 2012), liver (Takebe et al., 2013), esophagus (Trisno et al., 2018; Zhang et al., 2018), and even the endothelium (Wimmer et al., 2019). Organoid development in all of these examples follows a common theme: a stem cell population, either pluripotent or tissue-specific multipotent, is differentiated into the target tissue by recapitulating normal developmental pathways *in vitro*. In kidney organoids, human pluripotent cells are

differentiated first into intermediate mesoderm, the precursor population to the kidney, then into metanephric mesenchyme and ureteric bud populations (Takasato et al., 2015).

Technical challenges of kidney organoids

Although organoids have shown great promise for future novel tissue replacement therapies, there are still several limitations of this system (**Fig. 1.7**). First, transcriptional profiling of these organoids reveal that they are more similar to the fetal version of the tissue than to the adult counterpart (Combes et al., 2017). Therefore, additional steps are needed in order to generate an adult-like organoid. Next, these organoids are several orders of magnitude smaller than the intended organ and current culture techniques are not easily scalable to sizes necessary for transplantation. Previous kidney organoids are formed at an air-liquid interface on floating membranes similar to embryonic kidney explant models (Morizane et al., 2015; Takasato et al., 2015). The size of the organoid is limited by the extent to which nutrients in the media can diffuse across the membrane. More recent methods have generated organoids in suspension in low adhesion culture plates (Czerniecki et al., 2018; Kumar et al., 2019; Przepiorski et al., 2018). Although this greatly improves the scalability of organoids one can make, they are still limited in size by the extent nutrients can normally diffuse into the structure. Overcoming the diffusion limit in order to support larger organoids will require a perfusable vascular network; however, vascularization of the organoids remains fairly limited. Although $CD31^+$ cells can be identified in many of these systems, in many cases vascularization is variable and often the handful of positive cells within an organoid that can be observed are progressively lost over time (Takasato et al., 2015; van den Berg et al., 2018). These results mirror those seen in embryonic kidney explant culture, whereby ECs present within the developing kidney are lost within several days of culture

while the epithelial structures continue to grow (Murakami et al., 2019; Robert et al., 1998). The ability of these ECs to form mature capillary structures *in vitro* is also unclear, as some groups have identified vascularized glomerular structures (Freedman et al., 2015; Takasato et al., 2015; van den Berg et al., 2018) while others do not (Bantounas et al., 2018; Morizane et al., 2015; Taguchi and Nishinakamura, 2017). Additionally, CD31 sometimes marks regions of the cell other than the plasma membrane and is present in cells that do not exhibit normal endothelial morphology or form lumenized vascular structures (O. Cleaver, unpublished data). These issues must be addressed in order for organoids to become a viable therapeutic option.

Organoid vascularization – endogenous versus exogenous origins

The issue of vascularization in organoids may be solved through transplantation of these organoids into live hosts. The results of transplantations of the kidney explant model suggest that this will be a viable approach for organoids. Kidney explants transplanted in either the eye chamber, under the kidney capsule, or on the chorioallantoic membrane of quail embryos develop increased vascularization of the graft (Dekel et al., 2003; Hu et al., 2016; Hyink et al., 1996; Murakami et al., 2019; Robert et al., 1998; Robert et al., 1996; Sariola et al., 1983). The ECs found in the transplants are usually graft-derived with the exception of the vasculature of transplants placed under the newborn kidney capsule which arises from the host (Robert et al., 1996).

Recent work on transplantation of human organoids mirrors the encouraging results seen from transplantation of kidney explants. One group transplanted human-derived podocytes and proximal tubule cells with human umbilical vein endothelial cells (HUVECs) and mesenchymal stem cells under the kidney capsule (Sharmin et al., 2016). These transplants displayed vascularized glomeruli containing host-derived ECs. Likewise, transplantation of organoids grown

from an established human kidney organoid protocol (Takasato et al., 2015) led to increased vascularization, improved epithelial maturation including vascularized glomerular structures, and perfusion of these organoids when transplanted under the kidney capsule (van den Berg et al., 2018). Time-matched non-transplanted organoid controls remained in an immature state and did not show signs of increased vascularization. Additionally, the vasculature within the organoids contained a mix of human- and mouse-derived ECs anastomosed together. These studies stand in contrast to the majority of the explant transplantations above in that the majority of the vasculature is host-derived rather than graft-derived. Notably, the explants that did manifest host-derived vasculature were transplanted under the kidney capsule where the organoids were also transplanted, suggesting that whether the transplant contains host-derived or graft-derived vasculature depends on transplant location. Both of these studies show that transplantation of immature human pluripotent stem cell-derived renal organoids promotes further development and maturation than what can be achieved through current *in vitro* systems alone.

Importance of hemodynamic flow for vascular stability

The results from these transplantation experiments indicate that developing kidney tissues, including the vasculature, require systemic factors in order to fully mature. Indeed, ECs present within organoids regress over time even though the organoids continuously produce VEGF even after nearly 2 months *in vitro* (van den Berg et al., 2018). A major difference between the transplanted and non-transplanted organoids is the presence of blood flow. Although flow is dispensable for EC activity prior to lumenogenesis, the mechanical stimuli created by flow is critical for formation and maintenance of lumens, AV specification (as mentioned previously), and EC homeostasis (Baeyens and Schwartz, 2016; Culver and Dickinson, 2010; Lucitti et al., 2007;

Potter et al., 2014; Udan et al., 2013). Furthermore, the absence of flow in other contexts leads to vessel regression as seen in the current organoid models (Chen et al., 2012; Franco et al., 2015). Importantly, a fully perfused vascular network will be critical to scale these organoids to transplantable sizes.

This raises potential concerns with respect to tissue engineering: if flow within the vasculature is needed to generate fully mature vessels that can support the growth of the organoid, how can a fully perfused vascular network within an organoid or transplantable organ *in vitro* be generated? More simply, can any perfused vascular network be engineered and sustained *in vitro*?

Several groups have tackled the latter question through the creation of micro- and millifluidic devices (Alonzo et al., 2015; Grigoryan et al., 2019; Homan et al., 2019; Kolesky et al., 2016; Lin et al., 2019; Shirure et al., 2017; Wang et al., 2016; Zheng et al., 2012). These devices contain perfusable channels that can be lined with ECs. There are two main approaches to generating these devices. One method involves the creation of pre-formed channels – utilizing 3D printing or stereolithography in hydrogels – that are then lined with ECs by seeding purified EC populations through the same port where media flows (Grigoryan et al., 2019; Kolesky et al., 2016; Lin et al., 2019; Zheng et al., 2012). ECs attach to the channel walls, proliferate, and form polarized tight junctions indicating EC maturation (**Fig. 1.8A**). However, these systems are limited due to the high number of cells needed to seed the lumens, the purity of the population needed to seed the channels, and the current limitation in creating smaller lumens (<100 μm in diameter) that is more appropriate for capillary flow.

Alternative approaches take advantage of the inherent ability of individual ECs to form a lumenized vascular network by themselves. One approach first seeds a chamber with ECs and

perivascular cells, then generates fluid flow across the chamber (Alonzo et al., 2015; Shirure et al., 2017; Wang et al., 2016). In this system, there is 2 directions of flow: across the chamber that contains the ECs and parallel to this chamber (**Fig. 1.8B**). This organization mimics endogenous blood flow in which the flow moving parallel to the chamber represents larger caliber vessels and the flow across the chamber represents capillary flow. The main challenges with this approach are the inability to precisely control where and how lumens form and the lack of larger caliber vessels.

Recently, one group has attempted to determine the effects of flow on kidney organoid development. They created a millifluidic device in which kidney organoids can be grown embedded within gelatin-fibrin matrix and flow can be generated over (but not through) the embedded organoids. Organoids grown in this device and under flow exhibit increased vascular formation, including more abundant vascular structures, open vascular lumens, and enhanced expression of several vascular genes (Homan et al., 2019). Importantly, these organoids also showed enhancement of epithelial development with enhanced glomerular formation and an increase in expression of apical polarity markers, solute and small molecule transporters, and adult transcription factors. These findings were correlated with an increase in interactions between the endothelium and epithelium suggesting that the increase in endothelial-epithelial interaction may have contributed to the augmented epithelial maturation. These data support the hypothesis that proper vascular formation with flow is necessary for full kidney maturation *in vivo* and *ex vivo* as organoids. A major caveat of this approach is that flow is generated over the organoid but not through it; therefore, this system does not fully mimic normal development as perfusion of the organoid happens all around it and not exclusively through the vasculature.

The road ahead – Tackling challenges to create transplantable vascularized organs

The challenge of creating a purely *in vitro* perfused vascular network in an organoid may rely on a combination of these approaches. Initial perfusion of the organoid can be accomplished by first seeding organoids in microfluidic devices and stimulating the ECs within the organoid to form capillary-like vessels with patent lumens. These perfused organoids can then be fused to larger, pre-formed, EC-lined channels, mimicking the larger caliber renal artery and vein. Therefore, the combination of the approaches discussed here may successfully generate a fully vascularized organoid containing different vascular compartments in the correct series as seen *in vivo*. Alternatively, organoids with perfusable vascular networks may be able to form when grown on other scaffolding methods, including porous silk scaffolds and decellularized kidneys (Subramanian et al., 2010; Uzarski et al., 2015). It remains to be seen if any of these approaches will be viable for organoid biology moving forward. Additionally, there may be other systemic factors important for organoid maturation as seen in a transplant model that are not completely recapitulated by the introduction of perfusion *in vitro*. Lastly, these devices may need to be very finely tuned to generate properly patterned and perfused nephrons. This includes laying down the proper ECM matrix, incorporating the right growth factors in the correct location on a cellular level, and ensuring that each cell meets its own metabolic requirements.

The field of organoid biology is still very young and many challenges stand in the way to transform this approach into viable therapies. The combined effort of multiple disciplines, including developmental biology, bioengineering, and bioinformatics among others, will be absolutely necessary to move this field forward.

CONCLUDING REMARKS

Organ development is intricately tied to, and dependent on, vascular development. The endothelium is not simply an inert tube but rather a highly active coordinator of organogenesis. Any attempt to recapitulate development to create transplantable organs must find ways to promote and establish organ-specific vasculature to ensure full functionality. Transcriptional analyses of different vascular beds both between organs and within the same organ have revealed stark heterogeneity between these different EC groups (Nolan et al., 2013); however, the mechanistic analyses that clearly delineate the factors that determine these differences remain to be elucidated.

Studies that have investigated endothelial-epithelial crosstalk and endothelial patterning have mostly focused on well-established pathways that regulate endothelial activity, such as VEGF among others. Although these studies utilized the same general theme of inhibiting or over-activating these pathways in an organ-specific manner, the exact EC response to these perturbations was entirely location-dependent. These data demonstrate that, while these common signaling cascades are generally important for EC behavior in many organs, there are additional unknown modifiers that transform these common signaling pathways into an organ-specific signal. Determining EC heterogeneity, then, requires defining these unknown modifiers. Ultimately, identifying the mechanisms that determine EC heterogeneity, including their local character, signaling potential and behaviors, will help propel research into organoid systems or other *in vitro* organ generation approaches, which together will advance the translation of these approaches into viable regenerative therapies.

The aim of this body of work is to more thoroughly define EC heterogeneity during organogenesis. First, I will establish an atlas of vascular development in the kidney to serve as a

foundation for future experiments. I will determine the structure of ECs from the beginning of kidney development through the rest of embryogenesis, including AV specification and organization around different epithelial structures. I will also explore EC heterogeneity through protein and mRNA analyses and generate a putative list of novel EC-specific genes in the kidney. From this analysis, I chose Cyp26b1, a cytochrome P450 enzyme that catabolizes RA, as a candidate for future studies. Surprisingly, germ-line deletion led to drastic alterations in lung, but not kidney, development. Lastly, I identify a potential explanation for this phenotype through a mechanism that may protect the kidney, but not the lung, from loss of Cyp26b1. My goal in this thesis is to characterize organ-specific endothelial patterns in embryogenesis and introduce new ways in which crosstalk between ECs and other cell types impact organ development.

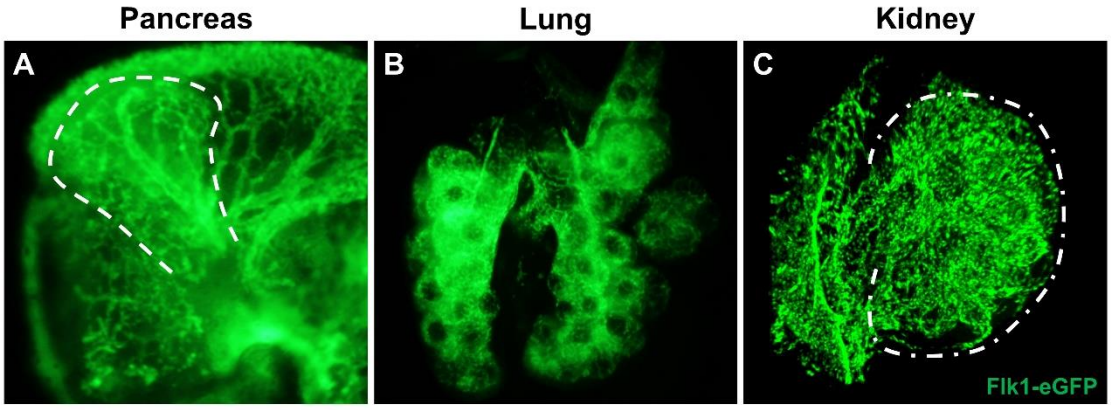

Figure 1.1. The vasculature of embryonic organs. Whole mount images of the vasculature in E12.5 Flk1-eGFP+ pancreas (**A**, outline), lung (**B**), and kidney (**C,** outline). Flk1-eGFP is expressed exclusively in the endothelium throughout development.

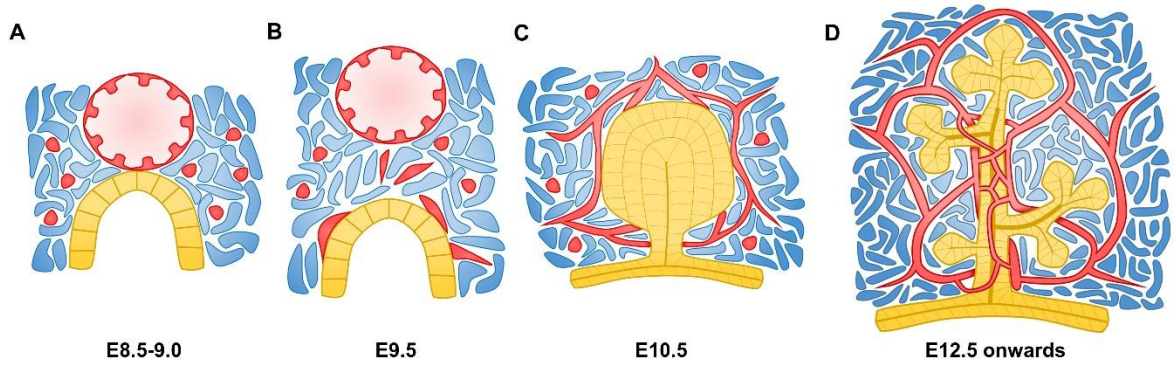

Figure 1.2. Vascular development in the pancreas. **A**) At E8.5 – E9.0 when the pancreas initially forms, the dorsal pancreas (endoderm epithelium in yellow) lies in direct contact with the dorsal aorta (red). The dorsal aorta communicates directly with the early pancreas to regulate early pancreatic morphogenesis and to maintain Pdx1 expression. Surrounding the dorsal aorta is the trunk mesenchyme (blue), which also regulates pancreatic development. Signals have identified as arising from the mesenchyme, trunk ECs and/or systemic blood circulation. A fine network of capillaries as well as isolated angioblasts can be identified in this mesenchyme. **B**) By E9.5, mesenchyme and capillaries intervene between the dorsal aorta and the dorsal pancreatic epithelium. **C**) At E10.5, the dorsal pancreatic epithelium has thickened into a stratified bud. An endothelial plexus surrounds this bud, making occasional direct contact with the epithelium, but not invading it. **D**) After the secondary transition beginning at E12.5, ECs preferentially enrich around the trunk of the pancreatic epithelial tree (thicker branches) and are more sparse around the distal tips, or acini.

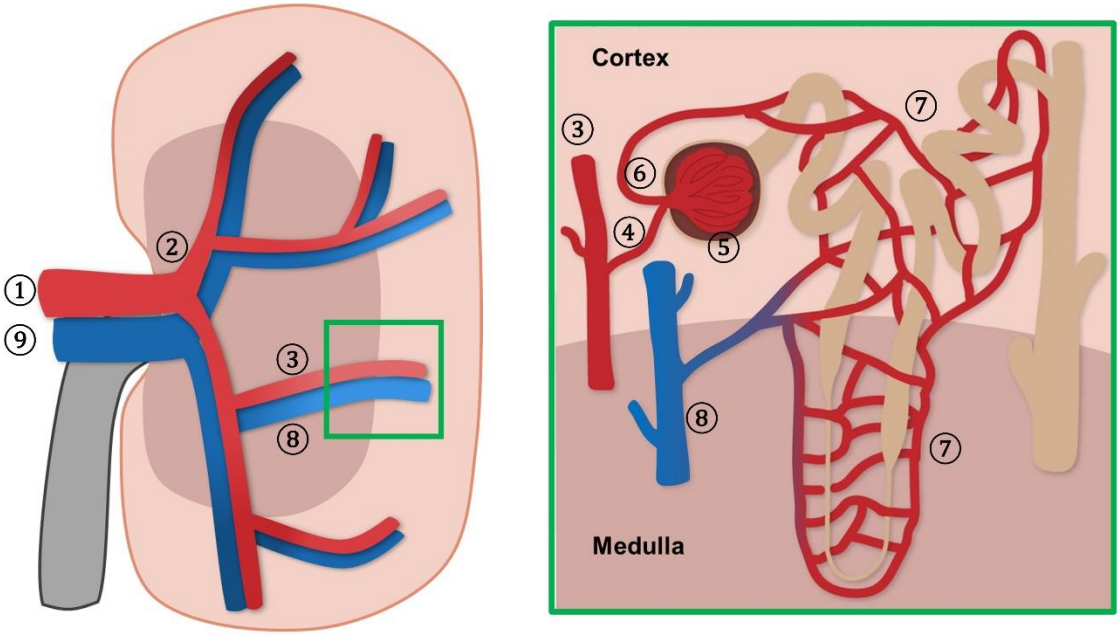

Figure 1.3. The path of blood flow through the kidney. Blood flow through the kidney progresses through a well-established path, on both the gross level and through each nephron (boxed area). Renal blood flow begins in the renal artery (1), which branches into the segmental arteries (2) and lobar arteries (3). Next, many afferent arterioles (4) branch off the lobar arteries, each feeding capillaries within a single glomerulus (5). Blood exits the glomerulus through the efferent arteriole (6) which drains into the second set of fine vessels called the 'peritubular capillaries' in the cortex (7, lighter area, top), and vasa recta in the medulla (7, darker area, bottom) that surround the nephron tubules. These capillaries then feed into lobar and segmental veins (8), which all eventually drain into the renal vein (9) and back into the systemic circulation.

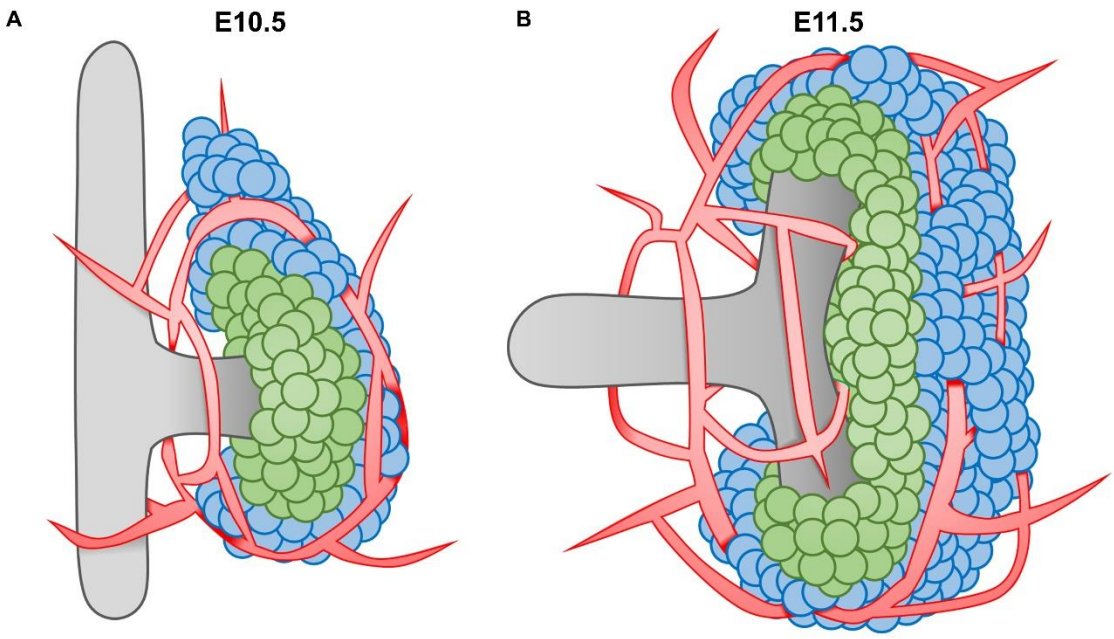

Figure 1.4. Vascularization of the early metanephros. **A**) At E10.5, the nephric duct (grey) or ureteric bud (UB) buds into the adjacent metanephric mesenchyme population, which consists of NPCs (green) and stromal progenitor cells (blue). The vasculature (red) exists as a plexus within the surrounding stroma, but does not penetrate the NPC clusters. **B**) At E11.5 after initial UB branching, the vascular plexus expands along with the developing kidney. Note that the vasculature still does not invade the NPCs.

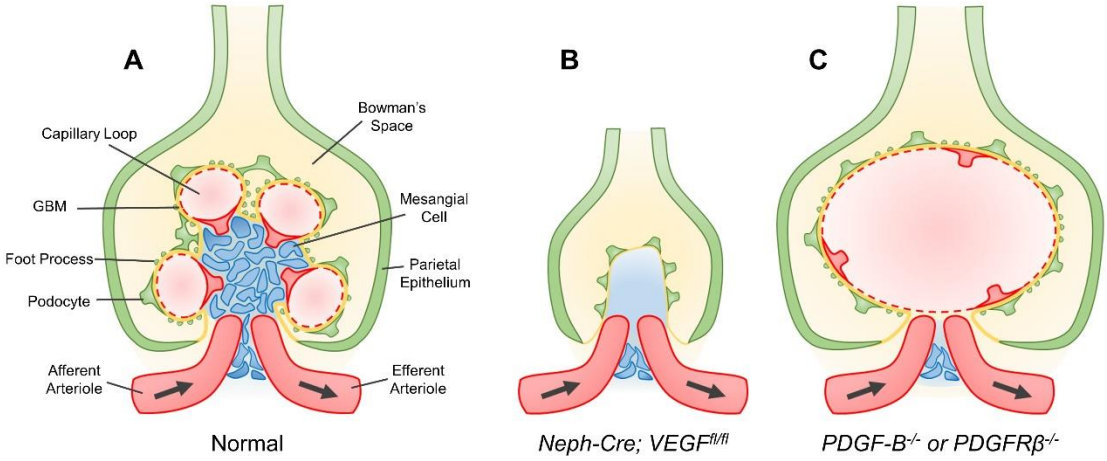

Figure 1.5. Models of mature glomeruli in specific genetic mutants. **A**) Healthy mature glomerulus. ECs (red) of the afferent arteriole (left red vessel) feed into multiple capillary loops, which drain into the efferent arteriole (right red vessel). These ECs interact with podocytes (green) to form the glomerular basement membrane or GBM (yellow). Mesangial cells (blue) are present around the ECs to support their activity. **B**) VEGF deletion from podocytes results in shrunken glomeruli with a loss of ECs and mesangial cells. Although podocytes are present, they lack foot processes and the GBM is noticeably thinner. **C**) Whole body deletion of PDGF-B or PDGFR-β results in loss of mesangial cells and large capillary aneurysms instead of multiple capillary loops. Podocytes and the GBM in these mutants appear normal.

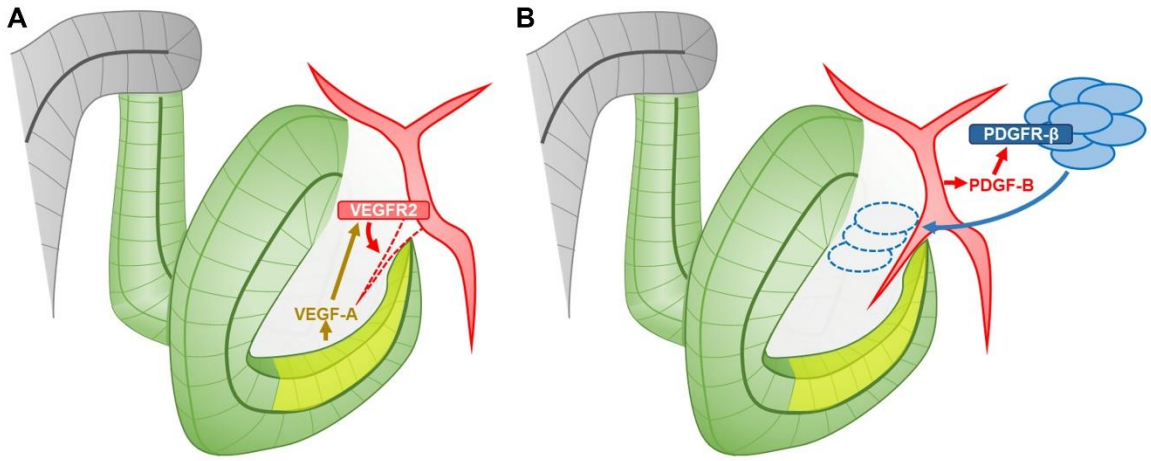

Figure 1.6. Glomerulogenesis requires coordinated communication between podocytes, ECs, and mesangial cells. **A**) During nephrogenesis, presumptive podocytes (yellow) within the S-shaped early nephron secrete VEGF-A. The VEGF-A ligand binds to VEGFR2 expressed on ECs (red), which are located in the plexus surrounding the developing nephron. This induces the ECs to undergo an angiogenic invasion of the developing nephron. **B**) As ECs invade the nephron, they secrete PDGF-B. PDGF-B binds to PDGFR-β on presumptive mesangial cells (blue) to promote chemotactic attraction of these cells and induce them to migrate into the developing glomerular cleft. Note that part of the developing nephron is hidden to allow for easier visualization of this process.

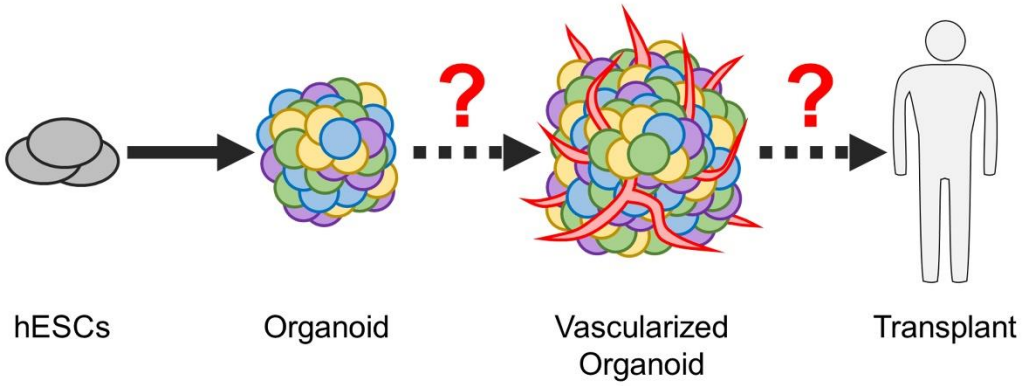

Figure 1.7. Flow chart for regenerative therapies. The goal of regenerative therapies is to recapitulate development ex vivo to create replacement tissues. To date, many groups have been able to differentiate human embryonic stem cells (grey) into tissue-specific organoids consisting of multiple different lineages. However, these organoids remain relatively small and immature due to, in part, the inability to create a perfused vascular network that is necessary to support larger scale tissues. Are there feasible ways to vascularize organoids such that it integrates properly with the developing tissue? If and when vascularization is achieved, the next major challenge will be to identify ways to successfully transplant the organoids into a recipient. Can these organoids successfully integrate into a recipient's vasculature and carry out a normal organ's function? These are the critical big picture questions that must be answered if organoids can become a viable regenerative therapy.

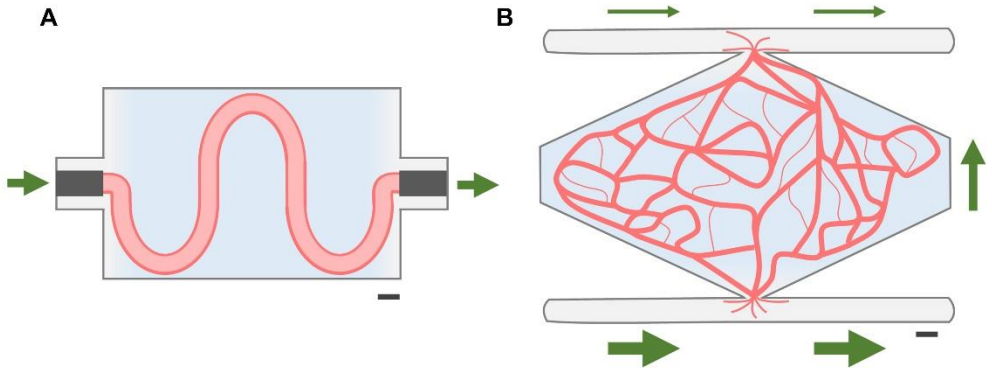

Figure 1.8. Microfluidic devices as methods to generate perfused organoids. **A**) An example of a 3D printed endothelial tube as described in Kolesky et al. (Kolesky et al., 2016). An initial cast of the tube is printed into the mold with an inlet and outlet. Next, an ECM matrix with or without cells (blue) is laid over the sacrificial cast and set. The inlet and outlets are attached to a microfluidic device to both flush out the original cast and ECs (red) are perfused through the now open channel. Flow in this system travels through the endothelial tube as marked by the green arrows. ECs will then adhere to the walls of the now empty tube and generate a patent vessel-like structure. Scale bar ≈ 100 μm. **B**) An example of an engineered capillary network after capillaries have formed as described in Wang et al (Wang et al., 2016). ECs (red) and fibroblasts (not pictured) are seeded in a fibrin gel (blue) within a mold. This mold lies adjacent and connected to two parallel channels, one with higher rate of flow (bottom, larger green arrows) and one with a lower rate of flow (top, small green arrows). Because these channels were connected to each other through the mold, additional direction of flow moves perpendicular to the channel orientation from the high-flow channel to the low-flow channel, perfusing the mold containing the ECs and fibroblasts (green arrow on right). Once seeded and subjected to this flow, ECs remodel, form cords, and open patent lumens that anastomose with the two channels allowing for flow through the newly generated endothelial lumens. Note the difference in vessel size between this system and 3D printed channels shown in A. Scale bar ≈ 100 μm.

Table 1.1. Table of pathways and genes affecting glomerular development

Gene	Cell type expressed	Mutated allele	Phenotype					Citation
			ECs	Podocytes	Mesangial Cells	GBM	Other	
VEGF-A	Podocytes	*Neph-Cre; VEGF$^{fl/fl}$*	Reduced or absent	N	A	Loss of EC fenestrations	Fatal within 18 hours	*Eremina et al., 2003; Eremina et al., 2006*
		Neph-Cre; VEGF$^{fl/+}$	Reduced or absent	Progressive loss	A	Loss of EC fenestrations		*Eremina et al., 2003*
		Neph-Cre; VEGF$^{hypo/fl}$	Progressive loss	N	Progressive loss	Loss of EC fenestrations	Fatal within 3 weeks	*Eremina et al., 2006*
		Neph-Cre; VEGF$_{164}$	Few, dilated capillary loops	N		Collapsed	Proteinurea	*Eremina et al., 2003*
PDGFR-B	Mesangium	*Pdgfr-β$^{-/-}$*	Aneurysm	N	A	Normal		*Soriano, 1994; Lindahl et al., 1998*
PDGF-B	ECs	*Pdgfb$^{-/-}$*	Aneurysm	N	A	Normal		*Leveen et al., 1994; Lindahl et al., 1998*
		Tie1-Cre; Pdgfb$^{fl/-}$	Aneurysm	N	A	Normal		*Bjarnegard et al., 2003*
Notch1	ECs	*Tie2-Cre; Notch1$^{fl/fl}$*	Hypercellular					*Alabi et al., 2016*
Notch2		*Notch2$^{hypo/hypo}$*	Absent or Aneurysm	Abnormal structure	A			*McCright et al., 2001*
RBP-J	Mesangium	*FoxD1-Cre; Rbp-J$^{fl/fl}$*	Aneurysm	N	A			*Lin et al., 2014*
Adam10	ECs	*Tie2-Cre; Adam10$^{fl/fl}$*	Enlarged, hypercellular	N	Normal	EC fenestrations contain diaphragms		*Farber et al., 2018*
Bmp4	Podocytes	*Bmp4$^{+/-}$*	Reduced or absent	N			Large glomerular cysts in Bowman's space	*Ueda et al., 2008*
	Podocytes	*Nephrin-Bmp4*	Reduced or absent	N	Reduced or absent			*Ueda et al., 2008*
Noggin	Podocytes	*Nephrin-Noggin*	Collapsed tufts, ECs in Bowman's capsule	N	Reduced or absent		Podocyte-like cells replace parietal epithelial cells	*Ueda et al., 2008*
Nrp1	Mesangium/ ECs	*Pdgfrb-Cre; Nrp1$^{fl/fl}$*	Aneurysm		A	EC detachment	Proteinurea, glomerular sclerosis	*Bartlett et al., 2017*
Sema3a	Podocytes	*Podocin-rtTA; tet-O-Sema3a* *	Progressive loss	Delayed differentiation		Loss of EC fenestrations, Immature foot processes.		*Reidy et al., 2009*
		Sema3a$^{-/-}$	Hypercellular	N		Loss of EC fenestrations. Foot processes effaced.	Proteinurea	*Reidy et al., 2009*
Angiopoietin-1	Podocytes	*ROSA26-rtTA; tetO-Cre; Angpt1$^{fl/fl}$* **	Aneurysm	N	Reduced	EC detachment		*Jeansson et al., 2011*

N = normal. A = Absent. Multiple different pathways regulate glomerular development. Genetic manipulation of these pathways can affect ECs, podocytes, mesangial cells, the GBM, or some combination of all 4. This table summarizes the phenotypes that manifest when some of the genes and pathways implicated in glomerular development are mutated. (*Tet system induced with doxycycline from E12 to birth. **Tet system induced beginning at E10.5).

CHAPTER TWO

MATERIALS AND METHODS

Mice and embryo handling

Experiments were performed in accordance with protocols approved by the UT Southwestern Medical Center IACUC. Cyp26b1 mutant alleles were generated using CRISPR/Cas9 as previously described (Yang et al., 2013). In brief, Cas9 mRNA and *in vitro* transcribed sgRNAs were injected directly into C57BL/6J oocytes. sgRNA sequences and genotyping primers used are **Table 2.1**. Successfully generated alleles were crossed into a CD1 background up to 5 backcrosses. RARE-hsp68-LacZ (Rossant et al., 1991) mice were acquired from The Jackson Laboratories. Images of whole embryos and organs were taken with an iPhone XS (Apple) and NeoLumar stereomicroscope (Zeiss) using a DP-70 camera (Olympus), respectively.

RA administration to pregnant dams was performed as previously described (Cadot et al., 2012; Okano et al., 2011). atRA (Sigma) was reconstituted in corn oil at 50 mg/mL in suspension. Pregnant dams were gavaged either 100 mg/kg atRA or equivalent dose of corn oil at E15.5, E16.5, and E17.5. Immediately prior to administration, atRA was resuspended to a consistent viscosity to ensure proper dosage. Reconstituted atRA was stored in the dark at 4°C in between dosings for the same experiment. Different experiments used freshly prepared atRA suspension prepared immediately before the first dose.

Measurements of embryo and lung weights

E18.5 embryos were dissected out of the uterus, blotted dry, and weighed. Wet and dry weights for the lungs were determined as previously described (Murata et al., 2007). Briefly, lungs were dissected out of embryos, blotted dry, and weighed on a pre-weighed piece of aluminum foil to determine the wet weight. Lungs on the aluminum foil were then dried overnight at 55°C and weighed again to determine the dry weight. Wet and dry weights were standardized to embryonic weight to determine relative wet and dry weights. Significance was determined using one-way ANOVA with Tukey multiple comparison test.

β-galactosidase reaction

E12.5-E14.5 Kidneys from ephrinB2-LacZ or EphB4-LacZ mice were fixed using 4% PFA for 20 minutes, rinsed in PBS and stained for β-gal for 3 hours to overnight as previously described (Villasenor et al., 2008). Images were taken with a NeoLumar stereomicroscope (Zeiss) using a DP-70 camera (Olympus).

Histologic and IF analysis on sections and quantifications

E12.5 – P5 embryos, lungs, or kidneys were dissected and fixed in 4% PFA/PBS overnight at 4°C. Tissues were washed in PBS the next day and were either embedded in Tissue-Tek O.C.T. Compound for cryoprotection (IF stains in Chapter 3) or dehydrated in a series of ethanol washes to 100% ethanol for paraffin embedding (IF stains in Chapter 4, all ISH and FISH, and H&E stains). Cryoprotected tissues were sectioned at 10 µm on a cryostat. Tissues for paraffin embedding were washed twice in 100% ethanol for 30 minutes, followed by 2 washes in xylene for 10 minutes each. Tissues were then moved to paraplast and washed

at least 3 times in 100% paraplast at 60°C before incubating overnight at 60°C. Tissues were then mounted and sectioned at 10 µm on a microtome.

For hematoxylin and eosin stains, paraffin-embedded sections were washed in xylene, 100% ethanol, and 95% ethanol 2 times for 3 minutes each. Slides were then kept under running water for 2 minutes followed by a 45 second incubation with hematoxylin (Gill's Method, Fisher Chemical, CS401-1D) and an additional 5 minutes under running water. Slides were submerged in acid alcohol (99 mL 70% ethanol + 1 mL 12N HCl) 4-5 times and washed under running water for 5 minutes. Slides were then submerged in 0.1% sodium bicarbonate for 1 minute and washed for 5 minutes under running water. Eosin staining was performed by incubating slides with Eosin Y (Acros Organics, 61181-5000) for 2 minutes followed by 3-4 1 minute washes under running water. Lastly, slides were dehydrated to 100% ethanol, washed in xylene, and mounted using Permount. Images were taken using a Zeiss Axiovert 200M scope and a DP-70 camera (Olympus).

For IF stains, slides were baked at 60°C for 10 minutes and allowed to cool down to room temperature (RT). Paraffin-embedded tissues only were deparaffinized in xylene 2 times for 5 minutes each and rehydrated through an ethanol series ending on brief wash in water. Slides were then washed in PBS + 0.1% Triton X-100 (Fisher Scientific) for 3 5-minute washes. When appropriate, slides were treated with heat-mediated antigen retrieval in 1 µM Tris pH 7.5, 5 µM EDTA pH 8.0 prior to blocking depending on the antibody. Primary antibody incubations were done at 4°C overnight (for antibody information, dilutions, and antigen retrieval conditions, see **Table 2.3**). Slides were then washed in PBS + 0.1% Triton X-100, incubated in secondary antibody for 1 hour at RT. To reduce autofluorescence from red

blood cells, slides were incubated in a 50 mM NH_4Cl, 10 mM $CuSO_4$, pH = 5.0 solution for 15 minutes followed by 2 5-minute PBS + 0.1% Triton X-100 washes. Slides were then incubated with DAPI for 10 minutes, washed in PBS + 0.1% Triton X-100, and mounted using Prolong Gold Mounting Medium. Images were obtained using an A1R Nikon confocal microscope.

To obtain semi-quantitative differences in antigen intensity between kidney regions from the immunofluorescent screen in **Fig. 3.10** and **Fig. 3.11**, I developed a system to score fluorescence levels. First, each antibody staining at each time point for all 5 regions is assigned a score of 3 or 0 based on the presence or absence of fluorescence. Next, 1 point is taken away if fluorescence is low (light green), 1 point is taken away if fluorescence is restricted to a subset within a region (R), and 2 points are taken away if both are present (light green and R). Therefore, every cell will have an integer score between 0 and 3. The score is based on cumulative assessment from 3 separate and blinded analyses of multiple images of each region from 3 independent experiments. Each antibody was imaged at the same settings at all 3 time points. The scores for all 3 time points per gene in each region are then added together to give a "cumulative score" of the expression pattern ranging from 0 to 9. For example, the cumulative score for Vegfr1 in the cortex is 7 (2+2+3) and Vegfr1 in the medulla is 5 (1+2+2). Next, I calculated the differences in cumulative scores between two regions per gene ("difference score"). This number represents how disparate the expression patterns for a given gene are between the two regions, with a larger number indicating a more pronounced difference in expression patterns. The difference score can range from 0 (no difference) to 9 (completely opposite patterns). For example, the difference score for Vegfr1 between the

cortex and medulla is 2 (|7-5|). Repeating this comparison for all 18 genes and taking the average and median of the difference scores in aggregate gives an estimation for variations in immunostaining patterns between any two regions. This was then repeated for every combination of two regions (10 comparisons total) to give the final figure.

Cell counting for $DAPI^+$, $proSP\text{-}C^+$, $Lamp3^+$, and $Sox9^+$ cells were performed using Bitplane Imaris v.9.0.2. Cells were counted using the spots function to generate an initial count followed by manual editing to ensure proper counts. $Lamp3^+/proSP\text{-}C^+$ cells were quantified using the "colocalize spots" function in the Imaris XT analysis package. Images used in these quantifications encompass at least 5 random views of distal epithelium from at least 3 embryos per genotype and treatment condition. Images were captured to avoid all proximal epithelial structures that may improperly skew the results. Airspace area and number were calculated using FIJI. First, a threshold was applied to images of distal airways using the DAPI stain such that the areas occupied by cells were mostly filled. Next, the number and sizes of all blank spaces greater than 100 μm^2 were calculated using the Analyze Particles function. The 100 μm^2 threshold was chosen to eliminate false positive blank spaces that are due to gaps in between adjacent $DAPI^+$ cells and not from actual open airspaces. Data and statistical analyses were plotted and performed in GraphPad Prism 8. Significance was determined using two-way ANOVA with Sidak multiple comparison test.

Whole-mount immunofluorescence

Fixed E10.5-E14.5 embryos and kidneys were washed in PBS and dehydrated to 100% methanol and then rehydrated in PBS with a 1 hour wash in 50% methanol. Tissues were then

incubated with 1% Triton X-100 in PBS for 2 hours and blocked in CAS-Block (Invitrogen) for at least 1 hour at RT. The tissues were incubated in primary antibodies overnight in CAS-Block (ThermoFisher) at 4°C. Tissues were then washed in PBS and incubated in secondary antibodies overnight at 4°C and then washed and dehydrated in methanol. Tissues were cleared by incubating them in a 1:2 mixture of benzyl alcohol/benzyl benzoate (BABB) for at least 10 minutes. Kidneys were visualized mounted in BABB using an LSM710 Meta Zeiss confocal to take optical sections every 2.5-3 µm.

Whole mount imaging processing, analysis, and statistical analysis

Confocal tiled z-stacks were rendered in 3D and analyzed using Bitplane Imaris v9.0.2 software. Generation of randomly generated spots and distribution of $Six2^+$ NPCs and random spots to the nearest blood vessel were determined as described previously (Acar et al., 2015). Briefly, $PECAM^+/Emcn^+$ vessels and $Six2^+$ NPCs were represented as surfaces and spots, respectively, using automatic functions to generate an initial structure, then manually edited to only those surfaces and spots within the kidney proper. Random spots were generated as described previously (Acar et al., 2015) and restricted to the kidney proper through manual circumscribing. Spots were generated in sufficient numbers such that the total spots remaining after editing was within ~5% of the total number of $Six2^+$ NPCs. To determine the distribution of the two spot populations to the nearest blood vessel, I first performed a distance transformation of the $PECAM^+/Emcn^+$ blood vessel surface, which generates a new channel with intensity directly proportional to distance from the surface. The distances between both spot populations and the area of max intensity of the generated channel were then calculated

and either grouped into bins of 2 µm or averaged. The data grouped into bins were converted into a proportion of the total number of spots to better assess distribution.

Significance in **Fig. 3.7D** (n=3) and **3.7E** (n=5-7) was determined using unpaired student's t test and Ordinary one-way ANOVA with Tukey's multiple comparison test, respectively. Error bars indicate standard deviation.

Digoxigenin-labeled RNA probes and *in situ* hybridizations

cDNA templates for digoxigenin-labeled probes were acquired from plasmid purchased from Dharmacon (GE) (Rsad2, Cyp26b1) or generated from E18.5 whole kidney cDNA by PCR (Gimap4). Rsad2 and Cyp26b1 plasmids were linearized using a one-cutter restriction enzyme. For PCR-based synthesis, I first isolated mRNA from E18.5 embryonic kidneys using the RNeasy Mini kit (Qiagen) and then generated cDNA using the Superscript III First-Strand Synthesis System kit (Invitrogen) following manufacturer's instructions. To generate the cDNA template containing a T7 promoter site in the anti-sense direction, PCR was performed on the cDNA using the gene-specific primers listed below. PCR program: 1) 94˚C for 5 minutes, 2) 35 cycles of 94˚C or 30 seconds, 60˚C for 45 seconds, 72˚C for 3 minutes, and 3) 72˚C for 5 minutes. The PCR product was purified by phenol:chloroform extraction. Probe synthesis for all genes was performed as described previously (Azizoglu et al., 2016). Briefly, probes were synthesized at 37˚C for 2-4 hours in digoxigenin-synthesis reaction mixture with T7 RNA polymerase (Roche) (Rsad2, Gimap4) or T3 RNA polymerase (Cyp26b1). After synthesis, DNA was eliminated by adding RQ1 DNase I (Promega) and RNA

probes were purified using Micro Bio-spin columns (Bio-RAD). 10x hybridization stock was prepared at 10 µg/mL by adding the appropriate volume of pre-hybridization buffer.

Accession numbers for clones: Rsad2 (BC057868), Cyp26b1: (BC059246). Primers for Gimap4: Forward: 5'-CTGGGATGGGAAAGAGCTTGT-3'. Reverse: 5'-TAATACGACTCACTATAGTCAAGGCAGCAGGCAGTAAT-3'.

In situ hybridizations were performed as described previously (Azizoglu et al., 2016). Briefly, fixed E15.5 or E18.5 kidneys and lungs were dehydrated to 100% ethanol and embedded in paraffin before sectioning with a microtome. Paraffin sections were de-paraffinized in xylene, then rehydrated to PBS before being treated with 15 µg/mL proteinase K for 15 minutes and fixed in 4% PFA. Slides were then washed and incubated with pre-hybridization buffer for 1 hour at RT before being hybridized with the specific probe at 1 µg/mL overnight at 65˚C. Next day, slides were washed in 0.2x SSC then transferred to MBST before blocking with 2% blocking solution (Roche) for at least 1 hour at RT. Slides were then incubated with Anti-Dig alkaline phosphatase conjugated antibody (Roche, 1:4000) overnight at 4C. Next day, slides were washed in MBST 3x and NTMT 3x before incubating with BM purple (Roche) for color reaction. After color reaction, slides were fixed with 4% PFA and mounted using Permount. Images were taken using a Zeiss Axiovert 200M scope and a DP-70 camera (Olympus).

Fluorescent *in situ* hybridizations were performed following the above *in situ* hybridization protocol up to the 0.2x SSC washes. After washes, slides were transferred to TNT and treated with 0.3% H_2O_2 for 30 minutes before washing again in TNT and blocking in 1% blocking buffer (Perkin Elmer) for at least 1 hour at RT. Slides were then incubated with

Anti-Dig peroxidase (Roche, 1:500), rat anti-PECAM, and rat anti-Endomucin overnight at 4C. Next day, slides were washed in TNT 3x before incubating with TSA Fluorescein Amplification Reagent (1:50 in Amplification Diluent, Perkin Elmer) for 15 minutes. Slides were washed in TNT following TSA incubation, incubated with Goat anti-rat Alexa Fluor 555 for 2 hours at RT, and subsequently incubated in DAPI. Slides were then washed in TNT and mounted using Prolong Gold Mounting Medium. Images were obtained using an A1R Nikon confocal microscope.

RNA Isolation and qRT-PCR

E18.5 lungs and kidneys were dissected and placed in RNAse-free Eppendorf tubes (Ambion) where they were manually dissociated using disposable plastic pestles. RNA extraction was performed using the RNeasy Mini Kit (Qiagen) following manufacturer's instructions. mRNA concentrations were quantified on a NanoDrop 2000c Spectrophotometer (Thermo Fisher). RNA was standardized to the sample with the lowest concentration and was reverse transcribed with SuperScript III (Invitrogen) kits following manufacturer's instructions using oligo-dTs. The resulting cDNA was diluted 1:6 in H_2O prior to qRT-PCR analyses.

Transcripts were quantified using Power SYBR Green PCR Master Mix (Applied Biosciences) on a QuantStudio 3 Real-Time PCR System (Applied Biosciences). Primers used for qRT-PCR are listed in **Table 2.2**. Relative levels of transcripts were determining using the ΔΔCt method by first standardizing mean Ct for a given gene to the housekeeping gene Cyclophilin in the same sample and then calculating changes between samples. Data and

statistical analyses were plotted and performed in GraphPad Prism 8. Significance was determined using two-way ANOVA with Sidak multiple comparison test.

Flow Cytometry

Primary lung cells were isolated from E16.5 – E18.5 lungs as previously described (Kim et al., 2005) using pan-CD45-FITC, CD31-APC, Sca1-APC-Cy7 (BD Pharmingen), EpCAM-PECy7 (BioLegend) with DAPI (Sigma) staining to eliminate dead cells. Briefly, whole E16.5 – E18.5 lungs were manually dissociated with a pestle in separate microcentrifuge tubes and then incubated with 2.5 mg/mL Collagenase A (Roche) and 20 ug/mL DNAse 1 (Sigma) for 45 minutes at 37°C on a nutator. Reaction was stopped by adding Wash media (PBS + 0.5% BSA + 2 mM EDTA + 1 mM $CaCl_2$) to each reaction. Cells were pelleted and incubated with ACK Lysis buffer for 10 minutes on ice to lyse red blood cells. Next, cells were washed and filtered through 40 μm cell filters before incubating with the antibodies listed above. Cells were then washed again and resuspended with wash media + DAPI for analysis. Samples were analyzed on LSR II (BD Biosciences).

Western Blot

Protein extraction and western blot analyses were performed as previously described (Azizoglu et al., 2017). Briefly, E18.5 lungs were mechanically dissociated with a pestle and homogenized in PBS with 10 μg/mL aprotinin, 10 μg/mL leupeptin, and 10 μg/mL pepstatin. Triton X-100 was added to each tube to a final concentration of 1%. Samples were frozen at -80°C overnight, thawed, and centrifuged at 10,000g for 5 minutes. Protein samples were

quantified using Pierce BSA protein assay (ThermoScientific), standardized in Laemmli's SDS-Sample Buffer (Boston Bioproducts). 40 µg of total protein from each lung lysate were run on a Western Blot. Antibodies and concentrations used are listed in **Table 2.3**.

RNA-seq of ECs from developing kidneys, lung, and pancreas

E12.5, E15.5, and E18.5 Flk1-eGFP kidneys, lungs, and pancreases were individually dissected in cold PBS, pooled, manually disaggregated with forceps, and digested in a mixture of 0.5% collagenase (Roche) and 20 U/mL RQI DNAse I (Promega) on a shaker for 40 minutes at 37°C. Digestion was stopped by adding ice cold FBS to a final concentration of 2%. Cell suspension was triturated with a progression of 18-, 23, and 25-gauge needles and filtered through a 70 µm filter yielding a single suspension. Cells were then washed twice with PBS + 0.5% BSA (Sigma Aldrich) + 5mM EDTA + 1mM $CaCl_2$ before proceeding to flow cytometry. GFP^+ cells were isolated by flow cytometry using a FACS AriaII and sorted into PBS + 0.5% BSA (Sigma Aldrich) + 5mM EDTA + 1mM $CaCl_2$. Sorted cells were lysed and the RNA was cleaned using miRVANA kit (Invitrogen) following manufacturer's instructions. RNA was isolated from cell lysates using RNAqueous Micro Total RNA Isolation kit (Invitrogen) following manufacturer's instructions. RNA sample quality and quantity was analyzed using Bioanalyzer with RNA 6000 Pico Kit (Agilent). Mouse TotalScript mRNA-seq libraries were combined into 10 nM pooled stocks, denatured and diluted to 7 pM with pre-chilled hybridization buffer and loaded into TruSeq SE v3 flowcells on an Illumina cBot followed by indexed single-end sequencing (50+7 bp) on an Illumina HiSeq 1500 using TruSeq SBS Kit v3 chemistry (Illumina). Base call files were generated by Real Time Analysis (RTA) software

(Illumina), which were then used to generate FASTQ files using bcl2fastq software (v. 1.8.4). Demultiplexed FASTQ files from RNA-seq libraries were trimmed for stretches of adapter sequences, and quality trimmed during the import to CLC Genomics Workbench 7.5 for alignment and quantification.

Differential gene expression from RNA-seq

Transcript abundance was estimated without aligning reads using Salmon (Patro et al., 2017) in R (v. 3.4.3) against an index of coding sequences from the Ensembl GRCm38 assembly. Transcript-level abundance was imported and count and offset matrices generated using the tximport R/Bioconductor package (Soneson et al., 2015). Differential expression analysis was performed using the DESeq2R/Bioconductor package (Love et al., 2014). To identify differentially expressed genes EC-specific, transcript abundance from FACS isolated ECs was compared to that from FACS isolated non-ECs from the same tissue and comparable developmental stage using publicly available datasets from the NCBI GEO database (**Table 2.4**).

Correlation patterns among genes across RNA-seq data sets were assessed using weighted correlation network analysis (WGCNA) (Langfelder and Horvath, 2008). A gene significance measure, GS_i, of the correlation between expression change across samples and the organ/cell type of the samples was calculated for each gene *i*. A p-value measuring the statistical significance of this correlation was obtained from a univariate regression model between the gene's expression across samples and the tissue/cell type of the samples. Overlap between gene sets whose expression were increased, at an FDR < 0.1, relative to non-

endothelial comparator at each developmental stage was determined. Code for analysis provided in supplemental data.

Table 2.1. Sequences of sgRNAs and genotyping primers

sgRNAs

Primer Name	**Sequence**
Cyp26b1_E3-M2	CACACGCACGGCCATTCGGA
Cyp26b1_E6-B2	TCCGGGTGGCCAGCTCGAAG

Genotyping

Primer Name	**Sequence**
Cyp26b1_KO-F	AGGCCCAGCGACTTACCACC
Cyp26b1_Exon6-F	TCGGACAGGTAAGTGGACCT
Cyp26b1_Exon6-R	TATACTGCAGCTCAACCGGC
Cyp26b1_d10-WT-F	CCAGCGACTTACCTTCCGAA
Cyp26b1_d10-KO-F	AGGAGGCCCAGCGACTTTGG
Cyp26b1_Exon3-R	TGGTCATCTCCTTGCCATGT
LacZ-F2	AACGTCGTGACTGGGAAAAC
LacZ-R2	CCGCCACATATCCTGATCTT

Table 2.2 Primers used for qRT-PCR

Primer Name	Sequence	Primer Name	Sequence
Acvrl1_RT-F	ACACCCACCATCCCTAACC	Pdpn_RT-F	GCCAGTGTTGTTCTGGGTTT
Acvrl1_RT-R	TGGGGTACCAGCACTCTCTC	Pdpn_RT-R	TCTCCTGTACCTGGGGTCAC
Ager_RT-F	GGGAAGAGGGGCAGACAG	Ptch1_RT-F	GCTCTGGAGCAGATTTCCAA
Ager_RT-R	TGATGTTCTGACCACCAGCTAC	Ptch1_RT-R	ACCCAGTTTAAATAAGAGTCTCTGAAA
Aqp5_RT-F	TAACCTGGCCGTCAATGC	Raldh1_RT-F	GCCATCACTGTGTCATCTGC
Aqp5_RT-R	GCCAGCTGGAAAGTCAAGATT	Raldh1_RT-R	CATCTTGAATCCACCGAAGG
Axin2_RT-F	CCATGACGGACAGTAGCGTA	Raldh2_RT-F	CATGGTATCCTCCGCAATG
Axin2_RT-R	GCCATTGGCCTTCACACT	Raldh2_RT-R	GCGCATTTAAGGCATTGTAAC
Bmp4_RT-F	GCCAACACTGTGAGGAGTTTC	Raldh3_RT-F	AACCTGGACAAAGCACTGAAG
Bmp4_RT-R	CACCTCATTCTCTGGGATGC	Raldh3_RT-R	AATGCATTGTAGCAGTTGATCC
Crabp2_RT-F	TTGAGGAAATGCTAAAAGCTCTG	RARa_RT-F	GTGCCATCTGCCTCATCTG
Crabp2_RT-R	TCCTGTTTGATCTCGACTGCT	RARa_RT-R	CAGCATGTCCACCTTGTCTG
Cyclophilin_RT-F	GGAGATGGCACAGGAGGAA	RARb_RT-F	AGCCCACCAGGAAACCTT
Cyclophilin_RT-R	GCCCGTAGTGCTTCAGCTT	RARb_RT-R	GTCAGCGCTGGAATTCGT
Cyp26a1_RT-F	CCGGCTTCAGGCTACAGA	RARg_RT-F	TGACAAGTCTTCTGGCTACCAC
Cyp26a1_RT-R	GGAGCTCTGTTGACGATTGTT	RARg_RT-R	TCTGAATGCTGCGTCTGAAG
Cyp26b1_E4-5-F	ACGCCCTGGACATTCTCA	Rbp1_RT-F	TAGACGACCGCAAGTGCAT
Cyp26b1_E4-5-R	AGATCAACTCCAGGGTTCCA	Rbp1_RT-R	TCTCCCTTCTGCACACACTG
Cyp26b1_RT-F	ACATCCACCGCAACAAGC	Rbp4_RT-F	AGACACGGAGGCTGGTGA
Cyp26b1_RT-R	GGGCAGGTAGCTCTCAAGTG	Rbp4_RT-R	GGCCTGCTTTGACAGTAACC
Cyp26c1_RT-F	GCGCACCTTTGAACTGGA	Ret_RT-F	CAAACTCTATGGCATGTCAGACC
Cyp26c1_RT-R	ATGCGTGTCTCGGATGCTAT	Ret_RT-R	ATCGGCTCTCGTGAGTGGTA
Dhrs3_RT-F	ATGTTCCAGGGCATGAGAGT	Sftpc_RT-F	GGTCCTGATGGAGAGTCCAC
Dhrs3_RT-R	TCCTCCGGGCTACTGTCTC	Sftpc_RT-F	GATGAGAAGGCGTTTGAGGT
Egr1_RT-F	GTCAGCAGCTTCCCGTCT	Shh_RT-F	TCCACTGTTCTGTGAAAGCAG
Egr1_RT-R	TGAAAGACCAGTTGAGGTGCT	Shh_RT-R	GGGACGTAAGTCCTTCACCA
Endoglin_RT-F	CATTGCACTTGGCCTACGA	Sox9_RT-F	GACAAGCGGAGGCCGAA
Endoglin_RT-R	GATGTTGACTCTTGGCTGTCC	Sox9_RT-R	CCAGCTTGCACGTCGGTT
Fgf10_RT-F	GATTGAGAAGAACGGCAAGG	Stra6_RT-F	TCAGGATCCTAAGATCTACAAGCA
Fgf10_RT-R	GTTGCTGTTGATGGCTTTGA	Stra6_RT-R	TCAGGAATCCAAGACCCAGA
Fgfr2_RT-F	ATCTGCCTGGTCTTGGTCAC	Tgfb1_RT-F	TGGAGCAACATGTGGAACTC
Fgfr2_RT-R	CTTCTCGGTGTTGGTCCAGT	Tgfb1_RT-R	GTCAGCAGCCGGTTACCA
Foxa1_RT-F	GAACAGCTACTACGCGGACA	Tgfb2_RT-F	AGGAGGTTTATAAAATCGACATGC
Foxa1_RT-R	CGGAGTTCATGTTGCTGACA	Tgfb2_RT-R	TAGAAAGTGGGCGGGATG
Fzd2_RT-F	CCGCTCTTCGTATACCTGTTC	Tgfb3_RT-3	TCAATATAAAGGGGGCGTACA
Fzd2_RT-R	CGGATGCGGAAGAGTGACA	Tgfb3_RT-F	CCCTGGACACCAATTACTGC
Gli1_RT-F	AGGAATTCGTGTGCCATTG	Tgfbi_RT-F	GAGCTGCTTATCCCAGATTCA
Gli1_RT-R	TCCGACAGCCTTCAAACG	Tgfbi_RT-R	GGCAGTGGAGACGTCAGATT
Gli2_RT-F	TGAAGGATTCCTGCTCGTG	Tgfbr1_RT-F	GCAGCTCCTCATCGTGTTG
Gli2_RT-R	GAAGTTTTCCAGGACAGAACCA	Tgfbr1_RT-R	AGAGGTGGCAGAAACACTGTAAT
Gli3_RT-F	CATTCCAATGAGAAACCGTATG	Tgfbr2_RT-F	CCATGGCTCTGGTACTCTGG
Gli3_RT-R	GAGCTGGGGTCTGTGTAACG	Tgfbr2_RT-R	ATGGGGGCTCGTAATCCTT

HOPX_RT-F	ACCACGCTGTGCCTCATC	Tgfbr3_RT-F	TGGCTGTGGTACTAGACATAGGAG
HOPX_RT-R	GCGCTGCTTAAACCATTTCT	Tgfbr3_RT-R	GGAGCCTGCACCACAATAG
Id1_RT-F	GCGAGATCAGTGCCTTGG	Wnt2_RT-F	CAGAGATCACAGCCTCTTTGG
Id1_RT-R	CTCCTGAAGGGCTGGAGTC	Wnt2_RT-R	GCGTAAACAAAGGCCGATT
Id2_RT-F	GACAGAACCAGGCGTCCA	Wnt4_RT-F	CTCCCTGTCTTTGGGAAGGT
Id2_RT-R	AGCTCAGAAGGGAATTCAGATG	Wnt4_RT-R	TCTCCAGTTCTCCACTGCTG
Id3_RT-F	GAGGAGCTTTTGCCACTGAC	Wnt5a_RT-F	TGAAGCAGGCCGTAGGAC
Id3_RT-R	GCTCATCCATGCCCTCAG	Wnt5a_RT-R	AGCCAGCACGTCTTGAGG
Lamp3_RT-F	GCTGTACTCTTCCTGTCCCTGA	Wnt7b_RT-F	GAACTCCGAGTAGGGAGTCG
Lamp3_RT-R	CTGTTCTGCTGATGTTGCAGT	Wnt7b_RT-R	GTCACAGCCACAATTGCTCA
Pbx1_RT-F	GCCAATATTTATGCTGCCAAA		
Pbx1_RT-F	ACATGTTAAAAGAACTGGAAGA ACC		

Table 2.3. List of antibodies

Antibody	Company	Catalog No.	Use	Conc.	AR
Aqp5	Abcam	ab78486	IF / WB	1:100 (IF) / 1:1000 (WB)	+
β-actin	Cell Signaling Technologies	3700	WB	1:2000	
β-Galactosidase	Abcam	ab9361	IF	1:100	+
CCSP	Millipore	07-623	IF	1:100	+
CD34	Abcam	ab8158	IF	1:100	
Claudin-5	Invitrogen	34-1600	IF	1:100	+
Connexin 40	Santa Cruz	sc-20466 (C-20)	IF	1:100	+
Cytokeratin	Sigma Aldrich	C2562	IF	1:100	+
Dhrs3	Proteintech	15393-1-AP	IF	1:100	+
E-Cadherin	BD Transduction	610182	IF	1:200	+
Endoglin	Rolf Brekken	N/A	IF	1:100	
Endomucin	Santa Cruz	sc-65495 (V.7C7)	IF	1:200	
GFP	Aves	GFP-1020	IF	1:200	
Icam1	Proteintech	10020-1-AP	IF	1:100	
Icam2	BD Pharmingen	553927	IF	1:100	
Foxj1	Invitrogen	14-9965-82	IF	1:100	+
Lamp3	Novus	DDX0191P-100	IF	1:100	+
LTL	Vector Laboratories	B-1325	IF	1:100	+
Lyve1	Abcam	ab14917	IF	1:100	+
Meis1/2/3	Active Motif	39795	IF	1:100	+
N-Cam	Sigma Aldrich	C9672	IF	1:100	+
NCC	Millipore	AB3553	IF	1:100	+
Nrp1	R&D Systems	AF566	IF	1:100	+
Nrp2	Cell Signaling	3366s	IF	1:100	+
Pdgfrα	R&D Systems	AF1062	IF	1:100	+
Pdgfrβ	Cell Signaling Technologies	3169	IF	1:100	+
PECAM	BE Pharmingen	55370 (MEC13.3)	IF	1:200	
Plvap	BD Biosciences	550563	IF	1:100	+
Podocalyxin1	R&D Systems	AF1556	IF	1:100	
Podoplanin	DSHB	8.1.1	IF	1:100	+

proSP-C	Millipore	AB3786	IF / WB	1:200 (IF) / 1:2000 (WB)	+
Six2	Proteintech	11562-1-AP	IF	1:200	
Slug	Cell Signaling Technologies	9585	IF	1:100	+
Sm22a	Abcam	ab14106	IF	1:100	
SMA	Sigma Aldrich	A5528	IF	1:100	+
Sox9	Millipore	AB5535	IF / WB	1:200 (IF) / 1:2000 (WB)	+
Sox17	R&D Systems	AF1924	IF	1:100	+
Tie2	R&D Systems	AF313	IF	1:100	+
VE-Cadherin	Santa Cruz	sc-6458 (C-19)	IF	1:100	+
VE-Cadherin	R&D Systems	AF1002	IF	1:200	+
Vegfr1	R&D Systems	AF471	IF	1:100	+
Vegfr3	BD Biosciences	552857	IF	1:100	+
vWF	Dako	A0082	IF	1:100	
Wt1	Santa Cruz	sc-7385	IF	1:100	+
CD45-FITC	BD Pharmingen	553080	FC	1:100	
CD31-APC	BD Pharmingen	551262	FC	1:200	
Sca1-APC-Cy7	BD Pharmingen	590654	FC	1:100	
EpCam-PE-Cy7	BioLegend	118216	FC	1:200	

AR = Antigen Retrieval. “+” indicates stain requires antigen retrieval. WB = Western blot. IF = Immunofluorescence. FC = Flow cytometry

Table 2.4. Publically available datasets used in RNA-seq analysis

Series	Run	Cell type	Developmental stage
GSE78772	SRR3195205	Nephron progenitor	E12.5
	SRR3195206	Nephron progenitor	E12.5
GSE64959	SRR1758421	Collecting duct	E15.5
	SRR1758423	Collecting duct	E15.5
	SRR1758428	Collecting duct	E15.5
GSE78772	SRR3195211	Nephron progenitor	P1
	SRR3195212	Nephron progenitor	P1

CHAPTER THREE

SPATIOTEMPORAL HETEROGENEITY AND PATTERNING OF DEVELOPING RENAL BLOOD VESSELS

INTRODUCTION

During embryogenesis, the vasculature develops coordinately with its host tissues. Vascular development has been analyzed in different organisms, with a focus on how the first blood vessels take shape (Cleaver et al., 1997; Coultas et al., 2010; Drake and Fleming, 2000; Herbert et al., 2009). Mechanisms of blood vessel development during embryogenesis include *vasculogenesis* which is *de novo* formation from isolated endothelial progenitor cells (or *angioblasts*), and *angiogenesis*, which is the formation of new blood vessels from sprouting or remodeling of existing vessels. However, recent interest has turned to trying to understand the dynamic interface between blood vessels and surrounding tissues as they grow together. During pancreas formation, for instance, ECs are initially present in the mesoderm surrounding the budding and branching endodermal epithelium (Azizoglu et al., 2016). These vascular progenitor cells coalesce and significantly remodel in the growing organ as blood flow is initiated, leading to elaboration and differentiation of vessels. What remains unknown is whether similar mechanisms exist in other organs including the kidney. This question is relevant to tissue engineering, as vascularization of replacement tissues is critical for therapeutic success. Currently, significant efforts are directed at generating *ex vivo* nephrons for those affected with chronic kidney disease and end stage renal failure (Oxburgh et al.,

2017). These efforts can be furthered by studying the process in murine mouse models, which, unlike human tissue, allow for developmental analyses using transgenic reporters and genetic modifications. A better understanding of murine kidney vasculature may also benefit therapeutic efforts in humans.

Murine kidney development begins at E10.5 when the Wolffian duct buds into the metanephric mesenchyme, which is comprised of NPCs expressing the transcription factor Six2 and stromal cells expressing the transcription factor FoxD1 (O'Brien and McMahon, 2014). Through reciprocal signaling, the Wolffian duct bud undergoes iterative branching events to form an epithelial tree, while NPCs aggregate at the UB tips to form "caps," proliferate, and undergo MET to begin nephrogenesis. NPCs that commit towards a nephron epithelial cell fate first condense to form PTAs at each distal ureteric tip. PTAs then undergo lumenogenesis to produce a RV, which then elongates to form an S-shaped body, ultimately generating a mature nephron (Gao et al., 2017; Yang et al., 2013). Nephrogenesis continues until NPCs are depleted at around P3, at which point the kidney grows through proliferative expansion of the established renal architecture (O'Brien and McMahon, 2014).

Despite the large body of knowledge documenting kidney epithelial patterning, less is known about the renal vasculature that develops in association with the epithelium. $Flk1^{+}$ (also KDR or VEGFR2) ECs have been identified within the metanephric blastema at E10.5 and the forming metanephros at E12.5 (Robert et al., 1998). Due to early technical limitations of interpreting 2D sections, previous studies considered the kidney prior to E14.5 as relatively avascular, or 'prevascular' (Tufro et al., 1999). Vascular structures appeared as isolated $Flk1^{+}$ angioblasts rather than continuous vessels. Recently, studies have advanced our understanding

of the early renal vasculature using 3D imaging (Munro et al., 2017b). In agreement with previous reports, they identify ECs around the E10.5 metanephric blastema but further show that they form a capillary plexus extending from vessels close to the nephric duct by E11.25. Therefore, ECs associate with the kidney from the onset of renal morphogenesis.

During the remainder of organogenesis, the vasculature develops in coordination with the maturing kidney by both organizing along maturing nephrons and undergoing AV specification; however, these processes remain poorly understood. Recent studies have shown that ECs circumscribe each $Six2^{+}$ NPC cap, but do not penetrate them (Munro et al., 2017b). Indeed, during nephrogenesis, ECs are thought to first interact with the developing nephron at the S-shaped body stage in which presumptive podocytes express VEGF to induce EC migration into the cleft (Gao et al., 2005; Tufro et al., 1999; Vaughan and Quaggin, 2008). Whether ECs interact with earlier stages of nephron development and whether they are patterned along developing renal structures remain unclear. Additionally, as vessels remodel, AV specification and subsequent development of arteries was shown to occur by E13.5, as vessels begin to express $Nrp1^{+}$ (Munro et al., 2017a). However, the structure and maturation of arteries, as well as the organization of veins, have not been assessed in the developing kidney. Many questions therefore remain regarding the developing architecture and fate of vascular cells within the developing kidney.

Here, I present an in-depth anatomical and molecular analysis of the developing renal endothelium. My studies provide an independent validation of recent studies from Munro and colleagues (Munro et al., 2017b), while extending their findings on several fronts. In addition, my transcriptomic data and spatiotemporal survey of vascular markers demonstrate molecular

diversification of ECs in the developing kidney. I assess the organization of ECs around the ureteric tree, progenitor caps, and developing nephrons, as well as the establishment of EC heterogeneity and changes in EC identity over time. Using whole mount 3D imaging, I show that the renal vasculature grows coordinately with the kidney from as early as E10.5, forming a plexus within and surrounding the metanephric blastema. Analysis of ECs relative to other renal cell types reveals that vessels organize in highly stereotyped patterns around the ureteric tree, $Six2^{+}$ NPCs and early nephron structures. Capillaries circumscribe NPCs, as well as differentiating RVs and emerging tubules, prior to the S-shaped body stage. Renal arterial development is first evident at E13.5, confirming previous studies (Hurtado et al., 2015; Munro et al., 2017a), and exhibits a predictable branching pattern as it grows. I find that the renal veins largely follow arteries, despite few established markers available. Using transcriptional profiling, I identify novel renal EC-enriched genes expressed in regionally-defined and organ-specific patterns. I show that the renal endothelium displays marked heterogeneity as early as E15.5 and that many EC gene expression patterns are highly dynamic over time. This study will serve as an atlas to guide our understanding of the developing renal vasculature.

RESULTS

Developing renal vasculature architecture is highly dynamic

To determine when, where, and how blood vessels arise in the kidney, I visualized embryonic vessels using a Flk1-eGFP reporter in both whole mount and sectioned tissue (Ema et al., 2006). Flk1 is known to be expressed widely throughout the embryonic vasculature, in both progenitor and mature ECs (Shalaby et al., 1995).

Kidney development begins at E10.5 when the UB evaginates from the Wolffian duct into the neighboring metanephric mesenchyme. Although ECs marked by Flk1-eGFP circumscribe the nephron progenitor population, they do not appear to invade it, in agreement with previous data (Munro et al., 2017b) (**Fig. 3.1A-A'**). In addition, capillaries largely remain approximately a few cell diameters away from the $Six2^+$ NPCs. My observations show that ECs surround but do not penetrate caps of NPCs, although they are in proximity to developing kidney structures as early as E10.5.

Kidney development proceeds through iterative rounds of UB branching while NPCs within the mesenchyme proliferate, condense, epithelialize, and differentiate into RVs. At E11.5, I observed a continuous vascular plexus around progenitor cells and the branching UB (**Fig. 3.1C-D**). I observed that the plexus surrounds the NPC caps, but does not invade them confirming previous findings (Munro et al., 2017b). Whole mount and section staining shows that as the NPCs expand and split following branching of the UB, ECs can be identified between the two epithelial populations (**Fig. 3.1D, F,** arrowheads). By E12.5, ECs connect across (peripheral to) the $Six2^+$ cell aggregates and along the outer periphery of the kidney to the interior plexus (**Fig. 3.1E-F**, arrows). As previously shown, these connections bisect the $Six2^+$ caps in a reiterative process (Munro et al., 2017b). By E13.5 through E15.5, the subcortical region (where nephron development occurs) is more highly vascularized than the outermost nephron progenitor and innermost medullary regions (**Fig. 3.1G-I'**).

Throughout late gestation, the vasculature continues to pervade the entirety of the kidney. Blood vessels orient longitudinally from the medulla out towards the cortex (**Fig 3.1J-**

J'). This organization is maintained after birth and after nephrogenesis is completed (**Fig. 3.1K-L**).

Arteries and veins of the kidney differentiate during midgestation

In the early embryo, ECs interconnect to form networks of cords prior to blood flow. Once cords open lumens and blood flow begins to exert hemodynamic force, vessels progressively remodel and differentiate into arteries and veins (Moyon et al., 2001). Studies have reported the onset of arterial specification and the presence a perfused arterial tree in the kidney as early as E13.5 (Hurtado et al., 2015; Munro et al., 2017a; Rymer et al., 2014). However, it has been unclear if arterial differentiation occurs in a stereotyped manner during kidney development.

To assess AV development in the early embryonic kidney, I first examined expression of reporter lines previously shown to be arterial-specific, ephrinB2-LacZ, or venous-specific, EphB4-LacZ. Interestingly, neither line showed significant endothelial expression in the E12.5 kidney (**Fig. 3.2A, C**). By E14.5, renal arteries exhibited ephrinB2-LacZ expression; however, LacZ expression was also present in the UB tree, preventing clear assessment of the arterial tree (**Fig. 3.2B**). Low EphB4-LacZ expression was detected in developing veins starting at E14.5, where it delineated three large branches (**Fig. 3.2D**). Thus, I found neither reporter, ephrinB2-lacZ nor EphB4-lacZ, to be a useful tool to assess AV specification due to low specificity or expression in early arteries or veins.

To better elucidate differentiation and architecture of forming arteries, I performed whole mount immunofluorescent staining with the known arterial-specific marker Cx40 to examine developing arterial vessels in 3D with confocal microscopy (Chong et al., 2011).

Cx40 whole mount stains revealed arterial connections extending from the aorta towards both the mesonephros and metanephros including an ephrinB2-LacZ^{+} vascular cord that connects the aorta and common iliac artery; however, these did not visibly penetrate the metanephros at E11.5 or E12.5, suggesting that AV fate within the kidney has not been specified at this stage (**Fig. 3.3A-B, Fig. 3.2**). The first evidence of arterial specification within the kidney was observed at E13.5, where a tree with multiple branches became distinguishable (**Fig. 3.3C**), in line with previous reports (Munro et al., 2017a; Rymer et al., 2014).

By E14.5, the renal arterial tree was further defined. I expanded on previous work by characterizing branching morphogenesis of the arterial tree at E14.5. The renal artery branched into two major arteries, each undergoing two to three additional branching events, leading to an additional three or four lobar arteries (**Fig. 3.3D**). Of note, these branches extended away from the renal hilum to the periphery of the organ, avoiding the central region of the kidney containing the papilla/medulla, but wrapping around the entire organ (**Fig. 3.3E-E'**). I found that, although these basic patterns were grossly similar, branching patterns differed slightly between age-matched individual kidneys (**Fig. 3.4**). This suggests that renal arterial patterning follows a predictable, but not stereotyped, ontogeny.

Next, I sought to determine if the arterial vessels exhibit properties of fully matured arteries. Mature arteries in the embryonic trunk express Cx40, but not Endomucin (Emcn) (Chong et al., 2011) (**Fig. 3.5**). Characterization of smaller arteries at E13.5 revealed that they express both Cx40 and Emcn, suggesting they have not fully matured (**Fig. 3.3F-H'**). At E14.5, arteries close to the renal hilum cease expression of Emcn, while those further from the hilum remain double-positive for Cx40 and Emcn (**Fig. 3.3I-K'**). Thus, arterial fate is specified in a

centripetal wave in the kidney, where differentiation progresses outward from the renal hilum towards the distal periphery of the organ.

Venous fate in the developing kidney proved to be difficult to assess, as I found no markers unique to venous cells. Nrp2, a known venous marker (Klagsbrun et al., 2002), did not exclusively label veins in the early embryonic kidney as it does in other tissues (data not shown) (Munro et al., 2017b). Although there are generally fewer useful vein markers available for the study of embryonic vessels (Chong et al., 2011), morphological differences between arteries and veins can distinguish them. Arteries display cuboidal ECs surrounded by a layer of SMCs, while veins are larger caliber vessels with thinner ECs that lack a clear outer layer of SMCs (dela Paz and D'Amore, 2009). By using pan-endothelial markers (PECAM or Flk1), I observed that renal arteries and veins often developed adjacent to one another, appearing as "artery-vein" doublets on sectioned tissue (**Fig. 3.5B-B"**). The co-alignment of arteries and veins, supported by observations of EphB4-LacZ whole mount stains and frequently observed in other tissues (Villasenor et al., 2010b), suggest that branching morphogenesis of the venous tree largely mirrors that of the arterial tree in the developing kidney.

ECs closely associate with the UB, but not NPCs

ECs are known to regulate epithelial branching and progenitor populations during pancreas and lung development (Lazarus et al., 2011; Magenheim et al., 2011; Zeng et al., 1998). Evidence of EC-tissue crosstalk suggests that an understanding of the anatomy of the organ vasculature may shed new light on developmental signaling events. I therefore asked how ECs organize around the collecting ducts, nephron progenitor cells, and developing nephrons.

I first examined endothelial organization around NPC caps located at UB tips. Throughout development (E10.5 to P3), each UB tip forms via the bifurcation and extension of existing tips, giving rise to "flattened Y"-shaped structures (Costantini and Kopan, 2010). At the tip of each UB, NPCs aggregate into distinct "caps." Munro and colleagues previously characterized EC organization around the tips (Munro et al., 2017b). In line with their data, I found ECs present at the point of each bifurcation, between two UBs, separating NPC caps (**Fig. 3.6A**). Using whole mount 3D imaging and viewing the NPC caps *en face*, I observed ECs circumscribing individual caps, but never invading the clusters of $Six2^{+}$ cells that form the caps (**Fig. 3.7A-B**). To quantitatively demonstrate that NPCs cluster away from ECs, I assessed the distribution of NPCs to their nearest blood vessel compared to randomly distributed spots. This analysis in E13.5 whole mount kidneys indicated that NPCs preferentially localize away from ECs (**Fig. 3.7C-D**). During the early stages of renal morphogenesis, this average distance from NPCs to the nearest blood vessel remains relatively stable at ~12-13 μm (**Fig. 3.7E**).

Our data and previous work establish that ECs circumscribe individual NPC caps, but some questions remain on how ECs organize with respect to the UB. I observed that bifurcating vascular cords rarely made contact with the UB tip epithelial cells (**Fig. 3.6A**). Instead, these ECs were mostly surrounded by stromal cells, which separated ECs from UB epithelium (**Fig. 3.6B**). Whole mount imaging of UB tips showed that ECs form loops not only through the bifurcation and around the epithelial stalk, but also around each tip separately (**Fig. 3.6C-E**). The same cruciform structure can be identified around each tip, indicating that the patterning of these vascular structures is predictable.

Next, I focused on endothelial organization around the UB trunk. I used a pan-cytokeratin antibody to delineate the UB and Flk1-eGFP or PECAM/Emcn to mark the ECs. I found that until E13.5, vessels surrounded the main trunk of each UB, but did not contact the epithelium (**Fig. 3.6F-I**). ECs surrounding the UBs remained at least 1-2 cell diameters away from UB stalks. At E14.5, this intervening distance disappeared, as the endothelium became intimately associated with the UB trunk and its early branches, coating most of the UB epithelium (**Fig. 3.6J-K**). This relationship was maintained throughout the rest of embryonic kidney development except at the renal pelvis, where ECs closely associate with epithelial cells in the renal papilla, but not those that comprise the ureter (**Fig. 3.6L-O**).

ECs form a plexus around the RV and S-shaped body

Nephron development begins when a subset of NPCs undergoes mesenchymal-to-epithelial transition and condenses into a PTA. This PTA undergoes tubulogenesis to form an RV, which then progresses to an S-shaped body as the nephron matures (Yang et al., 2013). ECs have long been believed to associate with the developing nephron at the S-shaped body stage (Eremina et al., 2003; Gao et al., 2005). This cleft contains podocyte progenitors expressing VEGF which attracts ECs (Eremina et al., 2003; Kitamoto et al., 1997; Tufro et al., 1999). However, relatively little is known about how blood vessels arise in and around the S-shape body and how they take shape during different stages of nephron development.

To assess the fine capillary structures around developing nephrons at different stages, our collaborator Denise Marciano, M.D., Ph.D. performed 3D imaging of thick sections (20 μm). This analysis revealed that a net-like endothelial plexus forms around the developing nephron as early as the RV stage (**Fig. 3.8A-A'**). Notably, ECs surround the RV except in the

region of direct cell-cell contact between the UB and RV epithelium, the point where these structures fuse (arrow, **Fig 3.8A-A'**). At the S-shaped body stage, we observed ECs within the cleft, as previously shown (Eremina et al., 2003). However, 3D imaging revealed that these ECs connect around the S-shaped body to form a plexus surrounding the developing nephron (**Fig. 3.8B-B''', Fig. 3.9**).

Using whole mount analysis, I was able to further characterize the changing anatomy of the renal vasculature at multiple stages of nephrogenesis. At the RV stage, when aggregated NPCs transform into an epithelial ball, ECs surround the RV on all sides, including between the lateral aspect of the vesicle and the UB (**Fig. 3.8C,** arrow, **Fig. 3.9a**). As the RV elongates and fuses to the UB epithelium, an EC collar forms around the most distal part of the RV (**Fig 3.8D-D',** white arrowheads), while a vascular 'basket' remains surrounding the rest of the developing nephron that only occasionally made direct contact with the epithelium (**Fig. 3.8D-D',** orange arrowheads**, Fig. 3.9B**). By the S-shaped body stage, the EC collar has elaborated into a plexus which envelopes the part of the S-shaped body destined to become the distal tubules (white outlines), while only sparsely covering the part that will form the glomerulus and proximal tubules (**Fig. 3.8E-E'', Fig. 3.9C**). Notably, this plexus is continuous with the surrounding endothelium, rather than consisting of a single invading sprout.

ECs of the developing kidney are heterogeneous

Recently, Lindstrom and colleagues utilized an immunofluorescent screen to demonstrate and map the heterogeneity of the epithelial cells in the RV and S-shaped body (Lindstrom et al., 2018d). Given that ECs display a high degree of heterogeneity between

different tissues and even within individual organs, I screened a variety of standard vascular markers in the developing kidney to assess potential regional differences as vessels take shape. I carried out a detailed qualitative characterization of expression patterns in E15.5, P1, and P5 kidneys, using Flk1-eGFP to confirm cells as endothelial. Marker fluorescence was scored for presence, intensity, and breadth of expression in capillaries of the renal cortex, medulla, and glomerulus, and ECs of the major vessels. Major vessels are defined as arteries and veins that appear as 'doublets', as shown above (**Fig. 3.5**). Importantly, this analysis should only be used to compare staining intensities for the same protein in different regions at different time points, but should not be used to directly compare staining intensities between different protein. For the purposes of this analysis, only expression in ECs was scored, although a few factors (E.g. Vegfr1, Claudin-5, Nrp1, Podxl1) also exhibited non-endothelial expression (Yang et al., 2016).

Strikingly, the endothelial markers tested displayed highly dynamic expression patterns during murine kidney development (**Fig. 3.10A**). Only 1 gene – PECAM– was strongly expressed in all renal ECs, at all time points. An additional 3 genes – Vegfr2, VE-Cad and Icam2 – were expressed in all ECs at all time points, but displayed differences in expression intensity in specific regions as the kidney matures. Therefore, only these 4 genes are pan-endothelial up through P5 of kidney development.

The remaining 14 factors displayed restricted endothelial expression patterns. Changes in expression over time were gene-dependent. The expression pattern of some genes became regionalized over time (e.g., Vegfr3, **Fig. 3.10B-I'**), while that of other genes broadened as the kidney matured (e.g., vWF, **Fig. 3.10J-Q'**). Other genes demonstrated region-specific

differences, whereby expression expanded in one region but became more restricted in another over time (e.g.Cx40, Claudin-5).

To better assess differences in overall expression patterns between two given regions, I developed a qualitative scoring system to compare the overall expression profile of a specific gene, comparing levels in one region to a different region (refer to Methods). These comparisons were arbitrary, but all assessments were carried out using identical experimental and imaging settings (as per (Lindstrom et al., 2018c)). Briefly, two regions that greatly differ in expression patterns will have a higher score (maximum of 9), while two regions with very similar expression patterns will have a lower score (minimum of 0). From this analysis, the two most similar regions are cortex and veins, while the two most divergent regions are arteries and veins (**Fig. 3.10R-S, Fig. 3.11**). The comparisons can be organized into two groups based on the difference score: 1. arterial and glomerular ECs (score ≥ 2), and 2. cortical, medullary, and venous ECs (score < 2). Thus, arterial and glomerular ECs have the most distinct molecular signatures within the kidney endothelium.

Transcriptome analysis of embryonic kidney ECs identifies regional molecular differences

In order to better characterize the expression profile of renal vasculature and to identify potential kidney-specific EC genes, we carried out transcriptional analysis on ECs isolated from the embryonic kidney and other embryonic organs. Utilizing the Flk1-eGFP transgenic line, a previous graduate student, Berfin Azizoglu, Ph.D., first isolated $eGFP^+$ ECs at three embryonic time points, E12.5, E15.5, and E18.5, from three different developing organs – kidney, lung, and pancreas – by FACS and performed RNA-seq on the isolated ECs (**Fig. 3.12A**)**.** Bioinformatic analysis, performed by our collaborator Christopher Chaney, M.D., was

used to compare these samples to each other and to publicly available datasets of non-EC types in the kidney (Gene Expression Omnibus). This analysis identified genes enriched in ECs that are specific to one organ or time point (**Fig. 3.12B-C, Fig. 3.13**). PCA verified the clustering of endothelial transcriptomes together, and that they were linearly separable from the comparator cell types along the first principal component (**Fig. 3.12**). To further enrich this set of genes for those most likely to be expressed in the kidney endothelium, WGCNA was performed on the genes with increased expression in the kidney endothelium at all 3 time points. This analysis yielded 417 genes likely to be significantly expressed in the renal endothelium (**Fig. 3.12, Table 3.1**). Of these, 35 genes demonstrated a significant monotonic increase in expression from E12.5 to E18.5 while only 2 genes showed a significant monotonic decrease in expression within the kidney (**Fig. 3.13**).

I found that 28 of the 417 genes were established EC markers, demonstrating that our analysis properly identified endothelial-specific genes (**Fig. 3.12D**). I first validated expression of the remaining genes using the publicly available www.genepaint.org and Genitourinary Development Molecular Anatomy Project (GUDMAP) databases, which contain *in situ* hybridizations of E14.5 embryos. I found that 180 genes did not have reported Genepaint data, leaving 209 potential novel EC genes (**Fig. 3.12D**). Each of these genes was assessed for both expression in the kidney in general and expression in kidney ECs. PECAM *in situ* hybridization data from www.genepaint.org was used as a positive control to confirm endothelial expression (**Fig. 3.12E**).

This analysis revealed that 66% (137/209) of the genes showed clear expression in the kidney with 76% (104/137) of those being expressed in renal ECs (**Fig. 3.12D**). The vast

majority of these genes were endothelial-specific (97/104), while the rest exhibited both stromal and endothelial patterns. Through this analysis, I also identified 12 genes that exhibited restricted expression patterns within the kidney. These patterns include arterial (Tm4sf1, **Fig. 3.12F**), outer cortical (Gpihbp1, **Fig. 3.12G**), and corticomedullary (Slfn5, **Fig. 3.12H**). I performed additional *in situ* hybridizations on E15.5 - E18.5 kidneys to verify that the genes identified are expressed in the renal endothelium (**Fig. 3.12I-J, Fig. 3.14A-B**) and validate genes not available on Genepaint (**Fig. 3.14C-D**). Of the genes I screened, Rsad2 appeared to be the most restricted to the kidney endothelium in the embryo with moderate punctate expression in the liver (**Fig. 3.14A**). FISH analysis revealed that Rsad2 is expressed in a subset of ECs in the E15.5 kidney (**Fig. 3.12J-J''**). Together these data provide a toolkit of new vascular markers, both region- and organ-specific, that will be useful to those studying the kidney and its blood vessels. In addition, it maps out emergence of EC heterogeneity in the kidney, demonstrating transcriptional and possibly functional regionalization of the vasculature occurs early in development.

DISCUSSION

Recent interest has focused on development of blood vessels in developing organs, especially to identify ways to apply these results to generating *ex vivo* transplantable organs for tissue replacement (Azizoglu et al., 2016; Lazarus et al., 2011). Although there are important differences between murine and human kidney development (Lindstrom et al., 2018b; Lindstrom et al., 2018c; Lindstrom et al., 2018d), the studies performed in the mouse can instruct the approaches carried out in human samples (O'Brien et al., 2016); therefore, annotation of mouse kidney development, understanding EC heterogeneity, and recognition of

regionalized gene expression, will aid efforts to engineer *ex vivo* kidneys. To date, ontogeny of the renal vasculature has remained poorly understood. In part, this has been due to a lack of useful markers for the kidney vasculature. Here, I analyze renal blood vessel anatomy from the onset of kidney morphogenesis and create a comprehensive atlas of the developing vasculature. Using whole mount imaging, I visualize the kidney in 3D to identify novel paradigms underlying formation of renal blood vessels. Specifically, I identify several patterns of capillary organization around epithelial sub-structures during metanephric development, including the progenitor pools, the developing nephron, and the collecting ducts, expanding upon previous studies (Munro et al., 2017b). In addition, using transcriptional and immunofluorescent profiling, I identify both known and novel vascular markers and map their regionalized expression within the kidney to better illustrate renal EC heterogeneity.

Emergence of the kidney vasculature

My detailed spatiotemporal analysis of the renal vasculature shows that the vasculature grows coordinately with each newly forming nephron. Fine renal capillaries form a meshwork that expands and remodels throughout metanephric development. My findings are in line with recent studies (Munro et al., 2017b), but extend our understanding of plexus remodeling in and around the early nephron. Fine capillaries emerge earlier than previously thought, and do not envelop all renal structures indiscriminately or uniformly. Vascular cords first surround the metanephros at E10.5, then expand around UBs and caps of NPCs from E11.5. I found no evidence for isolated angioblasts within or around the E11.5 metanephros in whole mount stained tissues. Instead, I observe in 3D elaboration of a capillary plexus around kidney progenitors. I note, however, that my results do not rule out the possibility of a more immature

angioblast population that is Flk1, PECAM/CD31, and Emcn negative and can give rise to mature ECs. In fact, re-aggregated E11.5 kidney organoids completely lacking $Flk1^{+}/CD31^{+}/Tie2^{+}$ ECs were able to generate bona fide ECs upon transplantation, suggesting that a non-EC population can differentiate into ECs (Murakami et al., 2019). However, it is unclear if this process is the predominant way that kidney ECs form in normal development.

Renal AV differentiation

In the present study, I also characterize AV differentiation during kidney development. I validate previous findings that the renal artery differentiation is first evident at E13.5, using an alternate arterial-specific marker (Munro et al., 2017a). At this time point, an arterial tree with at least three branching events can be distinguished. This organization is known to rely on cues from the surrounding stromal cells, as deletion of FoxD1-expressing stroma (Hum et al., 2014), FoxD1 (Sequeira-Lopez et al., 2015), or Pbx1 (Hurtado et al., 2015) all drastically impair arterial organization. Because these arteries are perfused by E13.5 (Hurtado et al., 2015; Rymer et al., 2014), I suggest that renal arterial maturation is – at least in part – dependent on blood flow, similar to many other vascular beds.

AV differentiation has been previously described in other systems. In the trunk of the early embryo and the pancreas, formation of arteries precedes that of veins, and developing vessels express for a time overlap of AV markers (Azizoglu et al., 2016; Chong et al., 2011). Venous development in the kidney occurs alongside arterial development. Although faint, EphB4-LacZ staining suggests that the venous tree mirrors the pattern of the arterial tree. This agrees with previous work in adult rat kidney that identified artery and vein co-alignment (Nordsletten et al., 2006). My work demonstrates that this paradigm is established early during

renal development. I further show that larger veins and arteries can be readily identified in cross sections of tissue as tubular "doublets", providing an anatomical tool to demarcate renal veins given the lack of proper venous markers.

Endothelial coordination with UB and RV formation

In agreement with work done by Munro and colleagues, I observed ECs reiteratively bisect distal UB tips to circumscribe individual NPC caps (Munro et al., 2017b). I expanded on this work by characterizing endothelial organization in and around all parts of the developing renal epithelium and identifying several new paradigms of renal blood vessel formation. First, ECs form a highly stereotyped cruciform pattern around the distal UB tip. Notably, a layer of cells immediately surrounding the bisecting ECs are not UB cells nor NPCs, but rather stromal cells. It is unclear if the stroma directly communicates with ECs, UB, or NPCs to regulate endothelial organization, or if there are signals from the endothelium that pattern the UB, NPCs, or stroma. A number of studies have suggested kidney-EC crosstalk (Abrahamson, 2009; Tufro, 2000), but the focus has primarily been on epithelial VEGFA (Eremina et al., 2003). Additionally, the endothelium closely associates with the UB trunk beginning at E14.5, but not earlier, suggesting that the UB trunk and tips pattern the endothelium differently.

I and others note that ECs circumscribe progenitor caps but avoid invading them. This organization raises the question of whether peripheral cap NPCs, which are located more closely to the endothelium, behave differently than those farther away. Hypoxia has been shown to be an important modulator of embryonic (Mazumdar et al., 2010), neural (Culver et al., 2013), hematopoietic (Takubo et al., 2010), and cardiac (Kimura et al., 2015) stem cells.

Some studies suggest vessels closest to NPCs are not perfused and hypoxia inhibits NPC differentiation in *ex vivo* kidney explants, suggesting that hypoxia may modulate NPCs (Rymer et al., 2014). Munro et al. did however identify red blood cells (RBCs) in these vessels. It remains an open question whether presence of RBCs definitively means that peripheral capillaries are perfused, as blood has been observed to arise in situ (Saxén, 1987). Given that there may be non-nutritional signals from ECs to peripheral cap NPCs, as observed in other tissues (Magenheim et al., 2011) or that oxygen levels may impact progenitors, future studies will be required to determine any functional relationship between the vasculature and NPCs.

Previous models of endothelial activity during nephrogenesis have posited that ECs first interact with the developing nephron during the S-shaped body stage, where they migrate into the cleft of the developing glomerulus (Eremina et al., 2003; Vaughan and Quaggin, 2008). These conclusions were based on 2D sections that can only image part of the nephron. However, imaging the entire nephron in 3D reveals new and unexpected microanatomy of endothelial and epithelial tissues. I find that a capillary plexus intimately surrounds the RV, prior to S-shaped body stage, and develops with the maturing nephron. Later, following formation of the S-shaped body, capillaries surround most of the developing nephron while maintaining connections to the surrounding plexus. These observations define clear patterns of capillary organization with developing nephrons. Due to the limitations of imaging fixed tissue, questions remain about how exactly ECs and developing nephrons dynamically remodel with respect to each other as they mature through these stages.

The close association between the RV and the endothelial plexus may point to active communication between these cell types. Indeed, ECs demonstrate clear differences in

patterning along the developing nephron, showing greater density around the region fated to become distal tubule. Proximodistal polarity in the developing nephron is established early in nephrogenesis during the RV stage when I observe the first signs of endothelial patterning (Costantini and Kopan, 2010; Lindstrom et al., 2018d). Whether endothelial patterning around the new nephron is regulated by the same mechanisms that establish nephron polarity remains to be determined. These findings also bring up the question of whether early fate commitment in the RV is regulated by ECs. Further studies are needed to uncover such potential functions of ECs in nephron development.

Transcriptional heterogeneity in ECs precedes functional heterogeneity

Solute movement and serum chemistries are carried out by the vasculature and regionalized along the nephron, implying that the associated endothelium is also specialized to specific renal compartments (Molema and Aird, 2012). However, the mechanisms that establish such differences between ECs remain largely unknown. Previous work looking at endothelial heterogeneity have focused on the organism as a whole, either characterizing differences between arterial or venous ECs (Aird, 2007a) or ECs across adult organs (Aird, 2012; Nolan et al., 2013), but not across embryonic organs. One study aimed to characterize endothelial heterogeneity in different regions of the adult kidney by identifying genes expressed in specific regions using microarray analysis (Brunskill and Potter, 2010). Although this study also screened E15.5 kidneys, the authors did not focus on distinct regions within the embryonic kidney.

The transcriptional and immunofluorescent screens reveal that heterogeneity evident in adulthood is established early during development, providing an initial foundation for EC

specification at early stages of metanephric development. Indeed, only a handful of known EC markers exhibited pan-endothelial expression throughout kidney development. Most were expressed in a regionally defined manner. Based on these data, it may be more appropriate to define each population of ECs by a panel of markers, rather than commonly used ones like PECAM or Flk1. My data further show that the endothelial transcriptome is spatiotemporally dynamic, as most genes display highly distinct expression patterns across the embryonic and postnatal stages tested. Thus, the immunofluorescent screen provides a powerful toolbox of markers that can be used to assess endothelial identity in the developing kidney in the absence of region-specific markers. However, the conclusions that can be drawn from the immunofluorescent screen are inherently limited because 1. it is a qualitative assessment of gene expression by immunofluorescence, 2. I cannot strictly compare intensities between markers, but only for the same gene across regions and time points, and 3. the absence of antigen expression does not rule out gene expression at a level below the threshold detected by immunofluorescence. However, these data will be useful for those investigating kidney vasculature as relative measures of marker levels.

Based on our RNA-seq analysis followed by Genepaint and GUDMAP screen, only a handful of validated genes exhibited some degree of regionality within the kidney. One potential explanation for this is that the resolution provided by Genepaint is not high enough to identify specific regional patterns unless the staining pattern is strong and specific. Additionally, vessels in E14.5 kidneys may not be as clearly differentiated and heterogeneous as their more mature counterparts. Consistent with this, ISH for Rsad2 at E15.5 appeared to be more broadly expressed in the kidney endothelium compared to that in the E18.5 kidney.

Lastly, our analysis identified genes that were highly expressed at all 3 time points during development. Overall, this screen can provide a valuable tool for identification of novel functional genes that regulate kidney vascular development or genes important for endothelial-epithelial crosstalk to the nearby nephron or the UB as they develop.

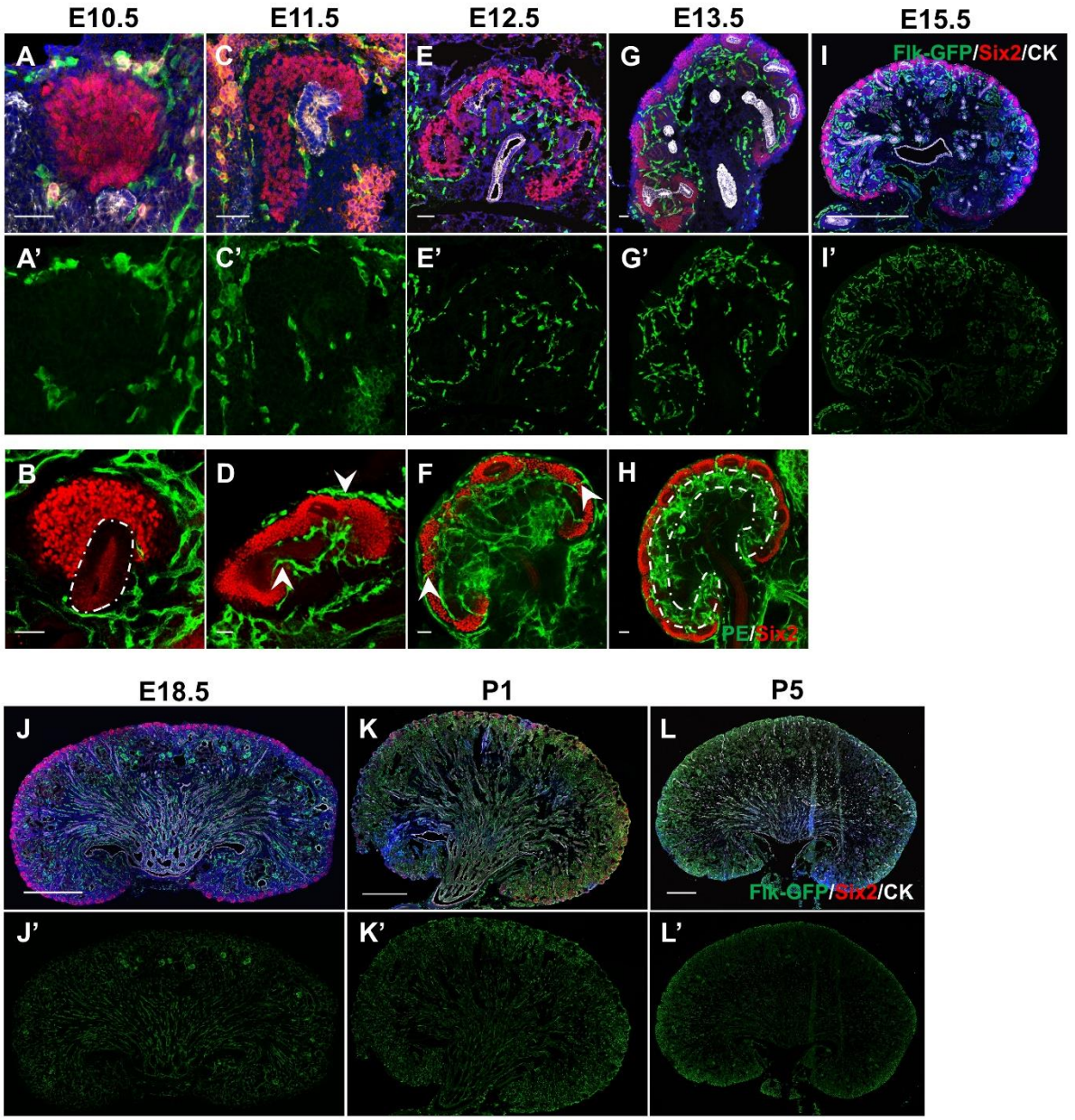

Figure 3.1. Basic anatomy of the vasculature during development of the kidney. **A-H)** Sections (**A**, **C**, **E**, **G**, **I-L**) or whole mount stains (**B**, **D**, **F**, **H**) of kidneys from E10.5-P5 stained with Flk1-eGFP, Six2, and CK to delineate the ECs, NPCs, and UB, respectively. White outline in **B** marks budding nephric duct (white outline). Arrowheads in **D** mark ECs surrounding UB or Six2 region, but not penetrating Six2 cells. Arrowheads in **F** highlight two examples of ECs that cross from outside to inside the kidney. Outline region in **H** marks area of enriched ECs deep to the NPCs. Scale bar = 50 μm (**A-G**) or 500 μm (**I-L**).

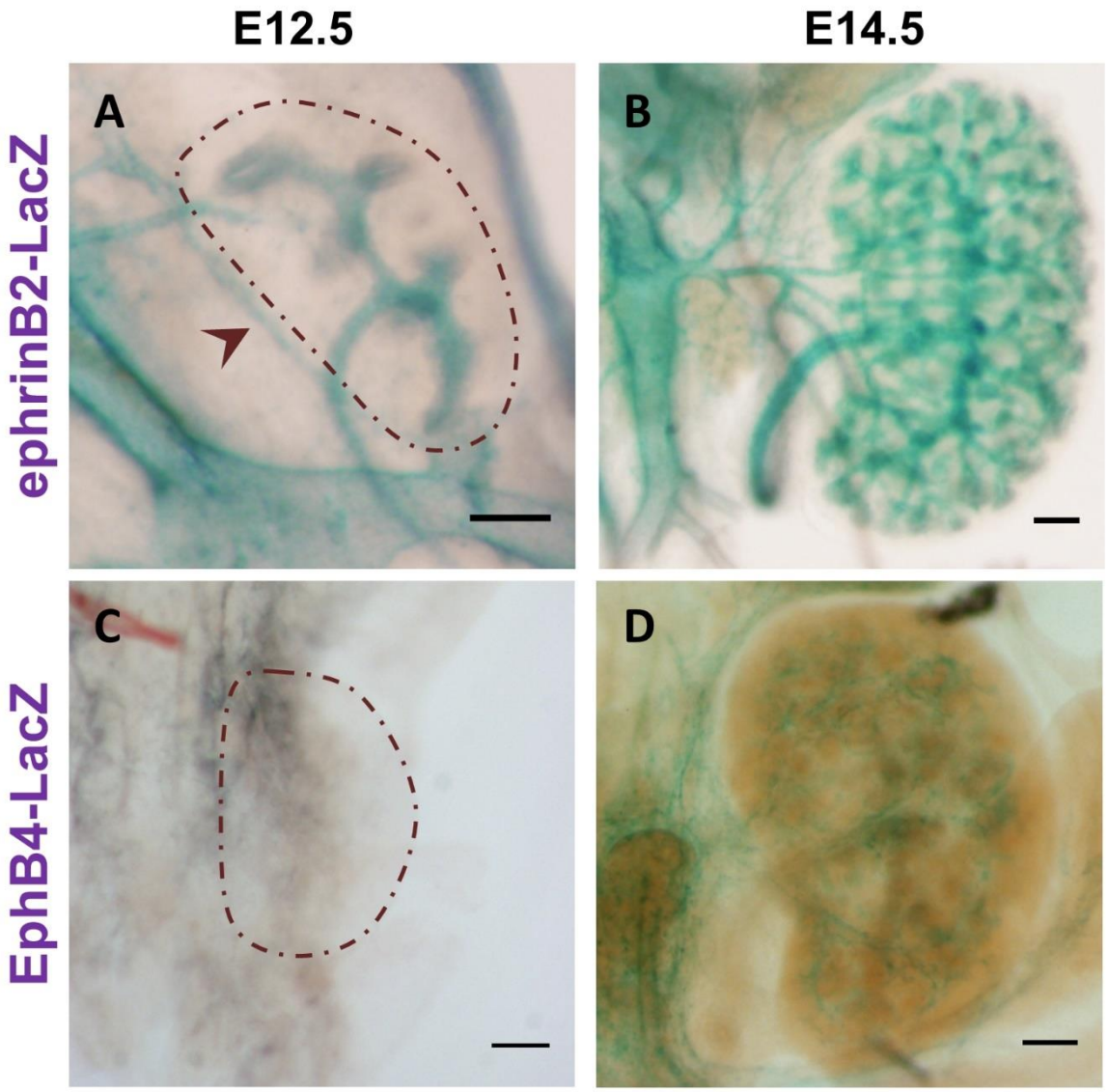

Figure 3.2. ephrinB2-LacZ and EphB4-lacZ stains reveal developing AV structures. A-B) ephrinB2-LacZ X-gal stain marks both arterial and ureteric bud tree at E12.5 (**A**) and E14.5 (**B**). Arrow marks vascular cord that connects aorta and common iliac artery (**C-D**) EphB4-LacZ X-gal stain demonstrates developing venous tree absent at E12.5 but present at E14.5. E12.5 kidneys marked with dotted line. Scale bar = 1 mm.

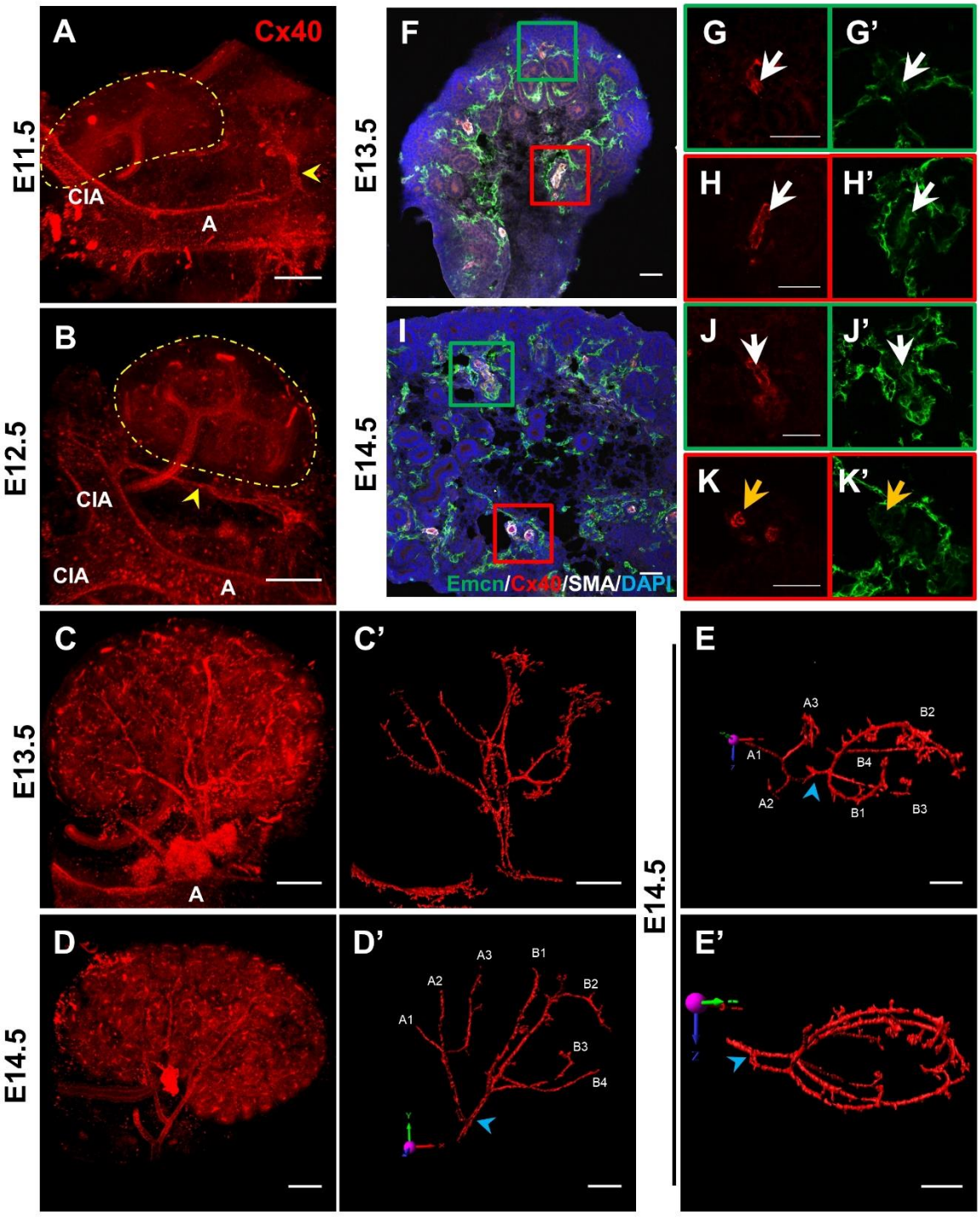

Figure 3.3. AV differentiation is first established at E13.5 and progresses towards the kidney periphery. **A-D**) Whole mount imaging of E11.5-E14.5 kidneys stained with Cx40 to mark the developing arterial tree. **A**) Yellow arrowheads mark $Cx40^{+}$ vessels extending from

the aorta to the mesonephros but not penetrating the metanephros (marked by yellow dotted line). **B**) Yellow arrowhead marks vascular cord extending from aorta to common iliac artery running alongside the E12.5 metanephros (marked by yellow dotted line). A = aorta, CIA = common iliac artery. **C'**, **D'**, **E**, **E'** 3D reconstruction of arterial surface at E13.5 (**C'**) and E14.5 (**D'**, **E**, **E'**) using Imaris software with manual editing to highlight arterial vasculature. **E**) 90˚ rotation of **D'** in x-axis (red arrow) to better demonstrate arterial branching morphogenesis. **E'**) Caudal view of the E14.5 kidney (90˚ rotation of **E** in z-axis [blue]) to highlight that renal arteries do not penetrate the renal medulla. Blue arrowheads mark first bifurcation point. Individual lobar branches are labeled by a letter to signify which major artery from which it arises and a number. **F-K**) Analysis of arterial differentiation on E13.5 (**F-H**) and E14.5 (**I-K**) kidney sections. Zoomed in images of boxed areas in the cortex (**G**, **J**) and medulla (**H**, **K**) show staining for arterial development in different parts of the kidney. White arrows demarcate $Emcn^{+}$, $Cx40^{+}$ vessels while orange arrows mark $Emcn^{-}$, $Cx40^{+}$ vessels. Scale bar = 150 µm (**A-E**) or 50 µm (**F-K'**).

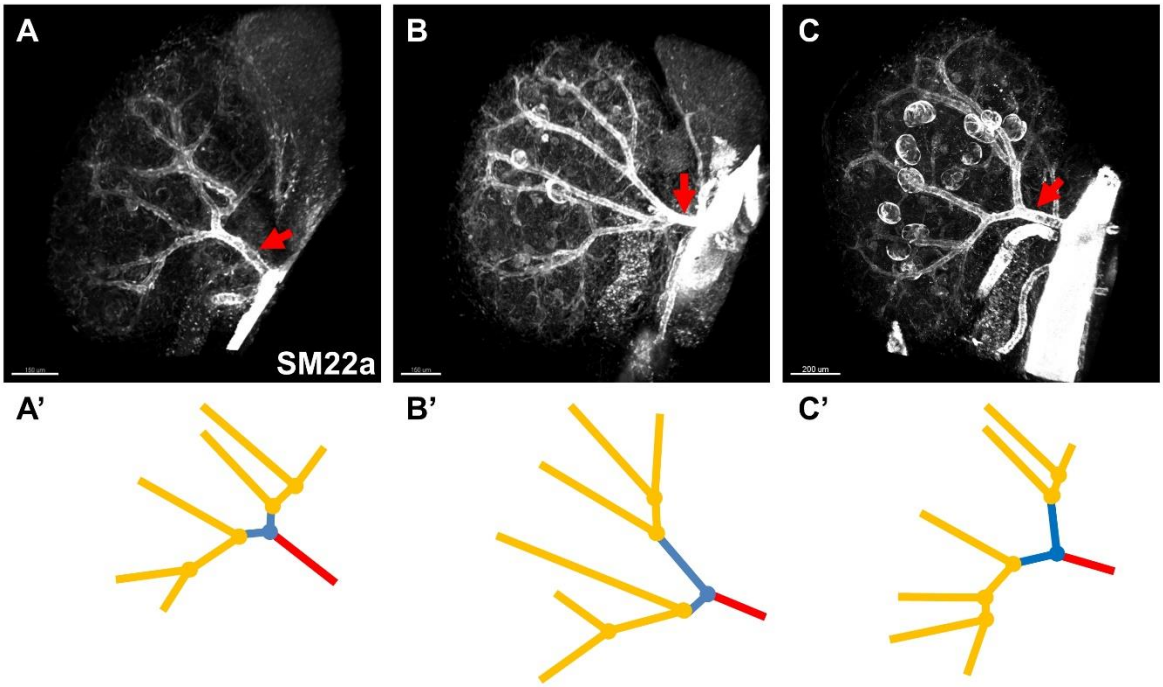

Figure 3.4. Renal arterial tree forms in a predictable but not stereotyped pattern. A-C) Whole mount imaging of 3 separate E14.5 kidneys were stained with the smooth muscle marker Sm22a to visualize the arterial tree. Red arrows mark the renal artery extending from the aorta. Balloon-like structures are parietal epithelial cells of Bowman's capsule. **A', B', C'**) Simplified 2D representation of the arterial branching pattern for each kidney. Each bar corresponds to a branch of the arterial tree and each circle is a branch point. Red branch represents the renal artery, blue branches represent the first major branching event, and the orange branches represent the lobar arteries. Lengths and angles of each branching event is roughly proportional to the in vivo stain, demonstrating the heterogeneity in the branching pattern.

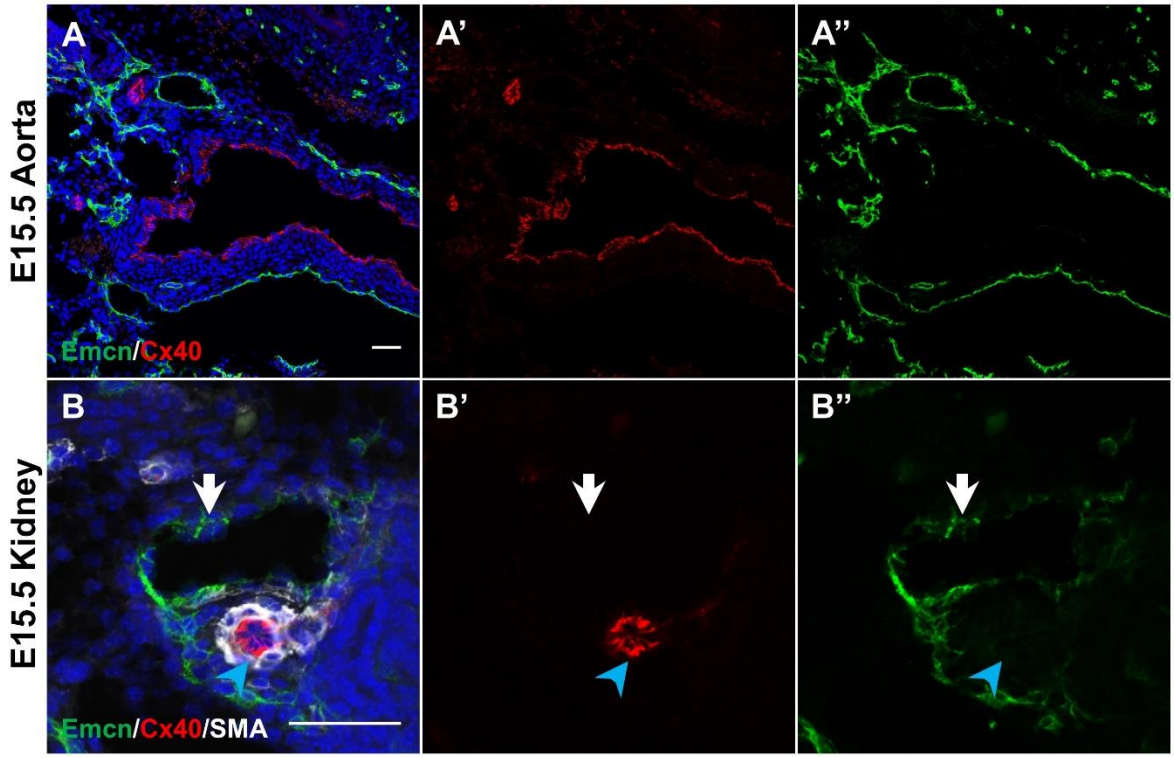

Figure 3.5. Arteries and veins express distinct genes in the midgestation kidney. A-A'') E15.5 aorta stained for Emcn and Cx40 demonstrating that the gene expressions are mutually exclusive in the aorta. **B-B'')** E15.5 kidney artery and vein doublet. Arteries and veins are marked with a blue arrowhead and a white arrow, respectively. Mature arteries express Cx40, but not Emcn, and are surrounded by SMA^+ cells. Mature veins express only Emcn and are not surrounded by any SMA^+ cells. Scale bar = 50 µm.

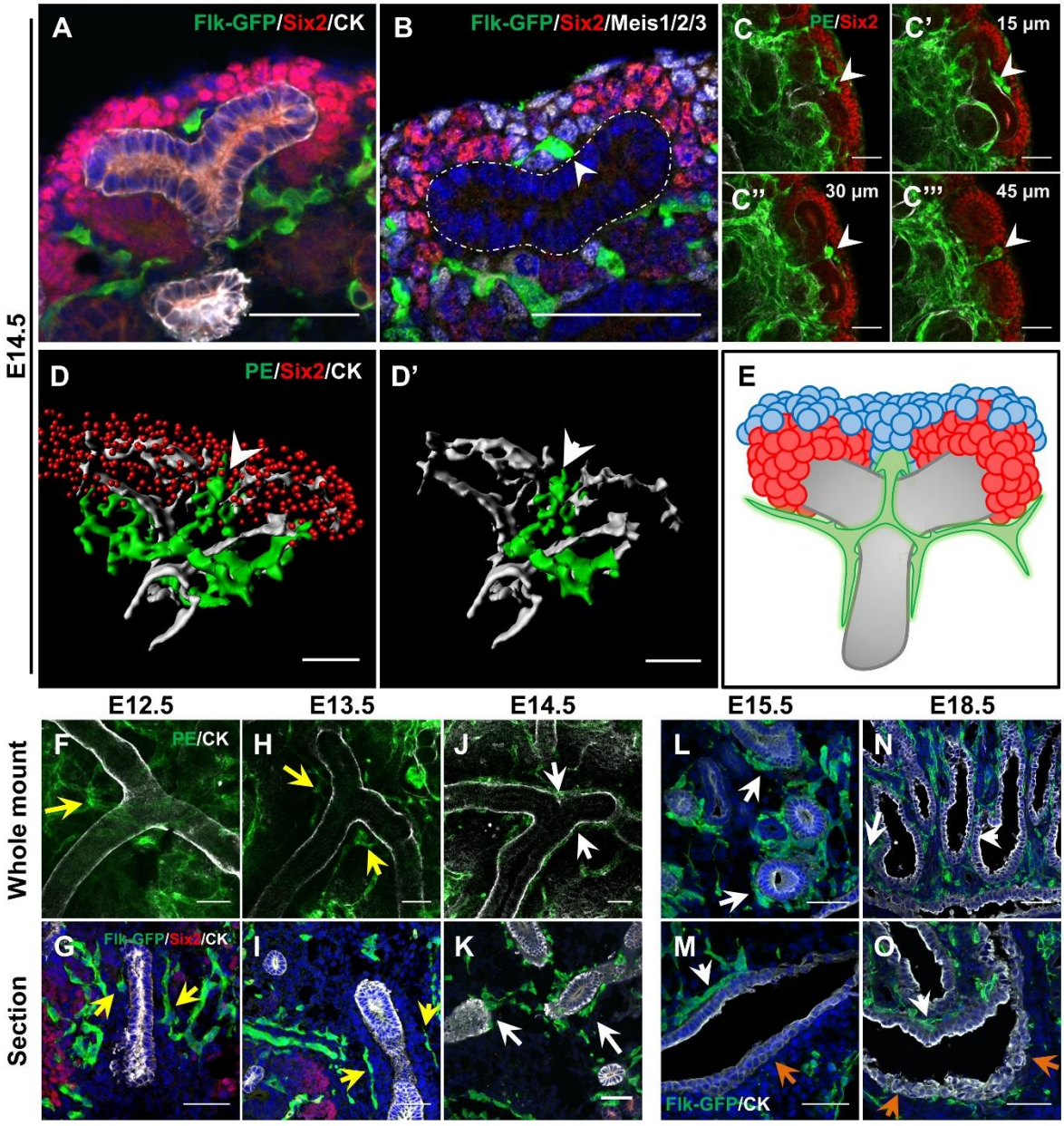

Figure 3.6. ECs avoid proximal ureteric stalk until 14.5 and bisect distal UB tips. **A**) E14.5 Distal tips of UB with EC in between the two NPC caps, bisecting the UB tips. **B**) Distal UB tip stained for the stromal marker Meis1/2/3 (white) demonstrating that the bisecting EC is surrounded mostly by stromal cells. White outline marks UB. White arrow marks connection between UB and bisecting EC. **C**) Whole mount analysis of EC looping around the distal UB (white arrowheads). Numbers in **C'-C'''** represent distance from **C** in Z-axis. **D**) 3D render of ECs around the distal UB tip with $Six2^{+}$ NPCs. **D'** highlights a single EC loop around the UB tip. White arrowhead marks bisecting EC. **E**) Model of EC organization at the distal UB tips.

ECs bisect the distal tips and circumscribe each branch of the UB tree, forming a cruciform structure around the bifurcation point. The EC that bisects the distal tip is almost entirely surrounded by stroma cells. Green = ECs, Red = NPCs, Blue = stromal cells, Grey = UB. Whole mount (**F**, **H**, **J**) and section (**G**, **I**, **K**) stains of the main trunk of the UB in E12.5 – E14.5 kidneys demonstrate ECs are separated from the UB trunk up to E13.5 (yellow arrows), but become tightly associated at E14.5 (white arrows). Immunofluorescent analysis on E15.5 (**L**, **M**) and E18.5 (**N**, **O**) sections show that ECs remain attached to the UB tree throughout development except on the side of the ureter facing the aorta (orange arrows). Scale bar = 50 μm.

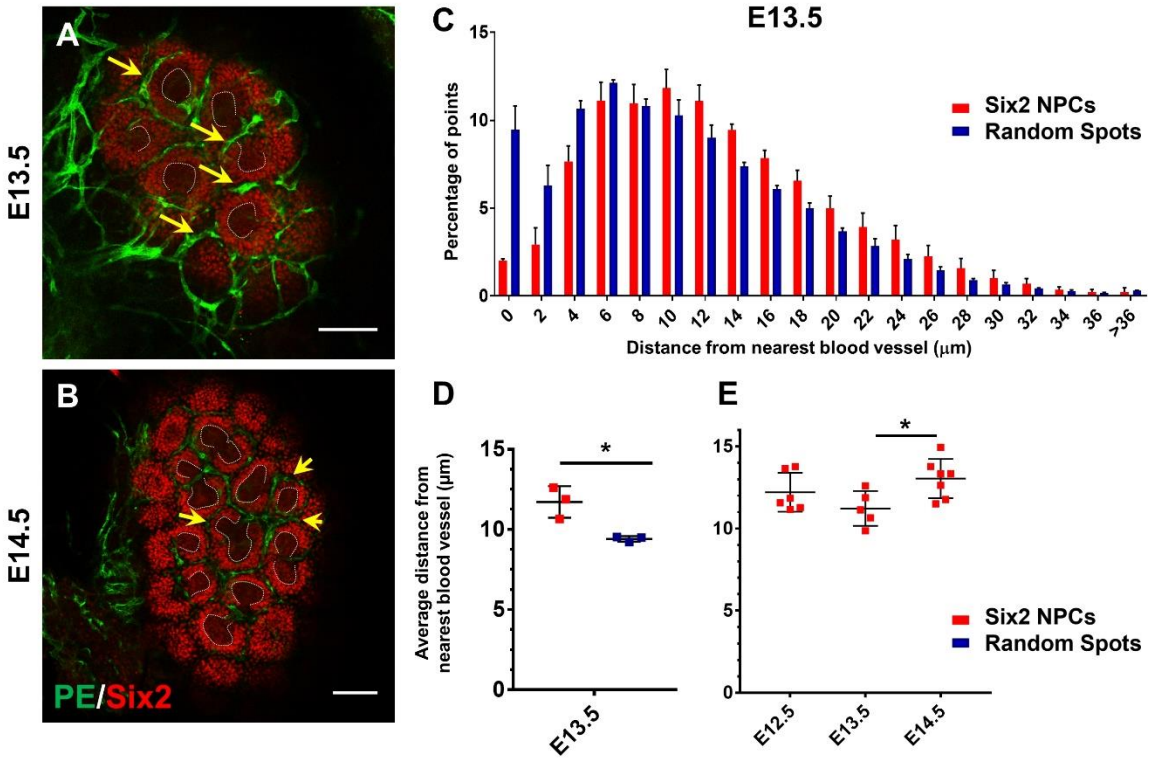

Figure 3.7. Endothelial cells avoid Six2$^+$ cells and circumscribe progenitor caps. A-B) Whole mount imaging of outer cortex in E13.5 (**A**) and E14.5 (**B**) kidneys. White dashed lines demarcate ureteric bud tips. Yellow arrows mark ECs circling the Six2$^+$ caps. **C**) Histogram of the distance between Six2$^+$ NPC or randomly generated spots and the nearest blood vessel. Histogram represents the average distributions across 3 different E13.5 kidneys. **D**) Average distance of all Six2$^+$ NPC and randomly generated spots to the nearest blood vessel at E13.5. n=3. **E**) Average distance of all Six2$^+$ NPCs to the nearest blood vessel from E12.5-E14.5. n=5-7 Error bars show standard deviation. Scale bar = 100 μm, **P*<0.05.

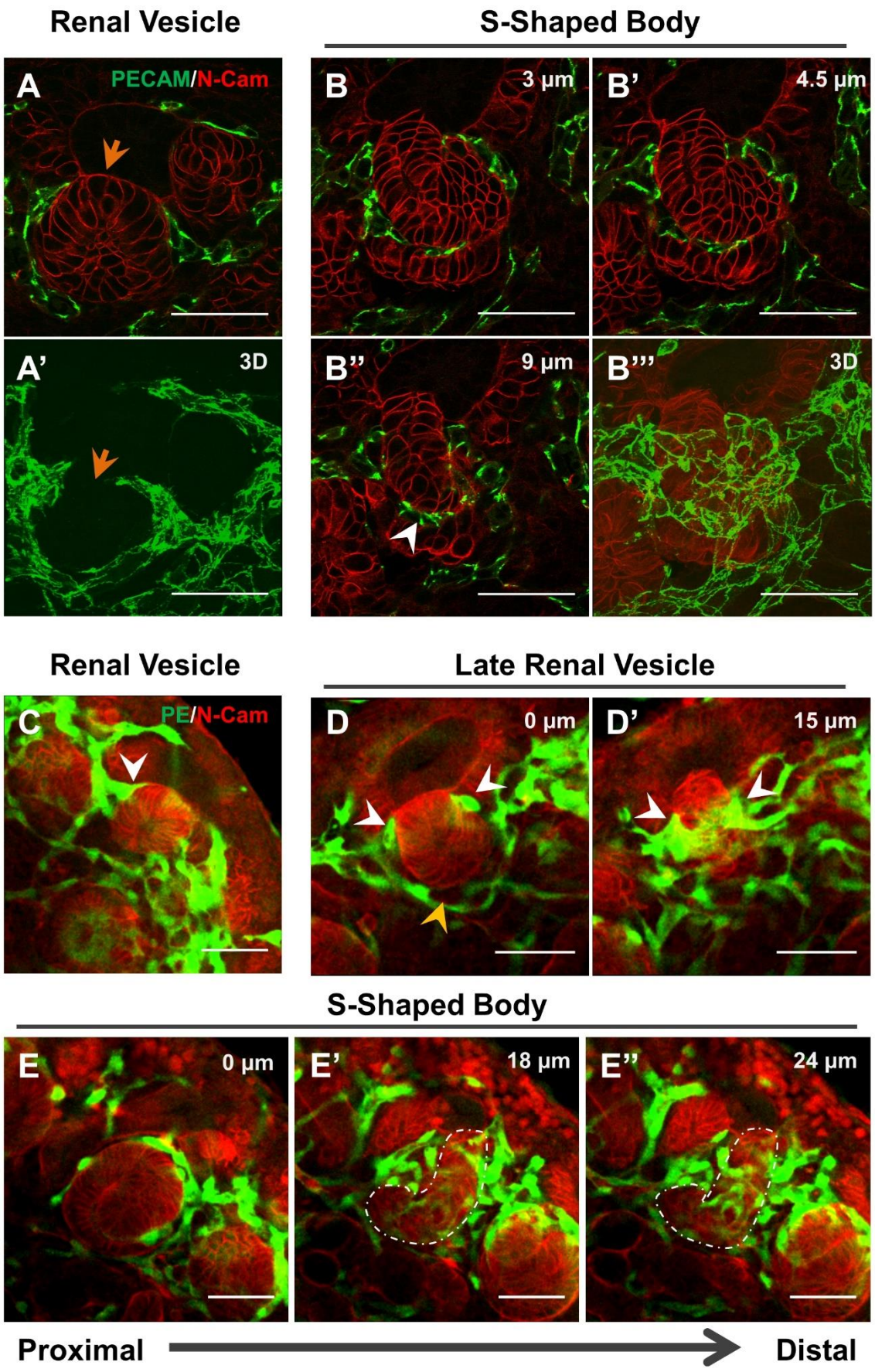
Renal Vesicle
S-Shaped Body
A
PECAM/N-Cam
B
3 µm
B'
4.5 µm
A'
3D
B''
9 µm
B'''
3D
Renal Vesicle
Late Renal Vesicle
C
PE/N-Cam
D
0 µm
D'
15 µm
S-Shaped Body
E
0 µm
E'
18 µm
E''
24 µm
Proximal
Distal

Figure 3.8. ECs form a plexus around the developing nephron. **A-B**) 20 μm sections of a developing RV (**A**) and S-Shaped Body (**B**) with 3D reconstruction of the structure (**A'**, **B'''**) demonstrating the developing endothelial plexus from the RV stage forward. Orange arrow marks region where RV and UB are fused together and no ECs can be seen. White arrowhead marks ECs in cleft of developing S-shaped body. **C-E**) Whole mount stains for the RV (**C**), late RV – when the RV elongates and connects to the UB tip (**D**), and S-shaped body stages (**E**). White arrowheads mark ECs in between the RV and UB (in **C**) or looping around the connection between the RV and the UB (in **D**). Orange arrowhead in **D** indicates areas devoid of direct epithelial contact as part of the vascular basket. White outline in **E'-E''** marks distal portion of S-shaped body. Scale bar = 50 μm.

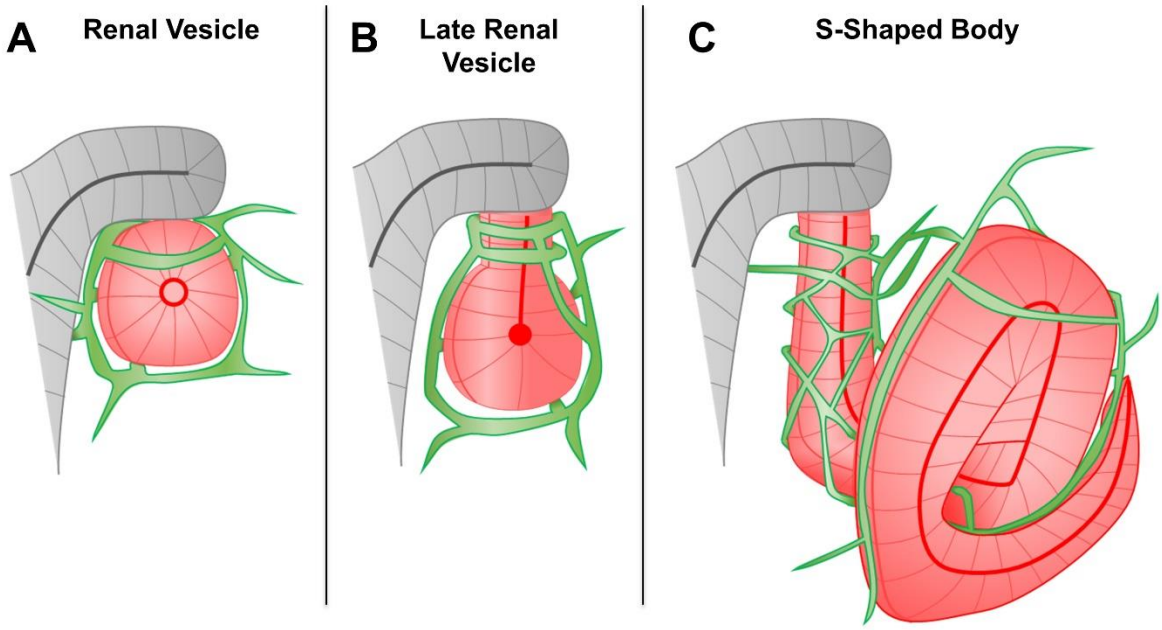

Figure 3.9. Models for endothelial organization around the developing nephron. Developing nephrons undergo multiple morphologic steps to form a mature nephron. (**A**) At the RV stage, ECs (green) form a plexus around the developing nephron structure (red) including in between the RV and UB (grey). (**B**) By the late RV stage when the RV elongates and attaches to the UB, the endothelial plexus begins to show signs of enrichment along the area of the vesicle destined to become the distal tubule. (**C**) Once the RV has reached the S-shaped body stage, the endothelial plexus has completely enveloped the distal part of the S-shaped body but is relatively sparse surrounding the proximal tubule portion (note that the proximal tubule portion has been slightly displaced to better visualize the distal tubule portion). The ECs that form along the cleft of the S-shaped body connect through the nephron to the rest of the endothelial plexus. At all stages, the plexus that surrounds the developing nephron is continuous with the rest of the cortical endothelium.

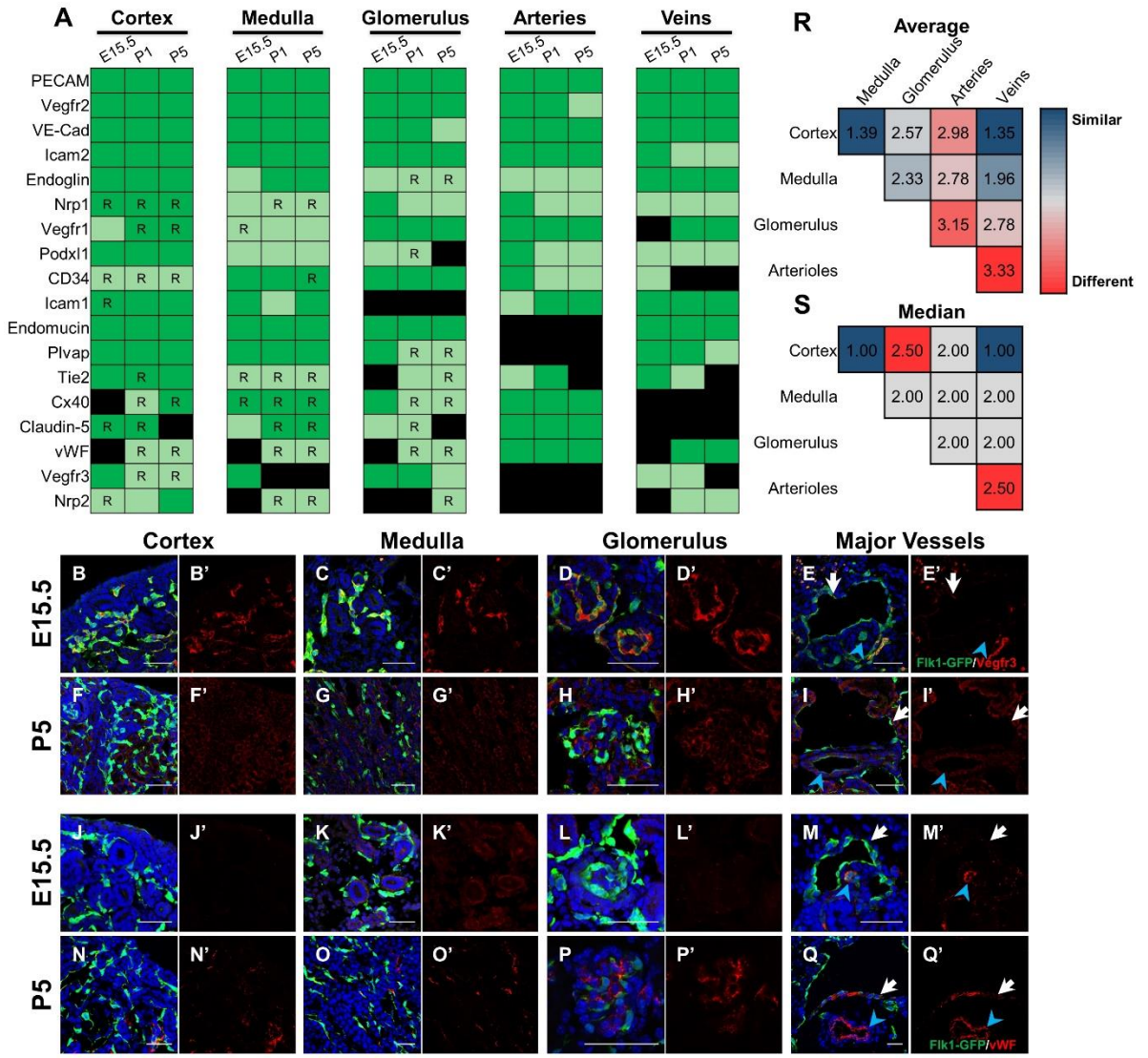

Figure 3.10. Standard endothelial markers display heterogeneous spatiotemporal expression in the developing kidney. **A**) Chart summarizing expression patterns for each endothelial gene in the kidney cortex, medulla, glomerulus, arteries, and veins at E15.5, P1, and P5. A gene was considered to be expressed in a region if the gene clearly colocalized with at least 1 Flk1-eGFP^{+} EC within a region. Strength of expression was determined qualitatively by comparing fluorescent intensity across different regions per gene. Expression in surrounding tissues was not considered. Dark green = strong expression, light green = weak expression, black = no expression, R = expression restricted to a subset of ECs within a region. *Vegfr3 and Nrp2 show strongest expression in lymphatics at all 3 timepoints. **B-Q**) Representative images for Vegfr3 (**B-I**) and vWF (**J-Q**) at E15.5 (**B-E**, **J-M**) and P5 (**F-I**, **N-Q**) costained with Flk1-eGFP (green) and DAPI (blue) to demonstrate changes in gene

expression by region over time. ECs of arteries and veins are marked with a blue arrowhead and white arrows, respectively. **R-S**) Average (**R**) and median (**S**) of the difference score between the regions (refer to Methods for how the score was determined). A score of 0 represents completely identical expression patterns while a score of 9 represents completely opposite expression patterns. Cells are shaded based off score. Red = higher score (more different) and blue = lower score (more similar). Scale bar = 50 μm.

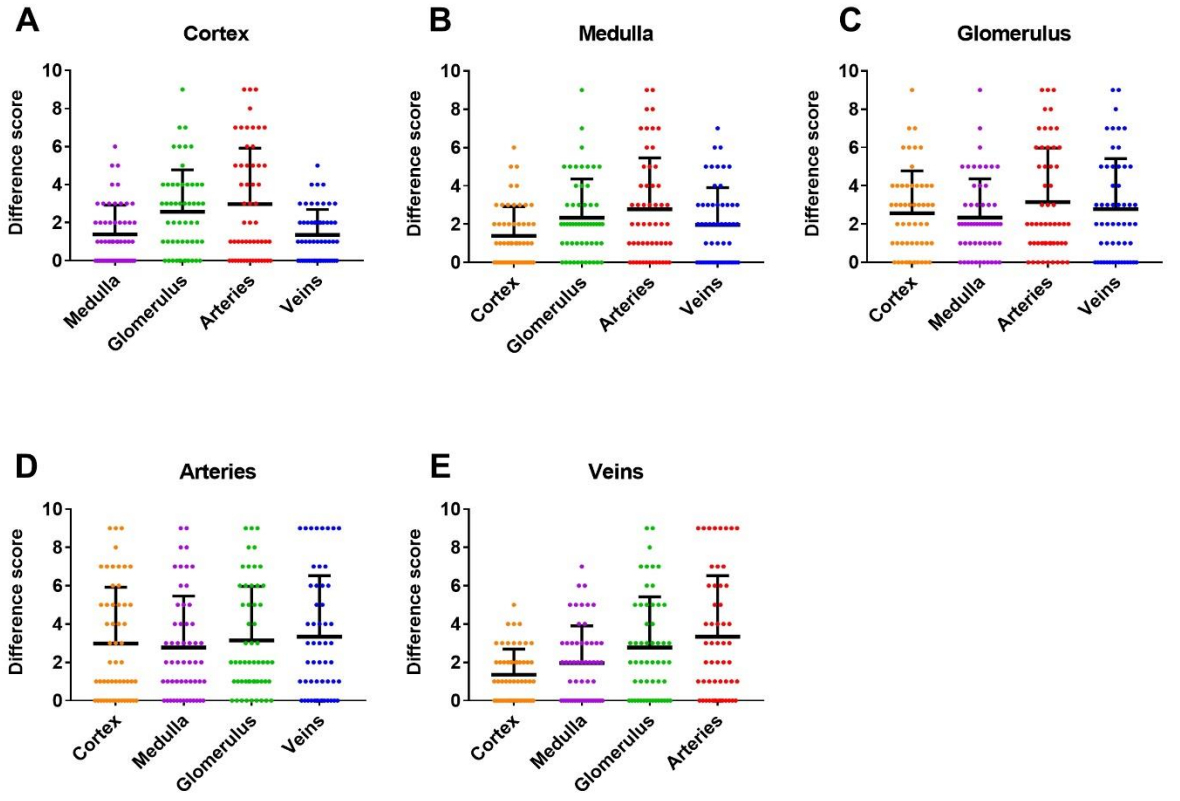

Figure 3.11. Differences in gene expression score between each region. Data summarized in **Fig 3.10R-S** organized by each region compared to the other 4 regions to better compare region expression patterns. All scores for all 3 independent analyses are shown. Line in each graph represents arithmetic mean and standard deviation. Each region is color-matched: cortex (**A**, orange), medulla (**B**, purple), glomerulus (**C**, green), arteries (**D**, red), and veins (**E**, blue).

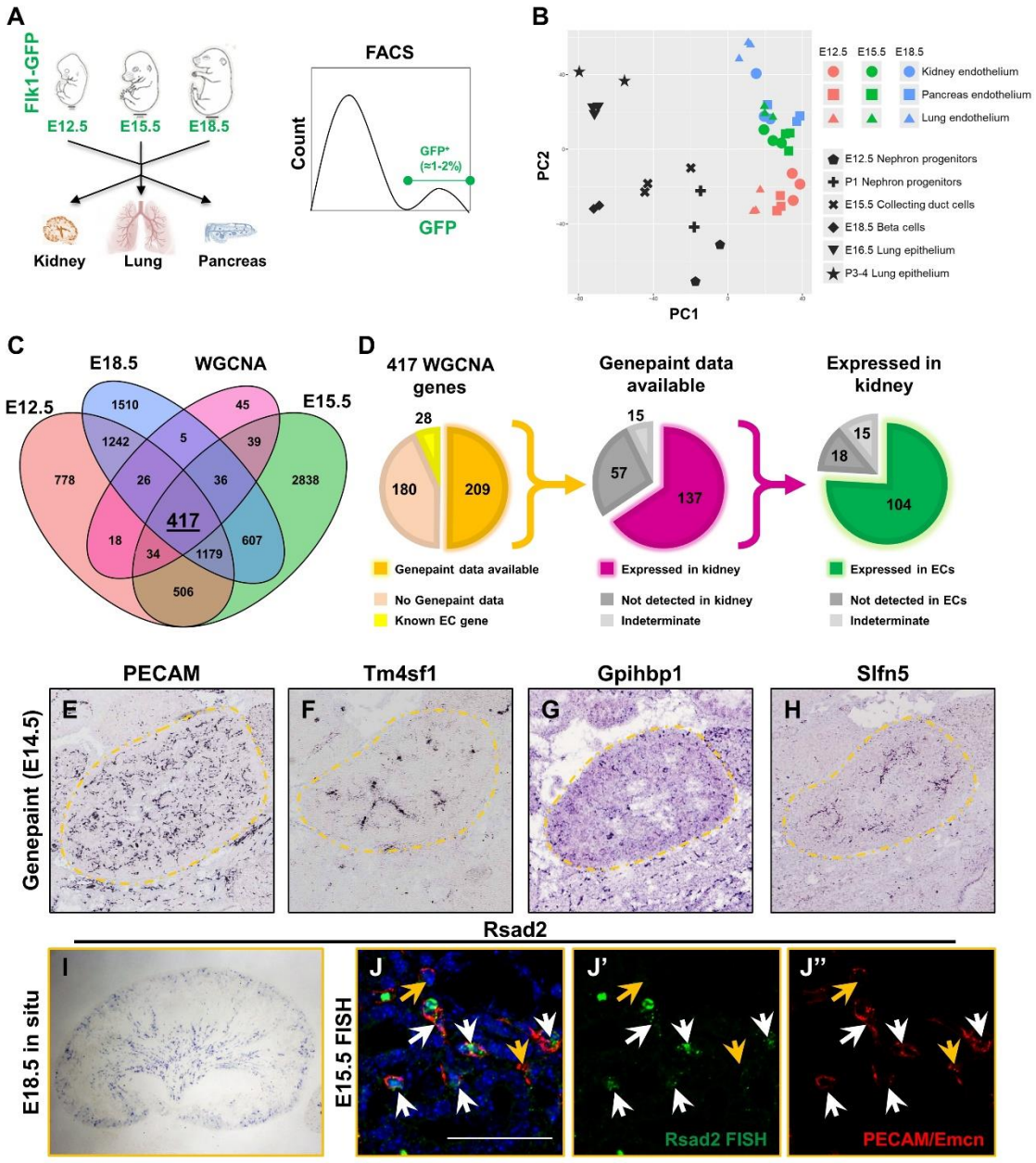

Figure 3.12. RNA-seq reveals endothelial spatiotemporal heterogeneity. A) Schematic for RNA-seq analysis. 3 organs – kidneys, lungs, and pancreas – were dissected out of E12.5, E15.5 and E18.5 Flk1-eGFP^{+} embryos (for a total of 9 samples) and digested to single cells. After digestion, GFP^{+} cells were isolated by FACS and subjected to RNA-seq analysis in bulk. **B**) Principal component analysis of 9 endothelial populations (colored) compared to six different outgroups (black). Endothelial populations cluster away from outgroups and show clear stratification over time. **C**) Venn diagram of genes enriched in the kidney endothelium

between E12.5, E15.5, E18.5, and those identified through WGCNA (p-value < 0.05). **D**) Graphs representing validation approach of the 417 genes identified through WGCNA of the gene enriched in the kidney endothelium at all 3 time points. Of the 417 genes identified, 28 of them are known EC genes (yellow) and 209 of them had data from genepaint.org available (orange, left graph). Of the 209 genes in which data was available, 137 of them were expressed in the kidney (middle graph, purple). Lastly, 104 of the 137 genes in kidney exhibited endothelial staining pattern in the kidney (green, right graph). **E-H**) ISH from genepaint.org. Kidneys are outlined in orange dotted lines to better visualize the kidney proper. **i** *In situ* hybridization of Rsad2 on E18.5 kidneys. **J-J''**) FISH on E15.5 kidneys demonstrating Rsad2 is restricted to ECs in the kidney (white arrows) but is not expressed in all ECs (orange arrows). Note that two large green dots on the FISH are autofluorescent blood cells. Scale bar = 50 µm.

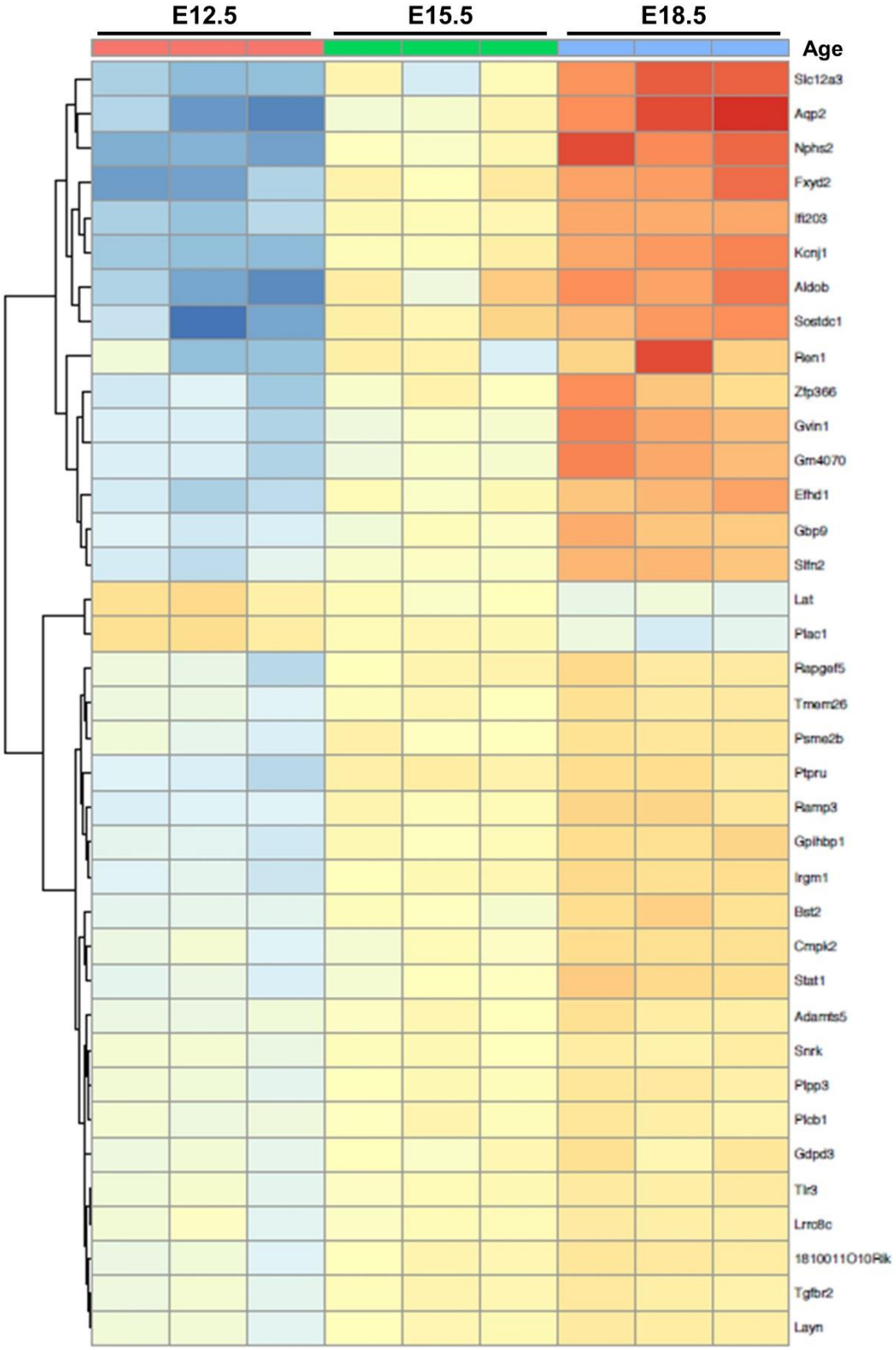
E12.5
E15.5
E18.5
Age
High
Low
Slc12a3
Aqp2
Nphs2
Fxyd2
Ifi203
Kcnj1
Aldob
Sostdc1
Ren1
Zfp366
Gvin1
Gm4070
Efhd1
Gbp9
Slfn2
Lat
Plac1
Rapgef5
Tmem26
Psme2b
Ptpru
Ramp3
Gpihbp1
Irgm1
Bst2
Cmpk2
Stat1
Adamts5
Snrk
Ptpp3
Plcb1
Gdpd3
Tlr3
Lrrc8c
1810011O10Rik
Tgfbr2
Layn

Figure 3.13. Temporal dynamics of gene expression in kidney endothelium. Heat map for all genes from the WGCNA that significantly increase or decrease their expression over time in the kidney endothelium. The relative expression levels for those genes whose expression either monotonically increased or decreased at an FDR < 0.1 across developmental time points and whose gene significance for the kidney EC type was positive at a p-value < 0.05 are shown. Red columns are E12.5 samples, green columns are E15.5 samples, and blue columns are E18.5 samples.

Gene Name					
1810006J02Rik	Atp10d	Cnr2	Entpd1	Gimap5	Ifi203
1810011O10Rik	Batf2	Cnrip1	Eogt	Gimap6	Ifi47
2610203C22Rik	Bcl6b	Col15a1	Epas1	Gimap8	Igf1
3110035E14Rik	Bik	Colgalt2	Ephb1	Gimap9	Igf2
4930429F24Rik	Bst2	Crmp1	Erg	Gja4	Igfbp3
4930486L24Rik	Btnl9	Crnde	Esam	Gja5	Igfbp4
4930555G01Rik	C230029F24Rik	Csgalnact1	Esm1	Gm10653	Il27ra
A330009N23Rik	C77370	Csn3	Ets1	Gm13889	Il2rg
A530016L24Rik	Cacna1e	Ctla2a	Exoc3l	Gm14207	Inpp4b
A630033H20Rik	Calml4	Ctla2b	Exoc3l2	Gm16897	Inpp5d
Abcg2	Casp4	Cyp26b1	Exoc3l4	Gm17757	Insl3
Abi3	Cbfa2t3	Cyyr1	F2rl3	Gm18853	Irgm1
Acr	Ccdc3	Dapk2	Fam102b	Gm3500	Irx3
Adam15	Ccm2l	Dhh	Fam13c	Gm3558	Irx5
Adam19	Cd109	Dkk2	Fam167b	Gm4070	Itga5
Adamts5	Cd1d1	Dll4	Fam184b	Gm5796	Jak3
Adcy4	Cd1d2	Dnah10	Fam196a	Gm5797	Kank3
Adgre5	Cd34	Dnm3	Fam212a	Gmfg	Kcnd3
Adgrf5	Cd38	Dnm3os	Fam43a	Gnb4	Kcne3
Adgrg3	Cd40	Dock4	Fam78a	Gng11	Kcnj14
Adgrl4	Cd47	Dok4	Fes	Gngt2	Kcnk6
Adh6b	Cd93	Dysf	Fgd5	Gpihbp1	Kctd12b
Adora2a	Cda	Ebf1	Fli1	Gpm6a	Kdr
Afap1l1	Cdc42ep1	Ecm2	Flrt2	Gpr182	Kif26a
AI662270	Cdc42ep2	Ecscr	Flrt3	Gpr183	Kitl
Alox12	Cdh5	Ednrb	Flt1	Grap	Klf7
Aplnr	Ces2e	Efna1	Flt4	Grrp1	Klhl4
Apold1	Chrm3	Egfem1	Fxyd5	Gvin1	Klhl6
Arap3	Chst1	Egfl7	Fyn	Gypc	Klk8
Arhgap18	Clca2	Egln3	Gas7	Hapln1	Lalba
Arhgap25	Cldn15	Ehd3	Gbp9	Hecw2	Lama4
Arhgap27	Cldn5	Ehd4	Gchfr	Hhex	Layn
Arhgap29	Clec14a	Elk3	Gdpd5	Hlx	Ldb2
Arhgap31	Clec1a	Elmo1	Gfi1b	Hpgd	Lhx6
Arhgef15	Clec1b	Emcn	Ggta1	Hrct1	Lmo2
Arhgef3	Clec9a	Endou	Gimap1	Ica1	LOC100861615
Art3	Cmtm3	Eng	Gimap3	Icam2	Lpar4
Atg9b	Cmtm8	Enpp3	Gimap4	Icos	Lrrc32

Gene Name				
Lrrc3b	Npl	Prnd	Sept1	Tcf15
Lrrc55	Npr1	Procr	Serpina3f	Tek
Lrrc8c	Nrarp	Pros1	Sez6l2	Tfpi
Lrrk2	Nrgn	Psme2b	Sgk1	Tgfb1
Ly6h	Nrp1	Ptchd1	Sh2d3c	Tgfbr2
Lyl1	Nrros	Ptgs1	Sh3bp5	Thsd1
Lyn	Oit3	Ptp4a3	Sh3tc2	Thsd7a
Man1c1	P2ry1	Ptprb	Shank3	Thy1
Map1b	Parvb	Pxdc1	She	Tie1
Marcks	Pcdh12	Ramp2	Shisa9	Timp3
Mb21d1	Pcdh17	Ramp3	Sigirr	Tll1
Mcam	Pcsk2os2	Rapgef3	Sipa1	Tlr4
Mef2c	Pde10a	Rapgef4	Slc25a45	Tm4sf1
Mest	Pde2a	Rapgef5	Slc43a3	Tm6sf1
Mfng	Pde8a	Raph1	Slc9a3r2	Tmc8
Mid2	Pdgfb	Rarb	Slfn3	Tmem132e
Mir682	Peak1	Rasgrp3	Slfn4	Tmem200c
Mir99ahg	Pecam1	Rasip1	Slfn5	Tmem204
Mmp25	Piezo2	Reep1	Smagp	Tmem255a
Mmrn1	Pik3c2g	Rftn2	Sncg	Tmem88
Mmrn2	Pik3cg	Rgl1	Snora33	Tnfaip2
Mn1	Pik3r6	Rgs14	Snrk	Tnfaip8l1
Msn	Plac1	Rgs7bp	Sox17	Tnfrsf11b
Msx1	Plaur	Rhoj	Sox18	Trim47
Myct1	Plcb1	Rinl	Sox7	Trpc3
Myzap	Pln	Ripply3	Sp110	Tspan18
N4bp3	Plpp1	Robo3	Ssu2	Ttc9
Nav3	Plpp3	Robo4	Stab1	Ttpa
Neurl3	Plvap	Rorb	Stab2	Unc45b
Nid2	Plxnd1	Rsad2	Stap2	Upp1
Nlgn1	Podxl	S100a10	Stard8	Ushbp1
Nlrc3	Pon3	S100a13	Stat1	Vamp5
Nlrp1b	Ppargc1b	S100a16	Stk10	Vsir
Nos2	Ppm1j	S1pr1	Tal1	Wipf1
Nos3	Prdm1	Samsn1	Tbata	Wisp1
Nov	Prkcdbp	Scarf1	Tbkbp1	Zeb1
Nova2	Prkch	Sema6b	Tbx18	Zfp69
Npdc1	Prkd2	Sema6d	Tbxa2r	

Table 3.1. List of kidney EC-enriched genes identified through WGCNA. 417 kidney EC-enriched genes were identified through WGCNA of Flk1-eGFP^{+} ECs isolated from E12.5, E15.5, and E18.5 kidneys, lungs, and pancreases compared to non-endothelial outgroups. Genes highlighted in green are novel kidney EC-enriched genes validated by Genepaint analysis.

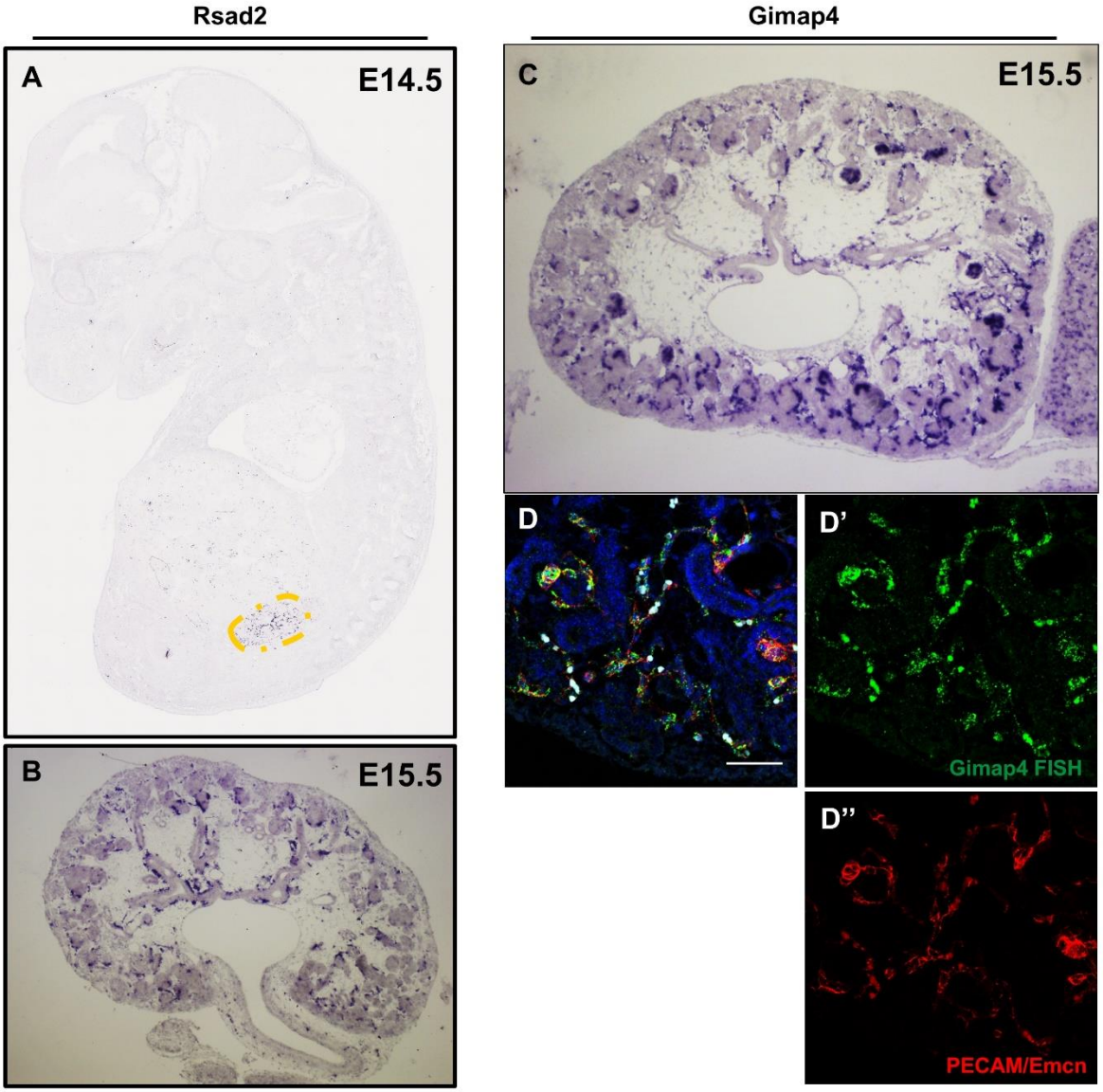

Figure 3.14. Validation of Genepaint.org data. **A**) E14.5 in situ of Rsad2 from genepaint.org demonstrating enriched expression in the kidney with some expression in the liver. Kidney is outlined in orange dotted line. **B**) ISH of Rsad2 on E15.5 kidney. **C-D)** ISH of Gimap4 on E15.5 kidneys to further validate WGCNA analysis on E16.5 kidneys. **D-D''**) FISH of Gimap4 demonstrate co-expression with PE. White cells are autofluorescent blood cells. Scale bar = 50 µm.

CHAPTER FOUR

ORGANOTYPIC ROLES OF CYP26B1 DURING LUNG AND KIDNEY ORGANOGENESIS

INTRODUCTION

Organogenesis requires highly orchestrated crosstalk between ECs, epithelial cells, and stromal cells in order to form a mature and functional organ. These cell types communicate with one another using a multitude of distinct signaling pathways that must be activated at the right place and time to promote proper development (Kraus and Grapin-Botton, 2012; Rankin et al., 2018). Coordination is central to development, and aberrations in any step of this multistep process can have catastrophic consequences in the developing embryo. Precisely how these signals are spatiotemporally controlled over the course of organogenesis remains poorly understood.

Both the lung and kidney are prime examples of cellular crosstalk regulating organ development. The general overview of kidney development has been discussed at length in the previous chapters and will not be reviewed here. Lung development begins at E9.0 with specification of the ventral side of the anterior foregut endoderm into early lung progenitors (Herriges and Morrisey, 2014; Shi et al., 2009; Warburton et al., 2010). These progenitors undergo initial bud formation, followed by a highly stereotyped and hierarchical branching pattern to form the lung airway tree (Metzger et al., 2008). During this process, the lung epithelial tree is stratified into 2 separate groups: the distal airways that give rise to the alveoli where gas exchange occurs and the proximal airways that form the conducting airways

consisting of bronchi and bronchioles. By E16.5, the distal airways begin to differentiate into pre-alveolar structures called canaliculi and saccules, consisting of alveolar type 2 (AT2) surfactant-producing cells and alveolar type 1 (AT1) gas-exchanging cells. These structures support gas exchange in neonates as full alveolarization occurs postnatally (Herriges and Morrisey, 2014; Morrisey and Hogan, 2010). In humans, failure to form the early saccules can result in respiratory distress syndrome (RDS), which can have a mortality rate as high as 50% depending on the size of the infant at birth (Gallacher et al., 2016). As such, the signaling pathways that promote proper distal epithelial formation must be precisely controlled for postnatal viability.

Retinoic acid (RA) is a critical signaling molecule that exhibits highly regulated spatiotemporal control during embryogenesis. RA directs cellular fate by binding to the RAR and RXR family of nuclear receptors to induce changes in gene transcription. RA is derived from Vitamin A (retinol) consumed in our diet. Vitamin A undergoes an initial step of dehydrogenation to form retinaldehdyde, then retinaldehyde undergoes an additional step of dehydrogenation by Raldh1-3 to form the active forms of RA with all-trans retinoic acid (atRA) being the most abundant and potent form. Once synthesized, RA can act as an autocrine signal in the cell that synthesized it or can freely diffuse to nearby cells as a paracrine signal, forming a local gradient (Duester, 2008). Opposing RA signaling is the Cyp26 family of P450 enzymes, consisting of Cyp26a1, Cyp26b1, and Cyp26c1, that can metabolize RA into inactive forms. Cells that express one of these P450 enzymes act as a local sink for RA to reduce RA signaling. The expression patterns of these genes require precise control as genetic or pharmacologic manipulations resulting in RA excess or deficiency can drastically affect nearly

every organ during embryonic development (Duester, 2008; Rhinn and Dolle, 2012). Therefore, spatiotemporal regulation of RA signaling is achieved through the proper expression of Raldh enzymes in RA-synthesizing cells and Cyp26 enzymes in RA-degrading cells to form local, tightly controlled RA gradients.

Both lung and kidney development require proper RA signaling. RA deficiency through genetic deletion of Raldh2 or Raldh3 or by feeding pregnant dams a Vitamin A deficient diet impairs the development of the lung and kidney (Rosselot et al., 2010; Wang et al., 2006; Wilson et al., 1953). During initial lung bud formation, RA activates the Wnt cascade via the Shh pathway and inhibits TGF-β signaling (Chen et al., 2010; Chen et al., 2007; Rankin et al., 2016; Rankin et al., 2018). Both of these effects, in turn, lead to upregulation of Fgf10, a critical factor necessary for lung bud formation and branching (Desai et al., 2004; Park et al., 1998; Wang et al., 2006). Once the lung begins to branch, RA performs the opposite role and blocks epithelial branching through downregulation of Fgf10 (Malpel et al., 2000). As distal airways begin to differentiate, RA activity is absent in the lung suggesting that maturation of these airways requires lower RA signaling. In line with this hypothesis, forcing increased RA signaling in distal lung epithelial cells through a constitutively active RAR prevented differentiation of distal epithelial structures into primitive saccules (Wongtrakool et al., 2003). RA has also been shown to affect kidney epithelial development although its role has not been as extensively studied as compared to that in the lung. Like the lung, RA is necessary for proper ureteric bud formation (Rosselot et al., 2010). Additionally, RA regulates proximo-distal organization of the developing zebrafish nephron whereby excess RA blocks formation of the

distal tubule and vice versa (Li et al., 2014; Naylor et al., 2016; Wingert and Davidson, 2011). These data indicate that RA can play similar roles between organs.

Despite these works detailing RA activity, little is known about the role that Cyp26 enzymes play during murine lung and kidney development. As stated previously, inhibition of RA activity is necessary for distal epithelial differentiation, suggesting that one of the Cyp26 family members may be required to promote proper distal epithelial formation by reducing RA activity through degradation (Li et al., 2014; Naylor et al., 2016; Wingert and Davidson, 2011; Wongtrakool et al., 2003). Indeed, inhibition of Cyp26a1 in zebrafish lengthens the proximal tubule and shortens the distal tubule (Naylor et al., 2016), but it is unclear whether this holds true in murine kidney development. Additionally, little is known of the role of Cyp26 enzymes during lung development. Cyp26a1 is expressed in the epithelium during early stages of lung branching, but its expression is absent by E16.5 when distal epithelial differentiation begins (Malpel et al., 2000). On the other hand, Cyp26b1 can be identified throughout the lung and kidney mesenchyme, but not the epithelium, at E18.5 (Abu-Abed et al., 2002). Additionally, deletion of Cyp26b1 leads to neonatal lethality presumably due to pulmonary dysfunction although this phenotype has not been further studied (Yashiro et al., 2004). Based on these data, I hypothesize that Cyp26b1 is required in both the kidney and lung in order to reduce RA signaling and promote proper distal epithelial differentiation.

In this chapter, I examine the role of Cyp26b1 during lung and kidney organogenesis. First, I identify Cyp26b1 to be highly enriched in both lung and kidney ECs throughout development. To further study how Cyp26b1 may direct development of both of these organs, I generated novel mouse models of whole-body Cyp26b1 deletion. Embryos lacking Cyp26b1

exhibited a delay in the formation of distal airways in late gestation that culminates in neonatal demise. Cyp26b1 null lungs displayed increased cellular density and contained an expansion of distal progenitors and AT2 cells at the expense of mature gas-exchanging AT1 cells. Exogenous administration of atRA during late gestation was able to partially phenocopy loss of Cyp26b1 suggesting that the phenotype is due, in part, to excess RA. By contrast, Cyp26b1$^{-/-}$ kidneys appear unaffected with no appreciable difference in epithelial, endothelial and stromal development. Instead, kidneys appear to be protected by upregulating Dhrs3 to maintain normal RA levels. These data highlight two similar, but distinct mechanisms that modulate RA signaling during organogenesis.

RESULTS

Cyp26b1 is highly enriched in lung and kidney ECs

In the previous chapter, I identified Cyp26b1 as an endothelial-enriched gene in the kidney at E12.5, E15.5, and E18.5 through RNA-sequencing. Previous data have demonstrated that Cyp26b1 is also expressed in the lung mesenchyme, suggesting that it may also be expressed in lung ECs (Abu-Abed et al., 2002). To better differentiate between lung ECs and stromal cells, I assessed Cyp26b1 expression in publically available single cell RNA-sequencing (scRNA-seq) of fetal, early postnatal, and adult kidneys and lungs. All of these studies demonstrate increased expression of Cyp26b1 in ECs in both organs compared to non-ECs (**Fig. 4.1**) (Du et al., 2015; Du et al., 2017; Guo et al., 2019; Hochane et al., 2019; Lindstrom et al., 2018a; Sabbagh et al., 2018; Tabula Muris et al., 2018). To validate these data, I performed in situ hybridization for Cyp26b1 at E12.5, E15.5, and E18.5 in both the kidney and lung. In situ hybridization for Cyp26b1 at E12.5 revealed an endothelial-like

expression pattern in both the kidney and lung (**Fig. 4.2A, E**). Consistent with previously published data, Cyp26b1 was also expressed in the developing limbs, the front of the face and palate, the tongue, the hindbrain, intersomitic regions along the back, in endocardial cushions extending into the great vessels, and the epicardium (**Fig. 4.3**) (Abu-Abed et al., 2002; Spoorendonk et al., 2008). By E15.5 and later, Cyp26b1 expression in the kidney becomes restricted to ECs in the outer cortex that surround developing nephron (**Fig. 4.2B-C, F-G**). Likewise, Cyp26b1 expression in E15.5 and E18.5 lungs becomes restricted to the ECs in the distal periphery (**Fig. 4.2F-G**). I validated that Cyp26b1 is highly expressed in ECs specifically through FISH analysis and co-staining with the PECAM and Emcn (**Fig. 4.2D, H**). Of note, $Cyp26b1^{+}$ punctae were observed in some epithelial and stromal regions in these organs at much lower levels compared to that in ECs (**Fig. 4.2D**, white arrows). Thus, Cyp26b1 expression is highly enriched in lung and kidney ECs throughout development.

Cyp26b1 is required for proper distal airway morphogenesis in late gestation

Previous work examining a Cyp26b1 germline deficient mouse model has stated that Cyp26b1-null mutants die shortly after birth due to respiratory distress (Yashiro et al., 2004). I generated two independently derived Cyp26b1-null mouse models using CRISPR/Cas9 in order to explore this phenotype further. The first model contains an in-frame 2.6kb deletion from Exon 3 to Exon 6 (referred to as $Cyp26b1^{-}$) and the second contains a 10bp deletion in Exon 3 leading to a frame-shift mutation (referred to as $Cyp26b1^{\Delta 10}$). Both $Cyp26b1^{-/-}$ and $Cyp26b1^{\Delta 10/\Delta 10}$ mice died shortly after birth and exhibited signs of respiratory distress including air hunger mirroring the previously generated null model. Due to this early postnatal lethality and to avoid the confounding effects of breathing on lung development, I focused my

analysis immediately prior to birth. E18.5 Cyp26b1$^{-/-}$ embryos exhibited many of the same developmental defects previously identified, including limb defects, craniofacial abnormalities, micrognathia, cleft palate, skin abnormalities, and spleen hypoplasia although edema and hemorrhages were not observed at this stage (**Fig. 4.4A-B**) (Bowles et al., 2014; Dranse et al., 2011; Lenti et al., 2016; Okano et al., 2012a; Okano et al., 2012b; Yashiro et al., 2004). E18.5 Cyp26b1$^{-/-}$ lungs were grossly smaller with decreased distal airspaces compared to WT littermates but exhibited normal lobation (**Fig. 4.4C-D**). On section, Cyp26b1$^{-/-}$ lungs appeared to be more cellular with increased septal wall thickness and smaller airspaces although the total number of airspaces were not different (**Fig. 4.4E-K**). To determine whether the phenotype is due to hypercellularity or increased density of the same number of cells, I measured the wet and dry weights of these lungs. Measurements of the wet and dry weight standardized to total body weight confirm that Cyp26b1$^{-/-}$ lungs are proportionally smaller at dissection without any difference in total body weight (**Fig. 4.4L-M**). This difference is primarily due to a decrease in fluid content as demonstrated by a decrease in wet/dry ratio even though the dry weights were trending downwards (**Fig. 4.4N-O**). These data indicate that the phenotype in Cyp26b1$^{-/-}$ lungs is due to an increase in cellular density and not due to increased total cellular mass.

Distal airspace formation appears to be abrogated in Cyp26b1$^{-/-}$ lungs. To see when this phenotype arises, I analyzed earlier stages of lung development. Distal airway differentiation begins at E16.5 when Sox9^{+} distal epithelial progenitor cells differentiate into proSP-C^{+} AT2 cells, which then give rise to Aqp5^{+} AT1 cells to begin forming saccules for gas exchange (Herriges and Morrisey, 2014; Shi et al., 2009; Warburton et al., 2010). In agreement with this

timeline, Cyp26b1$^{-/-}$ lungs begin to show gross morphological defects beginning at E16.5 characterized by increased cellular density and decreased distal airspace formation (**Fig 4.5**). During distal epithelial differentiation, epithelial cells undergo morphogenetic changes from a columnar, glandular-like structure to a more flattened or rounded morphology for AT1 or AT2 cells, respectively (**Fig. 4.6A, C, E**). In Cyp26b1$^{-/-}$ lungs, the epithelium exhibits a shift towards more rounded epithelium while the transition to flattened epithelium appears delayed (**Fig. 4.6B, D, F**). Although lumens in the mutant lungs can be identified at E16.5, these lumens are appreciably smaller and are only open in regions closest to the end of the proximal epithelium (**Fig. 4.6G-H**, magenta outlines).

Cyp26b1 is necessary for proper distal epithelial maturation

Based on these changes in epithelial morphology, I asked whether distal epithelial differentiation was affected in Cyp26b1$^{-/-}$ lungs. Immunofluorescent stains for Sox9^{+} and proSP-C^{+} at E18.5 to mark distal progenitor and AT2 cells, respectively, reveal that Cyp26b1$^{-/-}$ lungs contain relatively more progenitor and AT2 cells compared to control littermates (**Fig. 4.7A-F**). Of note, Cyp26b1$^{-/-}$ lungs contain a higher proportion of both cell types after standardizing for the increased number of DAPI^{+} cells per given area. Immunofluorescent stains for Aqp5^{+} AT1 cells confirmed that distal airway spaces are decreased in the mutants but were difficult to quantify by cell counting (**Fig. 4.7G-H**). To better assay the relative abundance of AT1 cells, I performed western blot and qRT-PCR analyses on E18.5 tissues. Western blot analyses demonstrated a decrease in the AT1 cell marker Aqp5 and an increase in Sox9 and proSP-C, validating the immunofluorescent data (**Fig. 4.7I**). Likewise, qRT-PCR

for Aqp5 revealed ~40% decrease in Aqp5 mRNA abundance in Cyp26b1$^{-/-}$ lungs; however, Sox9 and Sftpc mRNA levels were not significantly altered (**Fig. 4.7J**).

I further validated these data using other established AT2 and AT1 cell markers. Immunofluorescent stains and quantification of AT2 cells using the AT2 cell marker Lamp3 demonstrated a similar increase in Lamp3^{+} AT2 cells as compared to proSP-C^{+} AT2 cells in Cyp26b1$^{-/-}$ lungs with the vast majority of AT2 cells expressing both proteins (**Fig. 4.8A-F**). Likewise, the AT1 cell marker Pdpn mirrored the phenotypes seen with Aqp5 by immunofluorescence (**Fig. 4.8G-H**). Lastly, mRNA levels for the AT1 cell markers Pdpn, HOPX, and Ager/RAGE are all ~40% decreased in Cyp26b1$^{-/-}$ lungs while mRNA for Lamp3 was not significantly altered mirroring the results seen for Sftpc and Aqp5 (**Fig. 4.8I**). One possible explanation for these results is that there is an increase in the relative abundance of all epithelia and not specifically distal epithelial progenitors and AT2 cells. To rule out this possibility, I performed flow cytometry on E16.5 – E18.5 lungs with the general epithelial marker EpCam. This analysis indicated that relative proportions of all epithelial cells did not differ between WT and KO lungs at all 3 time points (**Fig. 4.7K**).

Because these mice were generated using CRISPR/Cas9-mediated mutagenesis, there may be off-target effects contributing to this phenotype. To confirm that the phenotype seen is due to loss of Cyp26b1 and not from potential off-target effects, I crossed the Cyp26b1^{-} allele with the Cyp26b1$^{\Delta 10}$ to generate compound heterozygotes. E18.5 Cyp26b1$^{-/\Delta 10}$ embryos completely phenocopied Cyp26b1$^{-/-}$ embryos including gross developmental defects, decreased distal airspaces, increased cellularity, and increased relative numbers of distal epithelial progenitors and AT2 cells (**Fig. 4.9**).

Taken together, these data demonstrate that loss of Cyp26b1 result in changes in distal epithelial morphology and differentiation (**Fig. 4.7L**). More specifically, distal epithelial progenitor and AT2 cells are increased at the expense of AT1 cells.

Proximal airways, stroma, endothelia, and lymphatics are unaffected in Cyp26b1$^{-/-}$ lungs

I further assayed for changes in other populations in Cyp26b1$^{-/-}$ lungs. Proximal airways in Cyp26b1$^{-/-}$ lungs appeared unaffected as there was no appreciable difference in gross morphology or in the abundance of CCSP^{+} secretory cells and Foxj1^{+} ciliated cells (**Fig. 4.10A-B**). At the transition from proximal to distal airways reside CCSP^{+}, Sca1^{+} Bronchioalveolar Stem Cells (BASCs) that can give rise to distal epithelium in the adult during lung regeneration (Kim et al., 2005; Lee et al., 2014). Analysis of BASCs by flow cytometry revealed no differences in this population at any stage in late gestation (**Fig. 4.10C-D**).

Several groups have established a link between RA signaling and proper vascular formation in the heart through directing proper vascular smooth muscle cell differentiation and association of the vasculature with these smooth muscle cells (Braitsch et al., 2012; Wang et al., 2018a; Xiao et al., 2018). I analyzed the vasculature and associated stroma in Cyp26b1$^{-/-}$ lungs to see if similar changes can be identified. Gross analysis of the vasculature and stroma revealed no overt changes (**Fig. 4.11A-D**). Co-stains for VE-Cad and Pdgfr-β to mark the ECs and pericytes, respectively, did not reveal any differences in EC-pericyte coupling (**Fig. 4.11E-F**). I also observed no differences in arterial, venous, and lymphatic development (**Fig. 4.11G-J**). Lastly, RA has been shown to direct the differentiation of stromal-derived smooth muscle cells during lung organogenesis (Chen et al., 2014). Analysis of these cells using the marker Sm22a (protein product of *Tagln*) revealed that smooth muscle cells around both airways and

vessels were not appreciably altered in Cyp26b1$^{-/-}$ lungs (**Fig. 4.11K-L**). These data suggest that formation of the vasculature, stroma, and related lineages is not affected in Cyp26b1$^{-/-}$ lungs.

Cyp26b1 mutant lungs demonstrate a mixed RA response

Cyp26b1 reduces RA signaling by catabolizing RA into an inactive metabolite; therefore, I wanted to determine if there is increased RA signaling in lungs lacking Cyp26b1. Because the main mechanism of RA is to modulate gene transcription, I first assayed for genes in RA metabolism by qRT-PCR, several of which are known RA targets (RARβ, Stra6, Crabp2, Rbp1, Cyp26 family) (Balmer and Blomhoff, 2002; Rhinn and Dolle, 2012; Ross and Zolfaghari, 2011; Wu and Ross, 2010). Transcriptomic analyses of these genes in whole lung lysates revealed upregulation of RARβ and Stra6, downregulation of the RA-synthesizing enzymes Raldh1 and Raldh3, and a trend towards increased and decreased expression of Crabp2 and Raldh2, respectively (**Fig. 4.12A**). Assaying directly for the Cyp26 family, Cyp26b1 was strongly upregulated in Cyp26b1$^{-/-}$ lungs when analyzed using primers outside of the deleted region (**Fig. 4.12B**). Repeating the PCRs with primers within the deleted region spanning the intron between Exon 4 and Exon 5 verified the mutation (**Fig. 4.12B**, "Cyp26b1-E4-5"). Expression levels of Cyp26a1 and Cyp26c1 were not affected (**Fig. 4.12B**). ISH/FISH for Cyp26b1 in mutant lungs validated the qRT-PCR data and revealed that ECs specifically upregulated Cyp26b1 transcripts (**Fig. 4.12C-H**). These data are consistent with the conjecture that RA signaling is increased in Cyp26b1$^{-/-}$ lungs.

These data suggest that there is increased RA activity and that ECs are at least one cell type that directly respond to these changes. I next asked whether other targets of RA signaling

are altered in Cyp26b1$^{-/-}$ lungs. I first analyzed for changes in expression levels of Ret, Egr1, Foxa1, and Pbx1, which have all been shown to be direct targets of RA signaling in other contexts (Balmer and Blomhoff, 2002; Probst et al., 2011; Rhinn and Dolle, 2012; Wong et al., 2012). qRT-PCR analyses of whole lung lysates for these genes revealed significant upregulation of Ret but not the other 3 genes (**Fig. 4.12I**). I next asked whether other signaling pathways may be differentially regulated. During early lung morphogenesis, RA is known to transcriptionally regulate multiple signaling pathways, including Fgfs, Tgf-β/Bmps, Wnts, and Shh (Chen et al., 2007; Desai et al., 2004; Malpel et al., 2000; Rankin et al., 2016; Rankin et al., 2018). Interestingly, qRT-PCR analysis for all of these pathways by qRT-PCR revealed that these pathways are unaffected overall except for downregulation of the Tgf-β target Tgfbi (**Fig. 4.13**). Lastly, I utilized the RARE-hsp68LacZ reporter line as a visual reporter of RA activity (Rossant et al., 1991). E16.5 Cyp26b1$^{+/+}$ lungs showed no discernable LacZ^{+} expression consistent with previous reports (Malpel et al., 2000) (**Fig. 4.12J**). Surprisingly, Cyp26b1$^{-/-}$ lungs also showed no discernable LacZ^{+} expression despite increased LacZ expression in the stomach epithelium (**Fig. 4.12K, Fig. 4.14**). These data suggest that loss of Cyp26b1 in the lungs only partially affects RA signaling.

RA partially contributes to the phenotype in the lung

I sought to more clearly determine if RA is sufficient to induce the changes seen in the Cyp26b1$^{-/-}$ lungs. Previous reports have shown that exogenous administration of atRA can partially phenocopy the defects in limb development, palate fusion, and skin barrier formation that are seen in Cyp26b1$^{-/-}$ embryos (Cadot et al., 2012; Okano et al., 2012b). Following a similar dosing regimen, I gavaged 100 mg/kg atRA to Cyp26b1$^{+/-}$ pregnant dams at E15.5,

E16.5, and E17.5, dissected out the lungs at E18.5, and assessed for changes in lung development (**Fig. 4.15A**). 100% of Cyp26b1$^{-/-}$ and ~30% of Cyp26b1$^{+/-}$ and Cyp26b1$^{+/+}$ embryos receiving exogenous atRA died in utero while the remainder died shortly after birth (**Fig. 4.15B**). Because all atRA-treated Cyp26b1$^{-/-}$ embryos died by E18.5, I focused on the lungs of atRA-treated Cyp26b1$^{+/+}$ and Cyp26b1$^{+/-}$ embryos for these analyses. atRA-treated Cyp26b1$^{+/+}$ and Cyp26b1$^{+/-}$ lungs exhibited a loss of distal airspaces and increased cellular density that were indistinguishable from control Cyp26b1$^{-/-}$ lungs (**Fig. 4.15C-L, W, Fig. 4.16A-E**). Sox9^{+} distal progenitor cells were relatively more abundant in atRA-treated lungs per given area compared to their matched controls, but not to the same degree as that in Cyp26b1$^{-/-}$ lungs (**Fig. 4.15M-Q, X**). Interestingly, proSP-C^{+} AT2 cells were only proportionally increased in atRA-treated Cyp26b1$^{+/-}$, but not Cyp26b1$^{+/+}$, lungs (**Fig. 4.15R-S, Y**). These data demonstrate that RA is sufficient to induce morphologic changes in Cyp26b1$^{-/-}$ lungs and can only affect distal epithelial cell differentiation depending on genetic context.

To further validate these data, I performed qRT-PCR to see whether RA treatment induces the same changes in transcription as observed in Cyp26b1$^{-/-}$ lungs. Consistent with previous results, exogenous atRA treatment induced expression of RARβ, Stra6, and Cyp26b1 (**Fig. 4.16F-G**). I also observed a small, but significant, increase in Cyp26a1 (**Fig. 4.16G**). Next, I assayed for changes in markers of each distal epithelial population. Whereas expression levels of Sftpc, Aqp5, Pdpn, Ager, and Hopx in atRA-treated lungs mirrored that of Cyp26b1$^{-/-}$ lungs, Sox9 expression was increased and CCSP expression was decreased in atRA-treated lungs only (**Fig. 4.15Z, Fig. 4.16H**). These data raise the possibility that exogenous RA may induce additional transcriptional changes not observed in Cyp26b1$^{-/-}$ lungs. Indeed,

transcriptomic analysis of potential signaling pathways downstream of RA reveal differential expression of several Shh, Wnt, and Tgfβ members that are not differentially expressed in control Cyp26b1$^{-/-}$ lungs (**Fig. 4.17**). Specifically, I saw upregulation of Gli2, Gli3, Wnt4, Tgfb2, and Tgfb3 in atRA-treated lungs compared to Cyp26b1$^{-/-}$ lungs. Additionally, several other genes – namely, Shh, Ptch1, Wnt2, Tgfbr2, Tgfbr3, and Id1 –were not differentially expressed between atRA-treated and Cyp26b1$^{-/-}$ lungs but showed significant differences when the atRA-treated lungs were compared to their genotyped-matched controls (**Fig. 4.17**). Taken together, these data indicate that exogenous administration of atRA and loss of Cyp26b1 can both lead to similar morphologic effects on lung development but may work through separate mechanisms.

Loss of Cyp26b1 does not affect kidney development

Cyp26b1 is highly enriched in ECs in both the lung and the kidney (Fig. 1). Additionally, RA regulates proximo-distal patterning in zebrafish kidneys by inhibiting distal tubule formation (Li et al., 2014; Wingert and Davidson, 2011). Based on these observations, I asked whether deletion of Cyp26b1 also affected nephron development. Analysis of the developing nephron at multiple stages revealed no differences in organization and structure of the nephron (**Fig. 4.18A-F**). Additionally, I observed no differences in proximo-distal patterning at any stage in nephron development (**Fig. 4.18G-L**). I broadened my approach to determine whether other lineages are also affected in Cyp26b1-/- kidneys. Examination of the stroma using the stromal markers Pdgfr-α and Pdgfr-β revealed no overt differences in stromal organization (**Fig. 4.19A-B**). Likewise, the endothelium exhibited no changes in organization,

arteriovenous specification, and arterial structure (**Fig. 4.19C-J**). These data indicate that kidney development is unaffected in Cyp26b1$^{-/-}$ embryos.

Excess RA abrogates distal nephron formation only in specific genetic contexts

I wanted to assess whether RA signaling is affected in Cyp26b1$^{-/-}$ kidneys. Interestingly, qRT-PCR for the members of the RA metabolic pathway reveal little changes in those genes except for Cyp26b1 (**Fig. 4.20A-B**). As in the lung, Cyp26b1 is strongly upregulated specifically in ECs throughout the Cyp26b1$^{-/-}$ kidney (**Fig. 4.20B-H**). Analysis for genes downstream of RA signaling reveal increased expression of Foxa1 and Ecm1, but of Ret and Egr1 (**Fig. 4.20I**). Lastly, RARE-LacZ expression was unchanged between Cyp261$^{+/+}$ and Cyp26b1$^{-/-}$ kidneys, both exhibiting expression exclusively in the ureteric bud as shown previously (Rosselot et al., 2010). These data indicate that RA signaling is most likely not affected in Cyp26b1$^{-/-}$ kidneys.

These data led me to ask whether there were kidney-specific mechanisms that can compensate for loss of Cyp26b1 and maintain a normal level of RA signaling. Outside of Cyp26-mediated degradation, RA levels can be reduced by converting the immediate precursor, retinaldehyde, back into retinol through the activity of Dhrs3 (Adams et al., 2014; Billings et al., 2013; Feng et al., 2010) (**Fig. 4.21A**). Additionally, Dhrs3 protein is highly expressed in the kidney at E14.5, but not in the lung (Billings et al., 2013). Based on these studies, I asked whether Dhrs3 expression is altered in Cyp26b1$^{-/-}$ kidneys and lungs. Although Dhrs3 expression was not significantly upregulated by qRT-PCR (**Fig. 4.19A**), immunofluorescent analysis for the protein revealed appreciably higher levels in Cyp26b1$^{-/-}$ kidneys, but not lungs (**Fig. 4.21B-E**). This observation suggests that Dhrs3 may be protecting

the kidneys from excess RA in the context of Cyp26b1 deletion. Dhrs3 cannot directly metabolize atRA (**Fig. 4.21A**); therefore I sought to circumvent the activity of Dhrs3 and directly test the effects of excess RA on kidney development by assaying the kidneys from pregnant dams that received exogenously atRA. Kidneys from atRA-treated embryos exhibited increased Dhrs3 protein levels similar to that in Cyp26b1$^{-/-}$ kidneys, indicating that excess RA does induce increased Dhrs3 protein expression (**Fig. 4.22A-E**). Because RA has been previously shown to inhibit distal tubule formation (Li et al., 2014; Wingert and Davidson, 2011), I assessed for changes in the distal tubules in atRA-treated kidneys. Immunofluorescent analysis and quantification revealed a significant decrease in distal tubule number in atRA-treated Cyp26b$^{+/-}$ kidneys only (**Fig 4.22F-K**). Taken together, these data suggest that kidneys are protected from excess RA through both Cyp26b1- and Dhrs3-mediated mechanisms.

DISCUSSION

Here I identify organ-specific roles for Cyp26b1 in lung and kidney development. Whereas loss of Cyp26b1 abrogates lung distal epithelial development, kidneys appear to be protected through increasing Dhrs3 expression to maintain normal RA levels. When Dhrs3 is bypassed through administration of exogenous atRA, there is a decrease in distal tubule formation in agreement with previous work (Naylor et al., 2016). In essence, excess RA causes the same effect on distal epithelium in both the lung and kidney, but each organ utilizes separate mechanisms to buffer RA levels (**Fig. 4.23**). It is unclear why there are two separate mechanisms between the lung and the kidney. Are kidneys exquisitely sensitive to excess RA such that they need both Cyp26b1 and Dhrs3 to ensure proper RA levels? Given the drastic results in the lungs, why do the lungs not upregulate Dhrs3? What are the mechanisms that

lead to these disparate responses? It is possible that Dhrs3, and not Cyp26b1, may be the primary regulator of RA levels in the kidney; however, the effects of loss of Dhrs3 in kidney development have not been explored.

Cyp26b1 is necessary for distal epithelial maturation in the lung

Loss of Cyp26b1 leads to profound changes in lung distal epithelial differentiation and morphogenesis resulting in neonatal lethality. Of note, I saw expansion of both distal progenitors and AT2 cells. Although death in these mutants was previously characterized as "respiratory distress" (Yashiro et al., 2004), RDS is characterized by a decrease in surfactant production from AT2 cells. In that regard, my work stands in contrast to other studies that have also identified similar defects in distal epithelial differentiation but saw a decrease in surfactant production or proSP-C^+ AT2 cells (Compernolle et al., 2002; Hogmalm et al., 2014; Kersbergen et al., 2018; Rockich et al., 2013; Woik et al., 2014; Yang et al., 2002). Whereas the defects seen in these studies most likely arise from an inability of distal progenitor cells to first differentiate into AT2 cells, loss of Cyp26b1 appears to reduce the differentiation of AT2 cells into AT1.

RA has been previously shown to block distal epithelial differentiation in other contexts. Human pluripotent stem cell derived lung bud tip organoids containing $Sox9^+$ distal progenitors can be maintained in a progenitor state when cultured with Fgf7, CHIR-99021, and RA (Miller et al., 2018). Removal of CHIR-99021 and RA lead to differentiation of these progenitors into the mature airway lineages. Although this group did not test the effect of removing RA individually, their results are consistent with the model that RA inhibits differentiation of the distal airways. Similarly, hyperactive RA signaling through constitutively

active RARα or RARβ lead to defects in distal airway formation (Wongtrakool et al., 2003). Interestingly, lungs with the constitutively active RARα transgene had a complete loss of AT2 and AT1 cells whereas lungs with the constitutively active RARβ transgene did contain AT2 and AT1 cells, more closely mirroring Cyp26b1$^{-/-}$ lungs. These data raise the question of whether the effects observed in Cyp26b1$^{-/-}$ lungs are primarily mediated through RARβ or other RARs and nuclear receptors. Whereas these studies utilized *in vitro* systems or specifically engineered transgenic lines, I identify Cyp26b1 as the endogenous physiologic mechanism that decreases RA signaling during normal lung development.

Exogenous administration of atRA beginning at E15.5 is able to partially phenocopy loss of Cyp26b1. Although morphologic changes between atRA-treated and Cyp26b1$^{-/-}$ lungs were indistinguishable from one another, cell fate changes in atRA-treated lungs did not completely match that in Cyp26b1$^{-/-}$ lungs. One possible explanation for this is that distal epithelial progenitors are specified as early as E13.5 and may not be receptive to changes in fate by the first dose of RA at E15.5 (Frank et al., 2019). Cyp26b1$^{-/-}$ lungs, on the other hand, are exposed to higher levels of RA throughout lung development allowing for a more severe difference in lineage specification. Despite these results that suggest that RA drives the defects in lung formation, my transcriptomic analyses suggest that this phenotype is modulated by an additional RA-independent mechanism. First, I saw little change in the expression of multiple signaling pathways known to be regulated by RA during lung development. Second, several genes in these pathways were differentially expressed in the atRA-treated lungs. These data indicate that loss of Cyp26b1 and exogenous atRA can both result in similar gross defects in lung development but do so through different transcriptomic responses. Additional studies

need to be performed in order to identify these RA-independent mechanisms that drive the defects in Cyp26b1$^{-/-}$ lungs.

ECs as a negative regulator of RA signaling

I and others show that Cyp26b1 is highly enriched in lung and kidney ECs throughout development, implicating ECs in directing this phenotype. ECs have been shown to regulate lung development during branching morphogenesis and alveolarization (Del Moral et al., 2006; Jakkula et al., 2000; Lazarus et al., 2011). Additionally, ECs are critical in directing distal epithelial development in models of adult lung regeneration (Ding et al., 2011; Lee et al., 2014; Rafii et al., 2015). My data suggest a new role for ECs during normal lung development in which ECs express Cyp26b1 to decrease RA signaling and promote distal epithelial differentiation. Although EC organization and specification appear unaltered in the mutants, I observed strong upregulation of Cyp26b1, but not Cyp26a1 or Cyp26c1, specifically in ECs of both Cyp26b1$^{-/-}$ lungs and kidneys. Both Cyp26b1 and Cyp26a1 are known targets of RA (Rhinn and Dolle, 2012; Ross and Zolfaghari, 2011; Wu and Ross, 2010) but it is unclear why loss of Cyp26b1 or exogenous atRA both strongly upregulate only Cyp26b1 and not Cyp26a1. Based on these expression patterns, there may be unidentified EC-specific mechanisms that lead to upregulation of Cyp26b1 in both Cyp26b1$^{-/-}$ lungs and kidneys. It must be stated that I cannot rule out that ECs exclusively drive the defects seen in Cyp26b1$^{-/-}$ lungs as other non-EC populations that express Cyp26b1 at much lower levels may also be contributing to this phenotype.

Cyp26b1 is essential to form a functional lung and is dispensable for kidney development; however, it remains to be seen how exactly loss of Cyp26b1 leads to the defects

observed in this study. More specifically, what are the downstream targets of RA that promote maintenance of lung progenitor cells and block differentiation? What are the other RA-independent pathways that may be contributing to this phenotype? Are these RA-independent pathways shared between the lung and the kidney? Is there a link between RA and these other pathways? Why are distal epithelial cells uniquely sensitive to loss of Cyp26b1 while other populations appear normal? Answering these questions will help shed new light on the key mechanisms that transform a simple cluster of cells into a multicellular, highly organized, and complex organ.

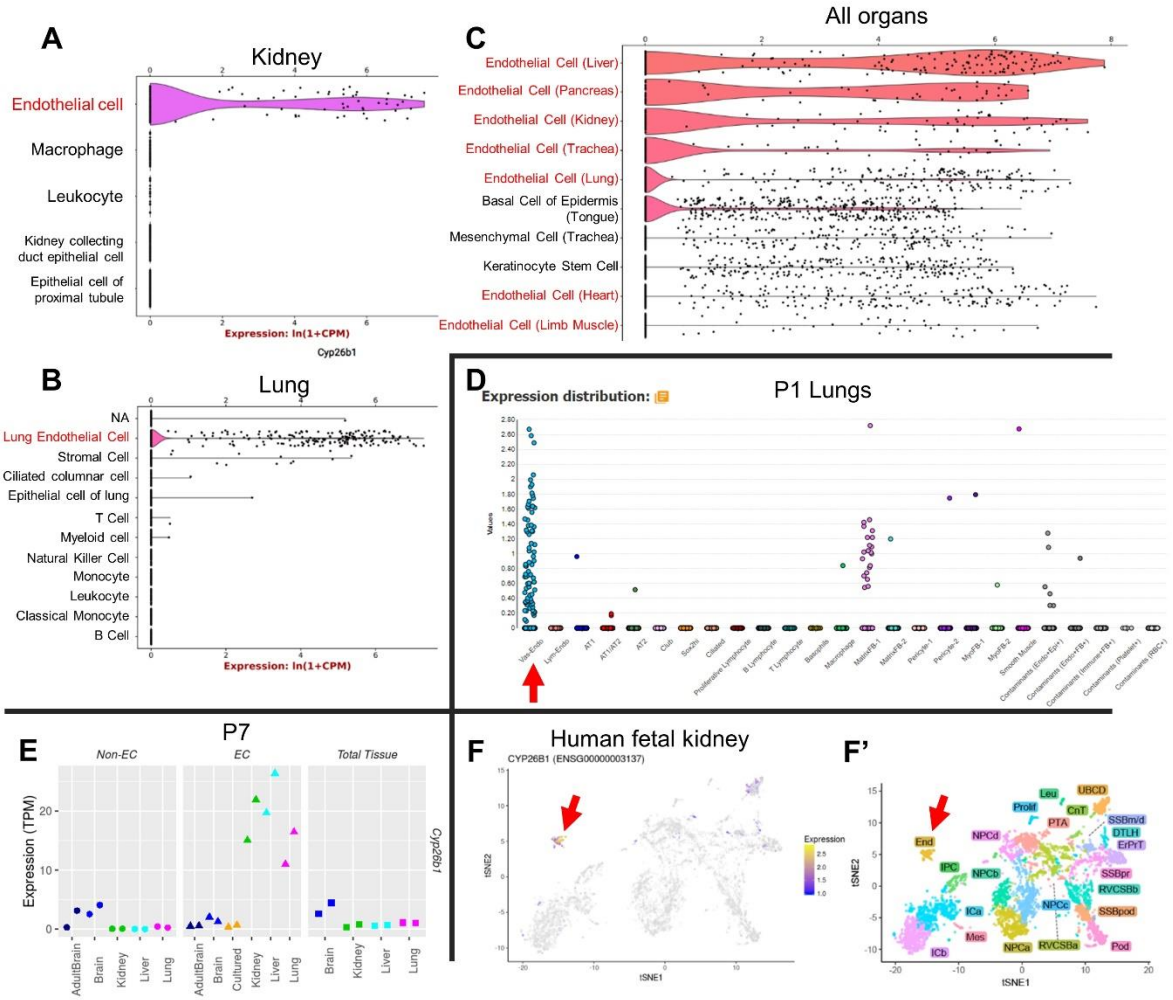

Figure 4.1. Cyp26b1 is highly enriched in lung, kidney, and other endothelial cell beds in post-natal mice. A-C) Violin plots of Cyp26b1 expression in scRNA-seq of adult kidneys (**A**), lungs (**B**), and in all adult organs combined (**C**) obtained from Tabula Muris consortium (Tabula Muris et al., 2018). Endothelial cell populations are highlighted in red. Data accessed through https://tabula-muris.ds.czbiohub.org/ **D**) Scatter plot of Drop-seq analysis of P1 lungs from LungGENS (Du et al., 2015; Du et al., 2017; Guo et al., 2019). Vascular-Endothelial cells are marked with Red arrow. Data accessed through https://research.cchmc.org/pbge/lunggens/SCLAB.html. **E**) Bulk RNA-seq of Tie2-GFP^{+} P7 ECs from brain, liver, lung, and kidney compared to GFP^{-} cells (Sabbagh et al., 2018). Data accessed through https://markfsabbagh.shinyapps.io/vectrdb/. **F-F'**) tSNE plot of scRNA-seq data of human fetal kidneys at week 16 of gestation (Hochane et al., 2019). Red arrow highlights endothelial cluster. Data accessed through https://home.physics.leidenuniv.nl/~semrau/humanfetalkidneyatlas/.

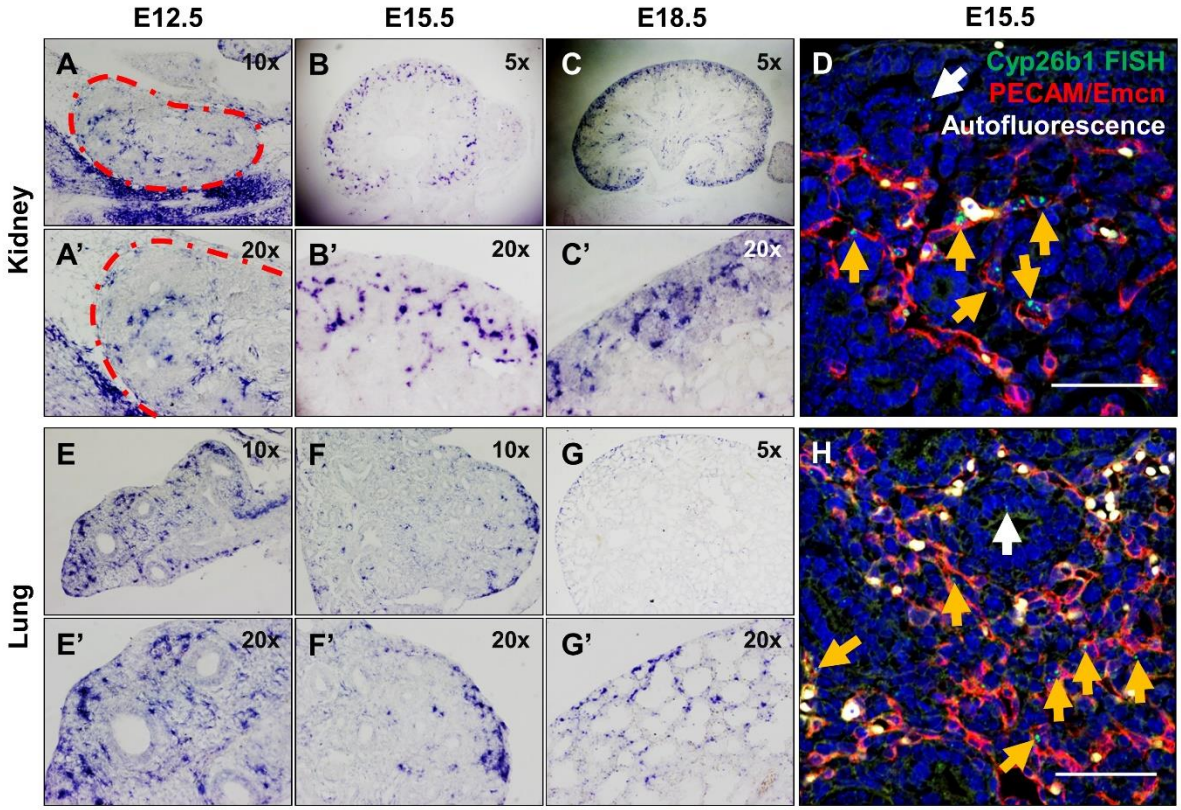

Figure 4.2. Cyp26b1 is highly enriched in lung and kidney endothelial cells during development. In situ hybridization of Cyp26b1 in the kidney (**A-D**) and lung (**E-H**) at E12.5 (**A, E**), E15.5 (**B, D, F, H**), and E18.5 (**C, G**). Magnifications for chromogenic assays shown. **D,H**) Fluorescent in situ hybridization for Cyp26b1 (green) co-stained with PECAM and Emcn (red) to mark ECs. Orange arrows are Cyp26b1^{+} punctae in PECAM/Emcn^{+} ECs. White arrow identifies Cyp26b1^{+} puncta in non-EC cell. Scale bar = 50 μm.

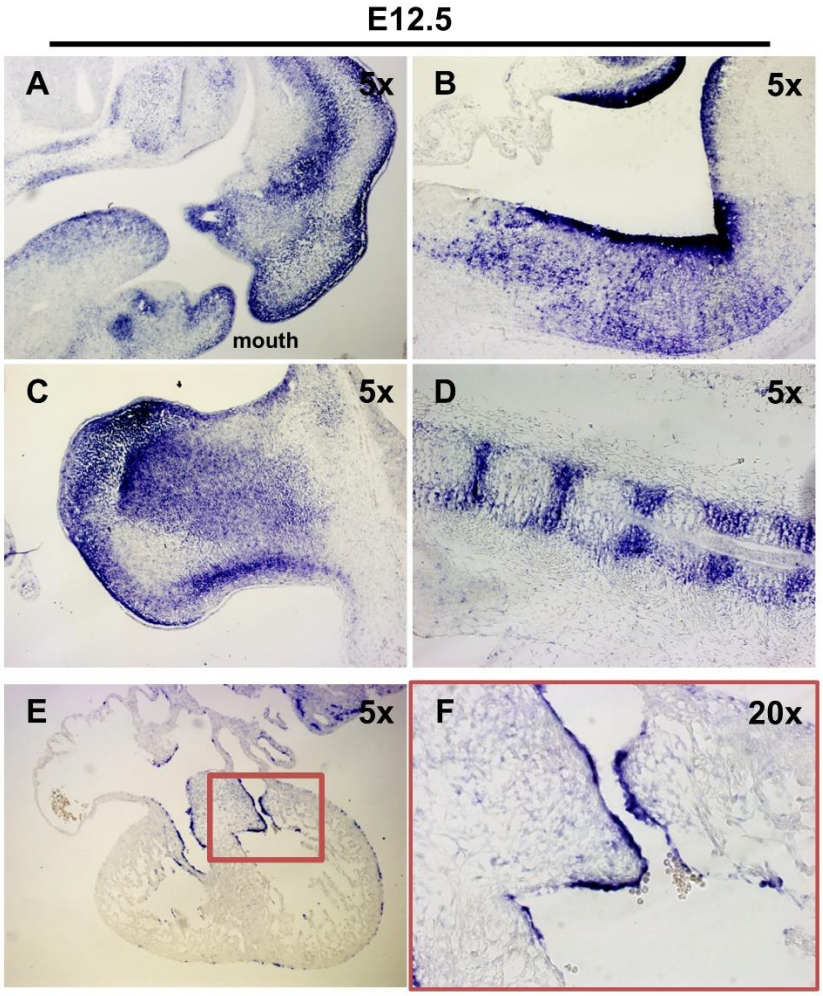

Figure 4.3. Cyp26b1 is expressed in multiple organs at E12.5. A-E) In situ hybridization for Cyp26b1 in the head (**A**), hindbrain (**B**), forelimb (**C**), somites (**D**), and heart (**E**). Mouth in (**A**) is marked for orientation. F) Zoomed in image of endocardial cushion shown in **E**. Magnifications for each image are shown.

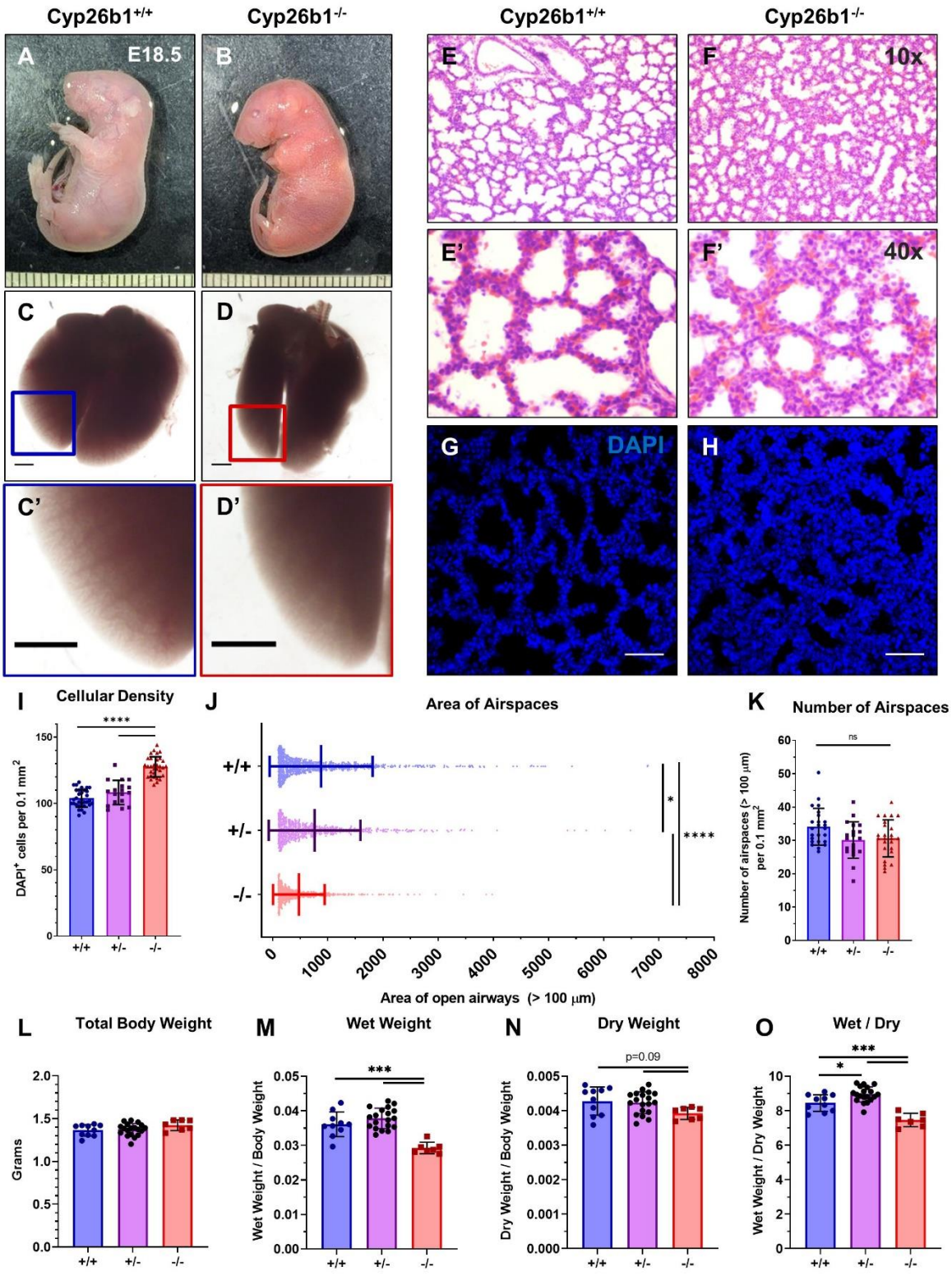
Cyp26b1+/+
Cyp26b1-/-
Cyp26b1+/+
Cyp26b1-/-
A
E18.5
B
E
F
10x
E'
F'
40x
C
D
G
DAPI
H
C'
D'
I
Cellular Density
****
DAPI+ cells per 0.1 mm2
150
100
50
0
+/+
+/-
-/-
J
Area of Airspaces
+/+
+/-
-/-
*
****
0
1000
2000
3000
4000
5000
6000
7000
8000
Area of open airways (> 100 μm)
K
Number of Airspaces
ns
Number of airspaces (> 100 μm) per 0.1 mm2
60
50
40
30
20
10
0
+/+
+/-
-/-
L
Total Body Weight
Grams
2.0
1.5
1.0
0.5
0.0
+/+
+/-
-/-
M
Wet Weight
***
Wet Weight / Body Weight
0.05
0.04
0.03
0.02
0.01
0.00
+/+
+/-
-/-
N
Dry Weight
p=0.09
Dry Weight / Body Weight
0.005
0.004
0.003
0.002
0.001
0.000
+/+
+/-
-/-
O
Wet / Dry
***
*
Wet Weight / Dry Weight
10
8
6
4
2
0
+/+
+/-
-/-

Figure 4.4. Cyp26b1 mutant lungs exhibit increased cellular density and decreased airspaces at late gestation. **A-B**) E18.5 Cyp26b1$^{+/+}$ and Cyp26b1$^{-/-}$ embryos at dissection. **C-D**) Lungs from Cyp26b1$^{+/+}$ and Cyp26b1$^{-/-}$ embryos. Zoomed areas in **C'** and **D'** highlight loss of distal airspaces in Cyp26b1$^{-/-}$ lungs. **E-F**) H&E stain of E18.5 Cyp26b1$^{+/+}$ and Cyp26b1$^{-/-}$ lungs at 10x (**E, F**) and 40x (**E', F'**) demonstrating increased septal wall thickness and smaller airspaces. **G-H**) Representative images of DAPI stains used in quantifications for **I-K**. **I**) Number of DAPI^{+} cells per 0.1 mm^2 demonstrating increased cellularity in the mutants. **J**) Area of open airspaces (>100 μm^2) in Cyp26b1$^{+/+}$, Cyp26b1$^{+/-}$, and Cyp26b1$^{-/-}$ lungs. **K**) The total number of open airspaces (>100 μm^2) per 0.1 mm^2. **L**) Total body weight of E18.5 embryos. **M**) Weight of lungs immediately after dissection (wet) relative to total body weight in E18.5 embryos. **N**) Weight of lungs after drying relative to total body weight in E18.5 embryos. **O**) Ratio of wet lung weight and dry lung weights. Scale bars = 1 mm (**A-D**), 50 μm (**G-H**). Significance was determined using one-way ANOVA with Tukey multiple comparison test. *P<0.05, ***P<0.001, ****P<0.0001.

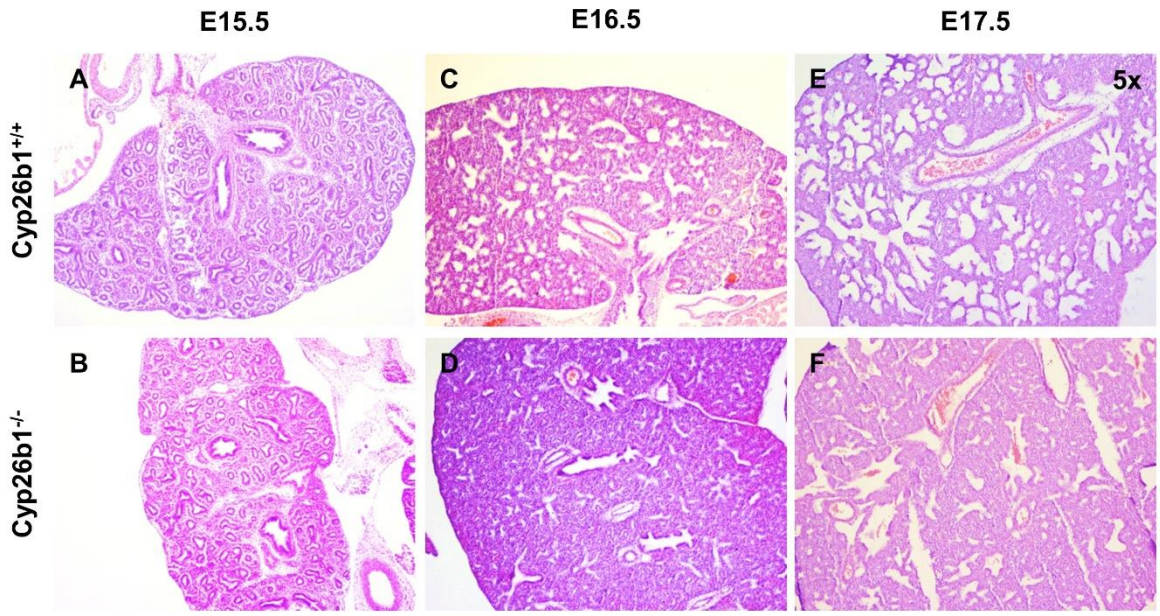

Figure 4.5. Gross histology of Cyp26b1$^{-/-}$ lungs in late gestation. **A-F**) H&E stains of Cyp26b1$^{+/+}$ (**A, C, E**) and Cyp26b1$^{-/-}$ (**B, D, F**) lungs at E15.5 (**A-B**), E16.5 (**C-D**), and E17.5 (**E-F**). Magnification for all images shown.

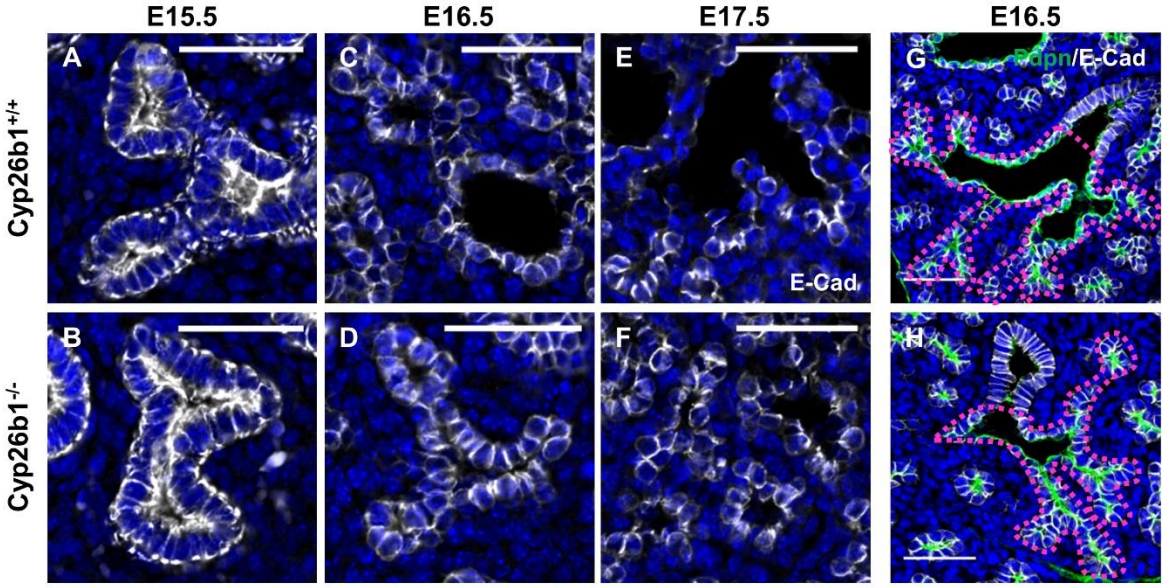

Figure 4.6. Defects in epithelial morphogenesis in Cyp26b1$^{-/-}$ lungs arise at E16.5. **A-F**) H&E of Cyp26b1$^{+/+}$ and Cyp26b1$^{-/-}$ lungs at E15.5 (**A-B**), E16.5 (**C-D**), and E17.5 (**E-F**). **G-L**) Immunofluorescent stains for E-Cad (white) to mark the epithelial structure at E15.5 (**G,H**), E16.5 (**I,J**), and E17.5 (**K,L**). **M-N**) Proximal to distal epithelial transition in E16.5 lungs stained with the AT1 cell marker Pdpn (green) and E-cad (white). Magenta outlines mark distal epithelial tree extending from the terminal bronchiole. Scale bar = 50 μm.

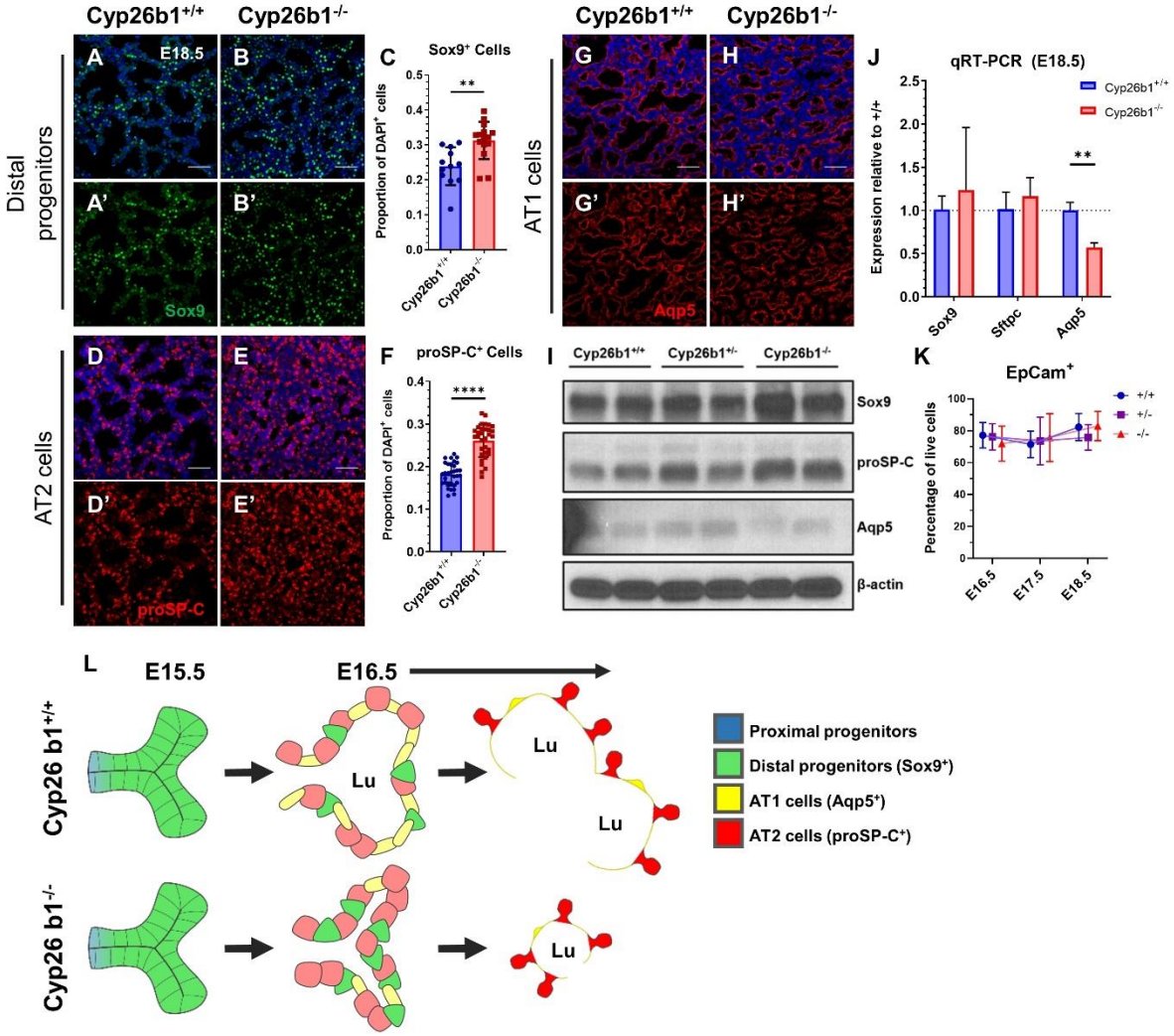

Figure 4.7. Distal epithelial progenitors and AT2 cells are expanded at the expense of AT1 cells in Cyp26b1$^{-/-}$ lungs. A-C) IF stain for the distal progenitor cell marker Sox9 (**A-B**) and quantification of cell counts (**C**). **D-F**) IF stain for the AT2 marker proSP-C (**D-E**) and quantification of cell counts (**F**). Note that the quantifications in both **C** and **F** are standardized to the total number of DAPI^{+} cells. **G-H**) IF stain for Aqp5 to mark AT1 cells. **I**) Western blot analysis of Sox9, proSP-C, and Aqp5 in E18.5 lungs with β-actin as loading control. **J**) qRT-PCR of Sox9, Sftpc, and Aqp5 at E18.5. **K**) Flow cytometry analysis of EpCam^{+}/CD31^{-}/CD45^{-} cells in E16.5 – E18.5 lungs. **L**) Model of distal epithelial maturation between Cyp26b1$^{+/+}$ and Cyp26b1$^{-/-}$ lungs. At E15.5 before Sox9^{+} distal progenitors (green) begin to differentiate, the epithelium resembles a glandular-like structure. Beginning at E16.5, these tips will undergo morphologic changes from a columnar to a squamous epithelium and start forming early AT1 (yellow) and AT2 (red) cells. Concurrently, lumens (Lu) open at this stage forming the early

saccules needed for gas exchange. These cells continue to mature for the rest of embryonic development and postnatally to form the mature functioning alveoli. In Cyp26b1$^{-/-}$ lungs, epithelial development is not affected through E15.5. Once distal differentiation commences, the epithelium is able to alter its morphology towards a more squamous epithelium; however, lumens fail to fully open and the proportion of distal progenitors, AT2, and AT1 cells have shifted. This ultimately results in fewer functional gas-exchanging units with smaller lumens, culminating in neonatal demise. Significance in **C** and **F** was determined using Student's T-Test. Significance in **J** was determined using two-way ANOVA with Sidak multiple comparison test. Scale bar = 50 μm. ***P*<0.01, *****P*<0.0001.

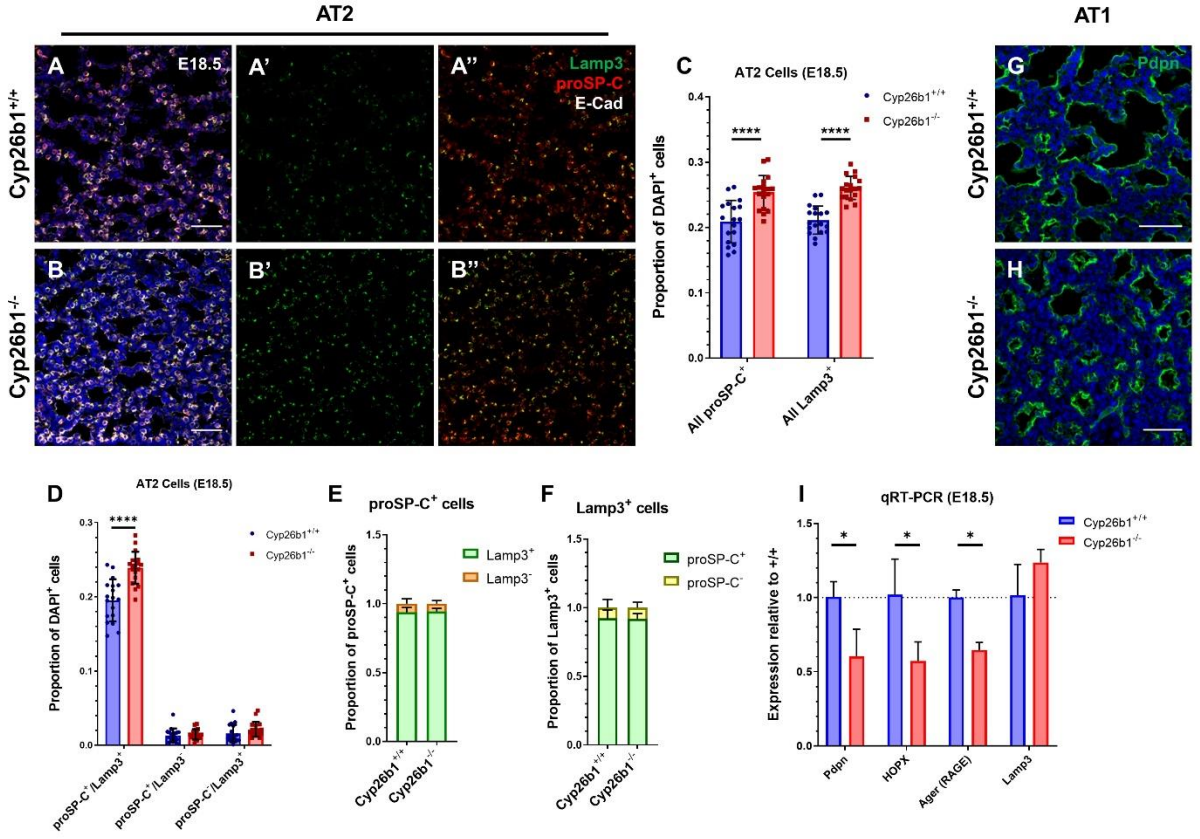

Figure 4.8. Validation of defects in distal epithelial differentiation using independent AT1 and AT2 cell markers. **A-C**) IF stain for the AT2 markers Lamp3 and proSP-C. **C**) Quantification of all proSP-C$^+$ cells and all Lamp3$^+$ cells with respect to DAPI. **D**) Stratification of data shown in **C** into proSP-C/Lamp3 Double positive cells (first set), proSP-C single positive cells (second set), and Lamp3 single positive cells (third set) as a proportion of DAPI$^+$ cells. **E**) Quantification of proSP-C/Lamp3 double positive cells (green) and proSP-C single positive cells (orange) with respect to all proSP-C$^+$ cells. **F**) Quantification of proSP-C/Lamp3 double positive cells (green) and Lamp3 single positive cells (orange) with respect to all Lamp3$^+$ cells. The proportions of proSP-C/Lamp3 double positive, proSP-C single positive, and Lamp3 single positive AT2 cells are the same between Cyp26b1$^{+/+}$ and Cyp26b1$^{-/-}$ lungs. Greater than 90% of all AT2 cells are proSP-C$^+$/Lamp3$^+$. **G-H**) IF stain for the AT1 marker Pdpn. **I**) qRT-PCR analysis for AT1 markers Pdpn, HOPX, and Ager and the AT2 marker Lamp3. Scale bar = 50 μm. Significance was determined using two-way ANOVA with Sidak multiple comparison test. *P<0.05, ****P<0.0001.

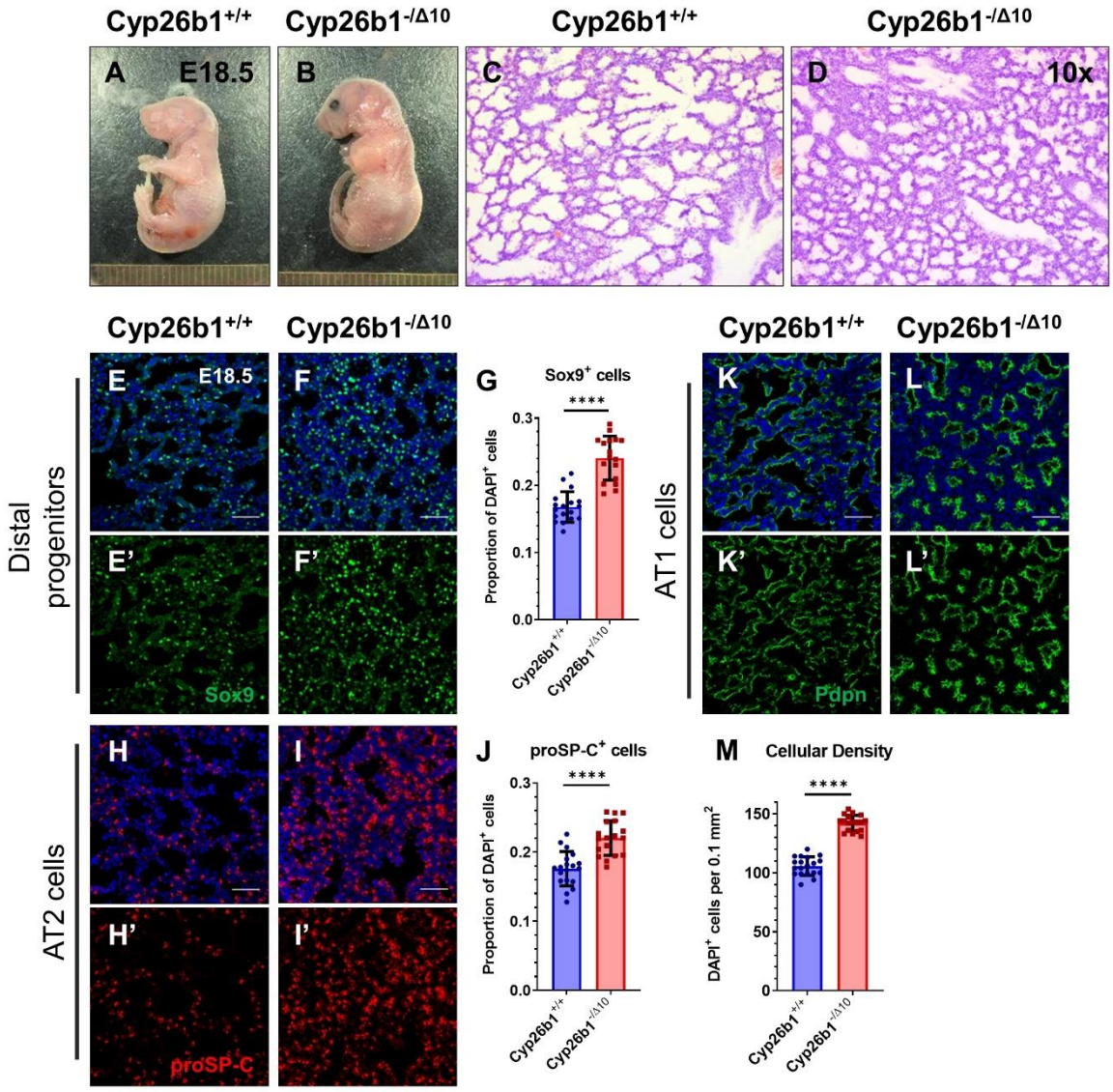

Figure 4.9. Cyp26b1$^{-/\Delta 10}$ lungs phenocopy Cyp26b1$^{-/-}$ lung defects in increased cellular density and distal epithelial differentiation. A-B) E18.5 Cyp26b1$^{+/+}$ and Cyp26b1$^{-/\Delta 10}$ embryos at dissection. **C-D**) H&E stain of E18.5 Cyp26b1$^{+/+}$ and Cyp26b1$^{-/\Delta 10}$ lungs at 10x. **E-G**) IF stain for the Sox9^{+} distal progenitors and quantification relative to DAPI^{+} cells. **H-J**) IF stain for the proSP-C^{+} AT2 cells and quantification relative to DAPI^{+} cells. **K-L**) IF stain for the Pdpn^{+} AT1 cells demonstrating smaller distal airspaces. **M**) Number of DAPI^{+} cells per 0.1 mm^{2} demonstrating increased cellularity in the compound heterozygous mice. Scale bar = 50 μm. Significance was determined using Student's T-Test. ****P<0.0001.

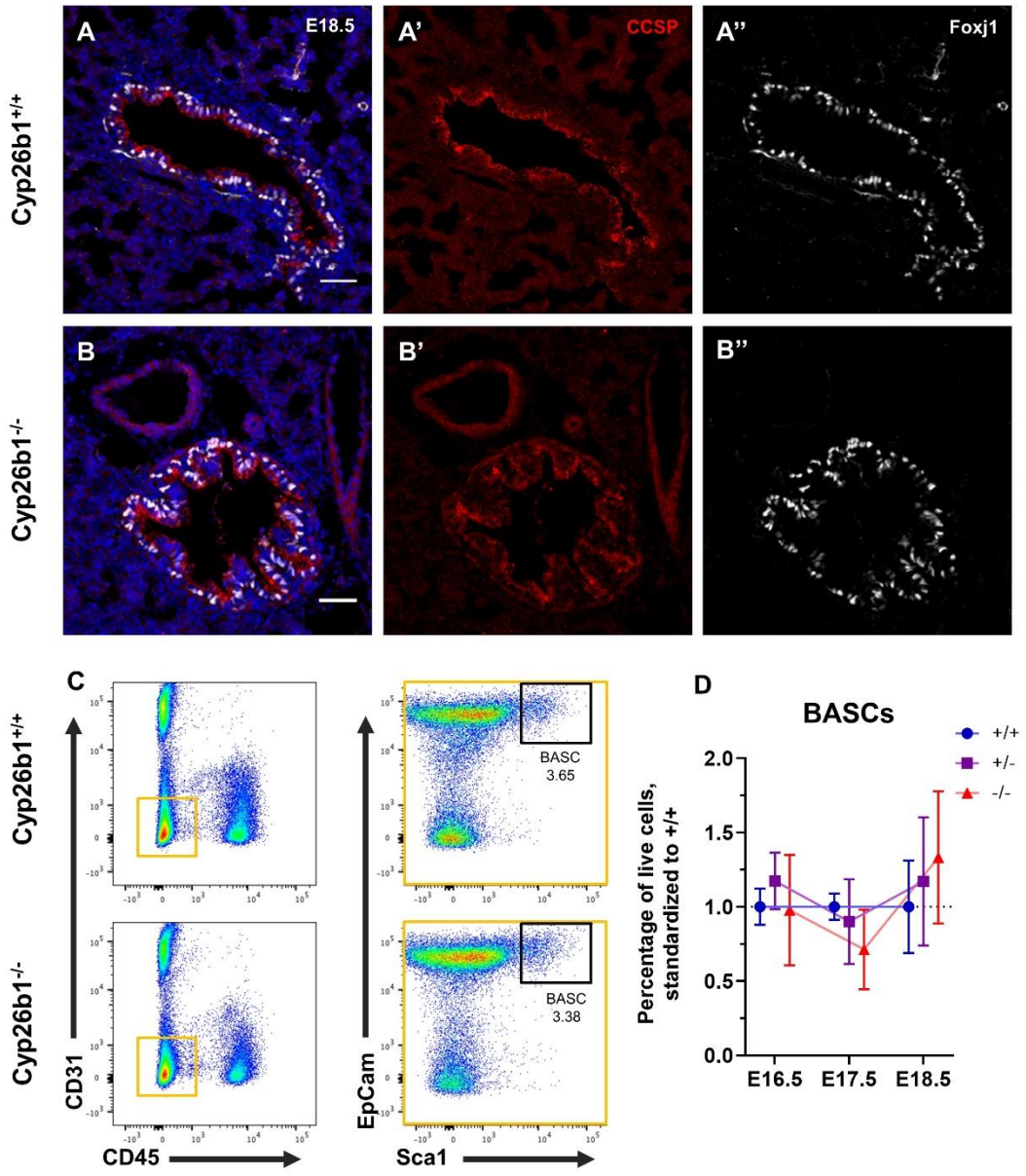

Figure 4.10. Proximal airways are unaffected in Cyp26b1$^{-/-}$ lungs. A-B) IF stains for CCSP (red) and FoxJ1 (white) in E18.5 Cyp26b1$^{+/+}$ (**A**) and Cyp26b1$^{-/-}$ (**B**) lungs. **C**) Flow charts for analysis of BASC populations. **D**) Quantification of the frequency BASCs (CD31^{-}/CD45^{-}/Sca1^{+}/Ep-CAM^{+}) as a proportion of all live cells in E16.5 – E18.5 lungs. Quantifications are standardized to the frequency of BASCs in Cyp26b1$^{+/+}$ samples per experiment. Scale bar = 50 μm.

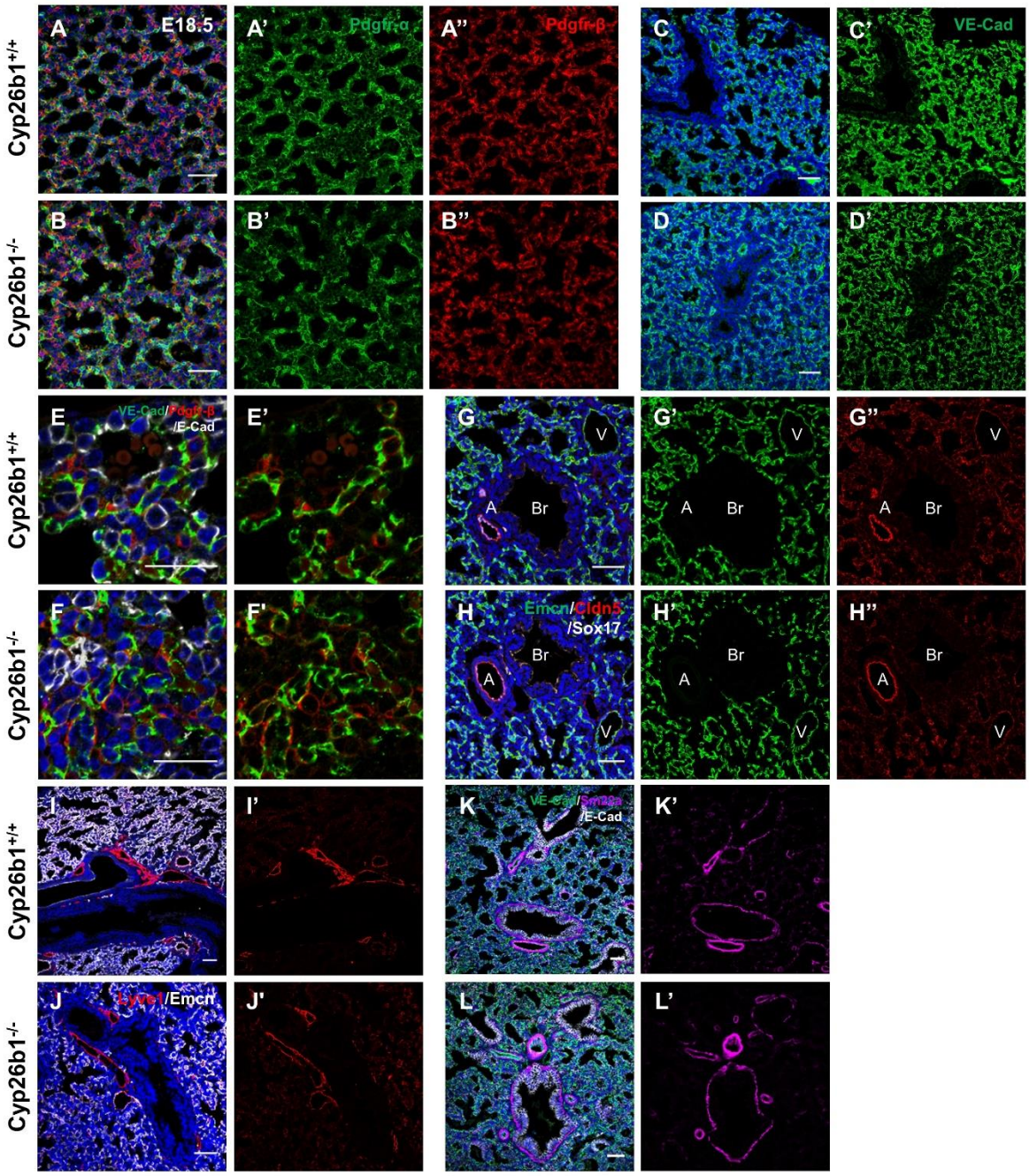
Cyp26b1+/+
Cyp26b1-/-
A
E18.5
A'
Pdgfrα
A''
Pdgfrβ
C
C'
VE-Cad
B
B'
B''
D
D'
E
VE-Cad/Pdgfrβ
/E-Cad
E'
G
V
A
Br
G'
G''
F
F'
H
Emcn/Cldn5
/Sox17
H'
H''
I
I'
K
VE-Cad/Sm22α
/E-Cad
K'
J
Lyve1/Emcn
J'
L
L'

Figure 4.11. Stromal and Vascular lineages are unaffected in Cyp26b1$^{-/-}$ lungs. A-B) If stain for the stromal markers Pdgfr-α (green) and Pdgfr-β (red) in E18.5 lungs. **C-D**) IF stain for the broad EC marker VE-Cad (green). **E-F**) IF stain for VE-Cad (green), Pdgfr-β (red), and E-Cad (white) to examine pericyte-EC interaction. **G-H**) IF stain for Emcn (green), Claudin-5 (red), and Sox17 (white) to differentiate arterial vs venous differentiation. A = artery, V = vein, Br = bronchi/bronchiole. Emcn is expressed in all but arterial ECs while Claudin-5 and Sox17 are more highly expressed in arterial ECs compared to capillary and veinous ECs. **I-J**) If stain for the lymphatic marker Lyve1 (red) and Emcn (white). **K-L**) IF stain for VE-Cad (green), Sm22a (magenta), and E-Cad (white). Scale bar = 50 μm (**A-D,G-L**), 25 μm (**E-F**).

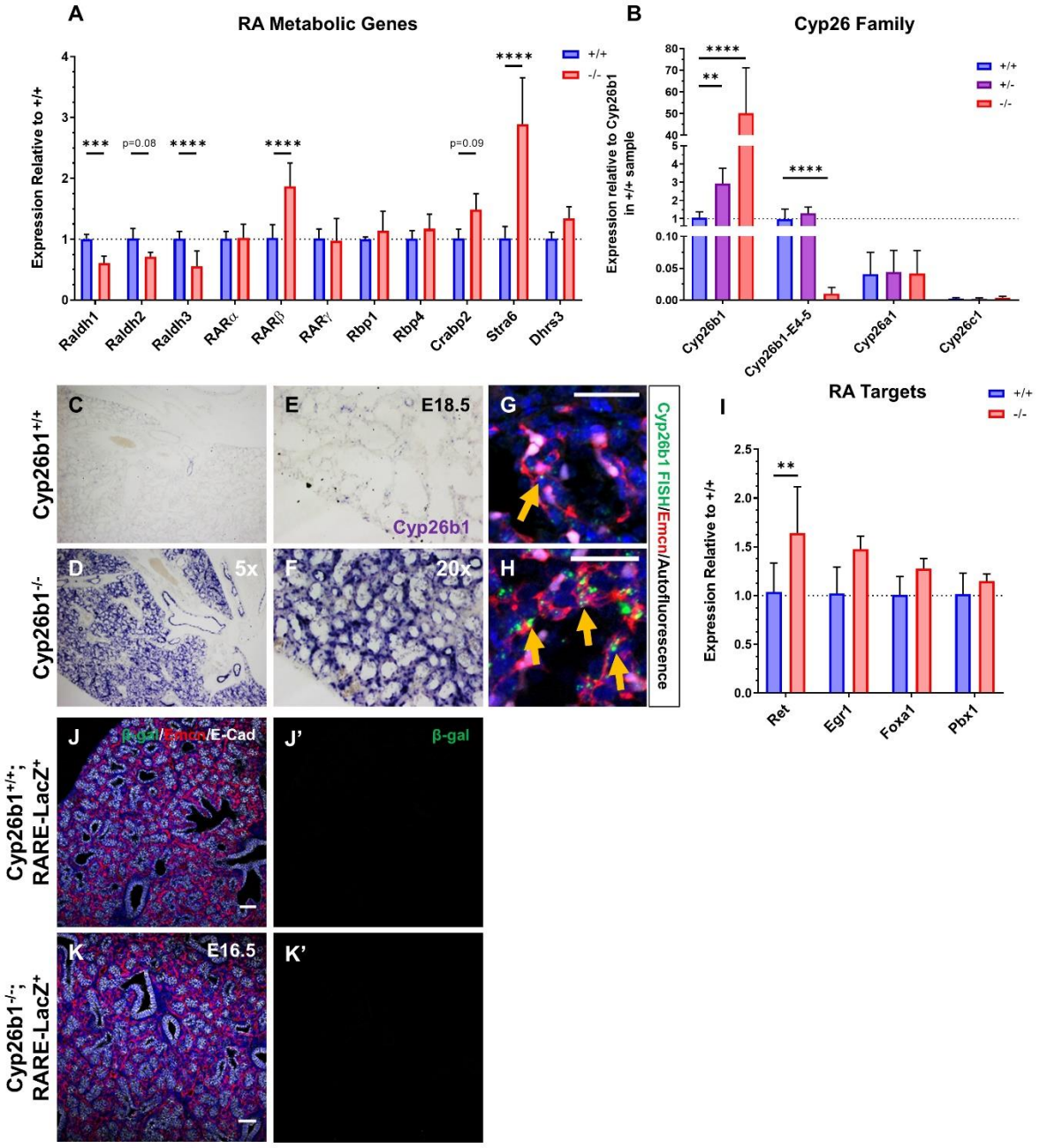

Figure 4.12. Cyp26b1$^{-/-}$ lungs exhibit a mixed RA response. **A**) qRT-PCR for several members of RA metabolism in whole E18.5 lungs. **B**) qRT-PCR for the three Cyp26 family members all standardized to the expression of Cyp26b1 in Cyp26b1$^{+/+}$ samples. Cyp26b1 utilizes primers outside of the deleted region (specifically spanning the intron between Exons 2 and 3) in Cyp26b1^{-} line whereas Cyp26b1-E4-5 utilizes primers designed within the deleted region (specifically spanning the intron between Exons 4 and 5). **C-F**) ISH for Cyp26b1 in

E18.5 Cyp26b1$^{+/+}$ (**C,E**) and Cyp26b1$^{-/-}$ (**D,F**) lungs at 5x (**C-D**) and 20x (**E-F**) zoom. **G-H**) FISH for Cyp26b1 (green) costained with Emcn (red). Orange arrows mark Cyp26b1^{+} punctae in ECs. **I**) qRT-PCR for Ret, Egr1, Foxa1, and Pbx1 in whole E18.5 lungs. **J-K**) IF stains for β-gal (green) to mark RARE-LacZ expression, Emcn (red), and E-Cad (white) in E16.5 RARE-LacZ^{+} Cyp26b1$^{+/+}$ and Cyp26b1$^{-/-}$ lungs. Scale bar = 25 μm (**G-H**), 50 μm (**J-K**). Significance was determined using two-way ANOVA with Sidak multiple comparison test. ***P*<0.01, ****P*<0.001, *****P*<0.0001.

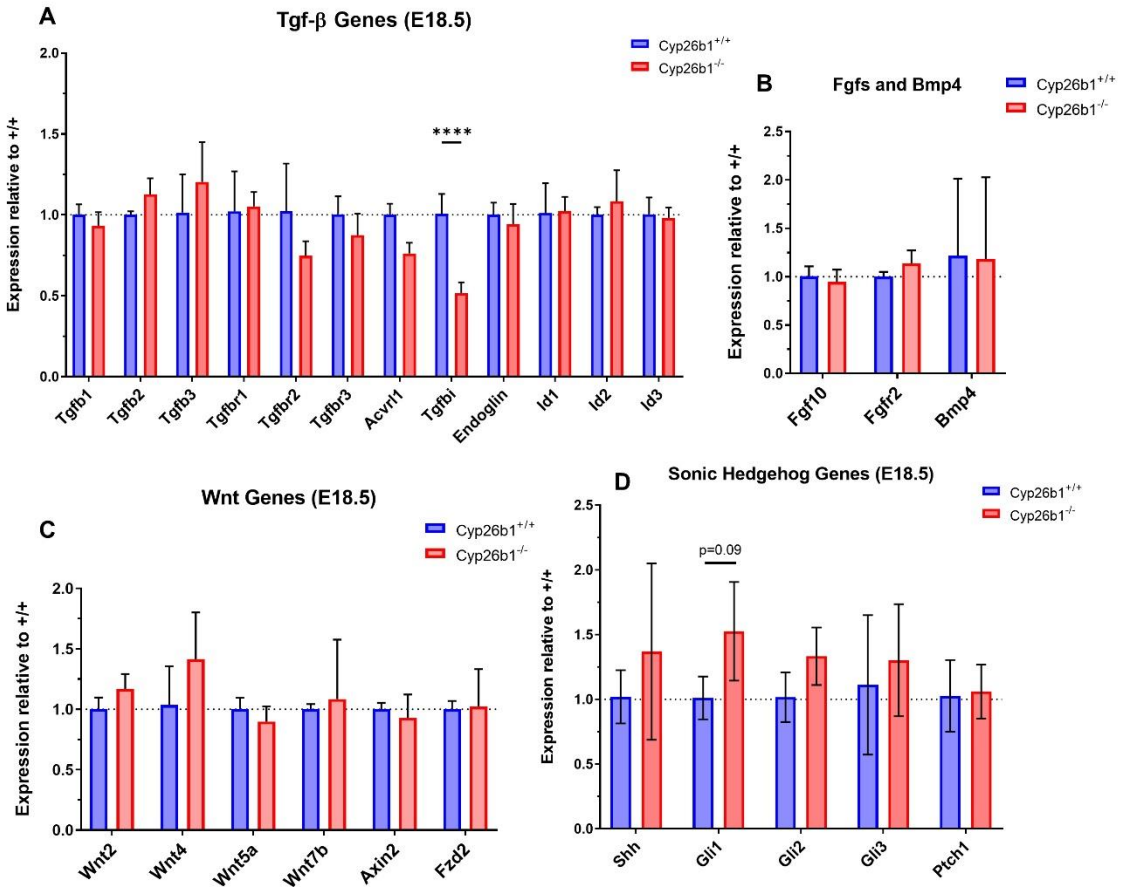

Figure 4.13. Other signaling pathways implicated in lung development are unaffected in Cyp26b1$^{-/-}$ lungs. A) qRT-PCR for members of the Tgf-β signaling pathway. **B**) qRT-PCR for established regulators of lung branching: Fgf10, Fgfr2, and Bmp4. **C**) qRT-PCR for members of the Wnt signaling pathway. **D**) qRT-PCR for members of the Shh signaling pathway. Expression levels are standardized to that in Cyp26b1$^{+/+}$ lungs for each gene. Significance was determined using two-way ANOVA with Sidak multiple comparison test. ****P<0.0001.

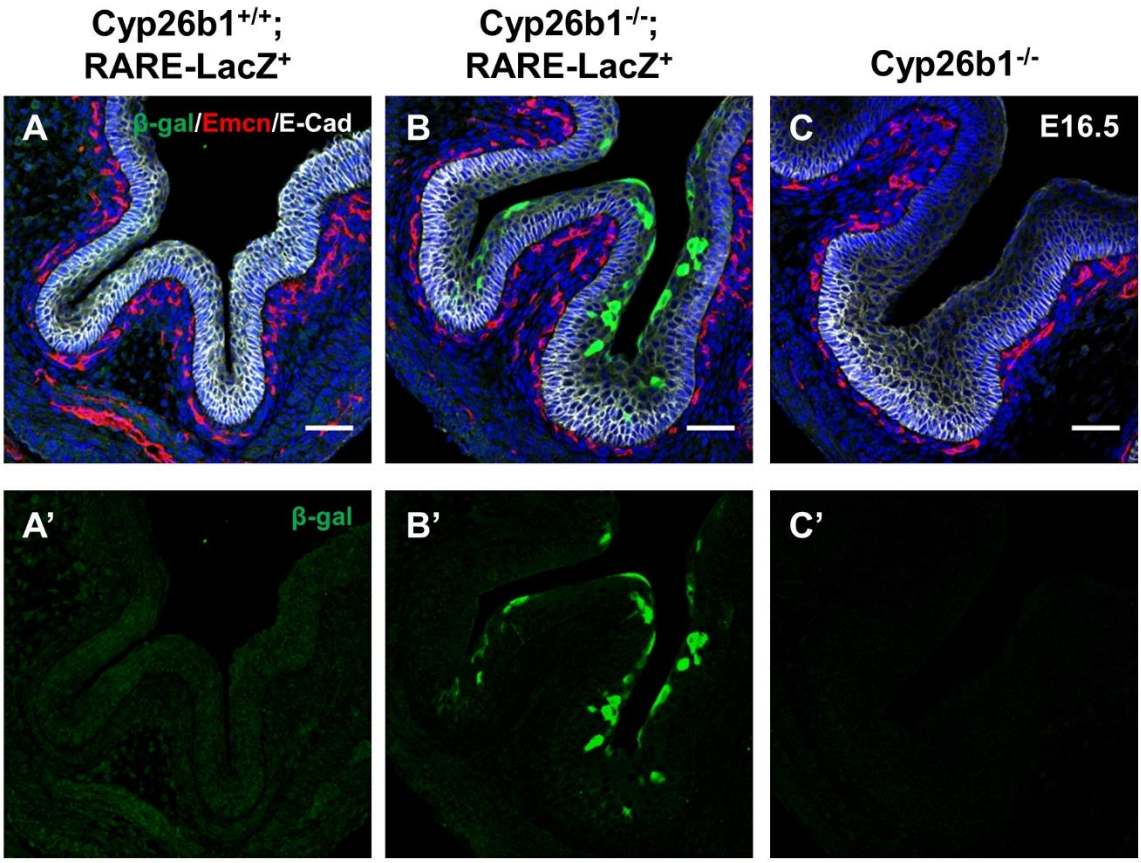

Figure 4.14. Expression of RARE-LacZ transgene in the stomach. A-C) IF stains of β-gal (green), Emcn (red), and E-Cad (white) in E16.5 Cyp26b1$^{+/+}$;RARE-LacZ^{+} (**A**), Cyp26b1$^{-/-}$;RARE-LacZ^{+} (**B**), and Cyp26b1$^{-/-}$ (**C**) stomachs. Scale bar = 50 μm.

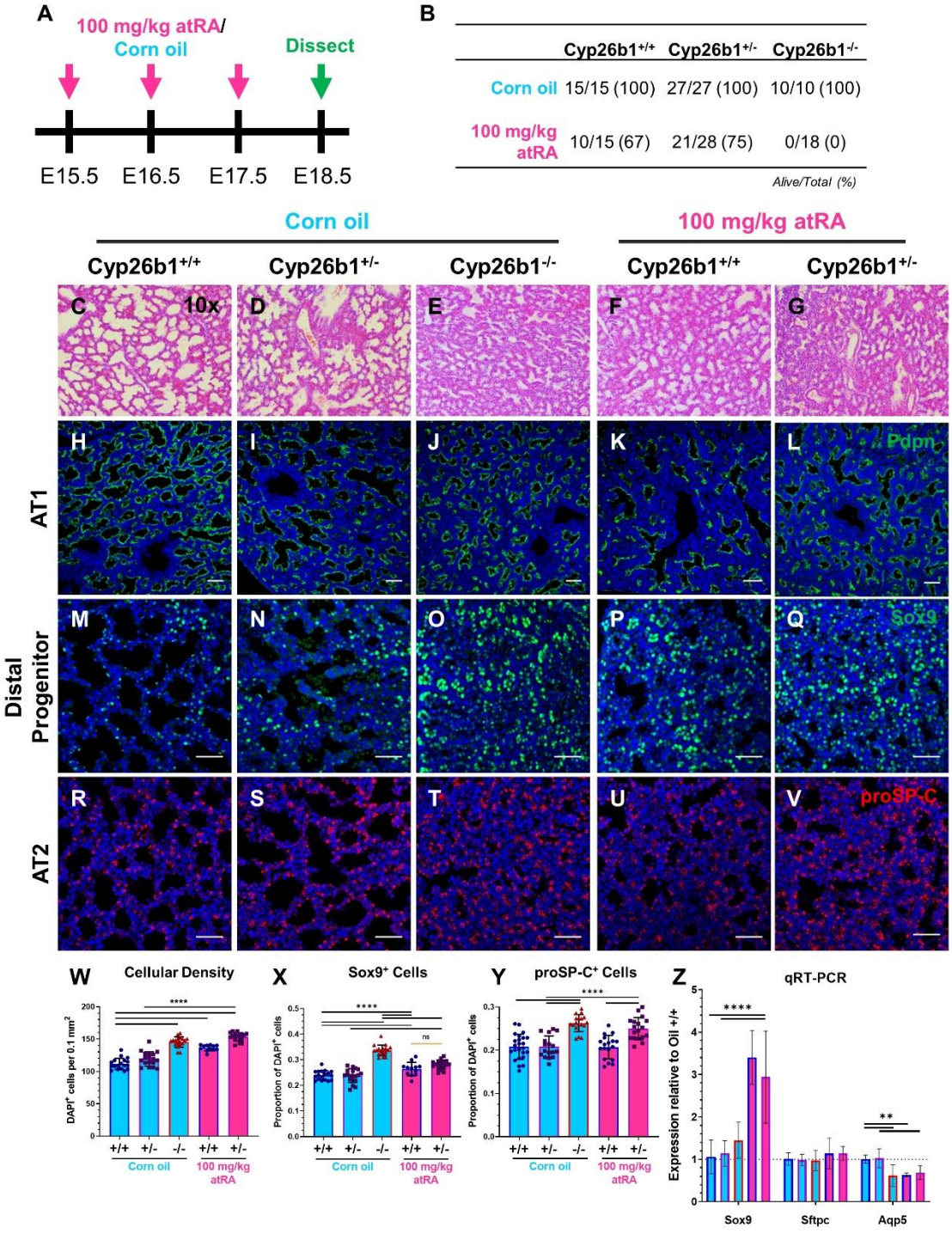

Figure 4.15. Exogenous atRA partially recapitulates loss of Cyp26b1. **A**) Experimental design for experiments with exogenous atRA. 100 mg/kg atRA (magenta) or equivalent dose of corn oil (control, cyan) will be gavaged to pregnant dams at E15.5, E16.5, and E17.5 and

dissected at E18.5. **B**) Survival chart for embryos at the time of dissection for each genotype and treatment option. **C-G**) H&E stains of control (**C-E**), and atRA-treated (**F-G**) lungs at 10x magnification. **H-L**) IF stain for the AT1 cell marker Pdpn in control (**H-J**) and atRA-treated (**K-L**) lungs. **M-Q**) IF stain for the distal epithelial progenitor marker Sox9 in control (**M-O**) and atRA-treated (**P-Q**) lungs. **R-V**) IF stain for AT2 cell marker proSP-C in control (**R-S**) and atRA-treated (**U-V**) lungs. **W**) Number of $DAPI^+$ cells per 0.1 mm^2 demonstrating increased cellularity in the control $Cyp26b1^{-/-}$ and atRA-treated $Cyp26b1^{+/+}$ and $Cyp26b1^{+/-}$ lungs. Outline color corresponds to genotype (blue = $Cyp26b1^{+/+}$, purple = $Cyp26b^{+/-}$, red = $Cyp26b1^{-/-}$) and fill color corresponds to treatment group (cyan = control, magenta = atRA) **X**) Quantification of $Sox9^+$ cells in **M-Q** following the same coloring scheme in **W**. **Y**) Quantification of proSP-C^+ cells in **R-V** following the same coloring scheme in **W**. **Z**) qRT-PCR for Sox9, Sftpc, and Aqp5 in control and atRA-treated lungs following the same coloring scheme in **W**. Scale bar = 50 μm. Significance in **W-Y** was determined using one-way ANOVA with Tukey multiple comparison test. Significance in **Z** was determined using two-way ANOVA with Sidak multiple comparison test. $^{**}P<0.01$, $^{****}P<0.0001$.

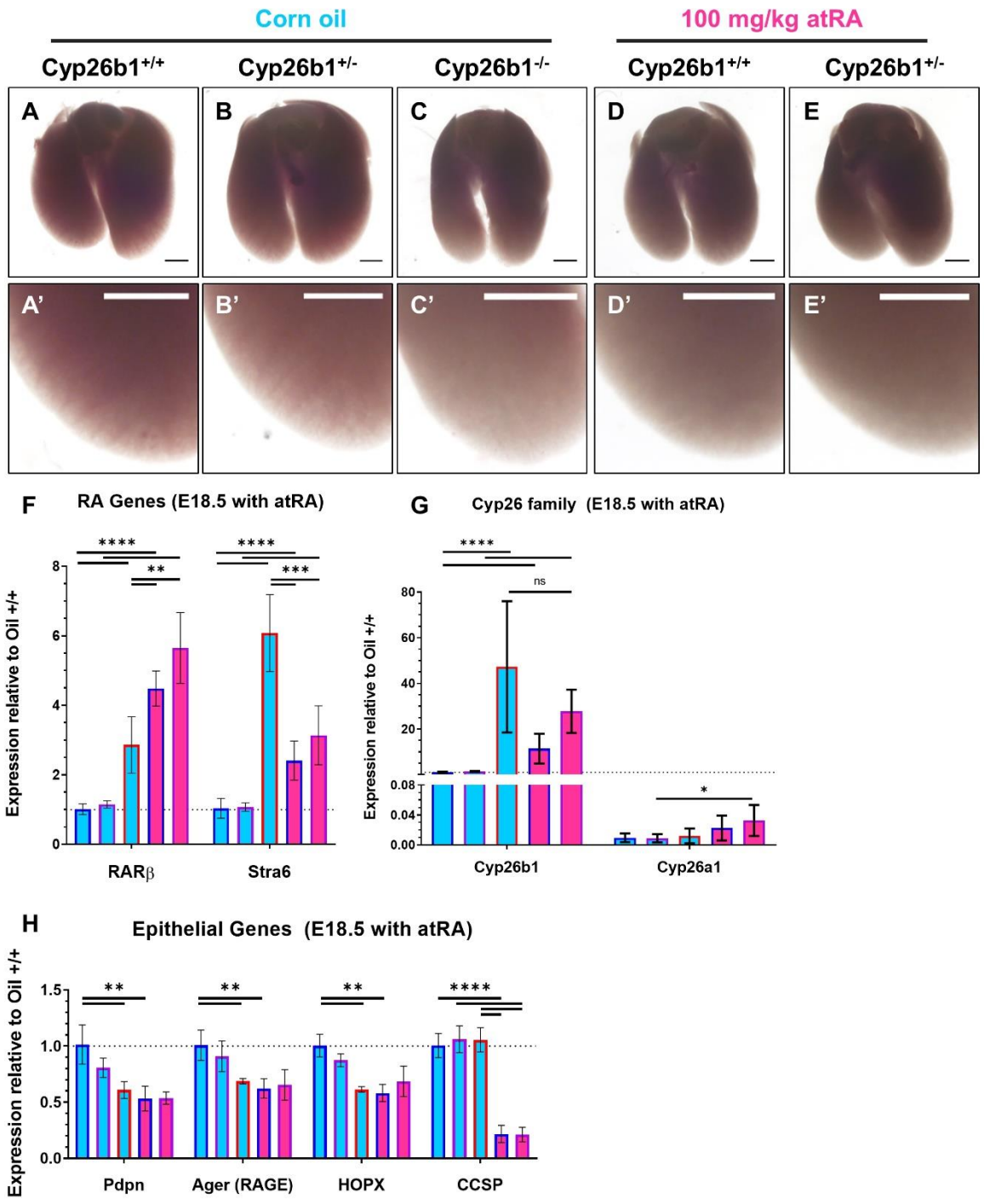

Figure 4.16. Morphologic and transcriptional changes in RA and epithelial genes with atRA treatment. **A-E**) Lungs from E18.5 control (**A-C**) and atRA-treated (**D-E**) Cyp26b1$^{+/+}$, Cyp26b1$^{+/-}$, and Cyp26b1$^{-/-}$ lungs at time of dissection. Magnified views of the left lobe are shown in **A'**, **B'**, **C'**, **D'**, and **E'** to highlight loss of distal airspaces in Cyp26b1$^{-/-}$ and atRA-

treated Cyp26b1$^{+/+}$ and Cyp26b1$^{+/-}$ lungs. **F**) qRT-PCR for RARβ and Stra6. Outline color corresponds to genotype (blue = Cyp26b1$^{+/+}$, purple = Cyp26b$^{+/-}$, red = Cyp26b1$^{-/-}$) and fill color corresponds to treatment group (cyan = control, magenta = atRA). **G**) qRT-PCR for Cyp26b1 and Cyp26a1 following the same coloring scheme in **F**. **H**) qRT-PCR for the epithelial genes Pdpn, Ager, HOPX, and CCSP following the same coloring scheme in **F**. Scale bar = 1 mm. Significance was determined using two-way ANOVA with Sidak multiple comparison test. **P*<0.05, ***P*<0.01, ****P*<0.001, *****P*<0.0001.

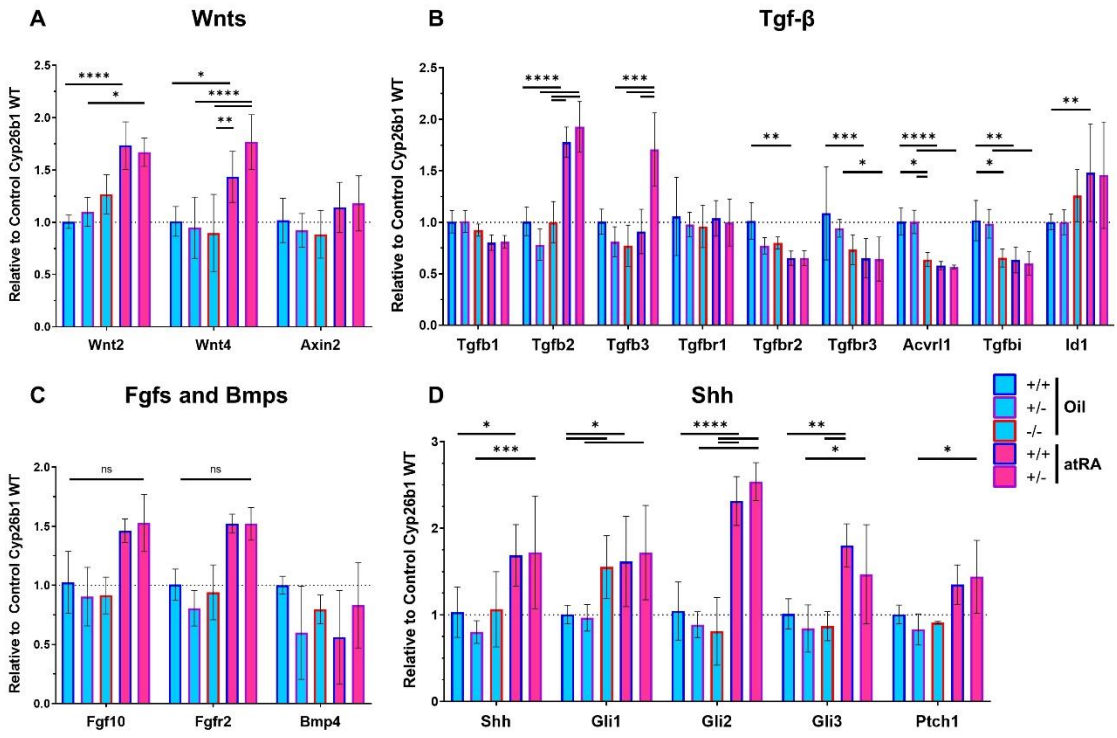

Figure 4.17. Exogenous atRA induces distinct transcriptional changes compared to Cyp26b1$^{-/-}$ lungs. **A**) qRT-PCR for the Wnt pathway genes Wnt2, Wnt4, and Axin2. Outline color corresponds to genotype (blue = Cyp26b1$^{+/+}$, purple = Cyp26b$^{+/-}$, red = Cyp26b1$^{-/-}$) and fill color corresponds to treatment group (cyan = control, magenta = atRA). **B**) qRT-PCR for members of the TGF-β signaling pathway following the same coloring scheme in **A**. **C**) qRT-PCR for established regulators of lung branching following the same coloring scheme in **A**. **D**) qRT-PCR for members of the Shh pathway following the flooring scheme in **A**. Significance was determined using two-way ANOVA with Sidak multiple comparison test. **P*<0.05, ***P*<0.01, ****P*<0.001, *****P*<0.0001.

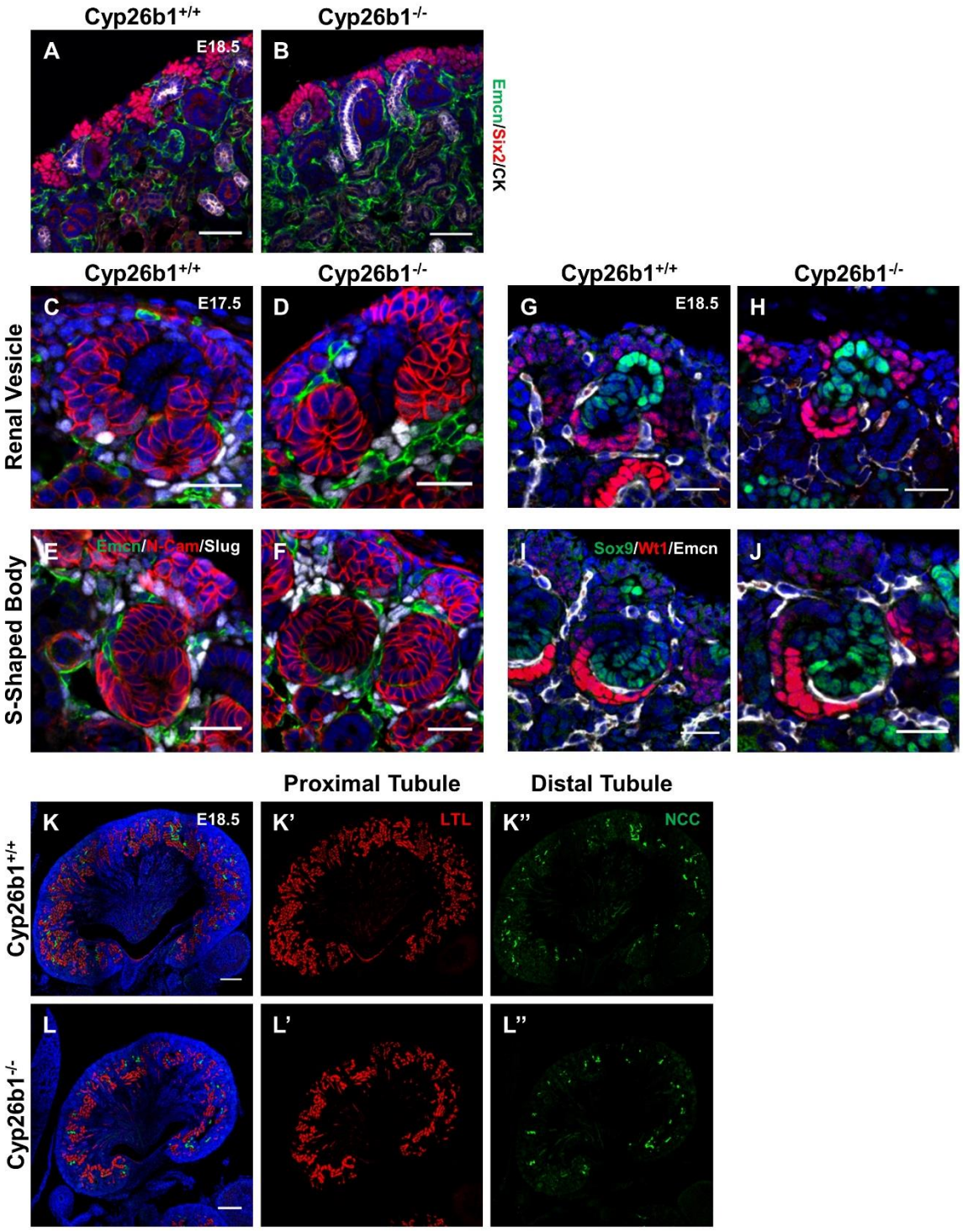

Figure 4.18. Kidney epithelial differentiation is unaffected in Cyp26b1$^{-/-}$ kidneys. A-B) IF stain of the outer cortex of E18.5 Cyp26b1$^{+/+}$ and Cyp26b1$^{-/-}$ kidneys for Emcn (green, ECs), Six2 (red, NPCs), and pan-Cytokeratin (white). **C-F**) If stain for N-cam (red) to highlight the

structure of the renal vesicle (**C-D**) and S-Shaped body (**E-F**) stages of nephron development. **G-J**) IF stain of renal vesicle (**G-H**) and S-Shaped body (**I-J**) stages marked with Wt1 (red) and Sox9 (green) to mark the cells destined to become proximal and distal tubules, respectively. **K-L**) E18.5 kidneys stained for LTL (red) and NCC (green) to mark mature proximal and distal tubules, respectively. Scale bar = 50 μm (**A-B**), 25 μm (**C-J**), 250 μm (**K-L**).

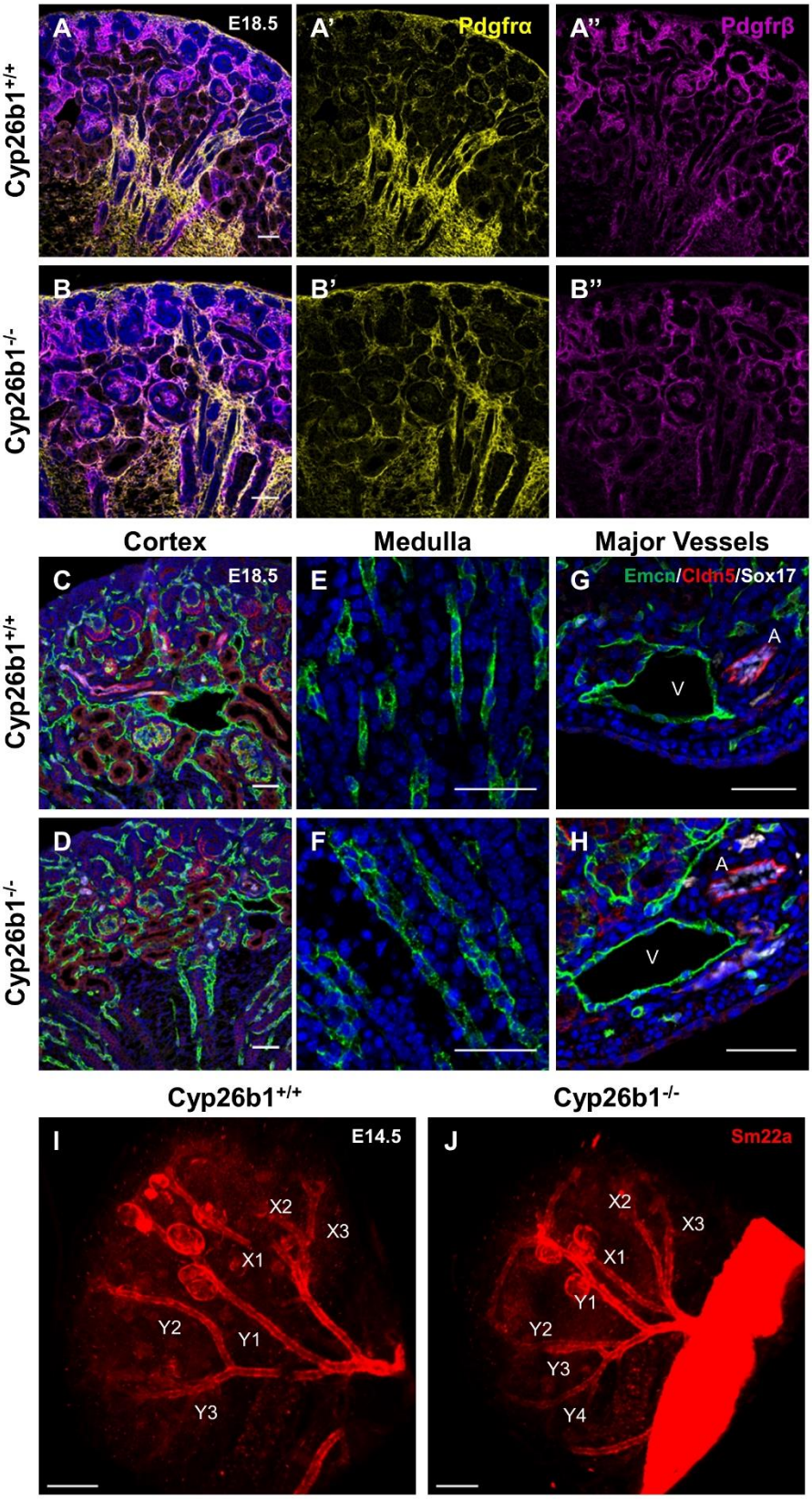
A
E18.5
A'
Pdgfrα
A''
Pdgfrβ
Cyp26b1+/+
B
B'
B''
Cyp26b1-/-
Cortex
Medulla
Major Vessels
C
E18.5
E
G
Emcn/Cldn5/Sox17
A
V
D
F
H
A
V
Cyp26b1+/+
Cyp26b1-/-
I
E14.5
X2
X3
X1
Y2
Y1
Y3
J
Sm22a
X2
X3
X1
Y1
Y2
Y3
Y4

Figure 4.19. Stromal and EC lineages are unaffected in Cyp26b1$^{-/-}$ kidneys. A-B) IF stain of the stromal markers Pdgfrα (yellow) and Pdgfrβ (magenta) in E18.5 kidneys. C-H) IF stain of Emcn (green), Claudin-5 (red), and Sox17 (white) focusing on the cortex (C-D), medulla (E-F), and major vessels (G-H) in E18.5 kidneys. A = artery, V = vein. I-J) IF of whole mount E14.5 stained with Sm22a to outline the arterial tree. Individual lobar branches are labeled by a letter to signify which major artery from which it arises and a number. Scale bar = 50 μm (A-H), 150 μm (I-J).

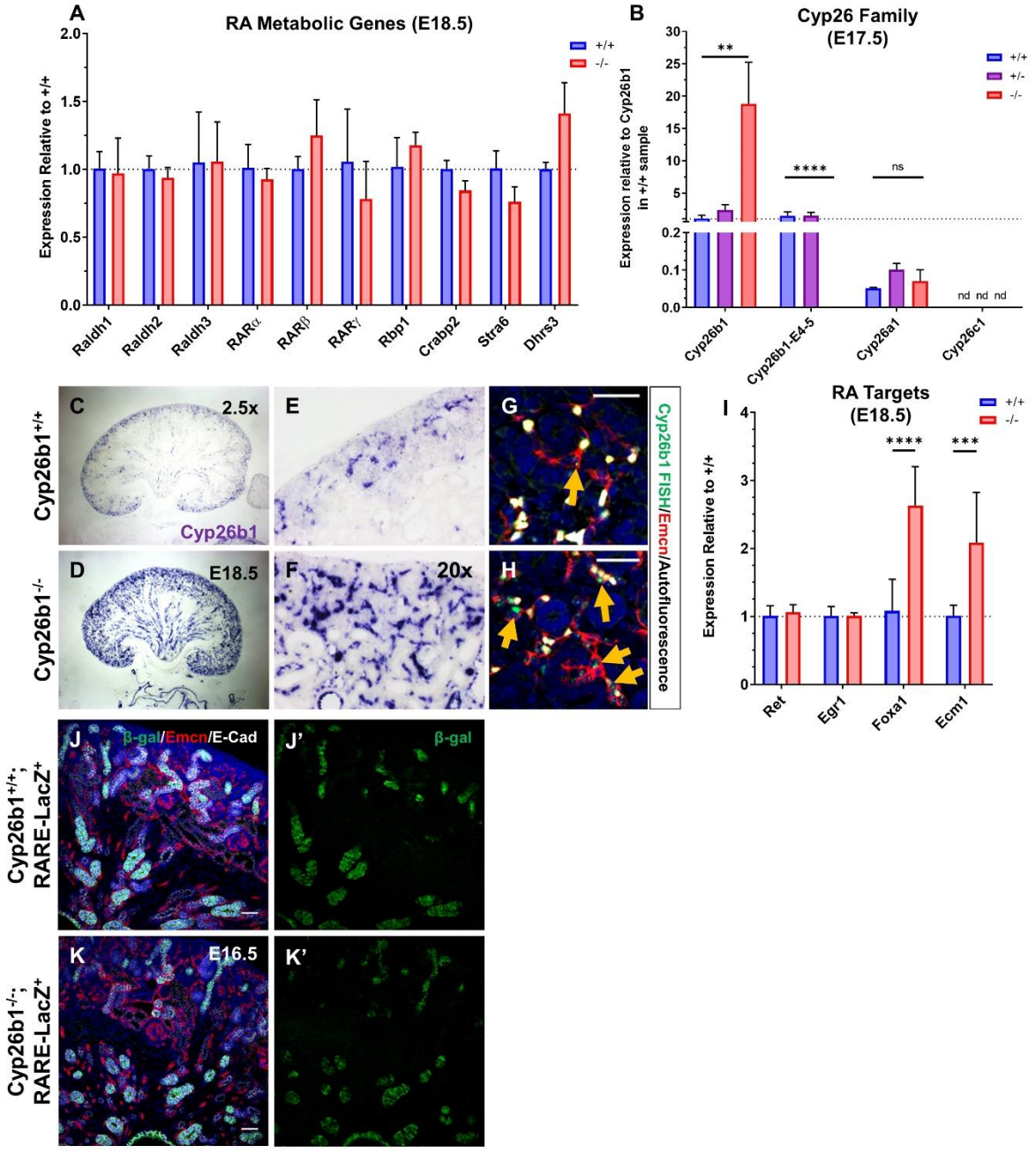

Figure 4.20. Cyp26b1$^{-/-}$ kidneys exhibit little RA response. **A**) qRT-PCR for several members of RA metabolism in whole E18.5 kidneys. **B**) qRT-PCR for the three Cyp26 family members all standardized to the expression of Cyp26b1 in Cyp26b1$^{+/+}$ samples in E17.5 kidneys. Cyp26b1 utilizes primers outside of the deleted region (specifically spanning the intron between Exons 2 and 3) in Cyp26b1^{-} line whereas Cyp26b1-E4-5 utilizes primers designed within the deleted region (specifically spanning the intron between Exons 4 and 5).

ND = not detected. **C-F**) ISH for Cyp26b1 in E18.5 Cyp26b1$^{+/+}$ (**C,E**) and Cyp26b1$^{-/-}$ (**D,F**) kidneys at 2.5x (**C-D**) and 20x (**E-F**) zoom. **G-H**) FISH for Cyp26b1 (green) costained with Emcn (red). Orange arrows mark Cyp26b1^{+} punctae in ECs. **I**) qRT-PCR for Ret, Egr1, Foxa1, and Pbx1 in whole E18.5 kidneys. **J-K**) IF stains for β-gal (green) to mark RARE-LacZ expression, Emcn (red), and E-Cad (white) in E16.5 RARE-LacZ^{+} Cyp26b1$^{+/+}$ and Cyp26b1$^{-/-}$ kidneys. Scale bar = 25 μm (**G-H**), 50 μm (**J-K**). Significance was determined using two-way ANOVA with Sidak multiple comparison test. ***P*<0.01, ****P*<0.001, *****P*<0.0001.

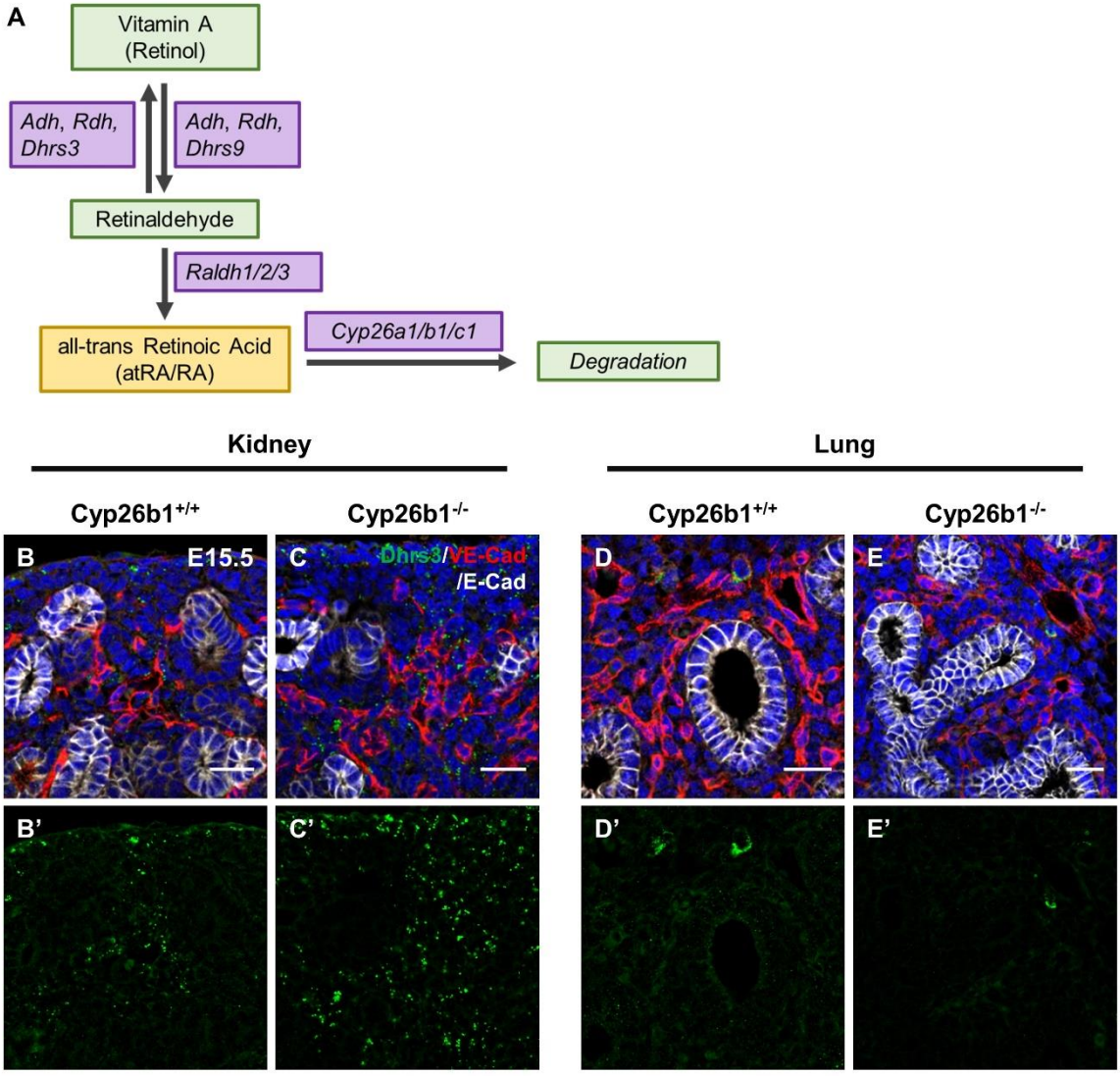

Figure 4.21. Dhrs3 protein is more abundant in Cyp26b1$^{-/-}$ kidneys, but not lungs. **A**) Model of RA metabolic pathway. Metabolites are marked in green or yellow boxes and enzymes are marked in purple boxes. **B-E**) IF stain for Dhrs3 (green), VE-Cad (red), and E-Cad in E15.5 kidneys (**B-C**) and lungs (**D-E**). Scale bar = 50 μm.

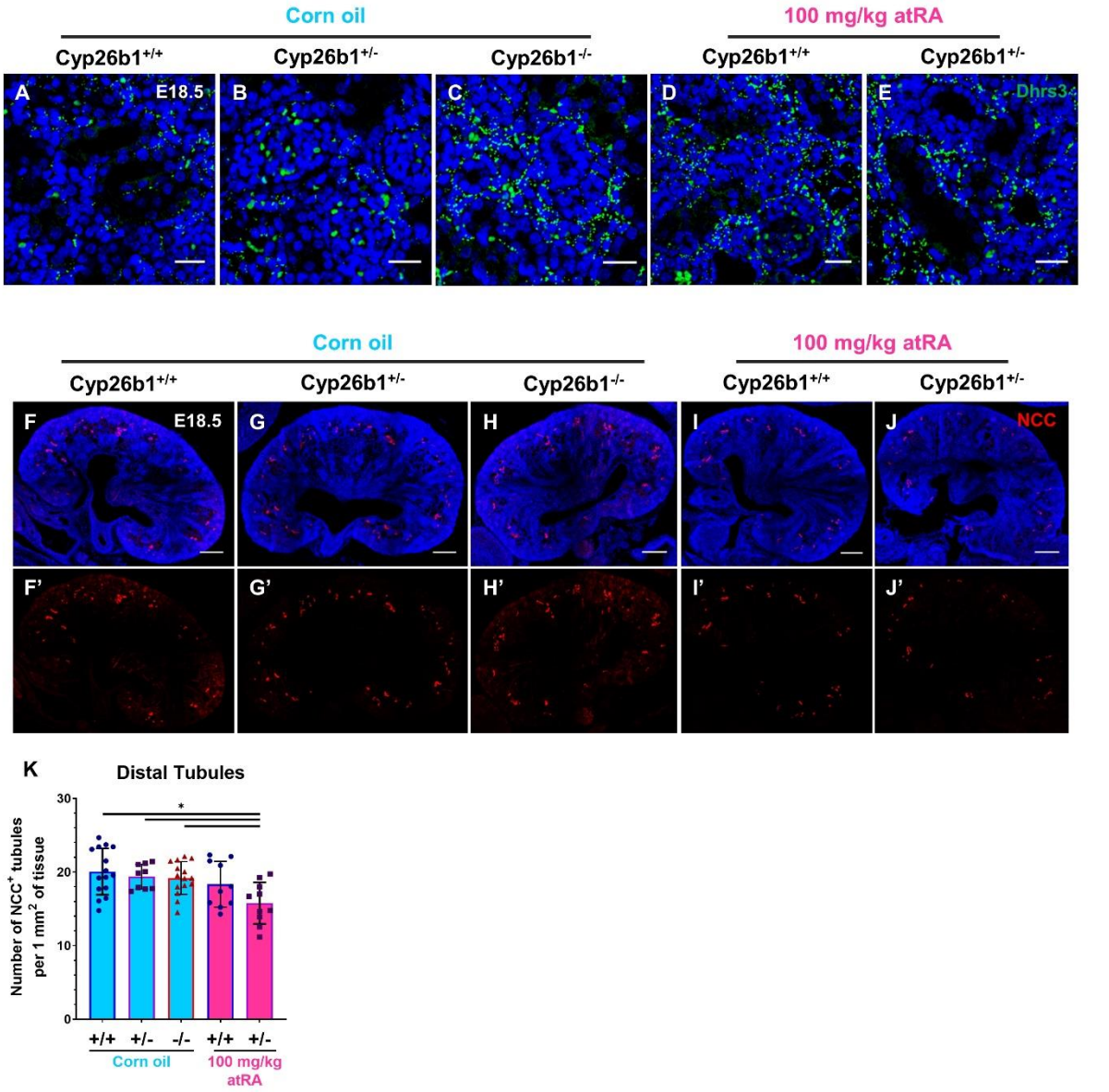

Figure 4.22. Exogenous atRA induces Dhrs3 expression and decreases distal tubule formation. **A-E**) IF stain of the cortex of control (**A-C**) and atRA-treated (**D-E**) kidneys for Dhrs3 (green) and DAPI (blue). **F-J**) IF stain of control (**F-H**) and atRA-treated (**I-J**) kidneys for the distal tubule marker NCC (red) and DAPI (blue). **K**) Quantification of the number of NCC+ tubules per section, standardized to the total area of the section. Scale bar = 25 μm (**A-E**), 250 μm (**F-J**). Significance was determined using one-way ANOVA with Tukey multiple comparison test. **P*<0.05.

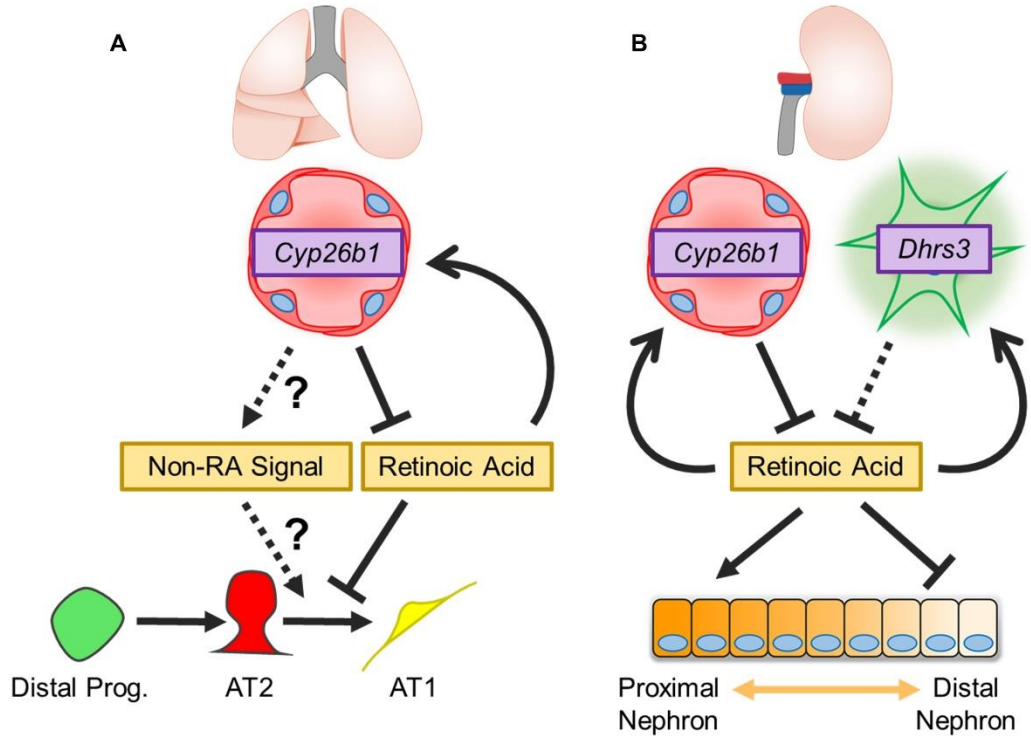

Figure 4.23. Mechanisms of RA inhibition between the lung and kidney. **A**) In the lung, Cyp26b1 is highly expressed in ECs. Cyp26b1 works through potentially two separate mechanisms to promote distal epithelial differentiation. First, Cyp26b1 directly decreases RA signaling through catabolism of RA. The decrease in RA signaling promotes differentiation of AT2 cells (red) into AT1 cells (yellow). Cyp26b1 itself is a target of RA, creating a negative feedback loop to maintain proper RA levels during development. Additionally, Cyp26b1 appears to affect a second, independent pathway – either inhibiting a pathway that blocks differentiation or activating a pathway that promotes differentiation – through an undetermined mechanism (dotted lines). **B**) RA handling during kidney development follows some of the same paradigms as that in the lung, but also exhibits unique differences. Analogous to what is observed in the lung, RA blocks the formation of distal nephron segments and kidney ECs express Cyp26b1 in order to decrease RA signaling. However, the kidneys possess an additional ability to reduce RA activity through Dhrs3. Unlike Cyp26b1, Dhrs3 – expressed predominately in stromal cells – modulates RA levels indirectly by reducing the amount of the immediate RA precursor retinaldehyde (Dotted line, refer to Fig. K4 for model). Dhrs3 and Cyp26b1 appear to be able to compensate for one another as both Dhrs3 and Cyp26b1 are targets of RA in the kidney and distal nephron development was abrogated only in Cyp26b1$^{+/-}$ kidneys treated with atRA. Therefore, the kidneys are protected from excess RA via two separate and compensatory mechanisms while the lungs rely exclusively on just one.

CHAPTER FIVE

CONCLUSIONS AND FUTURE DIRECTIONS

The research presented in this thesis aims to further define how ECs regulate organ development. The goal of my thesis was two-fold. First, I sought out to characterize renal vascular development and establish a set of tools that can be used for future work analyzing the kidney vasculature. Second, I identified and analyzed the EC-enriched gene Cyp26b1 and its role in regulating development of the lung and kidney. In this chapter, I will summarize each of these stories and discuss the relevant future directions to continue to move this science forward.

Chapter 3: Spatiotemporal heterogeneity and patterning of developing renal blood vessels

Summary

ECs during kidney organogenesis exhibit predictable patterns of organization. Kidney primordia are vascularized as early as E11.5 and contain a surrounding plexus of ECs. Arteries are first evident beginning at E13.5 and mature from the hilum towards the outer parts of the cortex. The renal arterial tree branches in a varied, but predictable structure with 2 major branches that divide into 3-4 smaller branches by E14.5. As the kidney continues to mature, ECs show clear signs of specification as “traditional” EC markers develop increasingly stark heterogeneity that varies by location and time. Similarly, ECs organize around the developing epithelial populations in easily identifiable patterns. ECs circumscribe NPC caps but generally

avoid NPCs. During nephron formation, ECs enrich along the portion of the nephron destined to become distal tubule and are relatively sparse around the region destined to become proximal tubule. Lastly, transcriptomic analysis identified at least 100 novel genes that are enriched in kidney ECs during development (**Table 3.1**).

Future Directions

The data presented in this chapter establish the normal pattern of renal endothelial development. Future studies that focus on genes or processes that alter kidney development can use these data as the benchmark to assess for changes in the developing renal vasculature. In this sense, the data presented provide a set of tools and a strong foundation for all future work analyzing renal vascular development. Additionally, these observations have generated new questions that can drive studies. First, where does the arterial tree come from? Does the arterial tree derive from an angiogenic sprout from the aorta, remodeling of the existing vascular plexus towards an arterial fate, or a mixture of both? Why does it arise at E13.5 and not earlier? At this stage, a large vascular plexus still exists that connects renal ECs with those in the surrounding mesenchyme in addition to the early arteries. How are these ECs pruned such that only a renal artery and vein are left in the mature organ? Additionally, what are the factors that determine its structure and specification? Previous studies have clearly implicated the stroma as a major signaling center that regulates regulating arterial formation (Hurtado et al., 2015; Lin et al., 2014) but it is unclear if there are EC-intrinsic mechanisms that determine this fate as well.

During epithelial development, ECs show clear patterning around different epithelial structures, hinting that endothelial-epithelial crosstalk may play key roles in their respective developmental trajectories. ECs preferentially cluster away from NPCs, circumscribing individual caps instead of penetrating them. This organization suggests that ECs may repel NPCs or vice versa. Although one study identified Sema3f as a potential repellant cue emanating from NPCs, they failed to observe any difference in the structure of ECs or NPCs when Sema3f or its EC-enriched receptor Nrp2 were deleted (Munro et al., 2017a). Despite these negative data, there is redundancy from the many chemotrophic factors that may influence proper EC-NPC organization that have yet to be identified. Likewise, EC enrichment around the developing distal nephron also suggests potential endothelial-epithelial interactions that promote distal nephron development or inhibit proximal nephron formation. Currently, there are no studies that have identified if and how ECs pattern the nephron outside of the glomerulus.

Key in answering these questions is identifying genes that may be important for these processes. To that end, our RNA-seq analysis has generated numerous novel EC-enriched genes that may be important for kidney endothelial, epithelial, and stromal developments. I chose Cyp26b1 to study further, but there are many other genes on that list that have not been explored at all in the context of kidney development. Furthermore, Genepaint analysis was only able to screen through approximately half of the 417 genes identified; therefore, there are most likely even more EC-enriched genes than our validation has identified. This list will be a treasure trove to identify key signals emanating from ECs that regulate kidney organogenesis.

Systematic and functional analyses of these genes through genetic and pharmacologic approaches will reveal new areas of renal developmental biology.

An additional advantage of this list is the identification of kidney EC-specific or regional genes that can lead to the generation of new tools for kidney research. Here, I highlighted Rsad2, a gene that appears to be expressed only in kidney ECs and hematopoietic cells in the liver throughout the entire embryo. To date, Rsad2 exhibits the most restricted expression in the kidney vasculature compared to all other cell types in the embryo. I attempted to take advantage of this expression pattern by generating a mouse line with an inducible Cre transgene driven by the endogenous Rsad2 promoter using CRISPR/Cas9. If successful, this will be the first instance of a kidney vascular-specific Cre line available. This mouse line will be an incredibly powerful tool to study kidney development as it bypasses a major limitation of the currently available vascular-specific Cre lines (VE-Cad-CreERT2 and Tie2-Cre). The main limitation of these Cre lines is that they are broadly expressed in the entire vascular system; therefore, deletion of specific genes that cause broad cardiovascular defects may lead to indirect effects on kidney development, confounding our ability to properly study kidney development. Because Rsad2 is specifically expressed in renal ECs, the Rsad2-CreERT2 mouse line circumvents this issue and allows us to more directly assess how loss of a gene in kidney ECs affects kidney development without affecting the vasculature as a whole. Although I was able to achieve proper insertion of the transgene, the CreERT2 allele did not appear to be functional. As disappointing as this is, I have still provided useful insight – such as the best sgRNA to use, and the sequence and size of the homology arms – that will help the next trainee

in creating this allele. Further analyses of the gene list may identify other genes like Rsad2 that can be used to create important tools to best study kidney development.

Chapter 4: Organotypic roles of Cyp26b1 during lung and kidney organogenesis

Summary

A major goal of my thesis was to identify ways in which ECs direct organ development. From the work done in Chapter 3, I chose Cyp26b1, a P450 enzyme that metabolizes RA into inactive forms, to study further. Cyp26b1 is highly enriched in ECs in both the lung and the kidney suggesting that ECs may regulate development of these organs through controlling RA signaling. Whole body knockouts of Cyp26b1 greatly impaired lung distal epithelial development while the kidneys did not appear affected. Cyp26b1$^{-/-}$ lungs exhibited decreased airway spaces, increased cellular density, and a delay in distal epithelial differentiation that abrogated the formation of mature AT1 gas-exchanging cells. Together these defects lead to neonatal demise. To verify whether these effects were due to excess RA, I administered atRA to pregnant dams in late gestation. Embryos that received atRA were able to partially phenocopy loss of Cyp26b1, exhibiting similar gross defects and changes in distal airway maturation. However, transcriptomic analyses revealed separate responses between Cyp26b1$^{-/-}$ and atRA-treated lungs, suggesting that there are other RA-independent mechanisms that drive the phenotype in Cyp26b1$^{-/-}$ lungs. Kidneys, on the other hand, appear protected from excess RA through upregulation of Dhrs3. Bypassing Dhrs3 by administering exogenous atRA was able to decrease distal nephron formation in Cyp26b1$^{+/-}$ kidneys only. These data suggest

that RA plays similar roles in both lung and kidney development, but is regulated through separate mechanisms.

Future Directions

The data presented here suggest that defects in Cyp26b1$^{-/-}$ lungs arise from RA-dependent and RA-independent mechanisms. The most salient next step is to identify those RA-independent mechanisms. Christopher Chaney in the Carroll lab and I have performed RNA-seq analysis of E18.5 Cyp26b1$^{+/+}$ and Cyp26b1$^{-/-}$ lungs to determine overall changes in the transcriptomes (data not presented here). Functional annotation clustering using the online tool DAVID (https://david.ncifcrf.gov/home.jsp) revealed that upregulated genes are primarily involved with chromatin remodeling while downregulated genes are involved in maintaining the ECM. Interestingly, DAVID analysis did not suggest enrichment of any pathways related to RA signaling or metabolism, supporting the hypothesis that RA-independent mechanisms partially drive this phenotype. These RNA-seq data will help identify the exact mechanisms that drive the defect in Cyp26b1$^{-/-}$ lungs. Additionally, it will be insightful to perform RNA-seq on atRA-treated and control lungs. Due to the differences in the transcriptomic responses between Cyp26b1$^{-/-}$ and atRA-treated lungs, RNA-seq analyses on these lungs will help determine the specific transcriptomic changes caused by RA-dependent and RA-independent processes.

My data implicate ECs in driving this phenotype; however, a major limitation of my work is that I analyzed whole body knockouts of Cyp26b1. Because Cyp26b1 is not exclusively expressed in ECs in both the kidney and lung, other cell types may be contributing

to this phenotype. To definitively demonstrate that the phenotype is due to loss of Cyp26b1 in ECs, I would need to acquire the Cyp26b1 conditional line (MacLean et al., 2007) and cross it to the EC-specific Tie2-Cre and VE-Cad-CreERT2 mouse lines. These experiments will be extremely valuable in furthering our understanding of Cyp26b1 for the following reasons. First, deletion of Cyp26b1 using Tie2-Cre will determine whether ECs directly regulate lung epithelial development through Cyp26b1. I hypothesize that EC-specific deletion of Cyp26b1 will recapitulate the defects seen in $Cyp26b1^{-/-}$ lungs. Even if this hypothesis is incorrect, this experiment will help identify the primary cell type that drives the defects observed in the $Cyp26b1^{-/-}$ lungs. Second, the inducible VE-Cad-CreERT2 line will provide important temporal control over Cyp26b1 deletion to identify the exact developmental window when Cyp26b1 is needed. Additionally, there may be postnatal defects in $Cyp26b1^{-/-}$ mice that cannot be observed because these mice die shortly after birth. The VE-Cad-CreERT2 line will allow us to bypass this neonatal lethality and study how loss of Cyp26b1 affects postnatal lung and kidney development. For these reasons, acquiring the Cyp26b1 conditional line is the critical next step to move this study forward.

Another important set of experiments to perform are rescue experiments. If the lung defects are mediated through excess RA, then depleting RA should prevent their formation. A common way to deplete RA is to feed mice a Vitamin A deficient diet. Vitamin A deficiency from E9.5 to E14.5 is sufficient to cause lasting changes in airway smooth muscle cell development (Chen et al., 2014). In data not shown here, I performed a similar experiment in which I fed pregnant dams a Vitamin A deficient diet from E9.5 to E18.5. $Cyp26b1^{-/-}$ lungs on the Vitamin A deficient diet were indistinguishable to $Cyp26b1^{-/-}$ lungs on the control diet.

Although these data suggest that Vitamin A deficiency does not rescue the defects, there are important caveats to this approach. First, the mother's liver contains large amounts of Vitamin A stored as retinyl ester that can maintain proper Vitamin A levels up to several weeks (Blomhoff and Blomhoff, 2006; Blomhoff et al., 1990). Second, RA is necessary for initial lung development; therefore, exogenous RA will be necessary to support embryonic development if true Vitamin A deficiency can be achieved. One group has designed an experimental approach to maintain females on a Vitamin A deficient diet for several weeks before breeding to fully deplete Vitamin A, then supplement these mothers with exogenous RA at critical moments during the pregnancy (See et al., 2008; White et al., 1998). A variation of this approach may be useful for the present study. Alternatively, a non-nutritional approach can also be performed through inhibiting the RA-synthesizing enzymes Raldh1-3 with the small molecule WIN18,446 *in vivo* (Wang et al., 2018a; Wang et al., 2018b). Lastly, the most rigorous approach would be to identify specific genes from the RNA-seq data that drive the Cyp26b1$^{-/-}$ phenotype, and then perform genetic experiments to try to rescue the defects.

Cyp26b1$^{-/-}$ kidneys appeared phenotypically normal; however, the data presented here provide tantalizing evidence that excess RA does affect murine kidney development and that both Cyp261 and Dhrs3 both act to reduce RA signaling in the kidney. The next step would be to generate Dhrs3$^{-/-}$; Cyp26b1$^{-/-}$ (or EC-specific Cyp26b1$^{-/-}$ as described above) mice to see if the deletion of both genes can cause defects in kidney development. Dhrs3 has not been studied in the context of kidney development despite its strong expression in the stroma (Billings et al., 2013); therefore, studying both Dhrs3$^{-/-}$ and Dhrs3$^{-/-}$; Cyp26b1$^{-/-}$ kidneys may lead to new and exciting findings about kidney development.

It is admittedly disappointing that Cyp26b1$^{-/-}$ kidneys did not show any overt defects. As such, these findings may dissuade further exploration of the RNA-seq data from Chapter 3 more thoroughly. However, I would argue these data should continue to be analyzed. My data highlight how specific organs shape the same signaling pathway to fit their needs. I find it absolutely fascinating that excess RA blocks distal epithelial development in both the lung and the kidney yet these organs utilize different mechanisms to protect themselves. One of the most exciting aspects of this project is being able to use one organ to generate hypotheses and experiments for another. For example, an alternative approach to rescue the lung defects may be to overexpress Dhrs3 in the lung, mirroring what occurs in the kidney. The prediction would be that Cyp26b1-dependent phenotypes might disappear. Although there are many more experiments left to do, what is clear is that the biology in these two organs is synergistic: the whole of studying both the lung and the kidney together is greater than the sum of studying the two organs separately. In essence, this story is emblematic of my future career as an M.D./Ph.D. Through both this project and my training so far, what I have learned is that the challenge to understand both sides – to find that common thread that links them together while distilling the differences – is well worth the reward in the end.

Final Conclusions

Overall, the work presented in this thesis details the importance of understanding cellular structure and communication during organogenesis. I defined the structure and organization of renal blood vessels throughout development and generated a list of novel EC-specific genes expressed in the kidney vasculature. I then characterized the function of one of

these genes, Cyp26b1, during organogenesis. Loss of Cyp26b1 specifically affected lung, but not kidney, epithelial development. The data presented demonstrate that regulation of RA signaling is both organ-specific and highly complex than previously appreciated. Several questions still remain about the role of Cyp26b1 and RA signaling between organs during embryonic development. Answering these questions will continue to shed light on the complex symphony that is organogenesis.

BIBLIOGRAPHY

Abrahamson, D.R. (2009). Development of kidney glomerular endothelial cells and their role in basement membrane assembly. Organogenesis *5*, 275-287.

Abu-Abed, S., MacLean, G., Fraulob, V., Chambon, P., Petkovich, M., and Dolle, P. (2002). Differential expression of the retinoic acid-metabolizing enzymes CYP26A1 and CYP26B1 during murine organogenesis. Mech Dev *110*, 173-177.

Acar, M., Kocherlakota, K.S., Murphy, M.M., Peyer, J.G., Oguro, H., Inra, C.N., Jaiyeola, C., Zhao, Z., Luby-Phelps, K., and Morrison, S.J. (2015). Deep imaging of bone marrow shows non-dividing stem cells are mainly perisinusoidal. Nature *526*, 126-130.

Adams, M.K., Belyaeva, O.V., Wu, L., and Kedishvili, N.Y. (2014). The retinaldehyde reductase activity of DHRS3 is reciprocally activated by retinol dehydrogenase 10 to control retinoid homeostasis. J Biol Chem *289*, 14868-14880.

Aird, W.C. (2003). Endothelial cell heterogeneity. Crit Care Med *31*, S221-230.

Aird, W.C. (2007a). Phenotypic heterogeneity of the endothelium: I. Structure, function, and mechanisms. Circ Res *100*, 158-173.

Aird, W.C. (2007b). Phenotypic heterogeneity of the endothelium: II. Representative vascular beds. Circ Res *100*, 174-190.

Aird, W.C. (2012). Endothelial cell heterogeneity. Cold Spring Harb Perspect Med *2*, a006429.

Akeson, A.L., Cameron, J.E., Le Cras, T.D., Whitsett, J.A., and Greenberg, J.M. (2005). Vascular endothelial growth factor-A induces prenatal neovascularization and alters bronchial development in mice. Pediatr Res *57*, 82-88.

Akeson, A.L., Greenberg, J.M., Cameron, J.E., Thompson, F.Y., Brooks, S.K., Wiginton, D., and Whitsett, J.A. (2003). Temporal and spatial regulation of VEGF-A controls vascular patterning in the embryonic lung. Dev Biol *264*, 443-455.

Alabi, R.O., Glomski, K., Haxaire, C., Weskamp, G., Monette, S., and Blobel, C.P. (2016). ADAM10-Dependent Signaling Through Notch1 and Notch4 Controls Development of Organ-Specific Vascular Beds. Circ Res *119*, 519-531.

Alonzo, L.F., Moya, M.L., Shirure, V.S., and George, S.C. (2015). Microfluidic device to control interstitial flow-mediated homotypic and heterotypic cellular communication. Lab Chip *15*, 3521-3529.

Aso, Y., Yoneda, K., and Kikkawa, Y. (1976). Morphologic and biochemical study of pulmonary changes induced by bleomycin in mice. Lab Invest *35*, 558-568.

Augustin, H.G., and Koh, G.Y. (2017). Organotypic vasculature: From descriptive heterogeneity to functional pathophysiology. Science *357*.

Azizoglu, D.B., Chong, D.C., Villasenor, A., Magenheim, J., Barry, D.M., Lee, S., Marty-Santos, L., Fu, S., Dor, Y., and Cleaver, O. (2016). Vascular development in the vertebrate pancreas. Dev Biol *420*, 67-78.

Azizoglu, D.B., and Cleaver, O. (2016). Blood vessel crosstalk during organogenesis-focus on pancreas and endothelial cells. Wiley Interdiscip Rev Dev Biol *5*, 598-617.

Baeyens, N., and Schwartz, M.A. (2016). Biomechanics of vascular mechanosensation and remodeling. Mol Biol Cell *27*, 7-11.

Balmer, J.E., and Blomhoff, R. (2002). Gene expression regulation by retinoic acid. J Lipid Res *43*, 1773-1808.

Bantounas, I., Ranjzad, P., Tengku, F., Silajdzic, E., Forster, D., Asselin, M.C., Lewis, P., Lennon, R., Plagge, A., Wang, Q., *et al.* (2018). Generation of Functioning Nephrons by Implanting Human Pluripotent Stem Cell-Derived Kidney Progenitors. Stem Cell Reports *10*, 766-779.

Bartlett, C.S., Scott, R.P., Carota, I.A., Wnuk, M.L., Kanwar, Y.S., Miner, J.H., and Quaggin, S.E. (2017). Glomerular mesangial cell recruitment and function require the co-receptor neuropilin-1. Am J Physiol Renal Physiol *313*, F1232-F1242.

Belteki, G., Haigh, J., Kabacs, N., Haigh, K., Sison, K., Costantini, F., Whitsett, J., Quaggin, S.E., and Nagy, A. (2005). Conditional and inducible transgene expression in mice through the combinatorial use of Cre-mediated recombination and tetracycline induction. Nucleic Acids Res *33*, e51.

Bhushan, A., Itoh, N., Kato, S., Thiery, J.P., Czernichow, P., Bellusci, S., and Scharfmann, R. (2001). Fgf10 is essential for maintaining the proliferative capacity of epithelial progenitor cells during early pancreatic organogenesis. Development *128*, 5109-5117.

Billings, S.E., Pierzchalski, K., Butler Tjaden, N.E., Pang, X.Y., Trainor, P.A., Kane, M.A., and Moise, A.R. (2013). The retinaldehyde reductase DHRS3 is essential for preventing the formation of excess retinoic acid during embryonic development. FASEB J *27*, 4877-4889.

Bjarnegard, M., Enge, M., Norlin, J., Gustafsdottir, S., Fredriksson, S., Abramsson, A., Takemoto, M., Gustafsson, E., Fassler, R., and Betsholtz, C. (2004). Endothelium-specific ablation of PDGFB leads to pericyte loss and glomerular, cardiac and placental abnormalities. Development *131*, 1847-1857.

Blomhoff, R., and Blomhoff, H.K. (2006). Overview of retinoid metabolism and function. J Neurobiol *66*, 606-630.

Blomhoff, R., Green, M.H., Berg, T., and Norum, K.R. (1990). Transport and storage of vitamin A. Science *250*, 399-404.

Bowles, J., Secker, G., Nguyen, C., Kazenwadel, J., Truong, V., Frampton, E., Curtis, C., Skoczylas, R., Davidson, T.L., Miura, N., *et al.* (2014). Control of retinoid levels by CYP26B1 is important for lymphatic vascular development in the mouse embryo. Dev Biol *386*, 25-33.

Braitsch, C.M., Combs, M.D., Quaggin, S.E., and Yutzey, K.E. (2012). Pod1/Tcf21 is regulated by retinoic acid signaling and inhibits differentiation of epicardium-derived cells into smooth muscle in the developing heart. Dev Biol *368*, 345-357.

Brunskill, E.W., and Potter, S.S. (2010). Gene expression programs of mouse endothelial cells in kidney development and disease. PLoS One *5*, e12034.

Cadot, S., Frenz, D., and Maconochie, M. (2012). A novel method for retinoic acid administration reveals differential and dose-dependent downregulation of Fgf3 in the developing inner ear and anterior CNS. Dev Dyn *241*, 741-758.

Cai, Q., Brissova, M., Reinert, R.B., Pan, F.C., Brahmachary, P., Jeansson, M., Shostak, A., Radhika, A., Poffenberger, G., Quaggin, S.E., *et al.* (2012). Enhanced expression of VEGF-A in beta cells increases endothelial cell number but impairs islet morphogenesis and beta cell proliferation. Developmental Biology *367*, 40-54.

Cao, G., O'Brien, C.D., Zhou, Z., Sanders, S.M., Greenbaum, J.N., Makrigiannakis, A., and DeLisser, H.M. (2002). Involvement of human PECAM-1 in angiogenesis and in vitro endothelial cell migration. Am J Physiol Cell Physiol *282*, C1181-1190.

Chen, F., Desai, T.J., Qian, J., Niederreither, K., Lu, J., and Cardoso, W.V. (2007). Inhibition of Tgf beta signaling by endogenous retinoic acid is essential for primary lung bud induction. Development *134*, 2969-2979.

Chen, F., Marquez, H., Kim, Y.K., Qian, J., Shao, F., Fine, A., Cruikshank, W.W., Quadro, L., and Cardoso, W.V. (2014). Prenatal retinoid deficiency leads to airway hyperresponsiveness in adult mice. J Clin Invest *124*, 801-811.

Chen, Q., Jiang, L., Li, C., Hu, D., Bu, J.W., Cai, D., and Du, J.L. (2012). Haemodynamics-driven developmental pruning of brain vasculature in zebrafish. PLoS Biol *10*, e1001374.

Chen, Y.W., Huang, S.X., de Carvalho, A., Ho, S.H., Islam, M.N., Volpi, S., Notarangelo, L.D., Ciancanelli, M., Casanova, J.L., Bhattacharya, J., *et al.* (2017). A three-dimensional model of human lung development and disease from pluripotent stem cells. Nat Cell Biol *19*, 542-549.

Chi, J.T., Chang, H.Y., Haraldsen, G., Jahnsen, F.L., Troyanskaya, O.G., Chang, D.S., Wang, Z., Rockson, S.G., van de Rijn, M., Botstein, D., *et al.* (2003). Endothelial cell diversity revealed by global expression profiling. Proc Natl Acad Sci U S A *100*, 10623-10628.

Chong, D.C., Koo, Y., Xu, K., Fu, S., and Cleaver, O. (2011). Stepwise arteriovenous fate acquisition during mammalian vasculogenesis. Dev Dyn *240*, 2153-2165.

Cleaver, O., Tonissen, K.F., Saha, M.S., and Krieg, P.A. (1997). Neovascularization of the Xenopus embryo. Dev Dyn *210*, 66-77.

Combes, A.N., Phipson, B., Zappia, L., Lawlor, K., Er, P.X., Oshlack, A., and Little, M. (2017). High throughput single cell RNA-seq of developing mouse kidney and human kidney organoids reveals a roadmap for recreating the kidney. bioRxiv.

Compernolle, V., Brusselmans, K., Acker, T., Hoet, P., Tjwa, M., Beck, H., Plaisance, S., Dor, Y., Keshet, E., Lupu, F., *et al.* (2002). Loss of HIF-2alpha and inhibition of VEGF impair fetal lung maturation, whereas treatment with VEGF prevents fatal respiratory distress in premature mice. Nat Med *8*, 702-710.

Costantini, F., and Kopan, R. (2010). Patterning a complex organ: branching morphogenesis and nephron segmentation in kidney development. Dev Cell *18*, 698-712.

Coultas, L., Nieuwenhuis, E., Anderson, G.A., Cabezas, J., Nagy, A., Henkelman, R.M., Hui, C.C., and Rossant, J. (2010). Hedgehog regulates distinct vascular patterning events through VEGF-dependent and -independent mechanisms. Blood *116*, 653-660.

Cowan, M.J., and Crystal, R.G. (1975). Lung growth after unilateral pneumonectomy: quantitation of collagen synthesis and content. Am Rev Respir Dis *111*, 267-277.

Culver, J.C., and Dickinson, M.E. (2010). The effects of hemodynamic force on embryonic development. Microcirculation *17*, 164-178.

Culver, J.C., Vadakkan, T.J., and Dickinson, M.E. (2013). A specialized microvascular domain in the mouse neural stem cell niche. PLoS One *8*, e53546.

Czerniecki, S.M., Cruz, N.M., Harder, J.L., Menon, R., Annis, J., Otto, E.A., Gulieva, R.E., Islas, L.V., Kim, Y.K., Tran, L.M., *et al.* (2018). High-Throughput Screening Enhances Kidney Organoid Differentiation from Human Pluripotent Stem Cells and Enables Automated Multidimensional Phenotyping. Cell Stem Cell *22*, 929-940 e924.

Dekel, B., Burakova, T., Arditti, F.D., Reich-Zeliger, S., Milstein, O., Aviel-Ronen, S., Rechavi, G., Friedman, N., Kaminski, N., Passwell, J.H., *et al.* (2003). Human and porcine early kidney precursors as a new source for transplantation. Nat Med *9*, 53-60.

Del Moral, P.M., Sala, F.G., Tefft, D., Shi, W., Keshet, E., Bellusci, S., and Warburton, D. (2006). VEGF-A signaling through Flk-1 is a critical facilitator of early embryonic lung epithelial to endothelial crosstalk and branching morphogenesis. Dev Biol *290*, 177-188.

dela Paz, N.G., and D'Amore, P.A. (2009). Arterial versus venous endothelial cells. Cell Tissue Res *335*, 5-16.

DeLisser, H.M., Christofidou-Solomidou, M., Strieter, R.M., Burdick, M.D., Robinson, C.S., Wexler, R.S., Kerr, J.S., Garlanda, C., Merwin, J.R., Madri, J.A., *et al.* (1997). Involvement of endothelial PECAM-1/CD31 in angiogenesis. Am J Pathol *151*, 671-677.

deMello, D.E., Sawyer, D., Galvin, N., and Reid, L.M. (1997). Early fetal development of lung vasculature. Am J Respir Cell Mol Biol *16*, 568-581.

Deng, Y., Larrivee, B., Zhuang, Z.W., Atri, D., Moraes, F., Prahst, C., Eichmann, A., and Simons, M. (2013). Endothelial RAF1/ERK activation regulates arterial morphogenesis. Blood *121*, 3988-3996, S3981-3989.

Desai, T.J., Malpel, S., Flentke, G.R., Smith, S.M., and Cardoso, W.V. (2004). Retinoic acid selectively regulates Fgf10 expression and maintains cell identity in the prospective lung field of the developing foregut. Dev Biol *273*, 402-415.

Dimke, H., Sparks, M.A., Thomson, B.R., Frische, S., Coffman, T.M., and Quaggin, S.E. (2015). Tubulovascular cross-talk by vascular endothelial growth factor a maintains peritubular microvasculature in kidney. J Am Soc Nephrol *26*, 1027-1038.

Ding, B.S., Nolan, D.J., Guo, P., Babazadeh, A.O., Cao, Z., Rosenwaks, Z., Crystal, R.G., Simons, M., Sato, T.N., Worgall, S., *et al.* (2011). Endothelial-derived angiocrine signals induce and sustain regenerative lung alveolarization. Cell *147*, 539-553.

Drake, C.J., and Fleming, P.A. (2000). Vasculogenesis in the day 6.5 to 9.5 mouse embryo. Blood *95*, 1671-1679.

Dranse, H.J., Sampaio, A.V., Petkovich, M., and Underhill, T.M. (2011). Genetic deletion of Cyp26b1 negatively impacts limb skeletogenesis by inhibiting chondrogenesis. J Cell Sci *124*, 2723-2734.

Du, Y., Guo, M., Whitsett, J.A., and Xu, Y. (2015). 'LungGENS': a web-based tool for mapping single-cell gene expression in the developing lung. Thorax *70*, 1092-1094.

Du, Y., Kitzmiller, J.A., Sridharan, A., Perl, A.K., Bridges, J.P., Misra, R.S., Pryhuber, G.S., Mariani, T.J., Bhattacharya, S., Guo, M., *et al.* (2017). Lung Gene Expression Analysis (LGEA): an integrative web portal for comprehensive gene expression data analysis in lung development. Thorax *72*, 481-484.

Duarte, A., Hirashima, M., Benedito, R., Trindade, A., Diniz, P., Bekman, E., Costa, L., Henrique, D., and Rossant, J. (2004). Dosage-sensitive requirement for mouse Dll4 in artery development. Genes Dev *18*, 2474-2478.

Dumont, D.J., Gradwohl, G., Fong, G.H., Puri, M.C., Gertsenstein, M., Auerbach, A., and Breitman, M.L. (1994). Dominant-negative and targeted null mutations in the endothelial receptor tyrosine kinase, tek, reveal a critical role in vasculogenesis of the embryo. Genes Dev *8*, 1897-1909.

Dunn, N.R., Winnier, G.E., Hargett, L.K., Schrick, J.J., Fogo, A.B., and Hogan, B.L. (1997). Haploinsufficient phenotypes in Bmp4 heterozygous null mice and modification by mutations in Gli3 and Alx4. Dev Biol *188*, 235-247.

Dye, B.R., Hill, D.R., Ferguson, M.A., Tsai, Y.H., Nagy, M.S., Dyal, R., Wells, J.M., Mayhew, C.N., Nattiv, R., Klein, O.D., *et al.* (2015). In vitro generation of human pluripotent stem cell derived lung organoids. Elife *4*.

Edsbagge, J., Johansson, J.K., Esni, F., Luo, Y., Radice, G.L., and Semb, H. (2005). Vascular function and sphingosine-1-phosphate regulate development of the dorsal pancreatic mesenchyme. Development *132*, 1085-1092.

Eiraku, M., Takata, N., Ishibashi, H., Kawada, M., Sakakura, E., Okuda, S., Sekiguchi, K., Adachi, T., and Sasai, Y. (2011). Self-organizing optic-cup morphogenesis in three-dimensional culture. Nature *472*, 51-56.

Eiraku, M., Watanabe, K., Matsuo-Takasaki, M., Kawada, M., Yonemura, S., Matsumura, M., Wataya, T., Nishiyama, A., Muguruma, K., and Sasai, Y. (2008). Self-organized formation of polarized cortical tissues from ESCs and its active manipulation by extrinsic signals. Cell Stem Cell *3*, 519-532.

Ema, M., Takahashi, S., and Rossant, J. (2006). Deletion of the selection cassette, but not cis-acting elements, in targeted Flk1-lacZ allele reveals Flk1 expression in multipotent mesodermal progenitors. Blood *107*, 111-117.

Eremina, V., Cui, S., Gerber, H., Ferrara, N., Haigh, J., Nagy, A., Ema, M., Rossant, J., Jothy, S., Miner, J.H., *et al.* (2006). Vascular endothelial growth factor a signaling in the podocyte-endothelial compartment is required for mesangial cell migration and survival. J Am Soc Nephrol *17*, 724-735.

Eremina, V., Sood, M., Haigh, J., Nagy, A., Lajoie, G., Ferrara, N., Gerber, H.P., Kikkawa, Y., Miner, J.H., and Quaggin, S.E. (2003). Glomerular-specific alterations of VEGF-A expression lead to distinct congenital and acquired renal diseases. J Clin Invest *111*, 707-716.

Farber, G., Hurtado, R., Loh, S., Monette, S., Mtui, J., Kopan, R., Quaggin, S., Meyer-Schwesinger, C., Herzlinger, D., Scott, R.P., *et al.* (2018). Glomerular endothelial cell maturation depends on ADAM10, a key regulator of Notch signaling. Angiogenesis *21*, 335-347.

Feng, L., Hernandez, R.E., Waxman, J.S., Yelon, D., and Moens, C.B. (2010). Dhrs3a regulates retinoic acid biosynthesis through a feedback inhibition mechanism. Dev Biol *338*, 1-14.

Ferrara, N., Carver-Moore, K., Chen, H., Dowd, M., Lu, L., O'Shea, K.S., Powell-Braxton, L., Hillan, K.J., and Moore, M.W. (1996). Heterozygous embryonic lethality induced by targeted inactivation of the VEGF gene. Nature *380*, 439-442.

Franco, C.A., Jones, M.L., Bernabeu, M.O., Geudens, I., Mathivet, T., Rosa, A., Lopes, F.M., Lima, A.P., Ragab, A., Collins, R.T., *et al.* (2015). Dynamic endothelial cell rearrangements drive developmental vessel regression. PLoS Biol *13*, e1002125.

Frank, D.B., Penkala, I.J., Zepp, J.A., Sivakumar, A., Linares-Saldana, R., Zacharias, W.J., Stolz, K.G., Pankin, J., Lu, M., Wang, Q., *et al.* (2019). Early lineage specification defines alveolar epithelial ontogeny in the murine lung. Proc Natl Acad Sci U S A.

Freedman, B.S., Brooks, C.R., Lam, A.Q., Fu, H., Morizane, R., Agrawal, V., Saad, A.F., Li, M.K., Hughes, M.R., Werff, R.V., *et al.* (2015). Modelling kidney disease with CRISPR-mutant kidney organoids derived from human pluripotent epiblast spheroids. Nat Commun *6*, 8715.

Gao, L., Yang, Z., Hiremath, C., Zimmerman, S.E., Long, B., Brakeman, P.R., Mostov, K.E., Bryant, D.M., Luby-Phelps, K., and Marciano, D.K. (2017). Afadin orients cell division to position the tubule lumen in developing renal tubules. Development *144*, 3511-3520.

Gao, X., Chen, X., Taglienti, M., Rumballe, B., Little, M.H., and Kreidberg, J.A. (2005). Angioblast-mesenchyme induction of early kidney development is mediated by Wt1 and Vegfa. Development *132*, 5437-5449.

Garcia, M.D., and Larina, I.V. (2014). Vascular development and hemodynamic force in the mouse yolk sac. Front Physiol *5*, 308.

Gerhardt, H., and Betsholtz, C. (2003). Endothelial-pericyte interactions in angiogenesis. Cell Tissue Res *314*, 15-23.

Grigoryan, B., Paulsen, S.J., Corbett, D.C., Sazer, D.W., Fortin, C.L., Zaita, A.J., Greenfield, P.T., Calafat, N.J., Gounley, J.P., Ta, A.H., *et al.* (2019). Multivascular networks and functional intravascular topologies within biocompatible hydrogels. Science *364*, 458-464.

Gu, G., Brown, J.R., and Melton, D.A. (2003). Direct lineage tracing reveals the ontogeny of pancreatic cell fates during mouse embryogenesis. Mech Dev *120*, 35-43.

Guillaume, R., Bressan, M., and Herzlinger, D. (2009). Paraxial mesoderm contributes stromal cells to the developing kidney. Dev Biol *329*, 169-175.

Guo, M., Du, Y., Gokey, J.J., Ray, S., Bell, S.M., Adam, M., Sudha, P., Perl, A.K., Deshmukh, H., Potter, S.S., *et al.* (2019). Single cell RNA analysis identifies

cellular heterogeneity and adaptive responses of the lung at birth. Nat Commun *10*, 37.

Hatini, V., Huh, S.O., Herzlinger, D., Soares, V.C., and Lai, E. (1996). Essential role of stromal mesenchyme in kidney morphogenesis revealed by targeted disruption of Winged Helix transcription factor BF-2. Genes Dev *10*, 1467-1478.

Havrilak, J.A., Melton, K.R., and Shannon, J.M. (2017). Endothelial cells are not required for specification of respiratory progenitors. Dev Biol *427*, 93-105.

Herbert, S.P., Huisken, J., Kim, T.N., Feldman, M.E., Houseman, B.T., Wang, R.A., Shokat, K.M., and Stainier, D.Y. (2009). Arterial-venous segregation by selective cell sprouting: an alternative mode of blood vessel formation. Science *326*, 294-298.

Herriges, M., and Morrisey, E.E. (2014). Lung development: orchestrating the generation and regeneration of a complex organ. Development *141*, 502-513.

Hochane, M., van den Berg, P.R., Fan, X., Berenger-Currias, N., Adegeest, E., Bialecka, M., Nieveen, M., Menschaart, M., Chuva de Sousa Lopes, S.M., and Semrau, S. (2019). Single-cell transcriptomics reveals gene expression dynamics of human fetal kidney development. PLoS Biol *17*, e3000152.

Hogmalm, A., Bry, M., Strandvik, B., and Bry, K. (2014). IL-1beta expression in the distal lung epithelium disrupts lung morphogenesis and epithelial cell differentiation in fetal mice. Am J Physiol Lung Cell Mol Physiol *306*, L23-34.

Homan, K.A., Gupta, N., Kroll, K.T., Kolesky, D.B., Skylar-Scott, M., Miyoshi, T., Mau, D., Valerius, M.T., Ferrante, T., Bonventre, J.V., *et al.* (2019). Flow-enhanced vascularization and maturation of kidney organoids in vitro. Nat Methods *16*, 255-262.

Hu, Y., Li, M., Gothert, J.R., Gomez, R.A., and Sequeira-Lopez, M.L. (2016). Hemovascular Progenitors in the Kidney Require Sphingosine-1-Phosphate Receptor 1 for Vascular Development. J Am Soc Nephrol *27*, 1984-1995.

Hum, S., Rymer, C., Schaefer, C., Bushnell, D., and Sims-Lucas, S. (2014). Ablation of the renal stroma defines its critical role in nephron progenitor and vasculature patterning. PLoS One *9*, e88400.

Humphreys, B.D., Lin, S.L., Kobayashi, A., Hudson, T.E., Nowlin, B.T., Bonventre, J.V., Valerius, M.T., McMahon, A.P., and Duffield, J.S. (2010). Fate tracing reveals the pericyte and not epithelial origin of myofibroblasts in kidney fibrosis. Am J Pathol *176*, 85-97.

Hurtado, R., Zewdu, R., Mtui, J., Liang, C., Aho, R., Kurylo, C., Selleri, L., and Herzlinger, D. (2015). Pbx1-dependent control of VMC differentiation kinetics underlies gross renal vascular patterning. Development *142*, 2653-2664.

Hyink, D.P., Tucker, D.C., St John, P.L., Leardkamolkarn, V., Accavitti, M.A., Abrass, C.K., and Abrahamson, D.R. (1996). Endogenous origin of glomerular endothelial and mesangial cells in grafts of embryonic kidneys. Am J Physiol *270*, F886-899.

Jacquemin, P., Yoshitomi, H., Kashima, Y., Rousseau, G.G., Lemaigre, F.P., and Zaret, K.S. (2006). An endothelial-mesenchymal relay pathway regulates early phases of pancreas development. Dev Biol *290*, 189-199.

Jakkula, M., Le Cras, T.D., Gebb, S., Hirth, K.P., Tuder, R.M., Voelkel, N.F., and Abman, S.H. (2000). Inhibition of angiogenesis decreases alveolarization in the developing rat lung. Am J Physiol Lung Cell Mol Physiol *279*, L600-607.

Jeansson, M., Gawlik, A., Anderson, G., Li, C., Kerjaschki, D., Henkelman, M., and Quaggin, S.E. (2011). Angiopoietin-1 is essential in mouse vasculature during development and in response to injury. J Clin Invest *121*, 2278-2289.

Jo, J., Xiao, Y., Sun, A.X., Cukuroglu, E., Tran, H.D., Goke, J., Tan, Z.Y., Saw, T.Y., Tan, C.P., Lokman, H., *et al.* (2016). Midbrain-like Organoids from Human Pluripotent Stem Cells Contain Functional Dopaminergic and Neuromelanin-Producing Neurons. Cell Stem Cell *19*, 248-257.

Kato, K., Dieguez-Hurtado, R., Park, D.Y., Hong, S.P., Kato-Azuma, S., Adams, S., Stehling, M., Trappmann, B., Wrana, J.L., Koh, G.Y., *et al.* (2018). Pulmonary pericytes regulate lung morphogenesis. Nat Commun *9*, 2448.

Katsumoto, K., and Kume, S. (2011). Endoderm and mesoderm reciprocal signaling mediated by CXCL12 and CXCR4 regulates the migration of angioblasts and establishes the pancreatic fate. Development *138*, 1947-1955.

Kawaguchi, Y., Cooper, B., Gannon, M., Ray, M., MacDonald, R.J., and Wright, C.V. (2002). The role of the transcriptional regulator Ptf1a in converting intestinal to pancreatic progenitors. Nat Genet *32*, 128-134.

Kenig-Kozlovsky, Y., Scott, R.P., Onay, T., Carota, I.A., Thomson, B.R., Gil, H.J., Ramirez, V., Yamaguchi, S., Tanna, C.E., Heinen, S., *et al.* (2018). Ascending Vasa Recta Are Angiopoietin/Tie2-Dependent Lymphatic-Like Vessels. J Am Soc Nephrol *29*, 1097-1107.

Kersbergen, A., Best, S.A., Dworkin, S., Ah-Cann, C., de Vries, M.E., Asselin-Labat, M.L., Ritchie, M.E., Jane, S.M., and Sutherland, K.D. (2018). Lung morphogenesis is orchestrated through Grainyhead-like 2 (Grhl2) transcriptional programs. Dev Biol *443*, 1-9.

Kim, C.F., Jackson, E.L., Woolfenden, A.E., Lawrence, S., Babar, I., Vogel, S., Crowley, D., Bronson, R.T., and Jacks, T. (2005). Identification of bronchioalveolar stem cells in normal lung and lung cancer. Cell *121*, 823-835.

Kimura, W., Xiao, F., Canseco, D.C., Muralidhar, S., Thet, S., Zhang, H.M., Abderrahman, Y., Chen, R., Garcia, J.A., Shelton, J.M., *et al.* (2015). Hypoxia fate mapping identifies cycling cardiomyocytes in the adult heart. Nature *523*, 226-230.

Kitamoto, Y., Tokunaga, H., and Tomita, K. (1997). Vascular endothelial growth factor is an essential molecule for mouse kidney development: glomerulogenesis and nephrogenesis. J Clin Invest *99*, 2351-2357.

Klagsbrun, M., Takashima, S., and Mamluk, R. (2002). The role of neuropilin in vascular and tumor biology. Adv Exp Med Biol *515*, 33-48.

Kolesky, D.B., Homan, K.A., Skylar-Scott, M.A., and Lewis, J.A. (2016). Three-dimensional bioprinting of thick vascularized tissues. Proc Natl Acad Sci U S A *113*, 3179-3184.

Kumar, S.V., Er, P.X., Lawlor, K.T., Motazedian, A., Scurr, M., Ghobrial, I., Combes, A.N., Zappia, L., Oshlack, A., Stanley, E.G., *et al.* (2019). Kidney micro-

organoids in suspension culture as a scalable source of human pluripotent stem cell-derived kidney cells. Development *146*.

Lammert, E., Cleaver, O., and Melton, D. (2001). Induction of pancreatic differentiation by signals from blood vessels. Science *294*, 564-567.

Lanahan, A., Zhang, X., Fantin, A., Zhuang, Z., Rivera-Molina, F., Speichinger, K., Prahst, C., Zhang, J., Wang, Y., Davis, G., *et al.* (2013). The neuropilin 1 cytoplasmic domain is required for VEGF-A-dependent arteriogenesis. Dev Cell *25*, 156-168.

Lanahan, A.A., Hermans, K., Claes, F., Kerley-Hamilton, J.S., Zhuang, Z.W., Giordano, F.J., Carmeliet, P., and Simons, M. (2010). VEGF receptor 2 endocytic trafficking regulates arterial morphogenesis. Dev Cell *18*, 713-724.

Lancaster, M.A., Corsini, N.S., Wolfinger, S., Gustafson, E.H., Phillips, A.W., Burkard, T.R., Otani, T., Livesey, F.J., and Knoblich, J.A. (2017). Guided self-organization and cortical plate formation in human brain organoids. Nat Biotechnol *35*, 659-666.

Lancaster, M.A., and Knoblich, J.A. (2014). Organogenesis in a dish: modeling development and disease using organoid technologies. Science *345*, 1247125.

Lancaster, M.A., Renner, M., Martin, C.A., Wenzel, D., Bicknell, L.S., Hurles, M.E., Homfray, T., Penninger, J.M., Jackson, A.P., and Knoblich, J.A. (2013). Cerebral organoids model human brain development and microcephaly. Nature *501*, 373-379.

Landsman, L., Nijagal, A., Whitchurch, T.J., Vanderlaan, R.L., Zimmer, W.E., Mackenzie, T.C., and Hebrok, M. (2011). Pancreatic mesenchyme regulates epithelial organogenesis throughout development. PLoS Biol *9*, e1001143.

Langfelder, P., and Horvath, S. (2008). WGCNA: an R package for weighted correlation network analysis. BMC Bioinformatics *9*, 559.

Lazarus, A., Del-Moral, P.M., Ilovich, O., Mishani, E., Warburton, D., and Keshet, E. (2011). A perfusion-independent role of blood vessels in determining branching stereotypy of lung airways. Development *138*, 2359-2368.

Le Cras, T.D., Spitzmiller, R.E., Albertine, K.H., Greenberg, J.M., Whitsett, J.A., and Akeson, A.L. (2004). VEGF causes pulmonary hemorrhage, hemosiderosis, and air space enlargement in neonatal mice. Am J Physiol Lung Cell Mol Physiol *287*, L134-142.

le Noble, F., Moyon, D., Pardanaud, L., Yuan, L., Djonov, V., Matthijsen, R., Breant, C., Fleury, V., and Eichmann, A. (2004). Flow regulates arterial-venous differentiation in the chick embryo yolk sac. Development *131*, 361-375.

Lee, J.H., Bhang, D.H., Beede, A., Huang, T.L., Stripp, B.R., Bloch, K.D., Wagers, A.J., Tseng, Y.H., Ryeom, S., and Kim, C.F. (2014). Lung stem cell differentiation in mice directed by endothelial cells via a BMP4-NFATc1-thrombospondin-1 axis. Cell *156*, 440-455.

Lenti, E., Farinello, D., Yokoyama, K.K., Penkov, D., Castagnaro, L., Lavorgna, G., Wuputra, K., Sandell, L.L., Tjaden, N.E., Bernassola, F., *et al.* (2016). Transcription factor TLX1 controls retinoic acid signaling to ensure spleen development. J Clin Invest *126*, 2452-2464.

Leveen, P., Pekny, M., Gebre-Medhin, S., Swolin, B., Larsson, E., and Betsholtz, C. (1994). Mice deficient for PDGF B show renal, cardiovascular, and hematological abnormalities. Genes Dev *8*, 1875-1887.

Li, Y., Cheng, C.N., Verdun, V.A., and Wingert, R.A. (2014). Zebrafish nephrogenesis is regulated by interactions between retinoic acid, mecom, and Notch signaling. Dev Biol *386*, 111-122.

Lin, E.E., Sequeira-Lopez, M.L., and Gomez, R.A. (2014). RBP-J in FOXD1+ renal stromal progenitors is crucial for the proper development and assembly of the kidney vasculature and glomerular mesangial cells. Am J Physiol Renal Physiol *306*, F249-258.

Lin, N.Y.C., Homan, K.A., Robinson, S.S., Kolesky, D.B., Duarte, N., Moisan, A., and Lewis, J.A. (2019). Renal reabsorption in 3D vascularized proximal tubule models. Proc Natl Acad Sci U S A *116*, 5399-5404.

Lindahl, P., Hellstrom, M., Kalen, M., Karlsson, L., Pekny, M., Pekna, M., Soriano, P., and Betsholtz, C. (1998). Paracrine PDGF-B/PDGF-Rbeta signaling controls mesangial cell development in kidney glomeruli. Development *125*, 3313-3322.

Lindstrom, N.O., De Sena Brandine, G., Tran, T., Ransick, A., Suh, G., Guo, J., Kim, A.D., Parvez, R.K., Ruffins, S.W., Rutledge, E.A., *et al.* (2018a). Progressive Recruitment of Mesenchymal Progenitors Reveals a Time-Dependent Process of Cell Fate Acquisition in Mouse and Human Nephrogenesis. Dev Cell *45*, 651-660 e654.

Lindstrom, N.O., Guo, J., Kim, A.D., Tran, T., Guo, Q., De Sena Brandine, G., Ransick, A., Parvez, R.K., Thornton, M.E., Basking, L., *et al.* (2018b). Conserved and Divergent Features of Mesenchymal Progenitor Cell Types within the Cortical Nephrogenic Niche of the Human and Mouse Kidney. J Am Soc Nephrol.

Lindstrom, N.O., McMahon, J.A., Guo, J., Tran, T., Guo, Q., Rutledge, E., Parvez, R.K., Saribekyan, G., Schuler, R.E., Liao, C., *et al.* (2018c). Conserved and Divergent Features of Human and Mouse Kidney Organogenesis. J Am Soc Nephrol.

Lindstrom, N.O., Tran, T., Guo, J., Rutledge, E., Parvez, R.K., Thornton, M.E., Grubbs, B., McMahon, J.A., and McMahon, A.P. (2018d). Conserved and Divergent Molecular and Anatomic Features of Human and Mouse Nephron Patterning. J Am Soc Nephrol.

Lindstrom, N.O., Tran, T., Guo, J., Rutledge, E., Parvez, R.K., Thornton, M.E., Grubbs, B., McMahon, J.A., and McMahon, A.P. (2018e). Conserved and Divergent Molecular and Anatomic Features of Human and Mouse Nephron Patterning. J Am Soc Nephrol *29*, 825-840.

Love, M.I., Huber, W., and Anders, S. (2014). Moderated estimation of fold change and dispersion for RNA-seq data with DESeq2. Genome biology *15*, 550.

Lucitti, J.L., Jones, E.A., Huang, C., Chen, J., Fraser, S.E., and Dickinson, M.E. (2007). Vascular remodeling of the mouse yolk sac requires hemodynamic force. Development *134*, 3317-3326.

MacLean, G., Li, H., Metzger, D., Chambon, P., and Petkovich, M. (2007). Apoptotic extinction of germ cells in testes of Cyp26b1 knockout mice. Endocrinology *148*, 4560-4567.

Magenheim, J., Ilovich, O., Lazarus, A., Klochendler, A., Ziv, O., Werman, R., Hija, A., Cleaver, O., Mishani, E., Keshet, E., *et al.* (2011). Blood vessels restrain pancreas branching, differentiation and growth. Development *138*, 4743-4752.

Malpel, S., Mendelsohn, C., and Cardoso, W.V. (2000). Regulation of retinoic acid signaling during lung morphogenesis. Development *127*, 3057-3067.

Marcu, R., Choi, Y.J., Xue, J., Fortin, C.L., Wang, Y., Nagao, R.J., Xu, J., MacDonald, J.W., Bammler, T.K., Murry, C.E., *et al.* (2018). Human Organ-Specific Endothelial Cell Heterogeneity. iScience *4*, 20-35.

Mazumdar, J., O'Brien, W.T., Johnson, R.S., LaManna, J.C., Chavez, J.C., Klein, P.S., and Simon, M.C. (2010). O2 regulates stem cells through Wnt/beta-catenin signalling. Nat Cell Biol *12*, 1007-1013.

McCright, B., Gao, X., Shen, L., Lozier, J., Lan, Y., Maguire, M., Herzlinger, D., Weinmaster, G., Jiang, R., and Gridley, T. (2001). Defects in development of the kidney, heart and eye vasculature in mice homozygous for a hypomorphic Notch2 mutation. Development *128*, 491-502.

Miller, A.J., Hill, D.R., Nagy, M.S., Aoki, Y., Dye, B.R., Chin, A.M., Huang, S., Zhu, F., White, E.S., Lama, V., *et al.* (2018). In Vitro Induction and In Vivo Engraftment of Lung Bud Tip Progenitor Cells Derived from Human Pluripotent Stem Cells. Stem Cell Reports *10*, 101-119.

Miner, J.H. (2012). The glomerular basement membrane. Exp Cell Res *318*, 973-978.

Mohamed, T., and Sequeira-Lopez, M.L.S. (2018). Development of the renal vasculature. Semin Cell Dev Biol.

Molema, G., and Aird, W.C. (2012). Vascular heterogeneity in the kidney. Semin Nephrol *32*, 145-155.

Morizane, R., Lam, A.Q., Freedman, B.S., Kishi, S., Valerius, M.T., and Bonventre, J.V. (2015). Nephron organoids derived from human pluripotent stem cells model kidney development and injury. Nat Biotechnol *33*, 1193-1200.

Moyon, D., Pardanaud, L., Yuan, L., Breant, C., and Eichmann, A. (2001). Plasticity of endothelial cells during arterial-venous differentiation in the avian embryo. Development *128*, 3359-3370.

Mukouyama, Y.S., Shin, D., Britsch, S., Taniguchi, M., and Anderson, D.J. (2002). Sensory nerves determine the pattern of arterial differentiation and blood vessel branching in the skin. Cell *109*, 693-705.

Munro, D.A.D., Hohenstein, P., Coate, T.M., and Davies, J.A. (2017a). Refuting the hypothesis that semaphorin-3f/neuropilin-2 exclude blood vessels from the cap mesenchyme in the developing kidney. Dev Dyn *246*, 1047-1056.

Munro, D.A.D., Hohenstein, P., and Davies, J.A. (2017b). Cycles of vascular plexus formation within the nephrogenic zone of the developing mouse kidney. Sci Rep *7*, 3273.

Murakami, Y., Naganuma, H., Tanigawa, S., Fujimori, T., Eto, M., and Nishinakamura, R. (2019). Reconstitution of the embryonic kidney identifies a donor cell contribution to the renal vasculature upon transplantation. Sci Rep *9*, 1172.

Nakano, T., Ando, S., Takata, N., Kawada, M., Muguruma, K., Sekiguchi, K., Saito, K., Yonemura, S., Eiraku, M., and Sasai, Y. (2012). Self-formation of optic cups and storable stratified neural retina from human ESCs. Cell Stem Cell *10*, 771-785.

Naylor, R.W., Skvarca, L.B., Thisse, C., Thisse, B., Hukriede, N.A., and Davidson, A.J. (2016). BMP and retinoic acid regulate anterior-posterior patterning of the non-axial mesoderm across the dorsal-ventral axis. Nat Commun *7*, 12197.

Newman, P.J., and Newman, D.K. (2003). Signal transduction pathways mediated by PECAM-1: new roles for an old molecule in platelet and vascular cell biology. Arterioscler Thromb Vasc Biol *23*, 953-964.

Nolan, D.J., Ginsberg, M., Israely, E., Palikuqi, B., Poulos, M.G., James, D., Ding, B.S., Schachterle, W., Liu, Y., Rosenwaks, Z., *et al.* (2013). Molecular signatures of tissue-specific microvascular endothelial cell heterogeneity in organ maintenance and regeneration. Dev Cell *26*, 204-219.

Nordsletten, D.A., Blackett, S., Bentley, M.D., Ritman, E.L., and Smith, N.P. (2006). Structural morphology of renal vasculature. Am J Physiol Heart Circ Physiol *291*, H296-309.

O'Brien, L.L., Guo, Q., Lee, Y., Tran, T., Benazet, J.D., Whitney, P.H., Valouev, A., and McMahon, A.P. (2016). Differential regulation of mouse and human nephron progenitors by the Six family of transcriptional regulators. Development *143*, 595-608.

O'Brien, L.L., and McMahon, A.P. (2014). Induction and patterning of the metanephric nephron. Semin Cell Dev Biol *36*, 31-38.

Okano, J., Kimura, W., Papaionnou, V.E., Miura, N., Yamada, G., Shiota, K., and Sakai, Y. (2012a). The regulation of endogenous retinoic acid level through CYP26B1 is required for elevation of palatal shelves. Dev Dyn *241*, 1744-1756.

Okano, J., Lichti, U., Mamiya, S., Aronova, M., Zhang, G., Yuspa, S.H., Hamada, H., Sakai, Y., and Morasso, M.I. (2012b). Increased retinoic acid levels through ablation of Cyp26b1 determine the processes of embryonic skin barrier formation and peridermal development. J Cell Sci *125*, 1827-1836.

Oxburgh, L., Carroll, T.J., Cleaver, O., Gossett, D.R., Hoshizaki, D.K., Hubbell, J.A., Humphreys, B.D., Jain, S., Jensen, J., Kaplan, D.L., *et al.* (2017). (Re)Building a Kidney. J Am Soc Nephrol *28*, 1370-1378.

Pan, F.C., and Wright, C. (2011). Pancreas organogenesis: from bud to plexus to gland. Dev Dyn *240*, 530-565.

Parera, M.C., van Dooren, M., van Kempen, M., de Krijger, R., Grosveld, F., Tibboel, D., and Rottier, R. (2005). Distal angiogenesis: a new concept for lung vascular morphogenesis. Am J Physiol Lung Cell Mol Physiol *288*, L141-149.

Patro, R., Duggal, G., Love, M.I., Irizarry, R.A., and Kingsford, C. (2017). Salmon provides fast and bias-aware quantification of transcript expression. Nat Methods *14*, 417-419.

Peng, T., Tian, Y., Boogerd, C.J., Lu, M.M., Kadzik, R.S., Stewart, K.M., Evans, S.M., and Morrisey, E.E. (2013). Coordination of heart and lung co-development by a multipotent cardiopulmonary progenitor. Nature *500*, 589-592.

Pierreux, C.E., Cordi, S., Hick, A.C., Achouri, Y., Ruiz de Almodovar, C., Prevot, P.P., Courtoy, P.J., Carmeliet, P., and Lemaigre, F.P. (2010). Epithelial: Endothelial cross-talk regulates exocrine differentiation in developing pancreas. Dev Biol *347*, 216-227.

Plopper, C.G., Suverkropp, C., Morin, D., Nishio, S., and Buckpitt, A. (1992). Relationship of cytochrome P-450 activity to Clara cell cytotoxicity. I. Histopathologic comparison of the respiratory tract of mice, rats and hamsters after parenteral administration of naphthalene. J Pharmacol Exp Ther *261*, 353-363.

Potter, C.M., Lao, K.H., Zeng, L., and Xu, Q. (2014). Role of biomechanical forces in stem cell vascular lineage differentiation. Arterioscler Thromb Vasc Biol *34*, 2184-2190.

Probst, S., Kraemer, C., Demougin, P., Sheth, R., Martin, G.R., Shiratori, H., Hamada, H., Iber, D., Zeller, R., and Zuniga, A. (2011). SHH propagates distal limb bud development by enhancing CYP26B1-mediated retinoic acid clearance via AER-FGF signalling. Development *138*, 1913-1923.

Przepiorski, A., Sander, V., Tran, T., Hollywood, J.A., Sorrenson, B., Shih, J.H., Wolvetang, E.J., McMahon, A.P., Holm, T.M., and Davidson, A.J. (2018). A Simple Bioreactor-Based Method to Generate Kidney Organoids from Pluripotent Stem Cells. Stem Cell Reports *11*, 470-484.

Pu, W., He, L., Han, X., Tian, X., Li, Y., Zhang, H., Liu, Q., Huang, X., Zhang, L., Wang, Q.D., *et al.* (2018). Genetic Targeting of Organ-Specific Blood Vessels. Circ Res *123*, 86-99.

Rafii, S., Cao, Z., Lis, R., Siempos, II, Chavez, D., Shido, K., Rabbany, S.Y., and Ding, B.S. (2015). Platelet-derived SDF-1 primes the pulmonary capillary vascular niche to drive lung alveolar regeneration. Nat Cell Biol *17*, 123-136.

Rankin, S.A., Han, L., McCracken, K.W., Kenny, A.P., Anglin, C.T., Grigg, E.A., Crawford, C.M., Wells, J.M., Shannon, J.M., and Zorn, A.M. (2016). A Retinoic Acid-Hedgehog Cascade Coordinates Mesoderm-Inducing Signals and Endoderm Competence during Lung Specification. Cell Rep *16*, 66-78.

Rankin, S.A., McCracken, K.W., Luedeke, D.M., Han, L., Wells, J.M., Shannon, J.M., and Zorn, A.M. (2018). Timing is everything: Reiterative Wnt, BMP and RA signaling regulate developmental competence during endoderm organogenesis. Dev Biol *434*, 121-132.

Reidy, K.J., Villegas, G., Teichman, J., Veron, D., Shen, W., Jimenez, J., Thomas, D., and Tufro, A. (2009). Semaphorin3a regulates endothelial cell number and podocyte differentiation during glomerular development. Development *136*, 3979-3989.

Reinert, R.B., Brissova, M., Shostak, A., Pan, F.C., Poffenberger, G., Cai, Q., Hundemer, G.L., Kantz, J., Thompson, C.S., Dai, C., *et al.* (2013). Vascular endothelial growth factor-a and islet vascularization are necessary in developing, but not adult, pancreatic islets. Diabetes *62*, 4154-4164.

Rhinn, M., and Dolle, P. (2012). Retinoic acid signalling during development. Development *139*, 843-858.

Robert, B., St John, P.L., and Abrahamson, D.R. (1998). Direct visualization of renal vascular morphogenesis in Flk1 heterozygous mutant mice. Am J Physiol *275*, F164-172.

Robert, B., St John, P.L., Hyink, D.P., and Abrahamson, D.R. (1996). Evidence that embryonic kidney cells expressing flk-1 are intrinsic, vasculogenic angioblasts. Am J Physiol *271*, F744-753.

Rockich, B.E., Hrycaj, S.M., Shih, H.P., Nagy, M.S., Ferguson, M.A., Kopp, J.L., Sander, M., Wellik, D.M., and Spence, J.R. (2013). Sox9 plays multiple roles in the lung epithelium during branching morphogenesis. Proc Natl Acad Sci U S A *110*, E4456-4464.

Ross, A.C., and Zolfaghari, R. (2011). Cytochrome P450s in the regulation of cellular retinoic acid metabolism. Annu Rev Nutr *31*, 65-87.

Rossant, J., Zirngibl, R., Cado, D., Shago, M., and Giguere, V. (1991). Expression of a retinoic acid response element-hsplacZ transgene defines specific domains of transcriptional activity during mouse embryogenesis. Genes Dev *5*, 1333-1344.

Rosselot, C., Spraggon, L., Chia, I., Batourina, E., Riccio, P., Lu, B., Niederreither, K., Dolle, P., Duester, G., Chambon, P., *et al.* (2010). Non-cell-autonomous retinoid signaling is crucial for renal development. Development *137*, 283-292.

Rymer, C., Paredes, J., Halt, K., Schaefer, C., Wiersch, J., Zhang, G., Potoka, D., Vainio, S., Gittes, G.K., Bates, C.M., *et al.* (2014). Renal blood flow and oxygenation drive nephron progenitor differentiation. Am J Physiol Renal Physiol *307*, F337-345.

Saarela, U., Akram, S.U., Desgrange, A., Rak-Raszewska, A., Shan, J., Cereghini, S., Ronkainen, V.P., Heikkila, J., Skovorodkin, I., and Vainio, S.J. (2017). Novel fixed z-direction (FiZD) kidney primordia and an organoid culture system for time-lapse confocal imaging. Development *144*, 1113-1117.

Sabbagh, M.F., Heng, J.S., Luo, C., Castanon, R.G., Nery, J.R., Rattner, A., Goff, L.A., Ecker, J.R., and Nathans, J. (2018). Transcriptional and epigenomic landscapes of CNS and non-CNS vascular endothelial cells. Elife *7*.

Sand, F.W., Hornblad, A., Johansson, J.K., Loren, C., Edsbagge, J., Stahlberg, A., Magenheim, J., Ilovich, O., Mishani, E., Dor, Y., *et al.* (2011). Growth-limiting role of endothelial cells in endoderm development. Dev Biol *352*, 267-277.

Sariola, H., Ekblom, P., Lehtonen, E., and Saxen, L. (1983). Differentiation and vascularization of the metanephric kidney grafted on the chorioallantoic membrane. Dev Biol *96*, 427-435.

Saxén, L. (1987). Vascularization of the nephron. In Organogenesis of the kidney, P.W. Barlow, P.B. Green, and C.C. Wylie, eds. (Cambridge: Cambridge University Press), pp. 129-142.

Saxen, L., and Sariola, H. (1987). Early Organogenesis of the Kidney. Pediatric Nephrology *1*, 385-392.

Schachtner, S.K., Wang, Y., and Scott Baldwin, H. (2000). Qualitative and quantitative analysis of embryonic pulmonary vessel formation. Am J Respir Cell Mol Biol *22*, 157-165.

See, A.W., Kaiser, M.E., White, J.C., and Clagett-Dame, M. (2008). A nutritional model of late embryonic vitamin A deficiency produces defects in organogenesis at a high penetrance and reveals new roles for the vitamin in skeletal development. Dev Biol *316*, 171-190.

Sequeira-Lopez, M.L., Lin, E.E., Li, M., Hu, Y., Sigmund, C.D., and Gomez, R.A. (2015). The earliest metanephric arteriolar progenitors and their role in kidney vascular development. Am J Physiol Regul Integr Comp Physiol *308*, R138-149.

Sequeira Lopez, M.L., and Gomez, R.A. (2011). Development of the renal arterioles. J Am Soc Nephrol *22*, 2156-2165.

Shah, S.R., Esni, F., Jakub, A., Paredes, J., Lath, N., Malek, M., Potoka, D.A., Prasadan, K., Mastroberardino, P.G., Shiota, C., *et al.* (2011). Embryonic mouse blood flow and oxygen correlate with early pancreatic differentiation. Dev Biol *349*, 342-349.

Shalaby, F., Rossant, J., Yamaguchi, T.P., Gertsenstein, M., Wu, X.F., Breitman, M.L., and Schuh, A.C. (1995). Failure of blood-island formation and vasculogenesis in Flk-1-deficient mice. Nature *376*, 62-66.

Sharmin, S., Taguchi, A., Kaku, Y., Yoshimura, Y., Ohmori, T., Sakuma, T., Mukoyama, M., Yamamoto, T., Kurihara, H., and Nishinakamura, R. (2016). Human Induced Pluripotent Stem Cell-Derived Podocytes Mature into Vascularized Glomeruli upon Experimental Transplantation. J Am Soc Nephrol *27*, 1778-1791.

Shi, W., Chen, F., and Cardoso, W.V. (2009). Mechanisms of lung development: contribution to adult lung disease and relevance to chronic obstructive pulmonary disease. Proc Am Thorac Soc *6*, 558-563.

Shirure, V.S., Lezia, A., Tao, A., Alonzo, L.F., and George, S.C. (2017). Low levels of physiological interstitial flow eliminate morphogen gradients and guide angiogenesis. Angiogenesis *20*, 493-504.

Siemerink, M.J., Klaassen, I., Van Noorden, C.J., and Schlingemann, R.O. (2013). Endothelial tip cells in ocular angiogenesis: potential target for anti-angiogenesis therapy. J Histochem Cytochem *61*, 101-115.

Simons, M., and Eichmann, A. (2015). Molecular controls of arterial morphogenesis. Circ Res *116*, 1712-1724.

Sison, K., Eremina, V., Baelde, H., Min, W., Hirashima, M., Fantus, I.G., and Quaggin, S.E. (2010). Glomerular structure and function require paracrine, not autocrine, VEGF-VEGFR-2 signaling. J Am Soc Nephrol *21*, 1691-1701.

Soneson, C., Love, M.I., and Robinson, M.D. (2015). Differential analyses for RNA-seq: transcript-level estimates improve gene-level inferences. F1000Res *4*, 1521.

Soriano, P. (1994). Abnormal kidney development and hematological disorders in PDGF beta-receptor mutant mice. Genes Dev *8*, 1888-1896.

Spence, J.R., Mayhew, C.N., Rankin, S.A., Kuhar, M.F., Vallance, J.E., Tolle, K., Hoskins, E.E., Kalinichenko, V.V., Wells, S.I., Zorn, A.M., *et al.* (2011). Directed differentiation of human pluripotent stem cells into intestinal tissue in vitro. Nature *470*, 105-109.

Spoorendonk, K.M., Peterson-Maduro, J., Renn, J., Trowe, T., Kranenbarg, S., Winkler, C., and Schulte-Merker, S. (2008). Retinoic acid and Cyp26b1 are critical regulators of osteogenesis in the axial skeleton. Development *135*, 3765-3774.

Stevens, P.E., Levin, A., and Kidney Disease: Improving Global Outcomes Chronic Kidney Disease Guideline Development Work Group, M. (2013). Evaluation and management of chronic kidney disease: synopsis of the kidney disease: improving global outcomes 2012 clinical practice guideline. Ann Intern Med *158*, 825-830.

Stolz, D.B., and Sims-Lucas, S. (2015). Unwrapping the origins and roles of the renal endothelium. Pediatr Nephrol *30*, 865-872.

Strilic, B., Kucera, T., Eglinger, J., Hughes, M.R., McNagny, K.M., Tsukita, S., Dejana, E., Ferrara, N., and Lammert, E. (2009). The molecular basis of vascular lumen formation in the developing mouse aorta. Dev Cell *17*, 505-515.

Subramanian, B., Rudym, D., Cannizzaro, C., Perrone, R., Zhou, J., and Kaplan, D.L. (2010). Tissue-engineered three-dimensional in vitro models for normal and diseased kidney. Tissue Eng Part A *16*, 2821-2831.

Suri, C., Jones, P.F., Patan, S., Bartunkova, S., Maisonpierre, P.C., Davis, S., Sato, T.N., and Yancopoulos, G.D. (1996). Requisite role of angiopoietin-1, a ligand for the TIE2 receptor, during embryonic angiogenesis. Cell *87*, 1171-1180.

Tabula Muris, C., Overall, c., Logistical, c., Organ, c., processing, Library, p., sequencing, Computational data, a., Cell type, a., Writing, g., *et al.* (2018). Single-cell transcriptomics of 20 mouse organs creates a Tabula Muris. Nature *562*, 367-372.

Taguchi, A., and Nishinakamura, R. (2017). Higher-Order Kidney Organogenesis from Pluripotent Stem Cells. Cell Stem Cell *21*, 730-746 e736.

Takasato, M., Er, P.X., Chiu, H.S., Maier, B., Baillie, G.J., Ferguson, C., Parton, R.G., Wolvetang, E.J., Roost, M.S., Chuva de Sousa Lopes, S.M., *et al.* (2015). Kidney organoids from human iPS cells contain multiple lineages and model human nephrogenesis. Nature *526*, 564-568.

Takebe, T., Sekine, K., Enomura, M., Koike, H., Kimura, M., Ogaeri, T., Zhang, R.R., Ueno, Y., Zheng, Y.W., Koike, N., *et al.* (2013). Vascularized and functional human liver from an iPSC-derived organ bud transplant. Nature *499*, 481-484.

Takubo, K., Goda, N., Yamada, W., Iriuchishima, H., Ikeda, E., Kubota, Y., Shima, H., Johnson, R.S., Hirao, A., Suematsu, M., *et al.* (2010). Regulation of the HIF-1alpha level is essential for hematopoietic stem cells. Cell Stem Cell *7*, 391-402.

Trisno, S.L., Philo, K.E.D., McCracken, K.W., Cata, E.M., Ruiz-Torres, S., Rankin, S.A., Han, L., Nasr, T., Chaturvedi, P., Rothenberg, M.E., *et al.* (2018). Esophageal Organoids from Human Pluripotent Stem Cells Delineate Sox2 Functions during Esophageal Specification. Cell Stem Cell *23*, 501-515 e507.

Tufro, A. (2000). VEGF spatially directs angiogenesis during metanephric development in vitro. Dev Biol *227*, 558-566.

Tufro, A., Norwood, V.F., Carey, R.M., and Gomez, R.A. (1999). Vascular endothelial growth factor induces nephrogenesis and vasculogenesis. J Am Soc Nephrol *10*, 2125-2134.

Tullius, S.G., and Rabb, H. (2018). Improving the Supply and Quality of Deceased-Donor Organs for Transplantation. N Engl J Med *378*, 1920-1929.

Udan, R.S., Vadakkan, T.J., and Dickinson, M.E. (2013). Dynamic responses of endothelial cells to changes in blood flow during vascular remodeling of the mouse yolk sac. Development *140*, 4041-4050.

Ueda, H., Miyazaki, Y., Matsusaka, T., Utsunomiya, Y., Kawamura, T., Hosoya, T., and Ichikawa, I. (2008). Bmp in podocytes is essential for normal glomerular capillary formation. J Am Soc Nephrol *19*, 685-694.

Uzarski, J.S., Bijonowski, B.M., Wang, B., Ward, H.H., Wandinger-Ness, A., Miller, W.M., and Wertheim, J.A. (2015). Dual-Purpose Bioreactors to Monitor Noninvasive Physical and Biochemical Markers of Kidney and Liver Scaffold Recellularization. Tissue Eng Part C Methods *21*, 1032-1043.

van den Berg, C.W., Ritsma, L., Avramut, M.C., Wiersma, L.E., van den Berg, B.M., Leuning, D.G., Lievers, E., Koning, M., Vanslambrouck, J.M., Koster, A.J., *et al.* (2018). Renal Subcapsular Transplantation of PSC-Derived Kidney Organoids Induces Neo-vasculogenesis and Significant Glomerular and Tubular Maturation In Vivo. Stem Cell Reports *10*, 751-765.

van Tuyl, M., Liu, J., Wang, J., Kuliszewski, M., Tibboel, D., and Post, M. (2005). Role of oxygen and vascular development in epithelial branching morphogenesis of the developing mouse lung. Am J Physiol Lung Cell Mol Physiol *288*, L167-178.

Vaughan, M.R., and Quaggin, S.E. (2008). How do mesangial and endothelial cells form the glomerular tuft? J Am Soc Nephrol *19*, 24-33.

Villasenor, A., Chong, D.C., and Cleaver, O. (2008). Biphasic Ngn3 expression in the developing pancreas. Dev Dyn *237*, 3270-3279.

Villasenor, A., Chong, D.C., Henkemeyer, M., and Cleaver, O. (2010a). Epithelial dynamics of pancreatic branching morphogenesis. Development *137*, 4295-4305.

Villasenor, A., Wang, Z.V., Rivera, L.B., Ocal, O., Asterholm, I.W., Scherer, P.E., Brekken, R.A., Cleaver, O., and Wilkie, T.M. (2010b). Rgs16 and Rgs8 in embryonic endocrine pancreas and mouse models of diabetes. Dis Model Mech *3*, 567-580.

Wang, S., Huang, W., Castillo, H.A., Kane, M.A., Xavier-Neto, J., Trainor, P.A., and Moise, A.R. (2018a). Alterations in retinoic acid signaling affect the development of the mouse coronary vasculature. Dev Dyn *247*, 976-991.

Wang, S., Yu, J., Jones, J.W., Pierzchalski, K., Kane, M.A., Trainor, P.A., Xavier-Neto, J., and Moise, A.R. (2018b). Retinoic acid signaling promotes the cytoskeletal rearrangement of embryonic epicardial cells. FASEB J *32*, 3765-3781.

Wang, X., Phan, D.T., Sobrino, A., George, S.C., Hughes, C.C., and Lee, A.P. (2016). Engineering anastomosis between living capillary networks and endothelial cell-lined microfluidic channels. Lab Chip *16*, 282-290.

Warburton, D., El-Hashash, A., Carraro, G., Tiozzo, C., Sala, F., Rogers, O., Langhe, S.D., Kemp, P.J., Riccardi, D., Torday, J., *et al.* (2010). Lung Organogenesis. In Organogenesis in Development, pp. 73-158.

White, J.C., Shankar, V.N., Highland, M., Epstein, M.L., DeLuca, H.F., and Clagett-Dame, M. (1998). Defects in embryonic hindbrain development and fetal resorption resulting from vitamin A deficiency in the rat are prevented by feeding

pharmacological levels of all-trans-retinoic acid. Proc Natl Acad Sci U S A *95*, 13459-13464.

Wimmer, R.A., Leopoldi, A., Aichinger, M., Wick, N., Hantusch, B., Novatchkova, M., Taubenschmid, J., Hammerle, M., Esk, C., Bagley, J.A., *et al.* (2019). Human blood vessel organoids as a model of diabetic vasculopathy. Nature *565*, 505-510.

Wingert, R.A., and Davidson, A.J. (2011). Zebrafish nephrogenesis involves dynamic spatiotemporal expression changes in renal progenitors and essential signals from retinoic acid and irx3b. Dev Dyn *240*, 2011-2027.

Woik, N., Dietz, C.T., Schaker, K., and Kroll, J. (2014). Kelch-like ECT2-interacting protein KLEIP regulates late-stage pulmonary maturation via Hif-2alpha in mice. Dis Model Mech *7*, 683-692.

Wong, Y.F., Wilson, P.D., Unwin, R.J., Norman, J.T., Arno, M., Hendry, B.M., and Xu, Q. (2012). Retinoic acid receptor-dependent, cell-autonomous, endogenous retinoic acid signaling and its target genes in mouse collecting duct cells. PLoS One *7*, e45725.

Wongtrakool, C., Malpel, S., Gorenstein, J., Sedita, J., Ramirez, M.I., Underhill, T.M., and Cardoso, W.V. (2003). Down-regulation of retinoic acid receptor alpha signaling is required for sacculation and type I cell formation in the developing lung. J Biol Chem *278*, 46911-46918.

Workman, M.J., Mahe, M.M., Trisno, S., Poling, H.M., Watson, C.L., Sundaram, N., Chang, C.F., Schiesser, J., Aubert, P., Stanley, E.G., *et al.* (2017). Engineered human pluripotent-stem-cell-derived intestinal tissues with a functional enteric nervous system. Nat Med *23*, 49-59.

Wu, L., and Ross, A.C. (2010). Acidic retinoids synergize with vitamin A to enhance retinol uptake and STRA6, LRAT, and CYP26B1 expression in neonatal lung. J Lipid Res *51*, 378-387.

Xiao, Y., Hill, M.C., Zhang, M., Martin, T.J., Morikawa, Y., Wang, S., Moise, A.R., Wythe, J.D., and Martin, J.F. (2018). Hippo Signaling Plays an Essential Role in Cell State Transitions during Cardiac Fibroblast Development. Dev Cell *45*, 153-169 e156.

Xu, K., Sacharidou, A., Fu, S., Chong, D.C., Skaug, B., Chen, Z.J., Davis, G.E., and Cleaver, O. (2011). Blood vessel tubulogenesis requires Rasip1 regulation of GTPase signaling. Dev Cell *20*, 526-539.

Yamamoto, H., Yun, E.J., Gerber, H.P., Ferrara, N., Whitsett, J.A., and Vu, T.H. (2007). Epithelial-vascular cross talk mediated by VEGF-A and HGF signaling directs primary septae formation during distal lung morphogenesis. Dev Biol *308*, 44-53.

Yang, H., Lu, M.M., Zhang, L., Whitsett, J.A., and Morrisey, E.E. (2002). GATA6 regulates differentiation of distal lung epithelium. Development *129*, 2233-2246.

Yang, Z., Zimmerman, S., Brakeman, P.R., Beaudoin, G.M., 3rd, Reichardt, L.F., and Marciano, D.K. (2013). De novo lumen formation and elongation in the developing nephron: a central role for afadin in apical polarity. Development *140*, 1774-1784.

Yang, Z., Zimmerman, S.E., Tsunezumi, J., Braitsch, C., Trent, C., Bryant, D.M., Cleaver, O., Gonzalez-Manchon, C., and Marciano, D.K. (2016). Role of CD34

family members in lumen formation in the developing kidney. Dev Biol *418*, 66-74.

Yashiro, K., Zhao, X., Uehara, M., Yamashita, K., Nishijima, M., Nishino, J., Saijoh, Y., Sakai, Y., and Hamada, H. (2004). Regulation of retinoic acid distribution is required for proximodistal patterning and outgrowth of the developing mouse limb. Dev Cell *6*, 411-422.

Yoshitomi, H., and Zaret, K.S. (2004). Endothelial cell interactions initiate dorsal pancreas development by selectively inducing the transcription factor Ptf1a. Development *131*, 807-817.

Yuan, L., Chan, G.C., Beeler, D., Janes, L., Spokes, K.C., Dharaneeswaran, H., Mojiri, A., Adams, W.J., Sciuto, T., Garcia-Cardena, G., *et al.* (2016). A role of stochastic phenotype switching in generating mosaic endothelial cell heterogeneity. Nat Commun *7*, 10160.

Zeng, X., Wert, S.E., Federici, R., Peters, K.G., and Whitsett, J.A. (1998). VEGF enhances pulmonary vasculogenesis and disrupts lung morphogenesis in vivo. Dev Dyn *211*, 215-227.

Zhang, Y., Yang, Y., Jiang, M., Huang, S.X., Zhang, W., Al Alam, D., Danopoulos, S., Mori, M., Chen, Y.W., Balasubramanian, R., *et al.* (2018). 3D Modeling of Esophageal Development using Human PSC-Derived Basal Progenitors Reveals a Critical Role for Notch Signaling. Cell Stem Cell *23*, 516-529 e515.

Zhao, Z., Nelson, A.R., Betsholtz, C., and Zlokovic, B.V. (2015). Establishment and Dysfunction of the Blood-Brain Barrier. Cell *163*, 1064-1078.

Zheng, Y., Chen, J., Craven, M., Choi, N.W., Totorica, S., Diaz-Santana, A., Kermani, P., Hempstead, B., Fischbach-Teschl, C., Lopez, J.A., *et al.* (2012). In vitro microvessels for the study of angiogenesis and thrombosis. Proc Natl Acad Sci U S A *109*, 9342-9347.